Non-Invasive Approaches for the Investigation of Intracortical Interactions in The Early Visual Cortex

Sébastien Proulx
Integrated Program in Neuroscience
McGill University, Montréal
April 18th, 2022

A thesis submitted to McGill University in partial fulfillment of the requirements of the degree of Doctor Philosophy in Neuroscience

CONTENT

ENGLISH ABSTRACT

Investigating the human mind requires non-invasive approaches. Yet, the relation between neural computations and non-invasive brain signals is indirect, complex and poorly understood.

To overcome this challenge, this thesis focusses on intracortical interactions between cortical columns at a major entry point of information in the cortex, the early visual cortex (EVC). The low-level computations this brain tissue carries are easily manipulated in established visual stimulation paradigms, and are well-studied in animals and preserved across many mammals. Intercolumnar interactions yet constitute a canonical substrate for computations across the cortex. By aiming a diverse set of non-invasive investigation tools on generalizable cortical computations in a well-known low-level sensory area, this thesis takes a principled approach to characterize non-invasive brain signals in terms of relevant neural computations.

The 1st study of this thesis clarifies how non-invasive brain modulation (NIBM) with transcranial magnetic stimulation (TMS) impacts neural computations from cortical columns representing different visual field locations, stimulus orientations and eye of origin. In a psychophysical visual masking paradigm, the "inhibitory" continuous theta burst stimulation (cTBS) treatment applied to the occipital pole reduced all tested cortical types of visual suppression, while leaving subcortical suppression and unsuppressed perception unaffected. Concordant with motor cortex findings, this suggests that behavioral and therapeutic effects of cTBS generalize across cortices and rely on a *reduction* of intracortical inhibition in the targeted brain area. It further highlights the potential of EVC TMS for dissecting the NIBM effects at the microcircuit level.

The 2nd study characterizes the computational relevance of non-invasive magnetic resonance spectroscopy (MRS) measures of bulk regional neurotransmitter concentrations. The poor specificity of these measures to specific subcellular compartments and to the various functions caried by the typically ~8-cm^3 sampled brain volume is alleviated by isolating interocular interactions in a post-pre protocol. Few hours of monocular deprivation (MD) induced a well-known adult-form visual plasticity that shifted ocular dominance (OD) toward the deprived eye. I report extensive behavioral, electrophysiological and MRS measures relating such OD

plasticity to *increased* occipital GABA concentrations in contradiction to previous findings. A behavioral follow-up attributed the discrepancy to the type of eye patch used for MD: opaque vs diffuser (translucent). Those triggered dissociable mechanisms—either disinhibition of the deprived eye *or* inhibition of the non-deprived eye—that ultimately lead to similar OD shifts. These results suggest that MR GABA signals can unveil the plasticity of specific microcircuits.

The 3rd study, focussing on functional MR imaging (fMRI), builds on evidence for cell-type specific neurovascular coupling to suggest that an fMRI voxel showing varying temporal shapes of the hemodynamic response (HR) may indicate differently active neural subpopulations, hence different neural computations. This was tested with blood-oxygenation-level-dependent (BOLD) fMRI in V1 optimized for detecting the delay of HRs to gratings or plaid stimuli, under the assumption that the latter stimulus involves stronger inhibition between simultaneously active orientation columns. The HRs to this inhibitory stimulus showed longer delays, but no difference in V1-average amplitudes despite clearly resolved stimulus-specific spatial patterns. This confirms that the shape of the hemodynamic response, usually discarded as a vascular artifact, provides relevant insight on neural computations otherwise indistinguishable from fMRI response amplitude alone.

This thesis concludes that carefully designed human studies complement animal studies in furthering our understanding of the neurobiological basis of non-invasive brain signals. This in turn better informs the interpretation of signals related to human specific brain functions. Findings here and from similarly principled approaches have the potential to unlock the study of the human mind and its afflictions.

RESUME EN FRANÇAIS

Comprendre l'esprit humain requière une approche non invasive. Cependant, la relation entre calculs neuronaux et signaux cérébraux non invasifs est indirecte, complexe et méconnue.

Afin de surmonter ce défi, cette thèse se concentre sur les interactions entre colonnes corticales, et ce à un point d'entrée majeur de l'information dans le cortex, le cortex visuel primaire (CVP). Les calculs de bas niveau opérés par ce tissu cérébral sont facilement manipulés dans des paradigmes établis de stimulation visuelle, et sont bien étudiés chez les animaux et préservés chez de nombreux mammifères. Les interactions entre colonnes représentent néanmoins un prototype de calculs à travers le cortex. En ciblant un ensemble diversifié de méthodes non invasives sur des cas type de calcul cortical dans une zone sensorielle de bas niveau bien connue, cette thèse adopte une approche raisonnée afin de caractériser les signaux cérébraux non invasifs de façon plus informative en termes de calculs neuronaux.

La 1ère étude de cette thèse clarifie comment la modulation cérébrale non invasive (MCNI) par stimulation magnétique transcrânienne (SMT) affect les calculs neuronaux entre colonnes corticales représentant différents points du champ visuel, orientations des stimuli et œil d'origine. Dans un paradigme psychophysique de masquage visuel, un traitement « inhibiteur » par stimulation thêta par bouffés en continue (STBC) appliqué au pôle occipital a réduit tous les types de suppression visuelle d'origine corticale, tout en laissant inchangées la suppression d'origine sous-corticale et la perception en absence de suppression. Concordant avec les résultats provenant du cortex moteur, cela suggère que les effets comportementaux et thérapeutiques de la STBC sont généralisables d'un cortex à l'autres et reposent sur une réduction de l'inhibition intracorticale dans la zone ciblée. Il est aussi mis en évidence le potentiel de la SMT du CVP pour disséquer comment la MCNI agit sur les microcircuits neuronaux.

La 2ième étude investigue comment la spectroscopie par résonance magnétique (SRM), par ses mesures de concentration régionale de neurotransmetteurs, peut nous informer sur les calculs neuronaux. La SRM confond les multiples fonctions opérées et les différents compartiments subcellulaires contenue dans le large volume cérébral—~8cm^3—typiquement

échantillonné. Ce problème est atténué en ciblant les interactions interoculaires dans un protocole bien connu de plasticité visuelle, où quelques heures de privation monoculaire (PM) altère l'équilibre interoculaire en faveur de l'œil couvert par le cache-œil. Je rapporte des mesures comportementales, électrophysiologiques et de SRM reliant cette plasticité à une augmentation des concentration occipitales de GABA, en contradiction avec des résultats précédents. Un suivi comportemental a attribué les divergences au type de cache-œil utilisé: opaque ou translucide. Ceux-ci ont produit le même débalancement de l'équilibre interoculaire, néanmoins dissocié selon l'œil affecté—désinhibition de l'œil privé dans un cas et inhibition de l'œil non privé dans l'autre. Ces résultats suggèrent que le GABA mesuré est SRM peut dévoiler une plasticité spécifique à différent microcircuits.

La 3e étude, axée sur l'imagerie par résonance magnétique fonctionnelle (IRMf), se base sur nos connaissances du couplage neurovasculaire spécifique au type de neurone pour suggérer que le décours temporel de la réponse hémodynamique (RH) peut indiquer l'implication de différentes sous-population de neurones à l'intérieur du voxel mesuré. Cette hypothèse est testée en imagerie BOLD (blood oxygenation level dependent) optimisée pour détecter le délai de la RH dans V1 en réponse à des stimuli visuelles en grille présentés seuls ou superposés en réseaux, et sous l'assomption que le stimulus en réseau implique une plus grande inhibition entre colonnes cortical d'orientation. Les RH de ce stimulus inhibiteur ont montré de plus longs délais, mais aucune différence de l'amplitudes moyennes dans V1 malgré des patrons d'amplitudes différents. Cela confirme que le décours temporel de la RH, généralement rejetée comme un artefact vasculaire, nous informes sur des calculs neuronaux autrement indissociable par l'amplitude de la RH.

Cette thèse conclut que des études humaines soigneusement conçues, en complément d'études animales, peuvent approfondir notre compréhension des bases neurobiologiques des signaux cérébraux non invasifs. À son tour, cette information permet de mieux interpréter les signaux émanant de fonctions cérébrales spécifiquement humaines. Ces découvertes, ainsi que d'autres guidées guide par des approches similaires, ont le potentiel de déverrouiller notre compréhension de l'esprit humain et de ses afflictions.

ACKNOWLEDGMENTS

I would like to first thank all the MVR unit for the warm welcome and the enlightening journal club from which I could absorb psychophysics.

Thanks all my great lab mates, past and present, for their technical, moral and existential support, not to mention the memorable parties.

Merci à mes colocs d'amour d'avoir fait de ce Manoir en ruine un vrai foyer où l'on a hâte de rentrer s'y réchauffer, et pour avoir fait de ces vacances et fin de semaine en chalet des aventures inoubliables.

I am thankful to the Mont-Royal for having hosted a refreshing and inspiring daily commute.

Merci à tous mes chers amis, ceux avec qui régulièrement ou ponctuellement j'ai pu échanger tant de niaiseries, ceux qui ont élevé ma vie avant dans sortir trop vite et que je sais seront toujours, reviendront toujours ou m'attendront toujours.

Big thanks to my codoers at AltPAP for turning this sanitary crisis into a wake-up call that brought back meaning to my life.

Merci particulier à ma famille qui malgré ne rien saisir à mon travail mon *toujours* supporté, peu importe à quel point je pouvais inutilement amplifier mes problèmes de privilégié.

Finally, special thanks to my supervisor Reza, for the indefectible support throughout these roller coaster projects and for teaching me that nothing is impossible.

CONTRIBUTION TO ORIGINAL KNOWLEDGE

Pointing an array of non-invasive investigational tools on the EVC of healthy humans, this thesis contributes original knowledge on the indirect relation from computationally relevant neural activity to non-invasive measurements and manipulations.

Chapter 2 introduces a general vision-science-based approach complementary to currently motor-cortex-centered approaches for dissecting the intracortical circuits modulated by popular transcranial magnetic stimulation (TMS) brain treatments. The approach itself is an original contribution—e.g. the perceptual effect of single TMS pulses is for the first time visualized projected onto the retinotopic cortex (Figure 2.3). Results contribute to knowledge by showing the generalizability of a standard cTBS brain treatment from motor to visual cortices (Figure 2.5), using an original selection of visual psychophysics for probing intracortical inhibitory circuits analogous to those typically measured in motor cortex studies (Figure 2.1).

Chapter 3 dissociated for the first time two similar MD plasticity protocols—opaque and diffuser eye patching both known to shift sensory eye dominance (SED) toward the deprived eye—on the basis of eye-specific perceptual measures (Figure 3.1H-J). These findings contribute to our understanding of microcircuit mechanisms of adult visual plasticity. Chapter 3 also originally dissociated the two MD treatments by comparing two other datasets—an originally reported in Chapter 3 and reported earlier by others—on MD-induced changes in occipital GABA concentrations (Figure 3.1G). Interpreted in more depth in Section 5.2.2 through the lens of *in silico* experiments (Figure 5.5) reported in full length in Annex B, Chapter 3's findings further contribute to our understandings of the origin of MR spectroscopy neurotransmitter signals and of the role of GABA in bistable neural dynamics.

Chapter 4 contributes to the quest for more computationally relevant interpretations of fMRI signals. It does so by linking the BOLD response delay to the excitation-to-inhibition balance of the underlying neural activation (Figure 4.5) in an original experiment using visual stimuli inducing visual suppression (Figure 4.1).

CONTRIBUTION OF AUTHORS

	Chapter 2				Chapter 3		Chapter 4	
CRediT (https://credit.niso.org/)	**Sébastien Proulx**	Abigail McLellan	Henry Yu	Reza Farivar	**Sébastien Proulx**	Reza Farivar	**Sébastien Proulx**	Reza Farivar
Conceptualization	X			X	X	X	X	X
Data curation	X	X	X		X		X	
Formal Analysis	X	X	X		X		X	
Funding acquisition				X		X		X
Investigation	X	X	X		X		X	
Methodology	X			X	X	X	X	X
Project administration	X			X	X	X	X	X
Resources				X		X		X
Software	X	X	X		X		X	
Supervision				X		X		X
Validation	X				X		X	
Visualization	X				X		X	
Writing – original draft	X				X		X	
Writing – review & editing	X			X	X	X	X	X

ABBREVIATIONS

%MSO	percent of maximum stimulator output
^{1}H-MR	proton magnetic resonance
AAM	arachidonic acid metabolites
ANOVA	analysis of variance
ASL	arterial spin labeling
AUC	area under the curve
BC	binocular combination
BF	bayesian factor
BOLD	blood-oxygen-level-dependent
BR	binocular rivalry
CBF	cerebral blood flow
CBV	cerebral blood volume
CBV_a	arterial cerebral blood volume
CBV_t	total cerebral blood volume
CBV_v	venous cerebral blood volume
cpd	cycles per degree
CRLB	cramer rao lower bound
cTBS	continuous theta burst stimulation
DE	deprived eye
depIndex	deprivation index
DLPFC	dorsolateral prefrontal cortex
dva	degree of visual angle
E-field	electric field
EI	excitation-inhibition
EPI	echo planar imaging
EVC	early visual cortex
fMRI	functional magnetic resonance imaging
fMRS	function magnetic resonance spectroscopy
GABA	γ-aminobutyric acid
GAD	glutamic acid decarboxylase
H_0	null hypothesis
H_1	alternate hypothesis
H_r	replication hypothesis
HR	hemodynamic response
I1 to I4	I-waves
iTBS	intermittent theta burst stimulation
LF-rTMS	low-frequency repetitive transcranial magnetic stimulation
LGN	lateral geniculate nucleus
LTD	long term depression
LTP	long term potentiation
LTPi	long term potentiation of inhibition
MD	monocular deprivation

MEG	magnetoencephalography
MEP	motor evoked potential
MM	macromolecule
mMRS	modulation magnetic resonance spectroscopy
MR	magnetic resonance
MRI	magnetic resonance imaging
MRS	magnetic resonance spectroscopy
NDE	non-deprived eye
negBOLD	negative blood-oxygen-level-dependent
NGF	neurogliaform
NIBM	non-invasive brain modulation
NIBS	non-invasive brain stimulation
nNOS	neuronal nitric oxide synthase
NO	nitric oxide
NPY	neuropeptide Y
OD	ocular dominance
OIS	optical intrinsic signal
OLS	ordinary least square
OVS	outer volume suppression
PAP	perisynaptic astrocytic processes
PC	pyramidal cell
posBOLD	positive blood-oxygen-level-dependent
PV	parvalbumin
RF	receptive field
RGC	retinal ganglionic cell
rmANCOVA	repeated-measures analysis of covariance
rmANOVA	repeated-measures analysis of variance
rmMANOVA	repeated-measures multivariate analysis of variance
rTMS	repetitive transcranial magnetic stimulation
sd	standard deviation
SDT	signal detection theory
SED	sensory eye dominance
SICI	short interval intracortical inhibition
SMC	smooth muscle cell
sMRS	static magnetic resonance spectroscopy
SOM	somatostatin
SVM	support vector machine
TCA	tricarboxylic acid
tCho	total choline
$tCrCH_3$	total of creatine (3^{rd} carbon)
tDCS	transcranial direct current stimulation
TE	echo time
TMS	transcranial magnetic stimulation
TR	repetition time

VASO	vascular occupancy
VEP	visual evoked potential
VIP	vasointestinal peptide
VSD	voltage sensitive dye

Chapter 1: General Introduction and Literature Review

The brain is best understood as an organ specialized for computations, which are fundamentally carried through the dynamics of ion flow across the neural membrane. The membrane potential roughly linearly integrates spatiotemporal synaptic inputs and, when depolarization crosses threshold, fires output through non-linear membrane dynamics—neurons compute through an *integrate-and-fire* process. The outputs of neurons serve as inputs to other neurons, forming neural circuits capable of simple computations that for example allow simple organisms to sense and react to environmental changes. Simpler circuits further assemble into larger more complex circuits supporting more complex computations. At the extreme, ~90 billion neurons are assembled in complex multiscale networks in the human brain, supporting exquisitely refined and potentially unique brain functions like synthetical-grammatical language, symbolic thought, art and pondering on the meaning of life (Mantini et al., 2013; Molnar & Pollen, 2014; Sousa et al., 2017). Yet, these fantastic abilities that make us human all fundamentally boil down to computations carried by neurons.

The gold standard for studying neural computations is electrophysiology, where neuron's electrical activity can be directly observed and manipulated, ideally in neural circuits that can be dissected at will. The human mind is however housed in a sacred box where no electrophysiology needle can penetrate just for the sake of understanding it. How to study it then? Post-mortem anatomical and histological studies have been instrumental in inferring human brain functions and identifying suitable *in vivo* animal models, but even primate brains fall short of recapitulating many features of the human mind (Monteggia et al., 2018). Human brain science must inevitably rely on non-invasive investigation tools.

All available non-invasive tools can only access poorly resolved and poorly identified populations of neurons—they are dwarfed by the specificity one can achieve by opening the cranial box of an animal and/or manipulating its genes. Worse, the measured signals are often only remotely related to the relevant electrical neural activity. There are rare cases where an epileptic brain is implanted with electrodes for presurgical investigation and where the patient generously allows neuroscientists to directly observe the electrical activity of a few tens of their

neurons; but even that is of limited value when considering that cognitive functions emerge from network dynamics involving hundreds of thousands of neurons. Modern functional brain imaging methods offer a bird's-eye view of these network dynamics, but at the cost of losing sight of the fundamental computing units supporting them.

Utterly understanding the unique features of the human brain will crucially require understanding non-invasively measured brain signals in terms of fundamental neural computations. It is not sufficient to infer that neurons in a 1-mm patch of cortex are *active*. We need to observe the *computation* this activation carries: the transformation of information as it flows from neuron to neuron (Annex A). To observe computations in non-invasive brain signals, one however first needs to understand how the physiological substrate of computations gives rise to those signals. This constitute a real challenge when dealing with human-specific brain processes—invasive access is denied and they can hardly be recapitulated in animal models. The challenge however must be tackled for cracking the human mind and its affliction.

1.1 A Roadmap for the Optimal Use of Non-Invasive Brain Signals

How can one develop a clear understanding of the human brain when the tools at hand provide an incomplete, blurred and distorted view? As described above, the challenge lies in linking the measured brain signals to relevant neural computations. I propose the latter will be best achieved by studying multiple non-invasive signals related to a single or limited set of evolutionary-preserved neural processes, while striving to frame these processes as generalizable computations associated with signature signal patterns. In this thesis that aims to unlock the potential of commonly used non-invasive investigational tools, the approach developed and applied is two pronged.

The first prong consists in targeting simple, well-studied and narrowly defined neural processes that are easily accessible to both non-invasive investigation in humans and invasive approaches in animal models. I opted for low-level visual processes for their ease of manipulation and quantification using consumer grade computers and monitors, thanks to clever stimulus and task designs born out of a century of visual psychophysics and electrophysiology. For generalizability to higher-level human functions, I further focus on the

early visual cortex: the first bit of neural tissue processing visual information through neurons that follow the cortical cytoarchitectonic. Finally, I specifically targeted lateral interactions between cortical columns as canonical computations—or as a canonical substrate for computations—that is potentially reused across the cortex. The essence here was to choose a relatively high-level model brain process that is low-level enough to exhibit clear cross-species similarity, allowing to leverage the animal literature (Priebe, 2016).

The second prong of this thesis' strategy consists in observing and manipulating the selected neural process from various angles. Each tool provides only a partial view of the investigated neural activity, each with its own often poorly specified distortions. For example, magnetic field perturbations around active neurons largely cancel out, biasing magnetoencephalography (MEG) toward picking only spatiotemporally coherent activity close to the scalp. Hemodynamic brain imaging signals do not suffer this bias, but the neural circuits within typical 1-8mm^3 imaging voxels may assume very different computational roles while driving hemodynamic responses of similar amplitude. Only by peeking at a neural process at different angles can someone gain a complete view of its nature.

In this thesis, I pointed multiple non-invasive tools at a class of neural processes well characterized from animal studies. The rest of this chapter outlines the background knowledge necessary for factoring out physiological epiphenomena from non-invasively measured brain signals and better observe computations. This includes (1) a simplified view of the main microcircuits for local cortical computations, (2) a framework for operationalizing these computations and (3) the neurophysiological basis of the brain signals recorded. The overarching goal of the thesis is to contribute to the identification of computationally relevant signature signals that can be of practical value for the study of human brain functions, healthy and diseased.

1.2 Neural Microcircuits and Computations in the Early Visual Cortex

The first cortical stage of the hierarchical processing of visual information, the early visual cortex, receives information mostly about local contrast in the retinal image. The computations it operates are mostly concerned with the physical aspects of stimuli and constitute important

preprocessing steps for the later-stage processes that are increasingly concerned with abstract aspects of perception (Mikellidou et al., 2016).

1.2.1 Neural Response Properties, Columns and Maps

V1 codes for various features of an image stimulus as evidenced by the response properties of single neurons (Hubel & Wiesel, 1962). The simplest code is that of spatial location, where neurons respond only to local luminance contrast within their receptive field (RF)—RFs near the fovea are generally less then 1 degree of visual angle in diameter (Smith et al., 2001). Many V1 neurons are also selective for the orientation of edges and therefore support orientation coding. In forward-facing-eye animals like humans, V1 neurons also show various degrees of ocular specificity, thereby maintaining an eye-of-origin code from which higher-level features like stereoscopic depth can be computed. With neurons tuned to spatial frequency, motion, chromaticity and others, V1 codes for a rich repertoire of low-level features. It is generally poor in or lacks neurons coding for more complex features like curvature, shapes or specific objects or faces. This conveniently reduces V1 computations to an experimentally tractable set.

Neurons with similar response properties tend to cluster into cortical columns: small domains spawning the full thickness of the cortex (Mountcastle, 1957) with widths in the order of 1mm in humans (Yacoub et al., 2008). They form intricated topological maps along the cortical surface (Figure 1.1) that constitute a major organization principle across visual areas (Hubel & Wiesel, 1974). These maps are first determined by patterns of feedforward thalamocortical inputs in layer IV (Figure 1.2B).

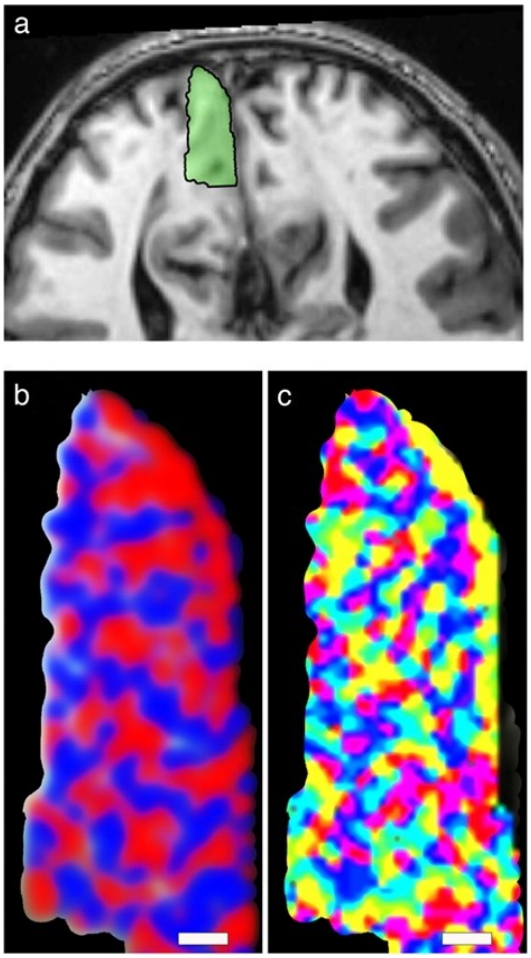

Figure 1.1 Example ocular dominance (b) and orientation preference (c) maps obtained with BOLD fMRI at 7T from an early visual cortex region-of-interest shown in green overlay in (a). Scale bar: 1mm. Reproduced with permission from Yacoub et al. (2008).

Adjacent retinal ganglionic cells (RGC) project, through the lateral geniculate nucleus (LGN) relay in the thalamus, to adjacent positions on the cortical sheet and dictate the retinotopic map. The visual field alignment of ON and OFF receptive fields from RGC and LGN neurons projecting to the same cortical neuron defines the latter's orientation preference (Lien & Scanziani, 2013) (Figure 1.3B), which vary smoothly across neighboring neurons and form the pinwheel pattern that tiles the cortical orientation map (Figure 1.1C and Figure 1.3A) (Liu et al., 2010; Reid & Alonso, 1995; Sedigh-Sarvestani et al., 2017). Finally, thalamocortical projections carrying information from one or the other eye are sharply segregated in narrow bands along the cortical sheet (Katz et al., 1989), forming V1's ocular dominance map (Figure 1.1B). Thalamocortical inputs therefore already code for visual features like visual field location and eye-of-origin when reaching the cortex. Cortical computations begin with the dendritic integration of patterned thalamocortical synapses—the orientation code is built on top of the visual-field-location code and binocular information emerges in dendrites crossing the monocular input bands. Cortical computations continue within V1 through complex microcircuitry described in the next two sections.

An important feature of intracortical connectivity is a sharp decrease in monosynaptic connection probability beyond ~½mm of lateral separation between neurons. This matches the scale of functionally defined cortical columns and supports the notion that the latter constitute distinct processing units (Roerig & Chen, 2002). Connections across columns, often referred to as lateral or horizontal connections, are however not uncommon. They often reach up to 4 to 6mm away (Figure 1.3A) and can powerfully influence another columns activity (Gilbert et al., 1996; Stettler et al., 2002). Moreover, proper calculations—accounting for the supralinearly increasing number of potential connection partners with increasing volume around a column—revealed that more than half the synapses in a 1mm-width column originate from outside that volume (Boucsein et al., 2011; Seeman et al., 2018; Stepanyants et al., 2009). Further considering the overall weak structural markers of a columnar organization (da Costa & Martin, 2010), the notion of columns largely rests on functional descriptions. *Intracolumnar* vs *intercolumnar* interactions however remain useful descriptive terms extensively used in this thesis (see section 1.2.4); but one should keep in mind that columns are probably more

accurately described as flexibly assembled rather than hardwired processing units (Gilbert et al., 1996; Kato et al., 2015), and as an epiphenomenonal rather than fundamental structure (Jang et al., 2020).

1.2.2 Intracortical Excitatory Microcircuitry and Computations

The cortical microcircuitry rests on a scaffold of pyramidal neurons, also called pyramidal cells (PC), that gates information in and out of an area. They integrate thalamocortical inputs and relay information down the visual hierarchy through long-range cortico-cortical[1] axonal projections—the *feedforward excitation* circuit motif (Figure 1.2B). Thalamocortical synapses however constitute only 15-20% of all excitatory synapses in input layer IV (Garcia-Marin et al., 2019). Excitatory circuits are dominated by collateral branches of pyramidal axons that feed excitatory outputs monosynaptically back to the same neuron and to other often reciprocally connected neurons—the *recurrent excitation* circuit motif (Figure 1.2C).

Feedforward excitation enables orientation and binocularity computations, as described in the previous section. Recurrent excitation powerfully amplifies weak feedforward signals (Douglas et al., 1995; Suarez et al., 1995), but does so in a feature selective fashion. For example some neurons preferentially send recurrences to similarly tuned neurons (Figure 1.3A and B), which importantly preserves the feature selectivities inherited or computed from patterned feedforward excitation (Lien & Scanziani, 2013). Recurrences also enable new computations. For example, those that extend laterally to neurons with a spatially displaced RF can preferentially connect neurons with colinearly aligned RFs (Iacaruso et al., 2017). This is thought to specifically amplify elongated edges and contribute to the computation of contour information (Figure 1.3C) (Niell & Scanziani, 2021).

1.2.3 Intracortical Inhibitory Microcircuitry and Computations

The above described excitatory circuits rely on glutamate, the main excitatory neurotransmitter. Second only to glutamatergic neurons, 10-20% of brain neurons instead use

[1] In this thesis, *cortico-cortical* qualifies monosynaptic connections made between neurons from different cortical areas, as opposed to *intracortical* connections that do not leave the cortical area of origin. For some authors, cortico-cortical connections also include within-area connections that extend laterally along the cortical sheet. To avoid confusion, the latter will be qualified lateral or horizontal *intracortical* connections.

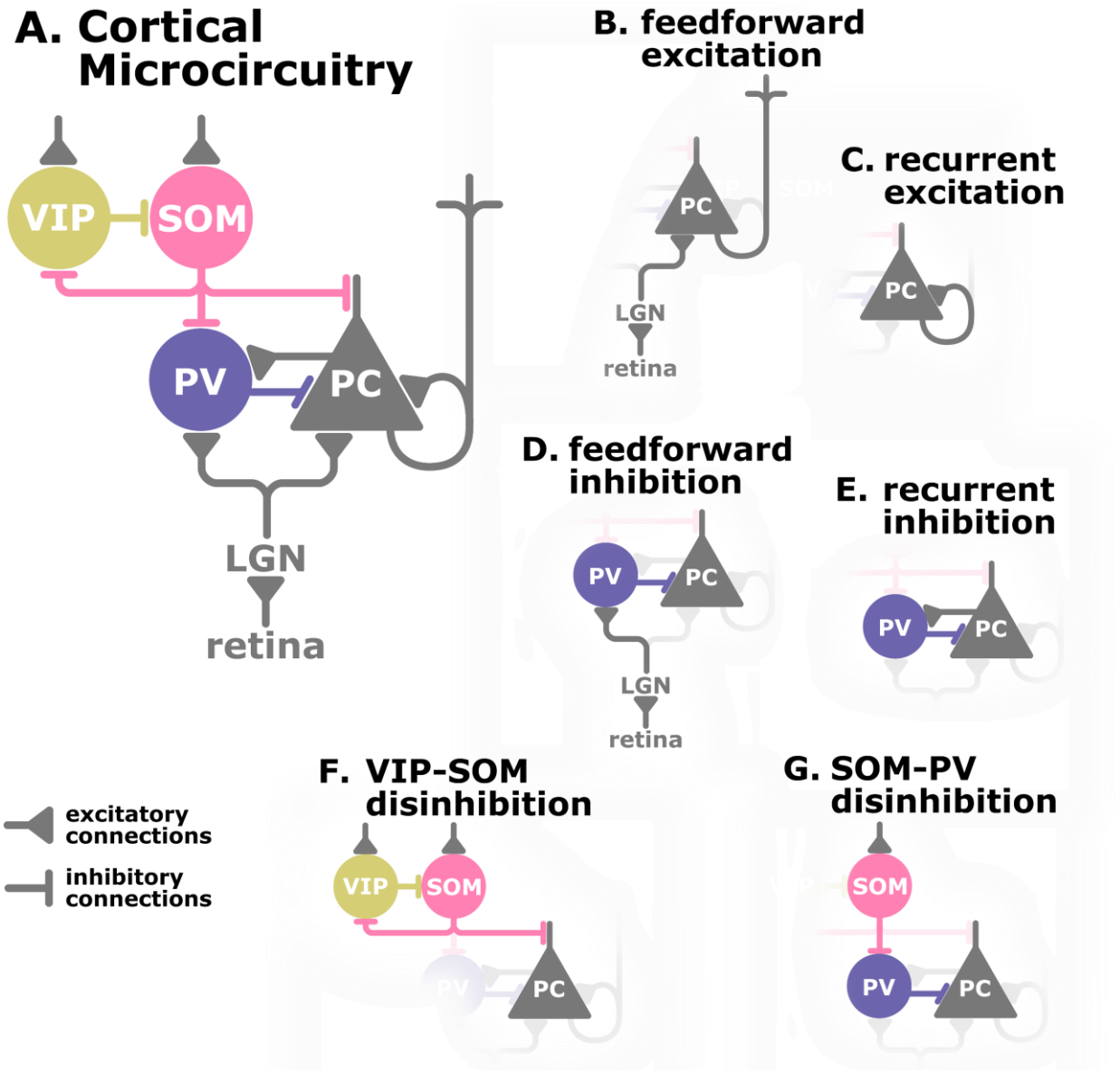

Figure 1.2 Canonical cortical microcircuits. A. Simplified view of cortical microcircuits, where inputs come from the retina through the LGN and outputs leave the cortical area through PCs axons (right upward projection). Excitatory connections on VIP and SOM neurons are left unspecified but can come from PC axon collaterals (intracortical) or from PC projections from other cortical areas (cortico-cortical). **B to G.** Common microcircuit motifs thought to carry specific computations. See main text for details. PV: parvalbumin-expressing neuron; SOM: somatostatin-expressing neuron; VIP: vasoactive intestinal peptide-expressing neuron; PC: pyramidal cell.

the main inhibitory neurotransmitter GABA. Most of the latter are interneurons—i.e. they project intracortically within the same brain area (Caputi et al., 2013). They crucially counterbalance recurrent amplification, preventing runaway excitation and maintaining optimal levels of activity through an adequate excitation-to-inhibition balance (EI). They however also directly support various cortical computations (Lee et al., 2017; Litwin-Kumar et al., 2016; Lourenco et al., 2020; Sadeh & Clopath, 2021; Tremblay et al., 2016) through a fauna of GABA

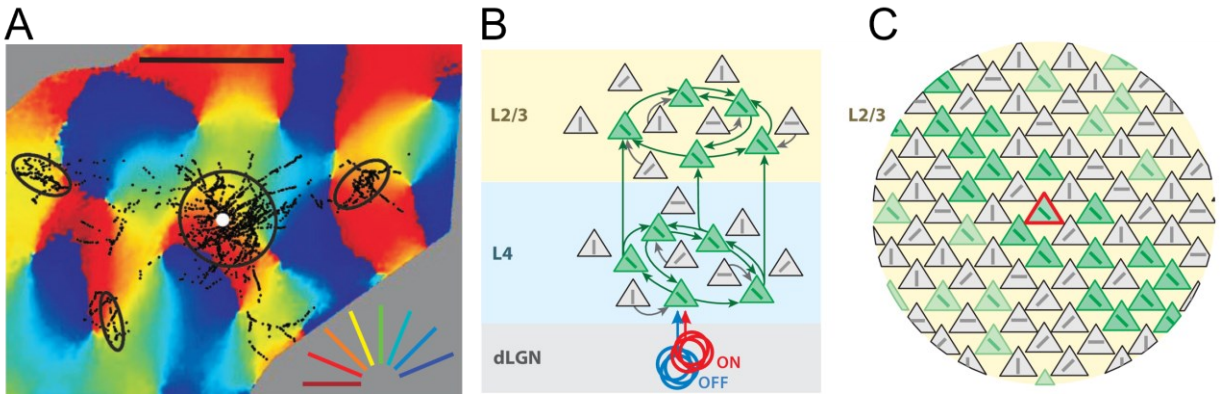

Figure 1.3 Intracortical excitatory circuits for processing orientation. **A.** Synaptic boutons (black points) from a single PC (white dot) overlaid on a standard orientation map obtained from optical intrinsic signal imaging. Black ellipses indicate bouton clusters. Note that boutons target areas of like orientations. Scale bar: 1mm. **B.** Representation of the spatial arrangement of the ON and OFF receptive fields of dLGN neurons (bottom section) that determines the orientation preference of PCs (triangles). PCs form recurrent networks preferentially connecting iso-oriented PCs (top two sections) and amplifying orientation signals. **C.** Representation of contour computation. The preferred stimuli of PCs that form strong recurrent excitatory connections (deep green triangles) tend to form a collinear arrangement, such that signals from elongated edges will be amplified. *A was adapted with permission from Martin et al. (2014). B and C were adapted with permission from Niell and Scanziani (2021).*

interneuron subtypes exhibiting an still incompletely characterized diversity of morphology, connectivity pattern and electrophysiological property (see Tremblay et al., 2016 for a comprehensive review).

The intracortical connectivity of different neuron types is overwhelmingly intricated (Bock et al., 2011)—caricaturally, everything seems connected to everything. Neuron-type-specific functions are therefore better understood through a simplified set of commonly observed connection motifs, or canonical microcircuits, thought to carry specific computations (Isaacson & Scanziani, 2011; Niell & Scanziani, 2021). Feedforward and recurrent excitation motifs were described in the previous section. Below I describe motifs involving three types of GABA neurons together comprising 80% of interneurons and defined by the expression of largely non-overlapping molecular markers, namely parvalbumin (PV), somatostatin (SOM) and vasointestinal peptide (VIP).

1.2.3.1 Feedforward and Recurrent Inhibition

PV interneurons constitute 40% of GABA interneurons and strongly influence pyramidal outputs through fast perisomatic synapses and sustained high frequency action potential bursts (Tremblay et al., 2016). Driven by thalamocortical projections, PV neurons form disynaptic

feedforward inhibition circuits (Figure 1.2D) that parallel monosynaptic feedforward excitation on PCs. PCs also drive their own inhibition through disynaptic *feedback inhibition* circuits (Figure 1.2D).

Feedforward and recurrent inhibitory motifs respectively track cortical inputs and outputs, providing a balanced inhibitory drive that allows recurrent amplification to operate without risking runaway excitation (Isaacson & Scanziani, 2011). Interestingly, feedback inhibition mediated by the mostly perisomatic PV synapses tends to somewhat indiscriminately gate PCs outputs, while the distal-dendrite-targeting SOM neurons enable a more refined gating of PCs inputs (Tremblay et al., 2016). These circuits contribute to various forms of gain control—recurrent amplification of weak signals is met with stronger inhibition when feedforward drive and intracortical activity increases, thereby reducing the gain of membrane responses and consequently expanding the dynamic range for encoding changes in stimulus intensity as spike rate variations (Pouille et al., 2009).

Beyond maintaining proper intracortical EI balance, feedforward and feedback inhibition also support important computations. For example, feedforward inhibition contributes to defining RFs for spikes—the impact of excitatory post-synaptic conductances on ON and OFF membrane potential subfields is sculpted by inhibitory post-synaptic conductances that form similar but slightly offset ON and OFF subfields (Liu et al., 2010) (Figure 1.4A). Also, inhibitory conductances on PCs are often more broadly tuned than excitatory conductances (Bock et al., 2011; Cardin et al., 2007; Monier et al., 2003) (Figure 1.4B), which contributes to sharpening

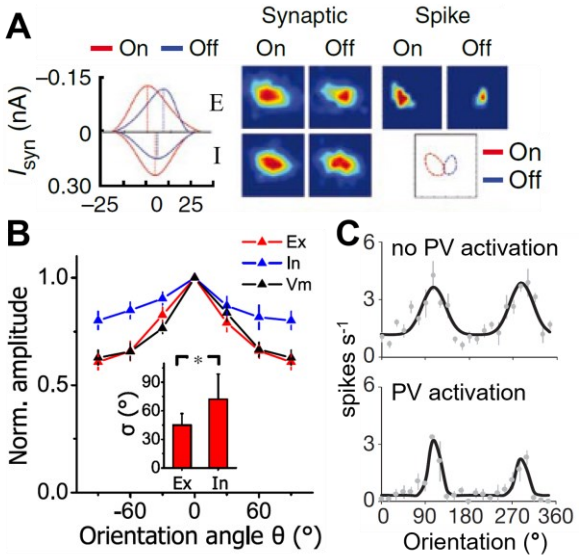

Figure 1.4 Feedforward and feedback inhibition computations. A. Left panel: example one-dimensional section of excitatory (positive) and inhibitory (negative) conductance RFs for ON (red) and OFF (blue) stimuli. Note the slight misalignment between excitatory and inhibitory RFs. Middle panel: two-dimensional version of the same RFs. Right panel: Spike RFs resulting from the combination of excitatory and inhibitory conductance RFs. **B.** Orientation tuning of excitatory (Ex) and inhibitory (In) conductances and membrane potentials (Vm). **C.** Direction tuning of spikes in an example neuron with (bottom) and without (top) concurrent optogenetic activation of PV inhibitory interneurons. *A, B and C respectively adapted with permission from Liu et al. (2010), Liu et al. (2011) and Lee et al. (2012)*

PCs' orientation selectivity (Isaacson & Scanziani, 2011; Liu et al., 2011; Lourenco et al., 2020) but see (Priebe & Ferster, 2008). The latter was nicely demonstrated through optogenetic overactivation of PV interneurons, which indeed sharpened PCs' tuning and additionally boosted orientation discrimination performances (Lee et al., 2012) (Figure 1.4C).

1.2.3.2 Disinhibition

Another microcircuit motif is disinhibition, where inhibition on PCs is lifted by inhibition targeting the PCs' inhibitors (Figure 1.2F and G). VIP inhibitory interneurons form 12% of the brain's interneurons and are considered the disinhibitor par excellence as they exclusively target other interneurons, mostly SOM (Kullander & Topolnik, 2021). In the simplest example of disinhibition, increasing inhibition through optogenetic activation of SOM or PV impaired visual contrast increment detection, while activating disinhibition from VIP facilitated it (Cone et al., 2019). Disinhibitory circuits—VIP→SOM (Figure 1.2F) and SOM→PV (Figure 1.2G) being the most studied—vary substantially in forms and functions: they mediate intracortical processes but also enable computational flexibility in intracortical circuits by integrating influences from ascending neuromodulatory and top-down cortico-cortical pathways (Cardin, 2019; Katzner et al., 2019; Lee et al., 2017).

Using optogenetics and modeling, Keller et al. (2020) provided a great lower-vision example of a VIP→SOM computation: orientation-specific surround modulation. When a circular grating was surrounded with an iso-oriented annulus grating, the response of L2/3 PCs to the center stimulus was suppressed by surround-driven inhibition from SOM interneurons (Figure 1.5A). VIP neurons however became more active when the surround was cross-oriented, thereby inhibiting SOM and consequently releasing inhibition on PCs (Figure 1.5B). Interestingly, such similar contextual modulation effects were related to other higher-level computations involving top-down cortico-cortical connections on V1 VIP disinhibitory circuits, including figure-ground segregation (Kirchberger et al., 2021), familiarity with

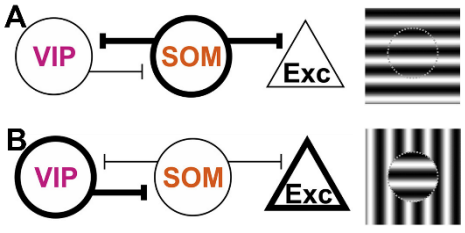

Figure 1.5 Disinhibitory circuit for orientation-specific surround modulation. **A.** Activity pattern when the PC (Exc) RF (dotted circle) is surrounded with a iso-oriented stimulus. **B.** Same as A but for a cross-oriented surround. *Modified with permission from Keller et al. (2020)*

stimuli (Garrett et al., 2020) and behavioral states (Millman et al., 2020).

1.2.4 Local and Lateral Recurrent Connectivity

Strictly speaking, a monosynaptic excitatory or disynaptic inhibitory connections is recurrent if it comes back to the same neuron. Connection motifs not strictly conforming to this definition can however functionally behave as recurrent given the dense interconnectedness of close neighbor neurons. Furthermore, the computational functions of recurrent connectivity are better described along a gradient that echoes the graded nature of the columnar organization (Section 1.2.1): from locally restricted to more laterally extending, and from *local* intracolumnar gain modulation among neurons with similarly selectivities to patterned *lateral* intercolumnar interactions among neurons with partially or non-overlapping feature selectivities.

1.2.5 Other Cortical Pathways

The above motifs by no means exhaustively account for the full complexity of cortical microcircuits. Significant heterogeneity in connectivity, function and other molecular markers within each class warrants further subdivisions that often overlap (Tremblay et al., 2016). Of note are GABA interneurons producing nitric oxide (NO) through the neuronal NO synthase (nNOS) and those expressing neuropeptide Y (NPY), two substances with neuromodulatory and vasomotor effects (Tricoire & Vitalis, 2012) (Section 5.3.1). The non-classical synapses of neurogliaform (NGF) cells defy the very notion of a neural circuit as, in a paracrine or volume transmission mode, the released GABA needs to diffuse through the extracellular space around the synapse to reach extrasynaptic receptors (Overstreet-Wadiche & McBain, 2015) (Section 5.2.1). Neuromodulatory pathways, cortico-thalamic loops and cortico-cortical connections are not considered further—or evoked *ad hoc*—in this thesis focusing on intracortical processes.

1.3 Operationalizing Intracortical Interactions in the Visual Cortex

How to drive and isolate intracortical computations in the human brain? This can be achieved by leveraging the intricated topographic functional maps of the EVC to drive activity in specific cortical patches using nothing more than carefully designed visual stimuli presented on a consumer grade monitor. Simultaneously driven, two intracortically connected patches can

interfere with one another's feedforward processing, measurably affecting sensitivities to the driving stimuli. Also, complex internally driven neural dynamics can emerge between the same two patches subjected to a sustained—time-invariant—feedforward drive. From this can emerge unstable perceptual dynamics with measurable characteristics that are tributary of the intracortical processes involved. It is through these two classes of phenomenon—namely visual contrast masking (Figure 1.6A) and bistable perception (Figure 1.6C and D)—that this thesis operationalizes intracortical interactions, as described below.

1.3.1 Driving Facilitatory and Suppressive Intracortical Interactions Between Patches of Cortex

Neighboring patches of V1 can be driven with luminance contrast stimuli—e.g. gratings—presented to neighboring patches of the visual field (Figure 1.6A, middle panel). In this case, the size and shape of the stimuli will define the size and shape of the activated retinotopic patches of cortex. Alternatively, stimuli can be overlaid in visual field space, but occupy orthogonal narrow bands in stimulus orientation space—two gratings overlayed at right angle (Figure 1.6A, right panel). Here, following V1's orientation representation map, one stimulus will activate an array of loosely but regularly tilled column-size patches, while the other stimulus will activate a similar array of patches intertwined with the first array (Figure 1.6B). A similar tilling of cortical patch activation can be obtained, following V1's ocular dominance map, by stimulation of one and the other eye.

In visual masking paradigms, comparing neural or perceptual responses evoked by two stimuli presented alone or simultaneously allows to isolate intracortical interactions between the corresponding cortical patches or sets of patches. A century of electrophysiology and visual psychophysics has delineated such interactions in the classic test-and-mask stimulus configurations used in this thesis: (1) center-surround (Cavanaugh et al., 2002; Petrov et al.,

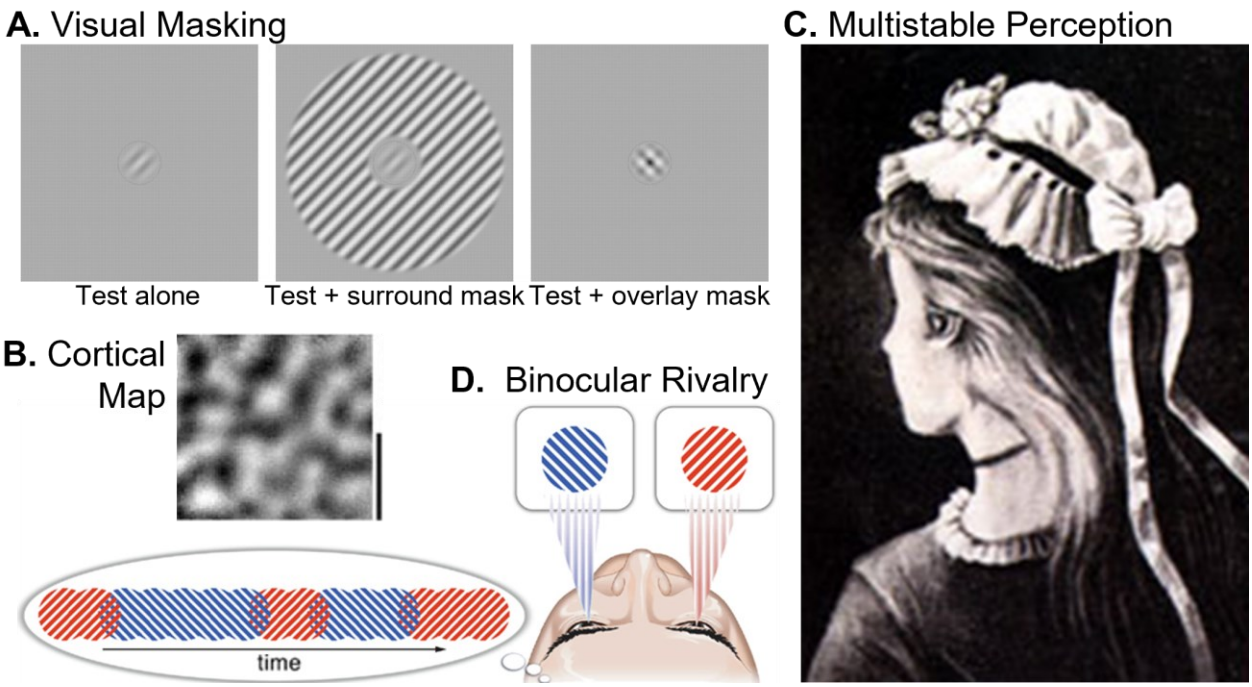

Figure 1.6 Visual stimuli and paradigms for operationalizing intracortical interactions. A. In visual masking paradigms, iso-oriented surround (middle panel) or cross-oriented overlay (right panel) mask stimuli measurably affect the detection of the test stimulus (left panel). **B.** Illustration of the intertwined pattern of cortical patches activated by one (white) or the other (black) of two orthogonal orientations (for example those of the test and overlay mask stimuli in A), obtained through intrinsic signal imaging. **C.** In this example of bistable perception, two characters can be perceived in this image but not at the same time. Hint 1: the top bright object is a hat in the two perceptual alternatives. Hint 2: the middle left bright object is the face profile of an older women in one alternative, but her left eye becomes the left ear of a younger women in the other perceptual alternative. **D.** In this binocular rivalry version of bistable perception, two incompatible images are presented one to each eye, leading to alternating perceptual states of measurable durations. Scale bar: 1mm. *Adapted with permission from (A) Petrov et al. (2005), (B) Huang et al. (2014), (C) anonymous German postcard from 1888 (https://en.wikipedia.org/wiki/My_Wife_and_My_Mother-in-Law) and (D) Dieter and Tadin (2011).*

2005) where a center *test* grating is presented with or without a surrounding annular *mask* grating (Figure 1.6A, middle panel), (2) cross-orientation (Li et al., 2005; Meese & Baker, 2009) where orthogonal orientations are spatially overlayed (Figure 1.6A, right panel) and (3) dichoptic (Petrov & Mckee, 2009; Sengpiel & Vorobyov, 2005) where different stimuli are presented to each eye (Figure 1.6D, right half of image; more details in section 2.3.3). Such paradigms invariably involve both excitatory and inhibitory intracortical interactions, and it is their balance that determines whether spiking responses or detection performances are facilitated or suppressed. The similarity—in orientation, spatial frequency, phase—and the spatial configuration of test and mask stimuli affect this balance in various ways, but the most consistent factor is contrast: high contrasts and high mask-to-test contrast ratios favor

suppressive effects (Meese et al., 2007; Nurminen et al., 2010; Ozeki et al., 2004). This thesis focusses on such visual stimulation regimes favoring inhibitory interactions (Chapter 2 and 4).

1.3.2 Driving Intrinsic Intracortical Neural Dynamics

A hallmark of high level cortical processes is their reliance on largely internally generated flexible neural dynamics. A striking example is a class of phenomena referred to as multistable perception, where an unchanging regime of sensorial stimulation evokes alternating perceptual states, or percepts—e.g. in Figure 1.6C's famous illusion, either a young or an old character is perceived, not both at the same time. There are countless instances of such perceptual multistability arising at various level of the visual hierarchy (Kovacs et al., 1996; Logothetis et al., 1996; Wilson, 2003), but a well-studied low-level example is binocular rivalry, where the competing percepts correspond to different simultaneously presented images, one to each eye (Figure 1.6D). Simple and easily parameterizable, binocular rivalry paradigms evoke a rich perceptual experience that can be quantified through continuous button press reports of the current percept (Brascamp et al., 2018).

A rich literature has linked the duration of alternating percepts and other features of binocular rivalry to various physiological and perceptual phenomena, including sensory eye dominance—during a tens-of-second-long binocular rivalry run, the retinal image of the dominant eye is perceived for longer periods of time. Importantly, the low-level intracortical dynamics involved—e.g. the interocular inhibition that maintains dominance (Mentch et al., 2019; Noest et al., 2007; van Loon et al., 2013) or the collinear excitation that supports the stereotypical spread of dominance during transitions (Wilson et al., 2001; Yang et al., 2015)—constitute an interesting and experimentally tractable low-level model for similar dynamics that are possibly at play throughout the cortex. Chapter 3 therefore operationalizes intracortical interactions using binocular rivalry. Findings are interpreted in more depth in section 5.2.2, in the light of model simulations of the underlying neural dynamics themselves reported fully in Annex A.

1.4 Non-Invasive Brain Signals

The direct and properly resolved observation of the fundamental neural membrane electrochemical dynamics supporting computations typically requires non-trivial surgical procedures and/or genetic manipulations, e.g. to place the tip of a microelectrode within micrometers of neurons in a live brain or a resected piece of it. Such observations are seldom possible in humans and limited to edge cases: consenting patients implanted with electrodes for pre-surgical evaluation of epilepsy (Jobst et al., 2020; Peyrache & Destexhe, 2019) or movement disorder treatment (Krauss et al., 2021), life threatening brain lesions resected with a safety margin that includes enough healthy tissue for *ex vivo* electrophysiology recordings (Park et al., 2022), and brain organoids cultured from human pluripotent cells (Koo et al., 2019). On the other hand, animal models can hardly achieve even face validity when it comes to many high-level cognitive abilities and related pathologies.

Non-invasive approaches are therefore essential, but the limited understanding on how non-invasive brain signals relate to neural computations is probably the most important barrier for understanding the human mind. Below I introduce current knowledge on this issue in relation to the main non-invasive tools used in this thesis and state the objectives of each chapter.

1.4.1 Psychophysics and Brain Modulation

1.4.1.1 Quantifying Perception with Psychophysics

The information conveyed by our senses about the physical environment is bound to be incomplete and ambiguous. For example, the 3D structure that constitutes a chair, once projected on the retina, should appear like a pile of pieces of wood. Yet, the observer undeniably experiences the perception of a chair. Conversely, the same regime of sensorial stimulation can lead to different percepts (see bistable and binocular rivalry in section 1.3.2). Perception is phenomenologically irreducible: it is not tightly determined by the physical aspects of stimuli—a 2D image in the first example above—but rather emerges from the activation of internal neural representations of the physical environment (Feinberg, 2012). Interestingly, one can learn a lot on the mechanisms of perception just from studying this relation between physical stimuli and subjectively reported perception. Humans effortlessly

perceive objects even when drawn summarily as cartoons, or when a natural image is filtered to only show luminance boundaries (Figure 1.7). From this simple observation, one can conclude that edge detection is a potent mechanism for activating internal representations and triggering perception (Marr & Hildreth, 1980).

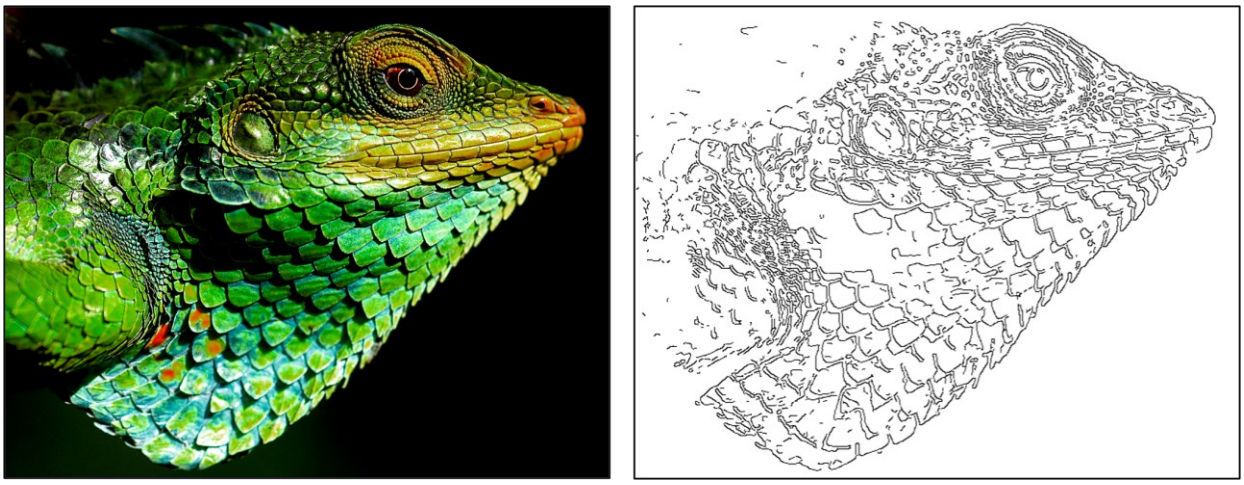

Figure 1.7 The importance of luminance edges for perception. The lizard is effortlessly perceived whether from a natural image (left) or from the same image filtered with Canny edge detector (Wikipedia) to show only luminance edges (right). Edges are sufficient to trigger perception, arguing for the importance of edge detection mechanisms in visual perception. *Images by Babujayan, distributed under a CC-BY-3.0.*

Psychophysics is the century-old science discipline that capitalizes on the careful quantification of such stimulus-to-perception relationships (Fechner, 1860). The strength of the discipline is to address computational principles directly, without explicitly addressing their neural substrate. A cardinal example of such principle involves the various parallel pathways, called *visual channels*, through which the visual system processes a retinal image (Braddick et al., 1978). A channel is a useful abstraction of computations carried by a population of neurons dedicated to a given image feature—it could be a column or an array of cortical patches (Figure 1.6B) activated by the specific orientation, spatial frequency and eye-of-origin of a grating (Figure 1.6A, left panel). A psychophysical experiment would typically quantify the channel's sensitivity by finding the minimum stimulus energy allowing above-chance detection of the grating. By comparing a channel's sensitivity across carefully chosen task or stimulus conditions, psychophysicists can gain insights on the computational architecture of vision or pinpoint the specific computation impaired in a given pathology.

In a series of standard overlay masking experiments like that depicted in Figure 1.6A, Baker et al. (2007) provided a great example of the psychophysical approach. When the test and mask stimuli were presented to opposite eyes and therefore processed through different ocular channels, suppression was weaker when both stimuli solicited different spatial frequency channels. However, when processed through the same ocular channel, suppression remains strong irrespective of the relative spatial frequency of the test and mask stimuli. Interpreted as potential intra and intercolumnar interactions, these within- and cross-channel interactions suggest the existence of a broadband—i.e. spatial-frequency insensitive—suppression mechanism that operates before ocular channel convergence in V1. Consistent with findings from other clever stimulus manipulations in the same study and backed by other theoretical, electrophysiological and brain modulation works (Freeman et al., 2002; Katzner et al., 2011; Li et al., 2005; Priebe & Ferster, 2006; Spiegel et al., 2012), this conclusion on the neural site of specific computations will be important for Chapter 2, but here it nicely illustrates the power of carefully studying perception alone.

With little to no specialized hardware or proprietary software required, psychophysical experiments on human can alone deliver important insights into the structure of visual computations. Importantly, models derived from psychophysics finding can guide the search of the neural substrate of specific computations, e.g. with modern non-invasive brain modulation methods as used in Chapter 2 and introduced below.

1.4.1.2 Modulating Brain Processing with Non-Invasive Brain Stimulation

The past three decades have seen the rise of various techniques for directly manipulating neural activity safely and non-invasively through the skull, with the two most important being transcranial direct current stimulation (tDCS) and transcranial magnetic stimulation (TMS) (Bergmann & Hartwigsen, 2021). In tDCS, scalp electrodes slowly inject safe amounts of current (≤1mA) into the brain, imposing a constant shift in resting membrane potential that affects spontaneous spiking rates (Stagg & Nitsche, 2011). TMS instead directly triggers action potentials through a brief but much stronger—2 to 3 orders of magnitude—and more spatially restricted electrical field, which is induced in brain tissues under the stimulation coil with a <1ms magnetic field pulse (Dayan et al., 2013; Polania et al., 2018).

Both non-invasive brain stimulation (NIBS) methods produce *online* effects: they trigger or alter neural activity and behavior while current flows between the tDCS electrodes or for tens to hundreds of milliseconds after the TMS pulse. With their decent spatial resolutions (Figure 1.8)—down to 1cm of less for TMS (Romero et al., 2019)—they proved instrumental for providing causal evidence in human mapping, connectivity and chronometry (Pascual-Leone et al., 2000). Spiegel et al. (2012) provides a great example, where they psychophysically measured overlay and surround monocular visual masking (see section 1.4.1.1) during tDCS over the EVC. They showed that anodal but not cathodal tDCS reduced surround suppression, a cortical phenomenon (Angelucci et al., 2017), whereas neither treatment affected overlay suppression. This polarity-specific *knock-out* of one suppression type but not the other provided causal evidence that, as suggested by Baker et al. (2007)'s psychophysical findings (section 1.4.1.1), monocular overlay suppression is mediated upstream of the EVC—a characteristic that will be leveraged in Chapter 2.

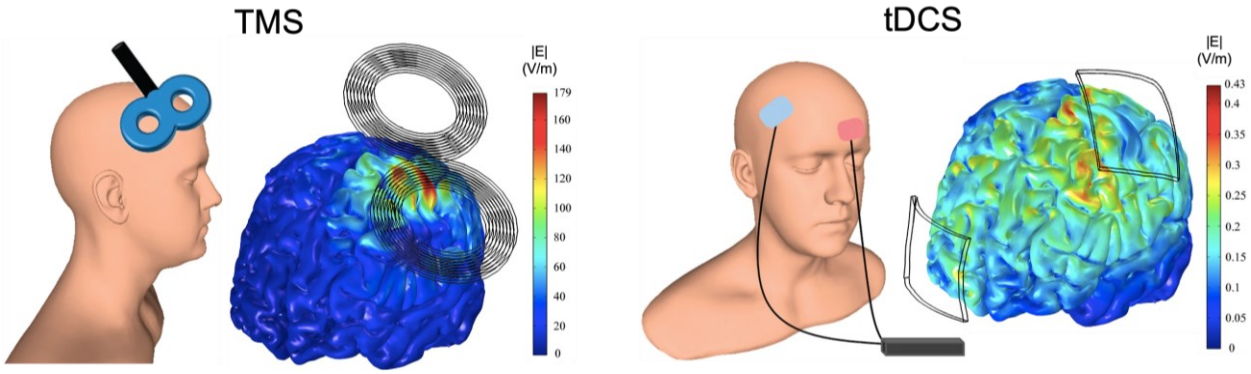

Figure 1.8 Typical TMS and tDCS set-ups for non-invasive brain modulation. Left sub-panels: coil or electrodes set-ups shown on skin models of the head. Right sub-panels: coil or electrode set-ups (black traces; not the same configuration as in left sub-panels) relative to the induced electric field modeled on the brain surface. An electric field of 100V/m is required to trigger action potential of cortico-spinal neurons. TMS typically shows better spatial specificity than tDCS. TMS: Transcranial Magnetic Stimulation; tDCS: transcranial Direct Current Stimulation. |E|: absolute induced electric field amplitude. Adapted with permission from Dayan et al. (2013) and Salvador et al. (2015).

Effects of NIBS are also observed *offline*, i.e. after the end of minutes to tens of minutes of treatment with tDCS or repetitive TMS (rTMS), the latter consisting in the repetitive application of single pulses in a given temporal pattern. NIBS experimental protocols seeking such offline modulatory effects—which I will refer to as non-invasive brain modulation (NIBM)—bear increasingly demonstrated potential as non-invasive brain therapies. From 2011 to 2020 inclusively, a steady average of ~700 human brain TMS papers per year were indexed on

PubMed®[2], with ~15% of those being clinical trials—a similar albeit less important trend is observed for tDCS papers[3]. This literature now provides level-A evidence (definite efficacy) supporting therapies for neuropathic pain, depression and stroke motor impairments (Lefaucheur et al., 2020).

Yet, even in healthy brains, mechanistic understandings of NIBM remain rudimentary and heavily based on motor cortex studies (Di Lazzaro et al., 2010), where effects are readily measurable from corticospinal muscle activations. More microcircuit-level and computationally-oriented investigations is required for guiding the principled, efficient and safe exploration of the immense parameter space of potential NIBM therapies (Pell et al., 2011). Although underutilized, the early visual system is well-suited for the task, as showcased in Chapter 2 focussing on TMS-based NIBM. In the sections below, I will outline the biophysical and neurophysiological underpinnings of NIBS and NIBM with TMS and highlight current knowledge on how specific intracortical circuits are affected.

1.4.1.2.1 Brain Stimulation with Single Pulses of TMS

A single TMS pulse induces a strong and focal electric field (E-field) that briefly depolarizes axons, directly triggering action potential within 1ms after the pulse (Mueller et al., 2014; Pashut et al., 2014). Over the next 6ms, these action potentials monosynaptically trigger volleys of secondary action potentials in connected excitatory and inhibitory neurons (Figure 1.9A) (Li et al., 2017; Mueller et al., 2014; Rusu et al., 2014). This initial surge of highly synchronized exogenously triggered activity is well characterized from epidural recordings of the successive volleys of corticospinal activity it generates (Figure 1.11) (Di Lazzaro et al., 2010; Rusu et al., 2014). Over the next hundreds of milliseconds (Figure 1.9B), the TMS-triggered neural activity appears to maintain itself and spread polysynaptically (Kozyrev et al., 2014; Li et al., 2017; Moliadze et al., 2003; Romero et al., 2019), producing successive phases of increased then suppressed firing rates followed by a rebound increase (Figure 1.9B). Different patterns are however observed in different neurons, with firing rate alterations sometimes detectable for up

[2] Search query: “Transcranial Magnetic Stimulation”[Mesh] AND “Humans”[Mesh] AND “Brain”[Mesh]
[3] Search query: “Transcranial Direct Current Stimulation”[Mesh] AND “Humans”[Mesh] AND “Brain”[Mesh]

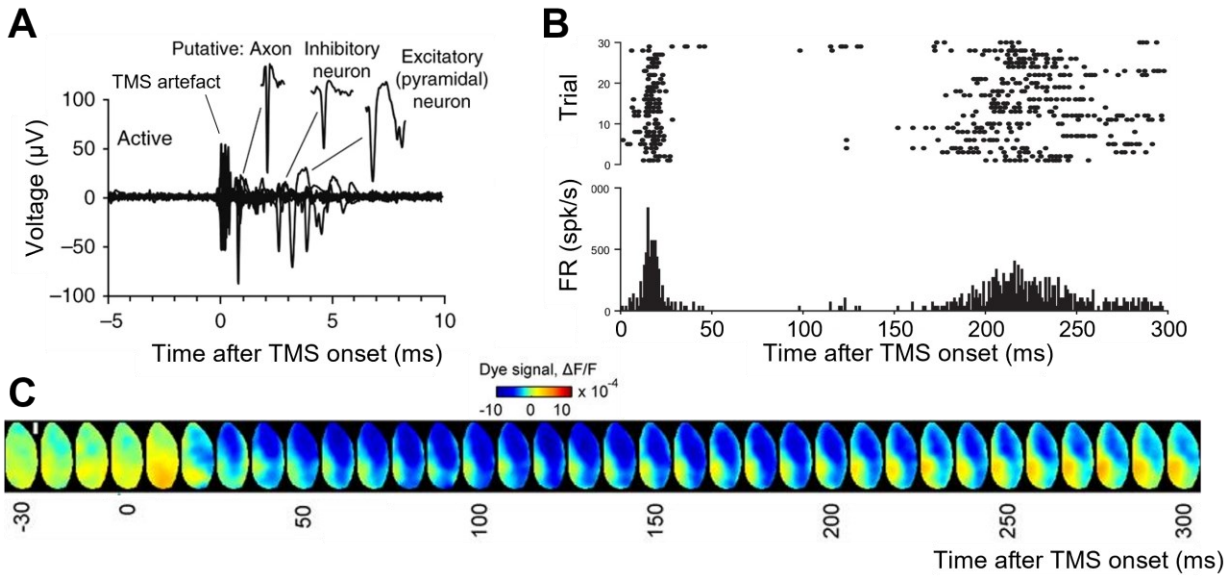

Figure 1.9. Effect of single-pulse TMS on electrophysiological recordings. A typical ~250-μs pulse directly triggers action potentials within the first millisecond. Activity then propagates polysynaptically through neural microcircuits over 300ms and beyond. **A.** Raw traces of multi-unit activity from 20 trials in the prefrontal cortex of an awake monkey. **B.** Single-neuron raster plot (top) and corresponding spiking frequency plot (bottom) aligned to TMS in the motor of an anesthetized rat. **C.** Voltage-sensitive dye intensity imaging timeseries from TMS over the EVC of an anesthetized cat. Note the early depolarization (ΔF/F>0 at 10ms) surrounded by delayed hyperpolarization (ΔF/F<0 at >10ms), reminiscent of typical center-surround patterns of sensory-driven activations. Scale bar: 1mm. *Adapted with permission from (A) Mueller et al. (2014), (B) Li et al. (2017) and (C) Kozyrev et al. (2014).*

to a few seconds (Moliadze et al., 2003; Romero et al., 2019). Interestingly, voltage-sensitive dye (VSD) imaging from Kozyrev et al. (2014) revealed that this intracortical polysynaptic spread of activity follows a spatiotemporal pattern of early focal excitation and late surround inhibition (Figure 1.9C), reminiscent of a pattern often observed with sensory-driven activations (Bergmann et al., 2016). Finally, activity also spread through long range cortico-cortical connections, triggering dose-dependent functional brain imaging responses in connected cortical and subcortical regions (Bergmann et al., 2016).

The initially highly synchronous TMS-triggered neural activity therefore seems to gradually mold into complex endogenous-like activity patterns (Samaha et al., 2017) as it dissipates through excitatory and inhibitory circuits. This exogenous activity most often interferes with computations carried by endogenous neural activity (de Graaf et al., 2014)—the so-call “virtual lesion” approach (Pascual-Leone et al., 1999) for establishing causal anatomofunctional relations. It is however important to note that—beyond disruptive effects—single TMS pulses can also activate the tissue’s function, triggering muscle twitches and the perception of

phosphenes when applied to motor and visual cortices, respectively. Importantly, the sensitivity to such TMS-triggered functional activation is heavily used as measures of brain tissue excitability. Moreover, increased behavioral performances with TMS are not uncommonly reported, particularly when the pulse is timed early during a behavioral trial (Luber & Lisanby, 2014), putatively because the exogenous activity has "naturalized" by the time the targeted brain area is required for the task. TMS therefore seems to interact with endogenous neural activity in complex and diverse ways, which can either disrupt, facilitate, or leave unaffected ongoing neural computations (Bergmann & Hartwigsen, 2021).

1.4.1.2.2 Brain Modulation with Trains of Pulses and rTMS

Applied in a short train, consecutive TMS pulses interact and can potentiate one another, altering neural activity for up to a few minutes. Within a 10-Hz train of 5 pulses, Kozyrev et al. (2014) observed that the suppression normally observed 50-100ms after a single pulse (Figure 1.9B and C) is obliterated, and that activity instead builds up over successive pulses (Figure 1.10A). For minutes after a similarly short 4-Hz train of 8 pulses in Allen et al. (2007), spontaneous and visually evoked firing rates are respectively modulated up and down (Figure 1.10B and C). Applied for longer periods, minutes to tens of minutes of rTMS modulates brain physiology for minutes to hours after the end of the treatment (George, 2019) and repeating such treatment within or across days can lengthen the offline effect to weeks and even months (Clavagnier et al., 2013). This makes for a sound strategy for therapy development: one can target a dysfunctional brain area to hopefully tip the brain dynamics back into a healthy state, then repeat the treatment to consolidate the therapeutic effect. The parameter space of rTMS treatments is however intractably large—one can use any combination of pulse shape, intensity, pulse train patterning, current orientation, target area, treatment repetitions, etc. The efficient and safe exploration of potential therapies therefore requires principled approaches, for which a deeper understanding of the molecular, neural and microcircuit mechanisms of rTMS is required.

The NIBM phenomenology described above is reminiscent of various brain plasticity phenomena, where stronger or longer inducing stimulation generally leads to more potent and durable plastic changes (Tang et al., 2021). Indeed, several parallels can be made between rTMS

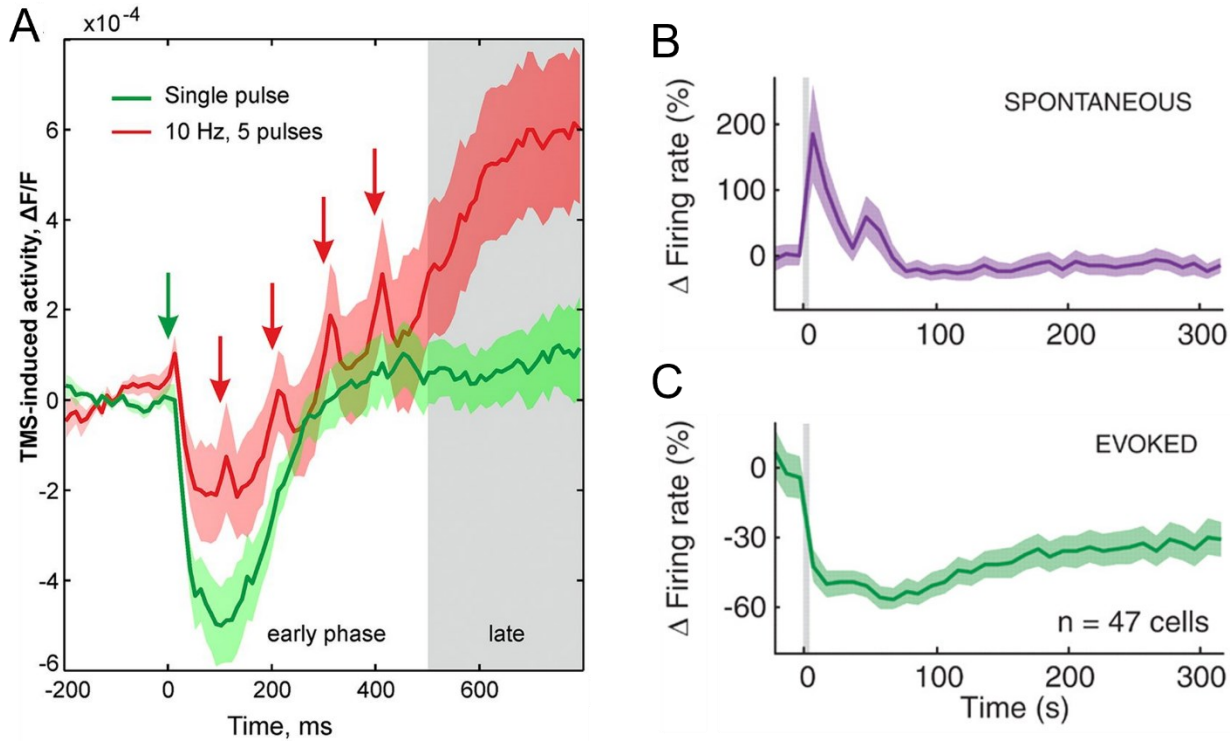

Figure 1.10 Effect of short trains of rTMS on electrophysiological recordings. A. Voltage-sensitive dye imaging data showing the response to single pulses applied alone (green arrow) or in short trains (red arrows). The suppressive phase after the first pulse of the train is interrupted by the following pulses, leading to a supra-linear building up of neural activity. **B and C.** Single-unit recordings after a short train of pulses (gray vertical shaded bars). Two-second visual stimuli were presented every 8s, allowing to assess the effect of the TMS train on spontaneous (B) and visually evoked (C) firing rates. *Reproduced and adapted with permission from (A) Kozyrev et al. (2014) and (B and C) Allen et al. (2007).*

and synaptic forms of plasticity (Kozyrev et al., 2018). The most obvious is the frequency dependence of established microelectric stimulation plasticity protocols and rTMS—high (≥10Hz) and low (≤3Hz) frequencies respectively lead to Long-Term Potentiation (LTP) and Long-Term Depression (LTD) of synapses after microelectric stimulation, and to LTP-like increases and LTD-like decreases in cortical excitability after rTMS (Huang et al., 2007). Moreover, synaptic reweighting and morphological restructuring are directly observable respectively after repetitive magnetic stimulation in slice cultures (Wolters et al., 2003) and rTMS in behaving mice (see Bergmann & Hartwigsen, 2021; Cirillo et al., 2017 for excellent reviews; Pell et al., 2011). Finally, excitability changes after rTMS in humans depend on the proper function of NMDA receptors and intracellular calcium signaling (Di Lazzaro et al., 1998; Kujirai et al., 1993), two crucial agents of synaptic plasticity. Although non-synaptic mechanisms are most likely also at play (Murphy et al., 2016), rTMS treatments seem to mostly leverage

endogenous synaptic plasticity mechanisms to tweak the connectivity and function of the stimulated neural circuits.

1.4.1.2.3 Modulation of Specific Intracortical Circuits

NIBM treatments are generally classified as either increasing or decreasing the excitability of the targeted brain tissue. This is best known from motor cortex studies, where excitability is indexed from the relation between the strengths of single-pulse TMS and motor evoked potentials (MEP) in electromyographic recordings of the target muscle. The oversimplified excitatory/inhibitory dichotomy can mislead one into thinking that rTMS simply tunes the tissue up or down—boosting the function or "virtually lesioning" the region. The cortical physiology of MEP generation however suggests that different rTMS protocols rather modulate specific intracortical and corticocortical microcircuits within the targeted brain tissues.

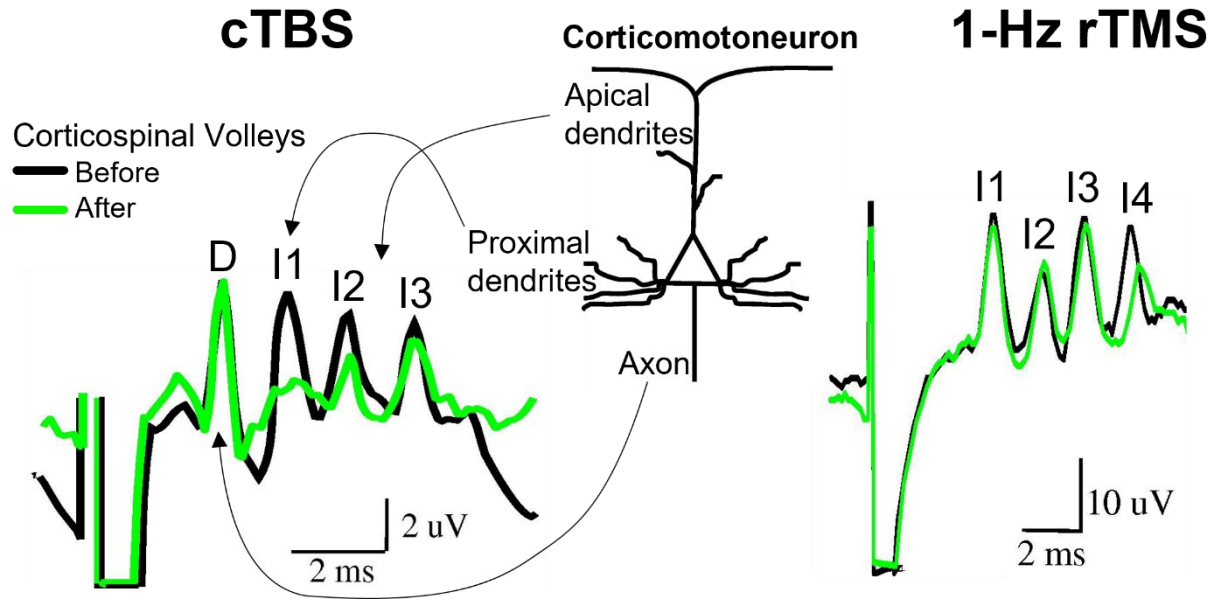

Figure 1.11 Physiology of MEP generation and the effect of rTMS. Traces represent corticospinal volleys in epidural spinal recordings, triggered by single-pulse TMS of the human motor cortex before (dark traces) and after (green traces) cTBS (left panel) or 1-Hz rTMS (right panel). Traces from the left panel show the D-wave (D) that originate from the direct activation of the axon of corticomotoneurons (middle panel) by the TMS pulse. The following I-waves (I1 to I4) result from the TMS pulse indirectly activating corticomotoneurons via synapses from other neurons. The early I-wave (I1) originates from synapses on proximal dendrites of corticomotoneurons whereas late I-waves (I2 to I4) most likely originate from synapses on distal dendrites or from polysynaptic pathways. The lower intensity of the single pulse of TMS used in the right panel did not trigger a D-wave at the expected delay but did activate the lower-threshold pathways for I-waves. *Adapted with permission from Di Lazzaro et al. (2010)*

MEP generation begins with TMS triggering an action potential in various axons (Figure 1.9A) that are favorably oriented in the E-field (Aberra et al., 2020; Shirinpour et al., 2021). Those axons belonging to corticomotoneurons directly signal to spinal motoneurons, producing the direct *D-wave* (D in Figure 1.11) of corticospinal volleys in epidural recordings of the human spine (Kozyrev et al., 2018; Tang et al., 2021). Axons within excitatory intracortical and corticocortical circuits are also activated, indirectly generating—through synapses on corticomotoneurons—respectively the early and late I-waves (I1 to I4 in Figure 1.11) that follow the D-wave (Ziemann, 2020). Intracortical inhibitory circuits are also recruited, synaptically counterbalancing excitatory circuits and limiting late I-wave amplitudes (Fumal et al., 2003). Importantly, these motor cortex intracortical excitatory and inhibitory microcircuits are commonly probed non-invasively in paired-pulse protocols (Figure 1.12).

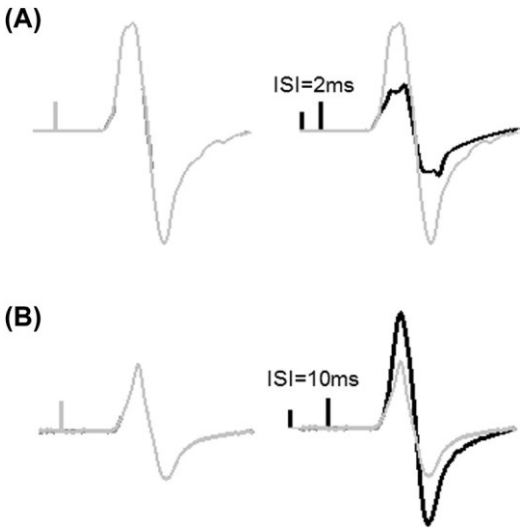

Figure 1.12 Probing motor cortex inhibitory and excitatory circuits. The MEP triggered by a single TMS test pulse (gray traces and vertical bars) is modulated when preceded by a subthreshold conditioning pulse (black traces and vertical bars). Depending on the interstimulus interval (ISI), such paired-pulse protocol probes the influence of intracortical inhibitory or excitatory circuits. *Reproduced with permission from (Zewdie & Kirton, 2016)*

Different rTMS protocols can produce similar modulations of cortical excitability but do so through modulations of different cortical microcircuits (see Di Lazzaro et al., 2010 for an excellent review). For example, both continuous theta burst stimulation (cTBS)—a temporally patterned form of rTMS inspired by microelectric stimulation studies (Suppa et al., 2016)—and 1-Hz rTMS of the primary motor cortex decrease MEP amplitudes, but epidural volleys show that they respectively do so by reducing the contribution of the early I-wave (I1 in left panel of Figure 1.11) or late I-waves (I2-I4 in right panel of Figure 1.11). Fast intracortical monosynaptic excitatory pathways targeting corticomotoneurons' soma and proximal dendrites likely underly the early I-wave, whereas late I-waves are instead proposed to emerge from slower polysynaptic excitatory intracortical pathways or from monosynaptic corticocortical pathways

targeting corticomotoneurons' apical dendrites (George, 2019). Importantly, these specific subcircuits targeted by different rTMS treatments most likely support different computations—e.g. primary motor cortex processes related to different phases of motor learning (Pell et al., 2011)—highlighting the specificity of rTMS to different microcircuits and computations in the targeted brain tissue.

A microcircuit-level mechanistic understanding of NIBM, beyond changes in brain tissue excitability, is required to predict therapeutic potentials and guide the principled design of new treatments. Motor cortex studies have been instrumental so far, but the generalizability of findings to other cortical areas remains relatively unknown. We have seen above that low-level visual psychophysics opens an underutilized window on objectifiable cortical functions, just like MEPs does on motor cortical functions. It therefore appears crucial to develop, validate and streamline a general visual TMS-psychophysics framework for dissecting the intracortical processes at play in NIBS and NIBM.

To achieve the above, **Chapter 2 aimed to**:

1. **show-case the various advantages of occipital pole TMS and psychophysics in assessing the computationally-relevant effects of rTMS brain modulation** and
2. **assess whether the reduction of motor cortex intracortical inhibition observed after cTBS generalizes to the visual cortex**.

1.4.2 MR Spectroscopy of Neurotransmitters

Cortical neurons mostly communicate through the synaptic release of glutamate or γ-aminobutyric acid (GABA) neurotransmitters. How the output of one neuron's computation contribute to the inputs of another neuron critically depends on the neurotransmitter used—presynaptic terminals releasing glutamate depolarize their post-synaptic partner, whereas those releasing GABA hyperpolarize them. Opposite post-synaptic effects—excitation or inhibition—can therefore arise from otherwise similar action potentials, highlighting the

importance of probing neurotransmitter functions non-invasively for understanding human neural computations.

The magnetic resonance (MR) proton signal (^{1}H-MR) from glutamate and GABA neurotransmitters has been observable in human brains for three decades (Bruhn et al., 1989). Water protons in a magnetic field resonate—they absorb and reemit radio-frequency energy—at a single frequency, giving rise to most of the signal recorded with clinical ^{1}H-MR systems. In MR Imaging (MRI) applications, this signal is spatially encoded during acquisition for later reconstruction into images (Figure 1.13, left panels). Using the same ^{1}H-MR systems, ^{1}H-MR spectroscopy (MRS) applications focus on protons in other molecules that also resonate, but at multiple frequencies defined by their unique spin structures—signals from different molecules are therefore tagged with different signature spectral patterns. Signals from about twenty small molecules, or metabolites, are therefore readily quantifiable from typical ^{1}H-MR spectra given appropriate suppression of the dominant water resonance (Figure 1.13, right panels). With

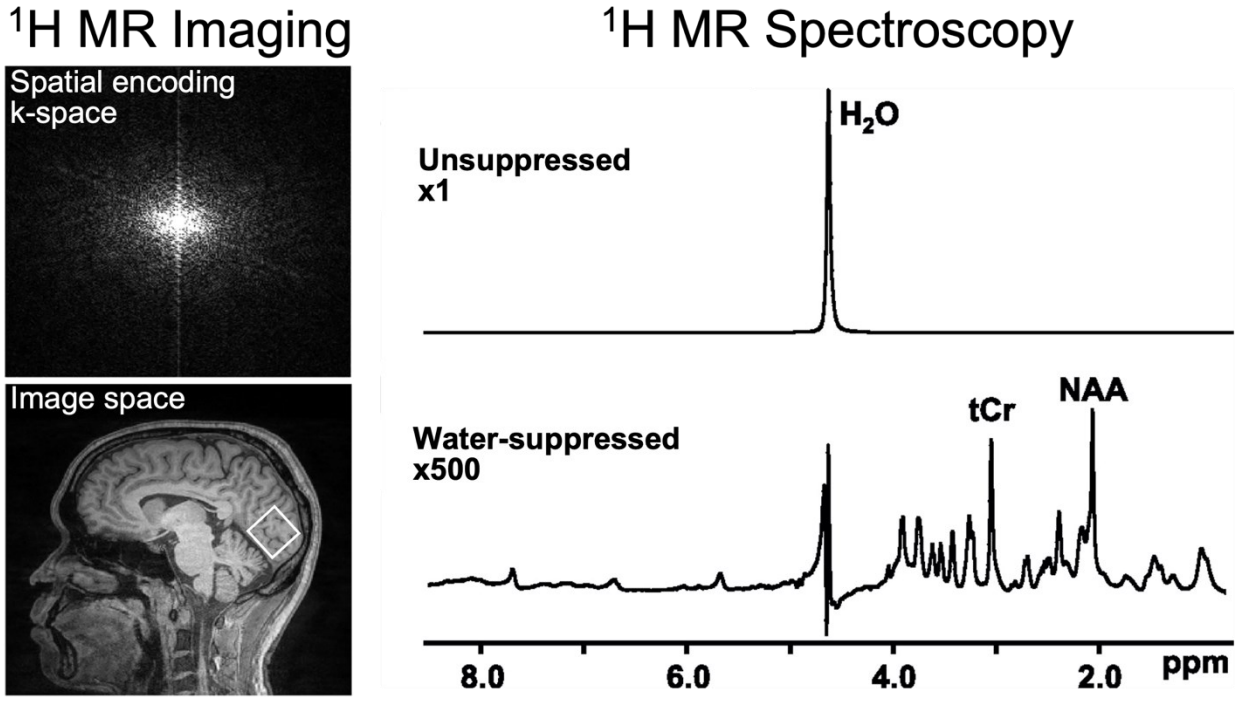

Figure 1.13 The ^{1}H-MR signal is dominated by water protons. Spatially encoding that signal during acquisition allows the reconstruction of images (left panels). When not spatially encoded, the signal is read as a spectrum (right panels), which again is dominated by water protons resonating at a single frequency (top right panel). Suppression of this water signal reveals complex peaks in the spectrum that arise from protons in small molecules (bottom right panel). In a typical MR spectroscopy application, such spectra are acquired from a single voxel (e.g. the white square in the bottom left panel) and allow the quantification of up to 20 metabolites. *Left and right panels respectively adapted with permission from Liu (2020) and Befroy and Shulman (2011)*

more modern technics—ultra-high-field ^{1}H-MR systems (Godlewska et al., 2017) and spectral editing pulse sequences (Hetherington et al., 1998; Mescher et al., 1998)—the low concentration glutamate (10-15mM) and GABA (1mM) neurotransmitters are routinely quantified at limited but biologically-relevant resolutions of several minutes for a single voxel of a few tens of cm^3. MRS studies of human brain neurotransmitters have seen a ~3-fold increase over the last 15 years, up to now ~150 studies yearly indexed on PubMed® and including a steady 5 clinical trials per year over the same period[4].

Drawing conclusions on neurotransmission from MRS measures of neurotransmitters is however not as straightforward as it may seem given their involvement in multiple unresolved biological processes at the subcellular scale. Below I outline current knowledge on the relevant cellular biology and metabolism, along with the different interpretational frameworks appropriate for different classes of MRS experiment.

1.4.2.1 Neurotransmitter Compartmentation and Static MRS Measures

MR spectroscopy applications are dominated by the non-invasive characterisation of pathological tissues—e.g. a snapshot of a brain tumor's chemical composition can inform on prognosis or treatment response (Wilson et al., 2019). In neuroscience applications, it is tempting to interpret cross-sectional studies using similarly static MRS (sMRS) estimates of glutamate and GABA concentrations as reflecting excitatory and inhibitory neurotransmission in the sampled brain region (Li et al., 2022). For example, Yoon et al. (2010) interpreted sMRS GABA measures as reflecting an inhibition trait—individuals with a strong trait should exhibit more of the GABA substrate for inhibition as well as stronger functional inhibition. Higher occipital GABA concentrations indeed related to stronger visual surround suppression, which is known to rely on intracortical inhibitory circuits (Adesnik et al., 2012).

For reasons that will come clear below, a direct link between sMRS GABA signals and inhibitory neurotransmission is unlikely. However, since 85-90% of the brain's glutamate (Andersen et al., 2017) and even more of GABA (Andersen et al., 2017) concentrate respectively

[4] Search query: "Glutamic Acid"[Mesh] AND "gamma-Aminobutyric Acid"[Mesh] AND "Magnetic Resonance Spectroscopy"[Mesh] AND "Brain"[Mesh] AND "Humans"[Mesh]

in excitatory and inhibitory neurons, sMRS GABA signals can reasonably be interpreted as reflecting the general capacity of the GABA cellular machinery for inhibitory neurotransmission. This is best illustrated in the observed decline of GABA concentrations with age (Gao et al., 2013) and in schizophrenia (Yoon et al., 2010). In senescent rats, dysfunctional inhibition—increased spike rates and reduced visual orientation selectivity—was accompanied by deficiencies in virtually all components of the machinery for GABA inhibition, namely GABA neuron density, GABA synthesis enzymes and GABA receptors (Ding et al., 2017). Similarly, schizophrenic human brains exhibit reduced number of GABA neurons post-mortem (Hashimoto et al., 2003) and showed lower occipital sMRS GABA signals that related to weaker visual surround suppression (Yoon et al., 2010).

Neurotransmission-related interpretations of sMRS neurotransmitter signals warrants caution because only ~30% of both glutamate and GABA is considered part of the neurotransmitter pool (Fonnum, 1984; Mangia et al., 2012; Martin & Rimvall, 1993). The remaining 70% is in the metabolic pool, functioning as metabolites in various neuroglial pathways for energy and amino acid metabolisms and ammonia homeostasis (Bak et al., 2006; Schousboe et al., 2013; Waagepetersen et al., 1999). Worse, 20-30% of total glutamate—i.e. most of the neurotransmitter pool—may be MR-invisible due to faster MR signal decay in the densely packed presynaptic vesicles (Jelen et al., 2018; Kauppinen & Williams, 1991; Pirttila et al., 1993). A similar faith is presumed for sMRS GABA signals. Consequently, sMRS is mostly sensitive to the metabolic pools of glutamate and GABA which are, at best, only indirectly related to neurotransmission.

The currently dominant view for relating sMRS GABA measures to inhibitory neurotransmission involves ambient extracellular GABA, which mediates a tonic form of inhibition through paracrine activation of extrasynaptic receptors (Farrant & Nusser, 2005; Rae, 2014; Stagg et al., 2011b). By some accounts (Myers et al., 2016), MRS was deemed hardly sensitive enough for μM-range extracellular concentrations. GABA transporters on the neural membrane however have the ability to reverse directions even under physiologic conditions (Sears & Hewett, 2021; Wu et al., 2007). The sMRS GABA signal may therefore indeed reflect tonic inhibition, but again indirectly through a dynamic equilibrium between the cytosolic

concentrations it is most sensitive to and the extracellular GABA that can actually reach extrasynaptic receptors. Glutamate may be similarly related to paracrine activation of extrasynaptic glutamate receptors, though the possibility of transporter reversal in physiological conditions is less clear (Mahmoud et al., 2019).

1.4.2.2 Neurotransmitter Cycling and the Compartment Shift Hypothesis for fMRS

There is a disconnect between, on one side, the incentives to draw conclusions on GABA and glutamate neurotransmission (Ip & Bridge, 2021; Kiemes et al., 2021)—many theories of neural dysfunction rest on imbalanced excitation and inhibition—and, on the other side, the lack of direct investigation of the biophysical origin and neurophysiological meaning of ^{1}H-MRS estimates of these neurotransmitters. On the other hand, ^{1}H-MRS is increasingly used in functional paradigms where changes in the glutamate or GABA signals of up to ~15% are observed in association with neural activation at the time scale of seconds to several tens of minutes (Jelen et al., 2018; Mullins, 2018). Although not devoid of interpretational challenges, this recently established reliability of such functional MRS (fMRS) paradigms may interestingly offer measures more directly related to synaptic neurotransmission, as we will see below.

As schematically represented in Figure 1.14, synaptic neurotransmission begins with the presynaptic release of vesicular neurotransmitters into the synaptic cleft. The spatiotemporal precision of postsynaptic receptor activation is ensured by rapid neurotransmitter recapture through high-affinity transmembrane transporters. Such transporters on the presynaptic membrane initiate a *short cycle* back to glutamate and GABA presynaptic vesicles. Transporters on the astrocytic membrane—often ensheathing individual synapses—initiate a *long cycle*. For glutamate, the latter is often referred to as the glutamate-glutamine cycle, as it involves the cytosolic conversion of recaptured glutamate to glutamine, then transportation back to glutamatergic terminals where glutamine is converted back to glutamate. GABA recaptured by astrocytes borrows the glutamate-glutamine route through cytosolic conversion to glutamate. Transported into GABAergic terminals, glutamine is converted back to glutamate then GABA.

Synaptically released neurotransmitters are moving from an MR-invisible to an MR-visible compartment. This should in theory lead to an immediate and possibly large increase—20-30%

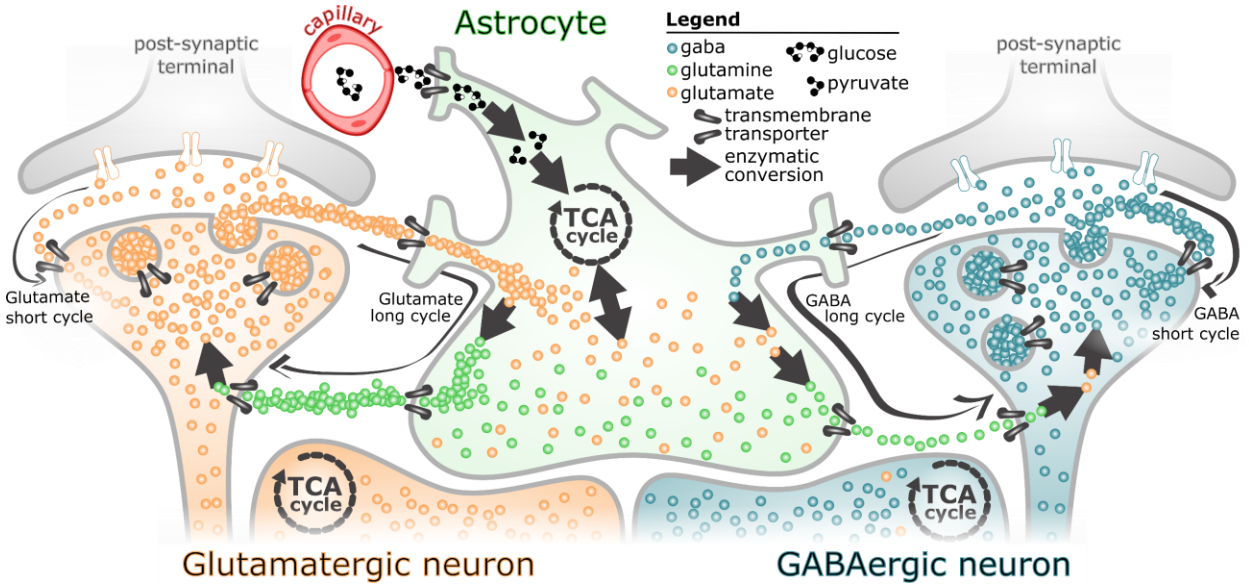

Figure 1.14 Neurotransmitter cycling and metabolic pathways. Recycling of synaptically released neurotransmitters begins with their recapture by transmembrane transporters, effectively terminating neurotransmitter receptor activation. In the *short cycle*, the presynaptic terminal repackages neurotransmitters directly recaptured from the synaptic cleft, whereas in the *long cycle*, neurotransmitters are recaptured by astrocytic processes ensheathing the synapse before being channeled back to presynaptic terminals in the form of glutamine. Recycling of glutamate and GABA respectively favors the long and short cycles. Glutamate and GABA respectively concentrate in glutamatergic and GABAergic neurons, particularly in presynaptic vesicles where, however, they are largely MR-invisible due to faster signal decay. Glutamate is also present in astrocytes, owing to its role in various metabolic pathways involving the TCA cycle. Glutamate is continuously catabolised, e.g. for energy, through the TCA cycle and replaced by *de novo* synthesis from glucose substrate taken up from capillaries. GABA is subjected to similarly catabolic and anaplerotic fluxes that however operate through conversion to glutamate. TCA: tricarboxylic acid.

of glutamate is likely invisible in presynaptic vesicles—in the recorded signal (Jelen et al., 2018; Mullins, 2018). Consistent with this *compartment shift hypothesis* are the +15% glutamate signal responses recorded within seconds of pain stimuli in several event-related fMRS designs (Archibald et al., 2020; Mullins, 2018). Similarly rapid changes were recently linked to visual memory by Koolschijn et al. (2021), who showed that early visual cortex glutamate-to-GABA ratios increased specifically during successful 5-s recall periods, and to magnitudes that correlated across individuals with hippocampal fMRI activation. The plausibility of this compartment shift effect is confirmed in yet unpublished realistic simulations by Lea-Carnall et al. (2021), where the 7-fold slower maximum rates for vesicular repackaging vs release produced changes in glutamate and MR GABA signals that were compatible with the size and time scale of *in vivo* observations. Finally, fMRS at less-commonly used ultra-short (<15ms) echo times—capturing more of the rapidly decaying vesicular neurotransmitter MR signal—

tend to show smaller changes (Jelen et al., 2018; Mekle et al., 2017; Mullins, 2018), consistent with a decreased sensitivity to the compartment shift effect.

There are therefore theoretical grounds—and some more direct evidence in animals (Takado et al., 2022)—for directly relating MR neurotransmitter signals to neurotransmission in fMRS paradigms. The latter are however not immune to confounds related to neurons' energy metabolism, as described in next section.

1.4.2.3 Energy Metabolism Confounding the Assessment of Neurotransmission with fMRS

About 80% of synaptically released glutamate is recycled through astrocytes in the long glutamate-glutamine cycle rather than the more direct short cycle (Bak et al., 2006) (Figure 1.14). This pathway allows significant mixing with the metabolic pool, where an estimated 25-30% of recycled glutamate is continuously catabolized for energy and replaced by *de novo* synthesis from glucose through tricarboxylic acid (TCA) cycle anaplerotic pathways (Schousboe et al., 2013). Furthermore, a 1:1 stoichiometry has been shown between glutamate-glutamine cycling and oxidative metabolism of glucose (Hyder et al., 2006; Rothman et al., 2003; Sibson et al., 1998). Interestingly, very-high-field fMRS in humans showed increased glycolysis—evidenced by decreased glucose and increased lactate—accompanied by a slow and modest ~5% increase in glutamate at the expense of aspartate concentrations tens of seconds into a block of visual stimulation (Ip et al., 2017; Lin et al., 2012; Mangia et al., 2007; Martinez-Maestro et al., 2019). This led to the influential proposition that neural activation imposes a new metabolic steady state and links glutamate concentrations, through the malate-aspartate shuttle, to oxidative metabolism rather than neurotransmission (Mangia et al., 2012).

With ~80-90% of synaptically released GABA taking the short cycle directly back to the presynaptic terminals (Schousboe et al., 2013), fMRS GABA may be somewhat less susceptible to metabolic confounds. It is however important to remember that non-synaptic GABA—80% of total GABA—mostly sits in the neuron's cytosol (Fonnum, 1984; Mangia et al., 2012; Martin & Rimvall, 1993). The metabolic functions of GABA—e.g. in shunting ~15% of the TCA cycle flux (Rae, 2014; Schousboe & Waagepetersen, 2007; Waagepetersen et al., 1999)—are less well

known, let alone their influence on fMRS signals, but nevertheless constitute a potential confound in fMRS.

Interestingly, by some accounts metabolic mechanisms are unlikely to support the larger ~15% changes not uncommonly reported (Jelen et al., 2018; Mullins, 2018). At least in these cases, the compartment shift hypothesis (previous section) and plasticity hypothesis (next section) may allow relatively safe conclusions on excitatory and inhibitory neurotransmission.

1.4.2.4 Brain Plasticity and Adaptation in MRS Modulation Paradigms

Another class of MRS experimental designs focuses on slower changes related to brain plasticity or adaptation phenomena. It particularly flourished in human sensorimotor cortex studies where various interventions—ranging from non-invasive brain modulation (Bachtiar et al., 2018; Stagg et al., 2011a; Stagg et al., 2010) to ischemic nerve block (Levy et al., 2002) and motor learning (Floyer-Lea et al., 2006; Kolasinski et al., 2019)—could all reduce the MRS GABA signal by over 15% within tens of minutes. These are not functional designs—they do not measure MRS changes closely related to the task or stimulus presentation time course. They instead seek to trigger neural adaptations or plasticity changes that will modulate neural processing, and they aim to relate the neuromodulation—measured through behavior or physiology—to post-intervention changes in MRS neurotransmitter signals. Given the focus on lasting modulation of neural functions, I will tentatively designate this class of MRS paradigms as modulation MRS (mMRS).

A good example of the level of insight mMRS paradigms can provide comes from studies by Frangou et al. (2018; 2019) using glass pattern visual stimuli to train healthy humans on different perceptual tasks. Behavioral improvements after training on signal-in-noise and feature-difference detection tasks were respectively related to decreased and increased occipitotemporal GABA concentrations (Frangou et al., 2018; Frangou et al., 2019). These mMRS changes built up slowly during the ~35min training period (Frangou et al., 2019), were maintained after the end of training in a 13-min MRS measure (Frangou et al., 2018) and showed regional specificity (Frangou et al., 2019). Importantly, while the mMRS effects could dissociate the two tasks, the fMRI signal from the same brain tissue did not (Frangou et al.,

2018). Similar task-specific mMRS findings were related to training-induced performance improvements and memory with other visual signal-in-noise (Shibata et al., 2017) and visuomotor (Chalavi et al., 2018) tasks.

The meaning of such mMRS findings for neurotransmission functions could be as diverse and context-specific as the plastic changes they relate to—a generic interpretation would at this stage be premature. However, by triggering presumably microcircuit-specific plasticity within a cortical area, the interpretational challenge could be turned into an advantage. Most importantly, contrary to sMRS protocols, many non-specific influences would subtract out in mMRS protocols. Moreover, with good *a priori* knowledge from animal and theoretical models, mMRS findings can contribute to better understand MR neurotransmitter signals themselves. For example, knowing that the dynamics of synaptogenesis and pruning in mouse cortex can be modulated within 4 hours (Zhou et al., 2020), if a plasticity protocol known to induce removal of GABA synapses on adult rat pyramidal neurons (van Versendaal et al., 2012) also reduces the MR GABA signal—as was indeed observed in human adults (Lunghi et al., 2015)—one could suggest that MR GABA is sensitive to GABA synapse density. This very conjectural proposition would need confirmation from mMRS and microscopic imaging of structural synaptic dynamics both performed in a single animal plasticity model, but it nicely illustrates the challenges and opportunities of these relatively new mMRS protocols.

Chapter 3 leverages an mMRS protocol in the context of an adult-form of human ocular dominance plasticity pioneered by Lunghi et al. (2011), where tens of minutes to hours of monocular deprivation (MD) shifts the interocular balance in favor the deprived eye. An mMRS experiment from the same group showed that MD reduces occipital GABA concentrations (Lunghi et al., 2015), but the influence of different deprivation regimes remained to be explored. Therefore, **Chapter 3 aimed to**:

1. **assess the generalizability of different MD treatments with regard to interocular inhibitory interactions** and
2. **better understand how interocular inhibition relates to MR GABA signals**.

The second aim will be further developed in Chapter 5 through the discussion of *in silico* simulation experiments reported in Annex A.

1.4.3 Hemodynamic Signals

The discovery by Ogawa et al. (1990) that MR imaging pulse sequences can be designed to yield a signal that depends on blood oxygenation—the blood-oxygenation-level-dependent (BOLD) signal—sparked a neuroscientific revolution (Van Horn, 2006). As BOLD changes colocalized with areas expected to show increased neural activity, e.g. in motor (Jack et al., 1994) and visual (Deyoe et al., 1994) cortices respectively during motor and visual tasks, the long-known functional hyperemia of active brain tissues (Roy & Sherrington, 1890) could finally be localized non-invasively. Despite poorly understood biophysical and physiological mechanisms, functional MR imaging (fMRI) techniques rapidly became a major tool for mapping human brain functions—PubMed® indexes ~800 publications featuring fMRI in the following decade, a number that steadily grows ~350 publications per year up to a peak of ~2,500 in 2015 alone[5].

Today, modern techniques—most notably the increased resolution afforded by more sensitive MR hardware (Wald & Polimeni, 2017) and the specificity of new fMRI contrasts to specific aspects of hemodynamics like cerebral blood flow (CBF) and volume (CBV) (reviewed in Huber et al., 2019; and Kim & Ogawa, 2012)—are unravelling more and more details about the complex spatiotemporal and non-linear dynamics that translate neural activity into measurable fMRI responses. Unwrapping these hemodynamic distortions can improve the localization of neural activity—down to tens of microns with cutting-edge technologies (Yu et al., 2014). More importantly for this thesis, these advances allow the extraction of signals that more directly relate to neural activity, bringing us one step closer to observing neural computations in human brains.

[5] Search query: (fMRI[Title/Abstract] OR "functional MRI"[Title/Abstract] OR "functional MR imaging"[Title/Abstract] OR "functional magnetic resonance imaging"[Title/Abstract]) AND "Humans"[Mesh] AND "Brain"[Mesh] AND "Brain Mapping"[Mesh]

Feedback mechanisms were long thought to drive functional hyperemia—by-products of energy metabolism trigger vascular responses that matches supplies to the increased demand (Ido et al., 2004; Raichle & Mintun, 2006). Such view makes sense given the tight *neurometabolic coupling* inferred from the observed 1:1 stoichiometry between synaptic neurotransmitter and glucose oxidation fluxes (Hyder et al., 2006; Rothman et al., 2003; Sibson et al., 1998). More recent research (see Drew, 2019; Howarth et al., 2021; Nippert et al., 2018 for excellent recent reviews) has however unveiled multiple transcellular signaling pathways more directly triggered by neural activity and converging on blood vessels. The *neurovascular unit*—neurons, astrocytes and blood vessel endothelial and contractile mural cells—integrates various signals and vasoactive messengers to enact a feedforward control of blood supplies. *Neurovascular coupling* mechanisms therefore appear to anticipate rather than react to neurometabolic needs.

More interestingly, both neurometabolic and neurovascular coupling vary between cell types (Cauli & Hamel, 2010; Drew, 2019; Howarth et al., 2021; Nippert et al., 2018). This suggests that different subsets of neurons active in a patch of brain tissue can trigger variable hemodynamics (Buxton et al., 2014; Uhlirova, Kılıç, Tian, Sakadžić, et al., 2016), which may inform on the computations being carried. This section briefly outlines the physiology of fMRI signals before highlighting emerging approaches for exploiting cell-type specific hemodynamics and bring fMRI beyond the mere localization of vaguely defined 'brain activations'. It concludes by introducing the aim of Chapter 4 and the approach proposed to obtain computationally-relevant information—the excitation/inhibition balance—from the delay of the BOLD response.

1.4.3.1 Vascular Anatomy and Functional Hyperemia

Hemodynamic signals are highly influenced by the fluid dynamics unfolding within the complex brain vasculature. Blood flows to the cortex at high pressure through a dense and redundant network of pial arteries that run along the cortical surface (Figure 1.15A). For each mm^2, about 12 penetrating arterioles of tens to few hundreds of µm in diameter (El-Bouri & Payne, 2016) branch off and dive at right angle into the cortical parenchyma (Figure 1.15B). There, parenchymal arterioles further branch several times, down to the ~3-µm diameter vessels—slightly smaller than red blood cells—that form the low-pressure capillary bed (Figure

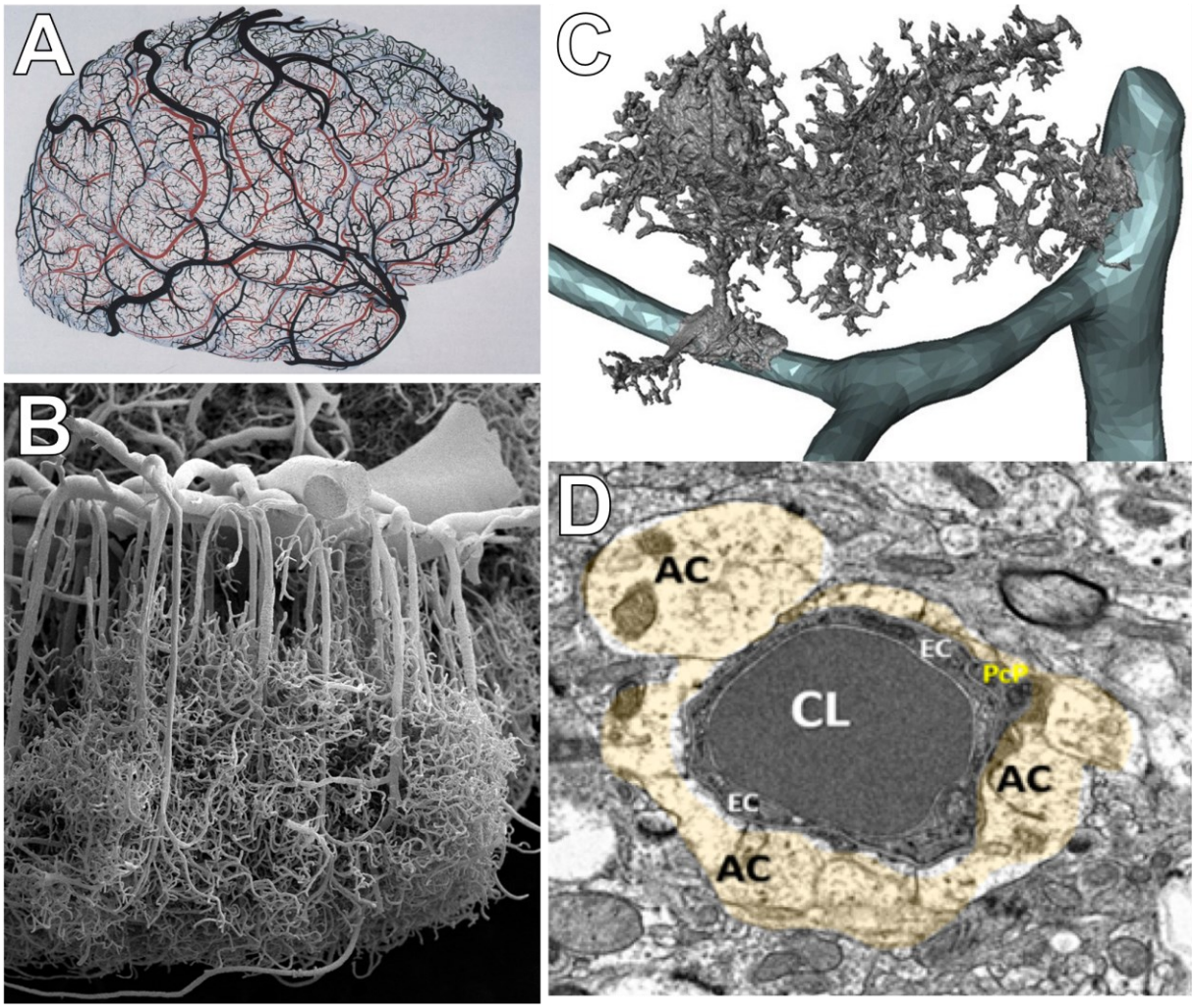

Figure 1.15 The brain vascular system. A. Drawing of pial vessels from a 50-year-old woman. Veins are in black, and red, blue and green represent arteries tributary of different upstream vessels. **B.** Vascular cast of the human cerebral cortex. From pial vessels (top horizontal structures), diving arterioles and venules (vertical structures) branch off to dive down and further ramify (bottom meshing structures) in the cortical parenchyma (here dissolved). **C.** Electron microscopy 3D reconstruction of a single astrocyte (grey) showing the apposition of its processes to a blood vessel (green). **D.** Electron microscopy showing the transection of a single capillary fully surrounded by astrocytic endfeet processes. CL: capillary lumen, EC: endothelial cell, AC; astrocyte. Reproduced with permission from (A) Duvernoy et al. (1981), (B) Alfonso Rodríguez-Baeza, MD PhD and Marisa Ortega from the Human Anatomy Lab of the Autonomous University of Barcelona (Spain), (C) Cali et al. (2019) and (D) Hayden (2019)

1.15B) where gases, water and small molecules exchange. This arterial topology is roughly mirrored by the venous system that drains low-pressure capillary blood through merging venules—larger and ~4 times less numerous than arterioles—back to the surface in the pial vein network (Duvernoy et al., 1981; Gagnon et al., 2015).

Blood supply is highly dynamic. Under sympathetic control, smooth muscle cells (SMC)—a type of mural cell wrapping around arterial vessels (Figure 1.16A)—maintain arterial pressure

under varying cardiac output (Payne, 2016). More importantly, SMCs on the more distal pial arteries and parenchymal arterioles (Figure 1.16B) are responsive to local levels of neural activity, allowing a remarkably fine control of local blood supply as observed with two-photon imaging of single vessels (Figure 1.16E) (Hall et al., 2014; Hill et al., 2015; O'Herron et al., 2016). Contractile pericytes—another type of mural cell—on precapillary arterioles or capillaries (Figure 1.16C and D) (Attwell et al., 2016) appear to respond first, within ~2sec of whisker stimulation, whereas the dilation of penetrating arterioles putatively governed by different neurovascular coupling mechanisms (Drew, 2019) lag by another ~1.4sec (Hall et al., 2014). Importantly, gap junctions between endothelial cells of the vessel wall propagate dilatory signals upstream to pial vessels then downstream to neighboring penetrating arterioles (Drew, 2019; Howarth et al., 2021; Kisler et al., 2017; Nippert et al., 2018). Drainage is less dynamic—venules and pial veins distend more slowly and passively to only ~⅓ of typical ~30% arterial

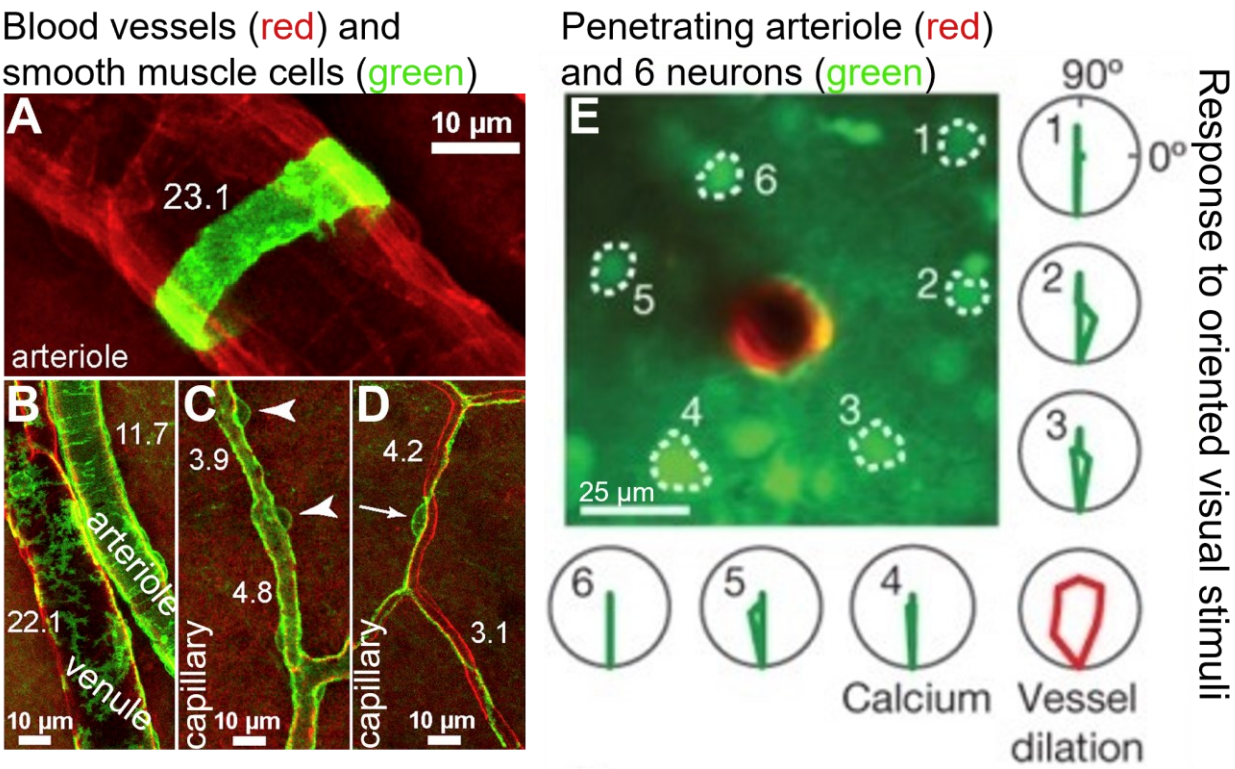

Figure 1.16 Neural control of arterial diameter. A to D. Mural cell types on differently sized arterial vessels (numbers indicate vessel diameter in µm) and one venule. Larger vessels exhibit smooth muscle cells (A and B). Capillaries/pre-capillary arterioles exhibit contractile pericytes (C) while the contractility of pericytes that do not enwrap the capillary is unclear (D). **E.** Two-photon imaging transection of a single penetrating arteriole surrounded by 6 neural somata in cat visual cortex. The polar traces in inset show the selectivity of neural calcium (green) and vessel dilation responses to the orientation of a visual stimulus. *Reproduced with permission from (A to D) Hill et al. (2015) and (E) O'Herron et al. (2016)*

dilation responses and only with prolong (>15sec) stimulation (Drew et al., 2011). Functional hyperemia is therefore actively triggered by neurons at the scale of cortical column or smaller, but then spreads to otherwise inactive brain tissues through active arterial propagation and—with prolong activation—passive venous distension.

1.4.3.2 Accessing Hemodynamics and Neuroenergetics with fMRI

The physiology of fMRI signals should be understood as dominated by two main phenomena, both related to neural activity through parallel mechanisms (Buxton et al., 2014). One involves neurovascular coupling: neurons signal their level of activity through the neurovascular unit to actively control the arteriolar dilation and constriction that is at the root of complex—hemodynamic—blood flow and volume responses. The other involves neurometabolic coupling: oxidative-metabolism-dominated neuroenergetics impact the extraction rate of oxygen from capillary hemoglobin and consequently affect signals dependent on the blood oxygenation level. Below I briefly describe how hemodynamics are accessible with fMRI tools for measuring blood flow and volume, and how hemodynamics and neuroenergetics together determine the BOLD signal.

Cerebral Blood Flow. Dilation of capillaries and/or arterial blood vessels have direct consequences CBF and CBV (Huber et al., 2019). CBF is most commonly estimated in fMRI with methods based on arterial spin labeling (ASL) (Calamante et al., 1999), which inverts the magnetization of spins (water protons) at the level of the neck to turn them into diffusible tracers. In brain capillaries, labeled water rapidly and almost completely exchanges with unlabelled tissue water, altering the MRI signal proportionally to blood flow. Upon capillary and arteriolar dilation, resistance to flow immediately drops and allows a rapid increase in blood flow. The reverse happens when the neural activation ends, terminating the flow response (Figure 1.17A, red trace), which may however undershoot.

Cerebral Blood Volume has mostly been measured in fMRI using iron-oxide contrast agents. The method was largely replaced in human studies by the safer and contrast-agent-free vascular space occupancy (VASO) method (Huber et al., 2019; Lu et al., 2003). When blood volume increases in a voxel, the consequently compressed surrounding parenchyma loses its

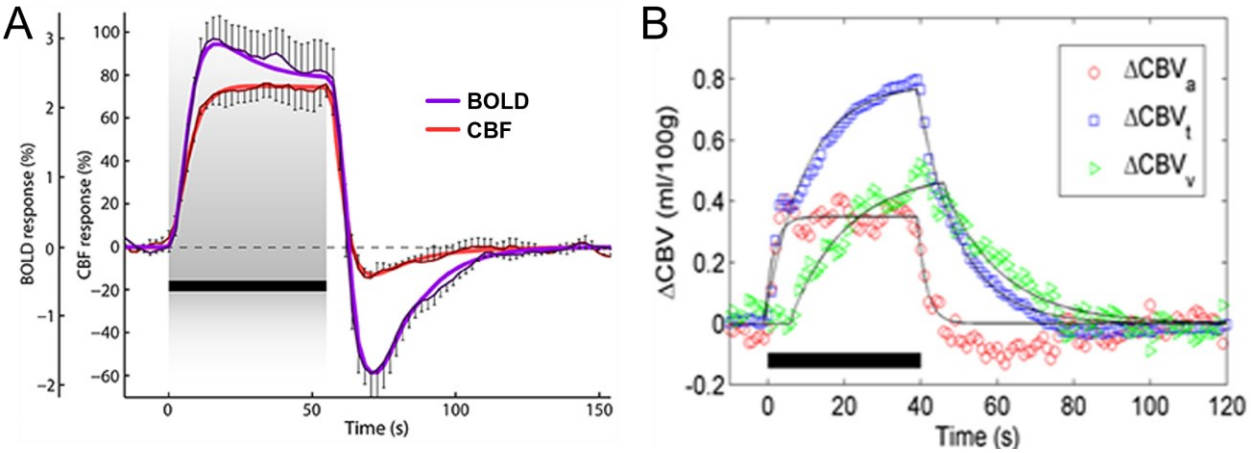

Figure 1.17 Hemodynamics. A. BOLD and CBF responses to minute-long block of flickering visual stimulation in humans. **B.** Total (CBV_t) and arterial (CBV_a) CBV responses to 40-s visual stimulation in cats. Venous CBV (CBV_v) is given by $CBV_t - CBV_a$. Reproduced with permission from (A) Havlicek, Ivanov, Roebroeck, et al. (2017) and (B) Kim (2018)

water to blood vessels and therefore contributes less to the voxel's volume. VASO exploits T_1 differences between blood and parenchyma to produce a signal proportional to 1-CBV (Figure 1.17B, blue trace). It is sensitive to all vascular compartments—arterial, capillary and venous—and therefore usually measures total blood volume (CBV_t). Other techniques can resolve the arterial compartment (CBV_a), but the capillary and venous compartments remain confounded in venous blood volume estimates ($CBV_v = CBV_t - CBV_a$) (Hua et al., 2019; Huber et al., 2014). Upon neural activation, CBV_a naturally increases with arteriolar dilation (Figure 1.17B, red trace) and closely follows the time course of CBF—the two are dynamically coupled. CBV_v responses result from the passive viscoelastic distension of veins and, as observed in microscopic imaging of veins, evolve more slowly over time and are detected only with longer (>15s) activations—CBV_v and CBF are dynamically uncoupled (Figure 1.17B, green trace) (Drew et al., 2011).

Blood Oxygenation Level Dependent Signals arise from deoxyhemoglobin acting as a paramagnetic contrast agent. Distorting the magnetic field tens of µm in and vessels, deoxyhemoglobin increases the dephasing of spins and the apparent T_2 relaxation of a voxel, making the BOLD signal chiefly dependent on the inverse the voxel's content in deoxyhemoglobin (Kim & Ogawa, 2012). Deoxyhemoglobin content is itself a complex function of oxygen consumption, blood flow and venous volume. Oxygen consumption and blood flow

have opposite effects—oxidative metabolism during neural activation extracts more oxygen from capillary hemoglobin, but deoxyhemoglobin is washed away below baseline by the excessive flow response, producing a net increase in BOLD signal. Early during an activation (<15s), CBV_v does not contribute much to BOLD, but the slow accumulation of deoxygenated blood in distending veins (Figure 1.17B, green trace) eventually draw the signal down, offsetting the wash out effect (Figure 1.17A, initial transient and plateau phases of the purple trace). When neural activation ends, the flow response abruptly ends but the drainage of accumulated venous blood lags behind—the now dominant CBV_v effect generates the post-stimulus undershoot in the BOLD signal (Figure 1.17A, negative phase of the purple trace). These complex hemodynamics obviously limit the interpretability of BOLD responses. The ease of implementation and high temporal SNR of BOLD—respectively ~2 and ~5-10 times than that of CBV and CBF (Huber et al., 2019)—however makes it the fMRI method of choice for most human applications.

Cerebral Metabolic Rate of Oxygen ($CMRO_2$). Interpreting stimulus-locked BOLD signal changes is relatively straightforward: neural activity is likely located in or close to voxels showing the BOLD modulations. Interpreting differences in the amplitude of BOLD responses is much less straightforward since opposing vascular and metabolic effects are conflated—a larger response could result from either a larger vascular or smaller metabolic response. These influences on the BOLD signal are best summarized in the following derivation of the Davis quantitative model of fMRI (Davis et al., 1998; Hoge et al., 1999a, 1999b):

$$\%BOLD = \mathrm{M}\left[1 - \left(\frac{CBF}{CBF_0}\right)^{-\beta}\left(\frac{CMRO_2}{CMRO_{2_0}}\right)^{\beta}\left(\frac{CBV_{\mathrm{v}}}{CBV_{\mathrm{v}_0}}\right)\right], \quad [1.1]$$

where $_0$ subscripts indicate baseline levels, β exponents account for the nonlinear relation between the deoxyhemoglobin content and its magnetic effect, and M is a subject- and voxel-specific calibration parameter. Deoxyhemoglobin content is modeled in the right-hand term by the three factors representing fractional changes in CBF, $CMRO_2$ and CBV_v, which respectively contribute to increasing, decreasing and decreasing the %BOLD signal. With measures of BOLD, CBV_v and CBF—or with only one of the latter two when additional assumptions are acceptable—one can solve equation [1.1] for $CMRO_2$, thereby disambiguating the vascular (CBF

and CBV_v) and metabolic ($CMRO_2$) determinants of the BOLD response (Gauthier & Fan, 2019; Hoge, 2012).

Quantitative fMRI methods are well-validated for estimating $CMRO_2$ during steady-state physiology, but less so for estimating its temporal dynamics (Hyder et al., 2010; Simon et al., 2013). An empirical approach to this consists in abolishing the blood flow response through hypotension or hypercapnia manipulations in animals to produce a $CMRO_2$-dominated *inverted* BOLD response (Nagaoka et al., 2006; Zappe et al., 2008). With negligible change in CBV_v at <15s stimulus durations, such empirically derived $CMRO_2$ estimates roughly follow the time course of the normal CBF-dominated BOLD signal. Therefore, and consistent with results from time resolved quantitative fMRI (Hyder et al., 2010; Sanganahalli et al., 2016), $CMRO_2$ and CBF appear dynamically coupled (Uludag et al., 2004), though faster $CMRO_2$ responses (Devor et al., 2003; Vazquez et al., 2012) may lead to an early dip in BOLD signal in some situations (Hu & Yacoub, 2012).

1.4.3.3 Taking fMRI Beyond Brain Mapping and Toward the Characterization of Intracortical Computations

By unwrapping hemodynamics, quantitative fMRI provides a neurometabolic signal more closely related to neural computations. Indeed, roughly 45% and 16% of the brain's energy budget goes respectively to chemical neurotransmission and action potentials (Dienel, 2019; Howarth et al., 2012)—the building blocks of neural computations—mostly through oxidative metabolism (Dienel, 2019; Lin et al., 2010). Masainoto et al. (2008) interestingly showed in anaesthetized cats that empirically derived $CMRO_2$ responses correlated better with local field potentials across trials than did optical intrinsic signal (OIS) and tissue P_{O_2}, two BOLD-like signals. $CMRO_2$ therefore appears as a better proxy of neural work and computations than other signals that conflate oxygen and vascular responses. However, Masainoto et al. (2008) showed that CBF also better correlates with synaptic activity than do BOLD-like signals. Purely vascular signals therefore remain relevant for studying neural functions, most certainly because of tight neurovascular coupling mechanisms (Howarth et al., 2021).

Perhaps neurometabolic ($CMRO_2$) and neurovascular (CBF) signals reflect different aspects of neural function (Buxton et al., 2014). $CMRO_2$ and CBF are linearly related across brains (Figure 1.18A) (Hoge et al., 1999b; Sheth et al., 2004; Stefanovic et al., 2004). This coupling is however not fixed within a given piece of brain and show various influences from caffein intake (Griffeth et al., 2011), neural adaptation (Lin et al., 2009; Moradi & Buxton, 2013), attention (Moradi et al., 2012), stimulus temporal frequency (Lin et al., 2010; Lin et al., 2008; Vafaee & Gjedde, 2000) and intensity (Figure 1.18B) (Liang et al., 2013) and activation vs post-stimulus deactivation (Mullinger et al., 2017). Buxton et al. (2014) elegantly proposed to leverage this rather loose coupling to extract more relevant information from fMRI signals. Formalized in Buxton (2021), the idea rests on $CMRO_2$ reflecting the neurometabolic consequence of excitatory activity (Dienel, 2019; Howarth et al., 2012; Howarth et al., 2021) while CBF depends on neurovascular signals from both excitatory and inhibitory neurons (Drew, 2019; Howarth et al., 2021; Nippert et al., 2018). The key consequence of the above is a CBF:$CMRO_2$ ratio that depends on the EI balance of the underlying neural activation.

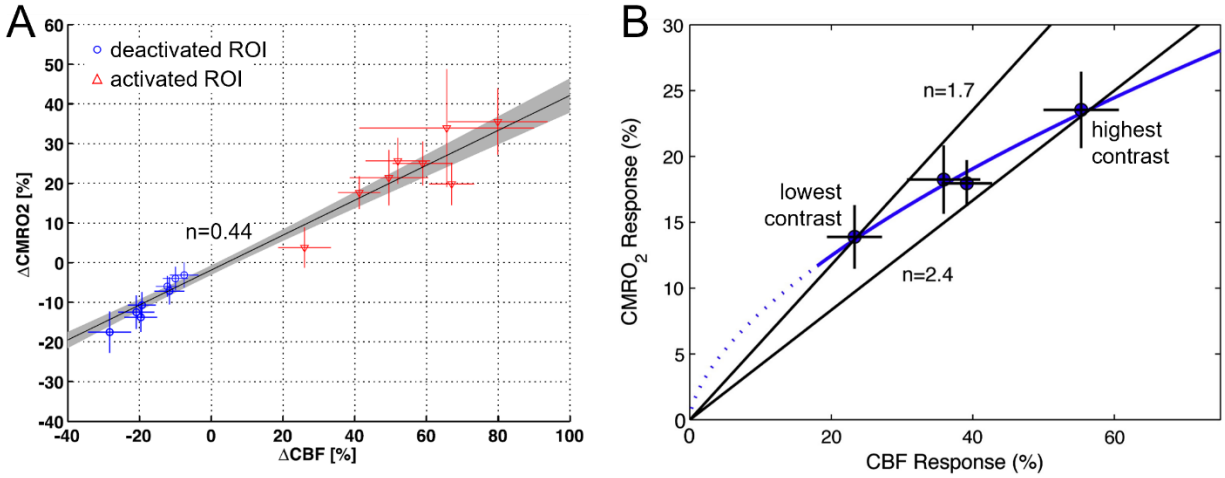

Figure 1.18. Loose coupling of vascular and metabolic responses. A. Linearly related CBF and $CMRO_2$ responses to hand movements across brains and across the activated contralateral and deactivated ipsilateral hemispheres. **B.** Sublinearly related CBF and $CMRO_2$ responses across visual stimulus intensities. Reproduce with permission from (A) Stefanovic et al. (2004) and (B) Liang et al. (2013).

The above view most tellingly accounts for visual fMRI data from Liang et al. (2013) and Moradi et al. (2012). In Liang et al. (2013), the CBF:$CMRO_2$ ratio increased with stimulus contrast (Figure 1.18B)—$CMRO_2$ saturated while CBF kept increasing, the latter being putatively driven by the stronger inhibitory activity required at high stimulus energy to prevent excessive excitation and energy consumption (Carandini & Heeger, 2012; Contreras & Palmer, 2003). In

Moradi et al. (2012), unattended stimuli also showed higher CBF:$CMRO_2$ ratios, which may here relate to top-down inhibition of irrelevant stimuli (Gilbert & Li, 2013). Quantitative fMRI may therefore not only provide more physiologically meaningful measures of neural activity, but also more computationally relevant properties like the underlying EI balance.

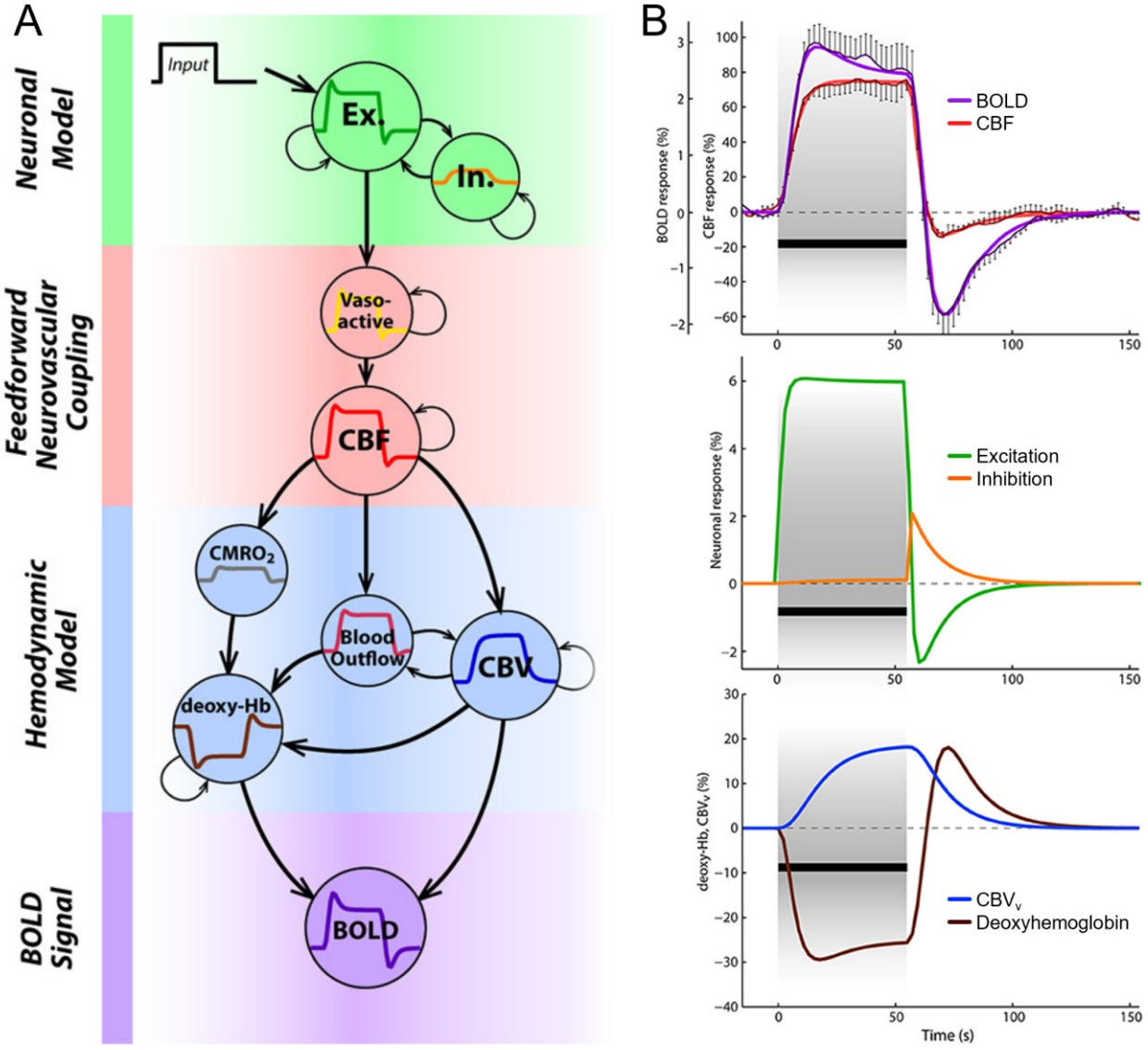

Figure 1.19 Detailed modeling of hemodynamics to unveil relevant neural dynamics. A. The output of a neural model involving excitatory and inhibitory neural populations is feed as input to a hemodynamic model. **B.** The model from A fitted to BOLD and CBF data (top panel) gives sensible predictions of the time course of excitation and inhibition (middle panel) and of CBV_v and deoxyhemoglobin (bottom panel). Adapted with permission from Havlicek, Ivanov, Roebroeck, et al. (2017).

Finally, the modeling work of Havlicek, Ivanov, Roebroeck, et al. (2017) is another example of leveraging detailed knowledge of hemodynamics to unveil relevant neural dynamics (Figure

1.19). In a nutshell, carefully constrained hemodynamic models (Figure 1.19A) can disambiguate vascular and neural contributions to transient phases of responses at the onset and offset of long stimulus blocks (Havlicek, Ivanov, Poser, et al., 2017; Havlicek et al., 2015; Havlicek, Roebroeck, et al., 2017). The particularly interesting touch in Havlicek, Ivanov, Roebroeck, et al. (2017)'s approach was to drive the hemodynamic model (Figure 1.19A, bottom three subpanels) with the output of a simple dynamic neural model involving excitatory and inhibitory neural populations (Figure 1.19A, top subpanel). Fitting such model to various fMRI data (Figure 1.19B) allowed to extract sensible time courses of neural excitation and inhibition (Figure 1.19B, middle panel).

Chapter 4 contributes to this quest for extracting neurally relevant information from fMRI signals. The novel approach taken relies, as in Buxton et al. (2014), on neuron-type-specific determinants of hemodynamic signals and, as in Havlicek, Ivanov, Roebroeck, et al. (2017), focuses on temporal aspects of the measured responses. It follows Farivar et al. (2011)'s hypothesis of a BOLD delay related to pathologically high interocular suppression in amblyopia. Conveniently by-passing the need for specialized fMRI sequences and for complex modeling and associated assumptions, **Chapter 4 aimed to**:

1. **modulate BOLD response delays through the manipulation of the EI balance with visual suppression stimuli in healthy adults**.

Chapter 2: TMS MODULATION OF PERCEPTUAL SUPPRESSION

PREAMBLE

TMS protocols for NIBM are making their way to patients' bedside despite little knowledge on their microcircuit-level mechanisms of action, which would be necessary for efficient and safe development of new brain therapies. This knowledge is so far virtually exclusively based on motor cortex studies, where microcircuit functions are accessible through measurable motor outputs carried by the corticospinal track upon a TMS pulse. We have however seen in Section 1.4.1.1 that that visual cortex microcircuitry also can be efficiently and non-invasively probed using well-established quantitative visual psychophysical methods. Moreover, the shape of the occipital pole exposes it to a particularly focal stimulation with TMS, the potency of which can be quickly assessed as in the motor cortex—though not as objectively—through a perceptual output taking the form of phosphenes. The combination of visual psychophysics and TMS of the occipital therefore bears untapped potentials for dissecting NIBM-induced microcircuit plasticity, assessing its cross-cortical and eventually predicting its therapeutic potential.

This potential is show-cased in this chapter's manuscript, under revision at Cerebral Cortex. It for the first time demonstrates that the effect of a popular NIBM protocol on intracortical inhibitory circuits generalizes from the motor to the visual cortex.

MANUSCRIPT TITLE: INHIBITORY RTMS OF THE OCCIPITAL POLE REDUCES INTRACORTICAL VISUAL SUPPRESSION

AUTHORS

Sébastien Proulx[1*], Abigail McLellan[1], Henry Yu[1] and Reza Farivar[1*]

AFFILIATIONS

[1]Department of Ophthalmology & Visual Sciences, McGill University, Montreal, Canada

* sebastien.proulx2@mail.mcgill.ca; reza.farivar@mcgill.ca

Montreal General Hospital, 1650 Avenue Cedar L11.409

Montréal, Québec, H3G 1A4, Canada

Tel: +1(514)-934-1934-44508

KEYWORDS

cTBS, interocular suppression, overlay suppression, surround suppression, visual masking

CONFLICT OF INTEREST

There are no known conflicts of interest associated with this publication and there has been no significant financial support for this work that could have influenced its outcome.

FUNDING

This work was supported by the Natural Sciences and Engineering Research Council (NSERC) Discovery grant (NSERC RGPIN 419235-2013) and NSERC and Fonds de la recherche en santé du Québec (FRSQ) PhD scholarships.

ACKNOWLEDGMENT

For pilot stages of this experiment, we would like to thank Robert F. Hess's lab for lending their TMS equipment and Danielle Krukowski for assisting with data acquisition. Thanks to Daniel Spiegel for his support in learning TMS methods.

2.1 Abstract

Transcranial Magnetic Stimulation (TMS) brain modulation with continuous Theta Burst Stimulation (cTBS) of the motor cortex reduces its excitability and TMS-measures of intracortical facilitation and inhibition. If cTBS effects generalize across cortices, targeting the visual cortex should decrease visual masking-measures of intracortical inhibition. To test that, we mapped and quantified phosphenes to target a titrated dose of cTBS to the unilateral occipital pole of 13 healthy humans. Visual contrast detection thresholds for a monocular luminance-modulated test grating were measured before and after cTBS in the targeted hemisphere, interleaving with measures in the opposite unstimulated control hemisphere. Four visual masks suppressed perception of the test stimulus: cross-oriented overlay or iso-oriented surround masks presented with the test in the same (monoptic) or in the opposite (dichoptic) eye. Monoptic overlay masking relying on sub-cortical processes, this condition controlled for non-specific changes in suppression. An additional no mask condition controlled for non-specific changes in contrast perception. Phosphene maps confirmed a well-lateralized TMS targeting of the cortical representation of the visual stimuli. cTBS reduced all three cortical types of suppression similarly, while sparing sub-cortical suppression and contrast perception. We conclude that inhibitory mechanisms of cTBS likely generalize across cortices, informing principled designs of cTBS therapies targeting non-motor cortices.

2.2 Introduction

Transcranial Magnetic Stimulation (TMS) pulses applied repetitively (rTMS) can trigger reversible plastic changes in the targeted brain tissue (Parkin et al., 2015; Wilson et al., 2018) and is widely used in cognitive and clinical research. Our knowledge of the neural underpinnings of these treatments heavily relies on studies of the motor cortex and measures of its excitability—the potency with which single TMS pulses can drive cortical pyramidal motoneurons and elicit a contraction of their target muscle. Depending mostly on the frequency or temporal pattern of rTMS, excitability can be driven up or down: rTMS at high frequencies (≥5Hz; HF-rTMS) or in intermittent theta bursts (iTBS) increases excitability (Huang et al., 2005; Pascualleone et al., 1994) whereas low-frequency rTMS (≤1Hz; LF-rTMS) and

continuous theta bursts (cTBS) decreases it (Chen et al., 1997; Chung et al., 2016; Wischnewski & Schutter, 2015).

cTBS increases bulk concentrations of GABA measured with Magnetic Resonance Spectroscopy (MRS) in the targeted motor (Stagg et al., 2009) and visual (Allen et al., 2014) cortices. The so-called "inhibition" of the targeted brain tissue by cTBS however does not seem to rely on increased function of inhibitory interneurons. GABA-dependent intracortical inhibition—specifically Short-interval IntraCortical Inhibition (SICI) measured with paired-pulse TMS in the motor cortex (Di Lazzaro et al., 2006; Ilic et al., 2002; Ziemann et al., 1996)—decreases after cTBS (Chung et al., 2016) or HF-rTMS (Fitzgerald et al., 2006). Furthermore, the few studies directly assessing TMS effects on neural activity in animals showed complex patterns of both facilitation and inhibition (Allen et al., 2007; Kozyrev et al., 2014; Kozyrev et al., 2018; Pasley et al., 2009), suggesting altered balance in the complex neural dynamics between facilitatory and inhibitory circuits (Wilson et al., 2018). Because of the importance of balanced excitation and inhibition in healthy cortical function, better understanding and generalization of these findings to inhibitory phenomena in non-motor areas will be crucial to interpreting behavioral and therapeutic effects of rTMS performed on cognitive brain areas.

In visual masking protocols, the perception of a visual *test* stimulus can be modulated—inhibited or facilitated—by the simultaneous presentation of a visual *mask* stimulus. Test and mask stimuli can be designed to separately drive and induce interactions between the different neural populations, which are embedded in the parallel topological representations of visual features such as visual field location, orientation and eye-of-origin. In *surround masking*, neural responses to visual gratings (Angelucci & Bressloff, 2006; Blakemore & Tobin, 1972; Zenger-Landolt & Heeger, 2003) and consequently their visibility (Nurminen et al., 2010; Petrov et al., 2005; Tolhurst & Thompson, 1975) changes when surrounded by an annular mask grating. Similar neural response (Li et al., 2005; Morrone et al., 1982) and visibility (Meese & Holmes, 2007; Petrov et al., 2005; Ross & Speed, 1991) modulations occur with *cross-oriented overlay masking*, where the mask overlays the stimulus in visual space but is orthogonally oriented. Masking can also be obtained by presenting stimuli to the same eye, *monoptic masking*, or to

opposite eyes, *dichoptic masking* (Deangelis et al., 1994; Kim & Mullen, 2015; Li et al., 2005; McKeefry et al., 2009; Sengpiel et al., 1998).

Proposed visual masking mechanisms involve lateral interactions between cortical columns through horizontal (Angelucci et al., 2017; Angelucci & Bressloff, 2006; Gilbert & Wiesel, 1989) or feedback connections (e.g. V2 to V1) (Angelucci & Bressloff, 2006; Bair et al., 2003; Nassi et al., 2013; Ozeki et al., 2009) influencing within-column recurrent amplification networks (Douglas et al., 1995; Ozeki et al., 2009) and normalizing cortical outputs (Carandini & Heeger, 2012). Interestingly, just like rTMS, masking involves both excitatory and inhibitory pathways (Foley, 1994; Meese et al., 2007; Ozeki et al., 2004; Xing & Heeger, 2001), leading to net facilitation or suppression depending on several stimulus parameters, high contrasts generally favoring suppression of neural responses (Sengpiel et al., 1998; Tajima et al., 2010) and perception (Nurminen et al., 2010; Petrov et al., 2005; Xing & Heeger, 2001). Visual masking protocols therefore offer the opportunity to dissect the intracortical excitatory and inhibitory effects of rTMS.

To the best of our knowledge, only two studies (Ling et al., 2009; Maniglia et al., 2019) adopted such an approach—measuring contrast sensitivity for masked stimulus in both the hemisphere targeted by 'inhibitory' 1Hz-rTMS and in the other unstimulated hemisphere. (Ling et al., 2009)'s results suggested increased suppression that did not depend on the orientation the mask that both overlayed and surrounded the test stimulus, while (Maniglia et al., 2019)'s results suggested increased facilitation from collinear flanker masks. These studies however lacked the crucial *no mask* condition to disambiguate changes in masking from changes in contrast perception *per se* (Antal et al., 2002; Clavagnier et al., 2013; Kaderali et al., 2015; Ling et al., 2009; Maniglia et al., 2019; Thompson et al., 2008).

This study takes advantage of visual masking protocols to probe the effects of rTMS on specific intracortical processes, while addressing limitations of previous studies (Ling et al., 2009; Maniglia et al., 2019) lacking a *no mask* condition crucial to disambiguate changes in masking vs changes in contrast perception *per se* (Antal et al., 2002; Thompson et al., 2008)}(Clavagnier et al., 2013; Kaderali et al., 2015). We used a heavily controlled, fully within-

subject single-session experimental design, where we targeted a titrated dose of rTMS to the unilateral occipital pole using quantified recordings of phosphene perception. We psychophysically probed the targeted brain tissue for its sensitivity to liminal luminance contrast gratings and susceptibility to different visual masks. Brain function localization was not a primary objective and we therefore did not use a control stimulation site. Unspecific rTMS effects were instead avoided by interleaving measures in the hemifield of the stimulated occipital pole with control measures in the hemifield of the unstimulated contralateral occipital pole, and by including stimulus conditions with no visual masking and visual masking of subcortical origin. Focusing on the "inhibitory" cTBS protocol (Huang et al., 2005) and on GABA-related intracortical inhibition (Cook et al., 2016; Ozeki et al., 2004; Yoon et al., 2010) with visual masks favoring suppression, our results show a hemisphere-specific reduction in visual suppression after cTBS, confirming the hypothesis that modulations of visual intracortical processes follow those found in the motor cortex.

2.3 Materials and Methods

2.3.1 Participants

We recruited selected participants based on stringent inclusion criteria, and controlled data quality for inclusion in final analyses. Twenty-six healthy adults, with normal or corrected-to-normal vision and properly performing the psychophysical task, were screened with occipital pole TMS. Sixteen reported reliable phosphenes and were recruited for the experiment. Data from three participants were excluded for unreliable TMS or psychophysical measures, leaving 13 for analysis (10 females; age: mean 25.8, range 18-35; Supplementary Table 2.1). The general procedure timeline is illustrated in Figure 2.1A, with details in sections below. Informed consent was obtained from all participants and the protocol NEU-13-043 approved by the Research Ethics Board of the Montreal Neurological Institute.

2.3.2 TMS: Phosphene-Guided Offline Modulation of the Unilateral Occipital Pole

2.3.2.1 Apparatus

All TMS used a commercial MagVenture MagPro X100 stimulator with the fluid-cooled Cool-B65 figure-of-eight stimulating coil (https://www.magventure.com/), with participants on a massage chair allowing to gently rest the coil on the back of the head, handle pointing rostrally

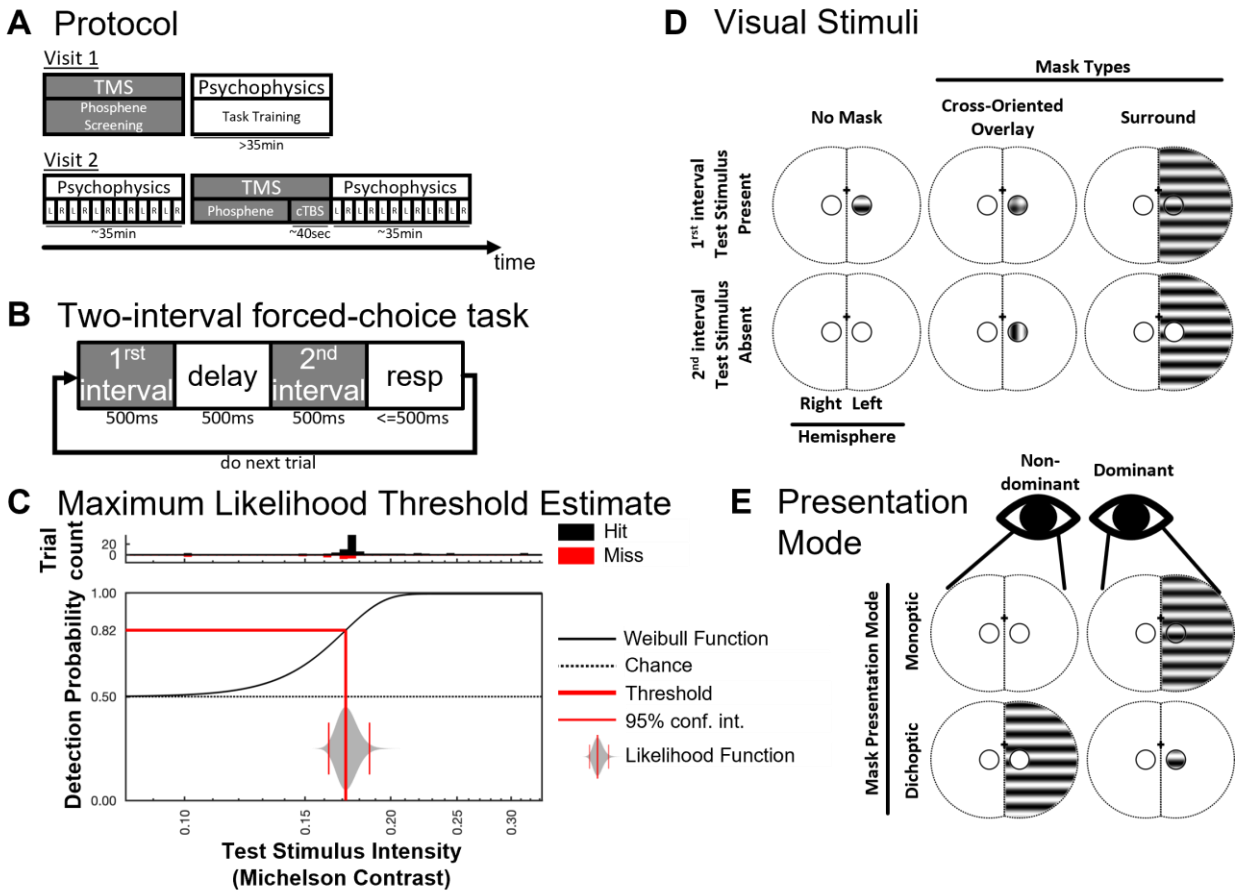

Figure 2.1 General Procedure and Psychophysics. A. On a first visit, participants underwent phosphene screening. Only those susceptible to occipital pole TMS were selected and trained on the psychophysical task, which estimated contrast sensitivity and visual suppression in alternating lower left (L) and right (R) quadrants, since the TMS-induced phosphenes could only be reliably induced in the lower visual field. On a second visit, the TMS session followed a phosphene-guided strategy to identify the single-hemisphere occipital pole target and titrate the dose of the cTBS treatment that followed within less than 5min (Figure 3A and C). **B.** Two-interval forced-choice psychophysical task, where participants are instructed to detect the interval within which the test stimulus was presented. **C.** Psychophysical data (top sub-panel) is analysed (bottom sub-panel) by computing the likelihood function (gray violin): the likelihood of a Weibull function (black trace) over a range of possible contrast values for its threshold parameter. The maximum of the likelihood is taken as the best estimate of the psychophysical threshold (thick red line), i.e. the contrast allowing 82% correct detection of test stimulus interval. **D.** Visual stimuli used for psychophysical measurements of contrast sensitivity and visual suppression. The black cross represents fixation, the small black-outline circles the test stimulus area and the large dotted-outline cropped circles the surround stimulus area. Stimuli shown here only for the right visual hemifield. The interval in which the test stimulus is present was randomized across trials. **E.** Representation of monocular on dichoptic presentation mode. For brevity of illustration, only surround mask type is shown here.

(upward), and using biphasic pulses with current direction set to normal. No neuro-navigation system was used. A 2×2cm grid of 0.5cm-spaced points on a rubber swim cap or thin fabric hat guided coil positioning.

All TMS (phosphene characterization and cTBS) was performed while fixating a faint 0.6-degrees of visual angle (dva) central cross on a 28.7×23.3 dva black background (Figure 2.3C) displayed on an LCD monitor at 47.5cm viewing distance. Participants' field-of-view was restricted to the black background with a black funnel attached between the massage chair and the monitor.

Verbal communication was possible at all times. A computer mouse and custom MATLAB code using Psychtoolbox-3 (Brainard, 1997; Kleiner et al., 2007; Pelli, 1997) allowed to collect "yes/no/maybe" reports (left/middle/right mouse clicks) of phosphene perception and their drawings, all displayed live to the experimenter.

2.3.2.2 Phosphene Characterization

Phosphene screening (Figure 2.1A) consisted of a heuristic ~10-minute "hunt" for the phosphene "hot spot" by applying single pulses within 1cm around the occipital pole target, i.e. 2cm above the inion on the midline (Salminen-Vaparanta et al., 2012; Salminen-Vaparanta et al., 2014). The experimenter sought clearly unilateral phosphenes reliably reported within the visual field area of our psychophysical measurements. It was performed on visit 1 to assess participants' eligibility.

The phosphene hunt was repeated at the beginning of the TMS session of visit 2, after which the coil's position was locked on the recovered hot spot with a mechanical arm. The position was maintained for the rest of the TMS session for the phosphene data collection and cTBS treatment described below.

Phosphene thresholds were obtained eyes-open with the visual field-of-view restricted to a dark background. Thresholds corresponded to the lowest stimulator power—in percent of maximum stimulator output (%MSO)—producing a phosphene on at least 4 out of 6 consecutive single pulses of TMS applied >5sec apart. Participants' forced yes/no choices (left/right mouse clicks) instructed the experimenter to lower the power in 2%-unit steps until phosphenes were no longer produced, i.e. below threshold power was reached (Sparing et al., 2005; Stokes et al., 2013; Waterston & Pack, 2010).

Phosphenes were then mapped relative to fixation with their outline and point of maximum intensity or center-of-mass drawn immediately after single pulses applied at phosphene threshold + 10%MSO. In most participants, a verbal cue switched attention from one lower visual field quadrant to the other on every pulse, for 10 pulses per quadrant. This was meant to avoid actually bilateral occipital pole stimulation appearing unilateral due to built expectations and attentional effects (Bestmann et al., 2007; Rangelov et al., 2015). Multiple or no drawings were allowed after a given pulse, but this was rarely required.

At any time, if the TMS coil's position was lost or large persistent changes in phosphene were observed, the whole TMS session started over.

2.3.2.3 cTBS

The cTBS treatment was applied while maintaining the TMS coil in position, immediately after phosphene characterization. The cTBS treatment used a standard protocol: 600 biphasic pulses in 50Hz bursts of 3 pulses, delivering bursts continuously at 5Hz for 40 seconds (Huang et al., 2005). Intensity was titrated at 80% of individual participant's phosphene threshold and was performed eyes opened fixating the cross on the dark background.

2.3.3 Psychophysics: Measurement of Visual Suppression

2.3.3.1 Apparatus and stimuli

All stimuli were generated using Psychtoolbox-3 (Brainard, 1997; Kleiner et al., 2007; Pelli, 1997) in MATLAB on a Windows workstation and displayed with 10-bit luminance levels over a mean gray background on a linearized analog CRT monitor (75-Hz refresh rate; 0.2164-mm pixel size) at an effective 34.4-cm viewing distance through a mirror stereoscope (~10×15dva field-of-view), forehead resting on the stereoscope. Permanently displayed binocular elements aided fusion (Supplementary Figure 2.2).

Visualized in Figure 2.1D, test and mask stimuli were built from vertical and horizontal 0.82-cpd sine-wave gratings, contrast-reversing every 100ms and presented at a 1.81-dva eccentricity position centered in a lower visual field quadrant. Stimulus intensities were defined as Michelson contrasts. The test stimulus had variable contrast expressed in natural log units

and was shown through a 1.51dva-diameter circular aperture. A faint circle indicated the test stimuli area. Fixed-contrast mask stimuli included (1) *cross-oriented overlay masks*, horizontally presented at 75% contrast through the same aperture as the test and (2) *surround masks,* vertically presented at 96% contrast through an annular aperture of 1.73-dva inner and 9.78-dva outer diameters centered around the test stimulus. The small portion of the surround mask overlapping the contralateral hemifield was masked out for strictly unilateral visual stimulation (see Figure 2.1D). The test stimulus was monocularly presented to the dominant eye identified from a quick binocular rivalry test of sensory eye dominance (Dieter et al., 2017). The mask stimuli were presented either (1) *monoptically* to the same eye as the test or (2) *dichoptically* to the other eye. Edges of all apertures were softened with a 0.25-cpd half-sine ramp. The actual psychophysical display is reproduced in Supplementary Figure 2.2.

2.3.3.2 Task and Visual Suppression Masking

Sensitivities for at-threshold perception of luminance contrast were inferred from the inverse of contrast thresholds for the detection of the test stimulus. They were obtained under several *stimulus conditions* using a two-interval forced-choice task with auditorily-cued 500-ms intervals separated by 500ms and followed by a minimum 500-ms response period (Figure 2.1B). On each trial, participants reported the randomly selected interval that contained the test stimulus through a key press, initiating the next trial.

Trials were obtained from 5 *stimulus conditions* (Figure 2.1D and E). Sensitivity to at-threshold contrast was evaluated in a control (1) *no mask* condition where the test was presented alone. Contrast sensitivities under visual suppression were evaluated in four *masking* stimulus conditions, where one of the above-described mask stimuli, namely the (2) *monoptic cross-oriented overlay*, (3) *monoptic surround*, (4) *dichoptic cross-oriented overlay* or (5) *dichoptic surround* masks, was added to both intervals. Trials from a given stimulus condition were grouped in ½-min mini-blocks of 16 consecutive trials of the same condition, with one mini-block per condition randomly interleaved within a ~3-min acquisition block. Each new mini-block began with brief blinks of the fixation and two dummy trials, using maximum then slightly above-threshold test contrasts, which allowed participants to confidently identify and prepare for the new stimulus conditions. Consecutive blocks alternated measurements in the 2

hemisphere conditions by moving the fixation across the stimulus field. Blocks were separated by short breaks of ½ to 1min or more if needed. A psychophysical session therefore totaled ~45 min for the acquisition of 96 trials per interleaved stimulus × hemisphere conditions.

Contrast of the test stimulus was independently controlled in the 10 (5 stimulus × 2 hemisphere) conditions by parallel realisations of an adaptive staircase procedure. The latter combined a QUEST Bayesian (Kingsmith et al., 1994; Watson & Pelli, 1983) with classic 2up-1down staircases (see Supplementary Methods for more details). From our simulations and experience, this allows for rapid yet robust convergence of data acquisition to a contrast range close to threshold.

2.3.4 Analysis

Phosphene count maps (Figure 2.3C) were built from cumulating phosphene area (convex hull of outlines) across drawings. Dividing by the number of trials (single-TMS pulses applied) yields the phosphene probability maps used for cross-participants averaging (Figure 2.4).

Analysis of psychophysical data relied on the likelihood function of thresholds (Figure 2.1C), derived for each stimulus and hemisphere conditions and each session using the QUEST toolbox (Kingsmith et al., 1994; Watson & Pelli, 1983). It expresses the likelihood of a psychophysical Weibull function (3.25 slope; 50% guess rate; 5% lapse rate) as a function of its 87%-correct threshold contrast, given the psychophysical data and (here non-informative) priors. Quality assurance sought narrow single-peaked likelihood functions. Contrast at the peak—the mode of the likelihood function—was taken as the best estimate of the psychophysical contrast detection threshold.

Repeated-measures ANOVAs (rmANOVA) used IBM SPSS Statistics 23 and in-house MATLAB scripts with Sidak correction for multiple comparisons. Bayesian one-sample and paired sample t-tests and Bayesian one-way rmANOVA were all performed in JASP 0.9.2.0 (Rouder et al., 2012; Verhagen & Wagenmakers, 2014; Wagenmakers et al., 2016) and used default Cauchy priors (scale=0.707). Bayesian Factors (BF) quantified evidence for the alternate two-tailed hypothesis of any change (BF_{10}), or one-tailed hypothesis a positive (BF_{+0}) or negative (BF_{-0}) changes, against the null hypothesis of no change. The inverse of these BFs correspondingly quantify

evidence for the null hypothesis (BF_{01}, BF_{0+} or BF_{0-}). BF qualitative interpretation followed Wagenmakers, Love, et al. (2018), where e.g. a BF_{10} (or BF_{01}) in the <1, 1 to 3, 3 to 10 or >10 range respectively indicates no, anecdotal, moderate or strong evidence for the alternate (or null) hypothesis. Moderate or strong evidence is analogous to a significant ($p<0.05$) frequentist inference test.

All error ranges shown represent non-parametric 95% confidence intervals from 100,000 bootstrapped resamples, except for likelihood functions where the Bayesian 95% Credible Intervals are represented (Figure 2.1C and Figure 2.3B and D).

2.3.5 Data and Code Availability

Psychophysics and phosphene data, along with example code, are available online (Proulx et al., 2020) at https://doi.org/10.5281/zenodo.4101627.

2.4 Results

We first report the results of our psychophysical assessment of visual suppression at baseline, showing potent visual masking as expected from previous psychophysical studies. We next report the results of the phosephene localization that shows we were able to effectively stimulate the occipital cortex in a reliable manner, and that the location of the induced phosphenes corresponded with our visual stimulus. Finally, we report our key findings of TMS-induced modulation of visual suppression.

2.4.1 Cortical Visual Suppression at Baseline

We expressed visual suppression as the elevation of contrast detection thresholds induced by the presence of a mask stimulus—high threshold elevation indicates strongly suppressed liminal perception of test-stimulus contrast. All visual masks potently suppressed perception in

all participants (Figure 2.2), with means(sd) of 0.54(0.11), 0.65(0.09), 0.39(0.13) and 0.40(0.15) log-unit threshold elevations respectively for *monoptic cross-oriented overlay*, *dichoptic cross-oriented overlay, monoptic surround* and *dichoptic surround* masks, relative to a mean(sd) of -1.72(0.05) log-unit contrast threshold in the *no mask* condition (Figure 2.1D). Despite their lower intensity (i.e. lower contrast), overlay masks were more potent than surround masks (main effect of Mask Type: $F_{1,12}$=36.3, p<0.001). Importantly, the impact of Mask Presentation Mode (monoptic vs dichoptic) depended on Mask Type (overlay vs surround) (Mask Presentation Mode × Mask Type interaction: $F_{1,12}$=8.4, p<0.05). Dichoptic presentation increased overlay suppression by 20.9% (*post-hoc* t-test: corrected p<0.01) but did not affect surround suppression (*post-hoc* t-test: p=0.85). This observation is consistent with published evidence that suppression arises subcortically for stimuli overlapping in the same eye (Freeman et al., 2002; Katzner et al., 2011; Li et al., 2005; Priebe & Ferster, 2006; Spiegel et al., 2012).

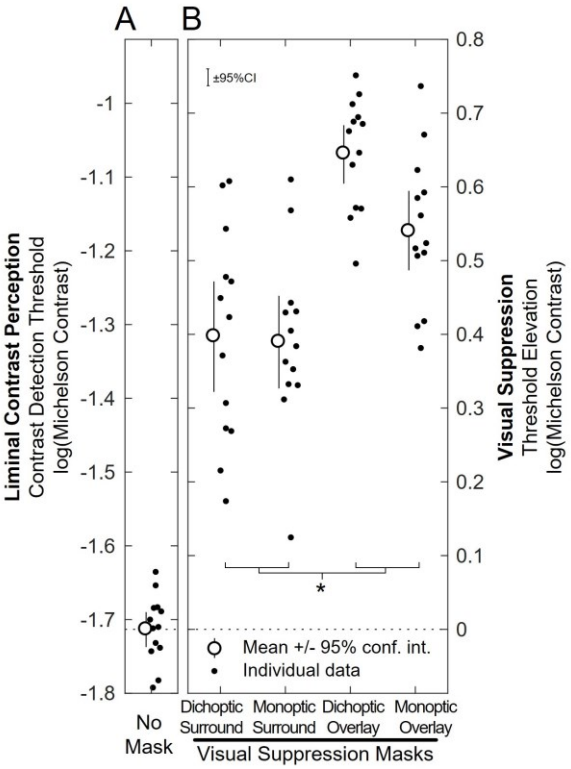

Figure 2.2 Visual Suppression. A. Contrast threshold for detection of the test stimulus when presented alone. Lower thresholds indicate higher sensitivities to luminance contrast. **B.** Visual suppression expressed as threshold elevation (mask – no mask) induced by the mask in each masking condition. Higher threshold elevations indicate stronger visual suppression. Data are averaged across hemispheres and pre/post cTBS sessions. *: p<0.05; Error bars: 95% bootstrapped confidence interval.

2.4.2 Phosphene-guided TMS of the Unilateral Occipital Pole

Phosphene thresholds averaged to 72.5 %MSO and ranged between 60 and 91 %MSO across participants (Supplementary Table 2.1 for details). Qualitative descriptions of phosphenes were overall consistent with TMS targeting early visual areas V1, V2 or V3 (Kammer, 1999; Kammer, Puls, Erb, et al., 2005; Kammer, Puls, Strasburger, et al., 2005; Kastner et al., 1998; Schaeffner & Welchman, 2017), with phosphenes being most often simple-shaped (a blob, ring or line), non-moving, non-colored (black or white) and generally showing no or little texture.

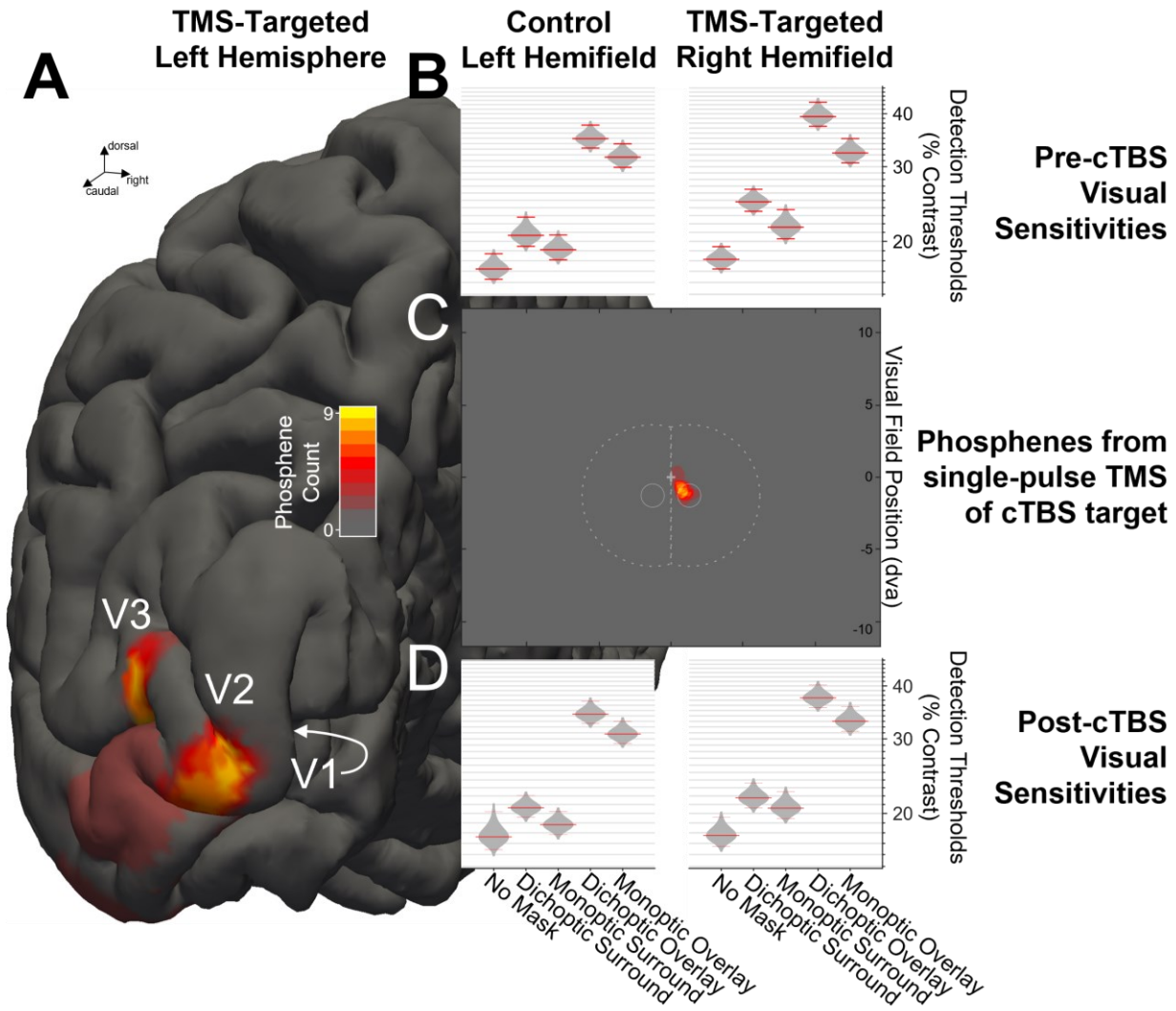

Figure 2.3 Single-Subject Example. A. 3D surface reconstruction of one participant (sp01) for whom anatomical MRI data was available. Retinotopy (not shown) and visual areas were obtained through the registration of a probabilistic retinotopic atlas (Benson et al., 2012; Benson et al., 2018). The overlay does not represent a physiological response, but rather the phosphene map in C, projected from the visual field space to the cortical space. In this participant and for illustrative purposes only, the patch retinotopic cortex representing the phosphenes' visual field location that appears closest to the TMS coil targeting the occipital pole is located in visual area V2, while the V1 representation of the phosphenes is buried into the calcarine sulcus. **B.** Psychophysical data from the pre-cTBS session, expressed as likelihood functions and 95% C.I. of test stimulus detection thresholds as in Figure 1C. **C.** Quantified representation in visual field space of phosphenes perceived upon single-pulse TMS applied at the site of the cTBS treatment. The size of the frame corresponds to the visual field area over which participants could outline their phosphenes over a dark background. The white cross represents fixation, and the other faint white graphic elements (not shown to participants) outline the visual stimuli used to collect the psychophysical data in B and D and visualized in **Figure 2.1**D and E. Participants were shown the outline of their phosphene drawing only while they were drawing it. The color scale indicates the number of phosphenes that covered a given visual field location. **D.** Psychophysical data from the post-cTBS session, expressed as in B.

Phosphene count maps revealed well-lateralized phosphenes concentrating on a center point and well overlapping the stimulus field in all participants (Figure 2.3C and Supplementary Figure

2.1). Group-level phosphene probability maps (Figure 2.4) further showed TMS mostly targeted the cortical representation of the psychophysical test stimulus. Shifting attention between hemifields did not reveal consistent phosphenes contralateral to the main focus (Figure 2.4 and Supplementary Figure 2.1). For visualization only, Figure 2.3A shows the projection of the phosphene count map onto retinotopic visual areas rendered as an overlay on the reconstructed cortical surface of a participant for which a brain MRI was available. These results overall suggest focal stimulation of a single occipital pole, targeting the brain tissue from which visual suppression was measured and leaving the contralateral occipital pole unstimulated.

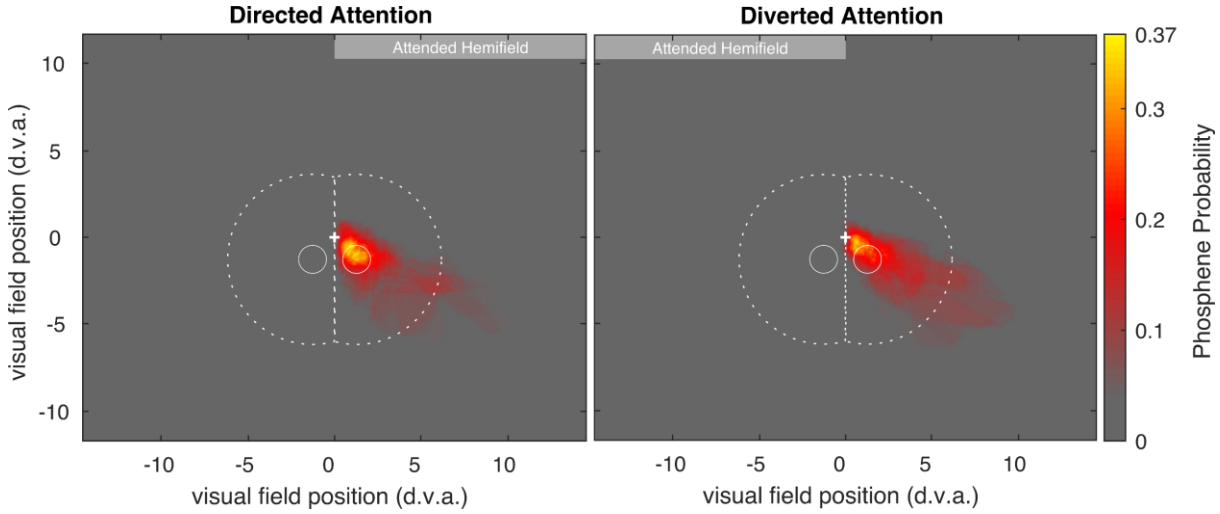

Figure 2.4 Group-Level Phosphene Probability Map. Maps were obtained when participants attention was directed to the phosphene location (A) or away to the contralateral hemifield (B). Attention was not modulated in two participants and their map were included in the condition of attention directed to the phosphene location. The effect of contralaterally directed attention was minimal, slightly shifting the probability mass toward the fixation. Importantly, it did not significantly uncover phosphenes in the contralateral hemifield, suggesting unilaterally restricted TMS. See supplementary Figure 1 for data from individual participants.

2.4.3 Occipital Pole cTBS Reduces Cortical but not Subcortical Visual Suppression

By decreasing intracortical suppression as in the motor cortex (Chung et al., 2016), occipital pole cTBS should release the suppressive effect of visual masks. Using the unstimulated contralateral hemisphere as a control, cTBS did show moderate evidence for increased

detection performance measured under visual suppression (four masking conditions averaged: BF_{-0}=4.57, data not shown).

Supported by subcortical processes, visual suppression between stimuli overlaid in the same eye should be spared by cortical cTBS (Freeman et al., 2002; Katzner et al., 2011; Li et al., 2005; Priebe & Ferster, 2006; Spiegel et al., 2012); performance under monoptic overlay suppression was indeed unaffected (Figure 2.5; BF_{0-}=6.16, moderate evidence). Performance under the three cortical types of visual suppression all showed anecdotal evidence for decreased suppression (Figure 2.5's three light red bars; BF_{-0}=1.79, 1.05 and 1.50 from left to right). These effects were similar to one another (one-way rmANOVA, BF_{01}=5.17, error=0.67%, moderate evidence) and when averaged provided strong evidence for decreased visual suppression (Figure 2.5; BF_{-0}=11.3) that was specific to the cortical types (Figure 2.5; average of cortical masks vs subcortical mask: BF_{-0}=4.34, moderate evidence).

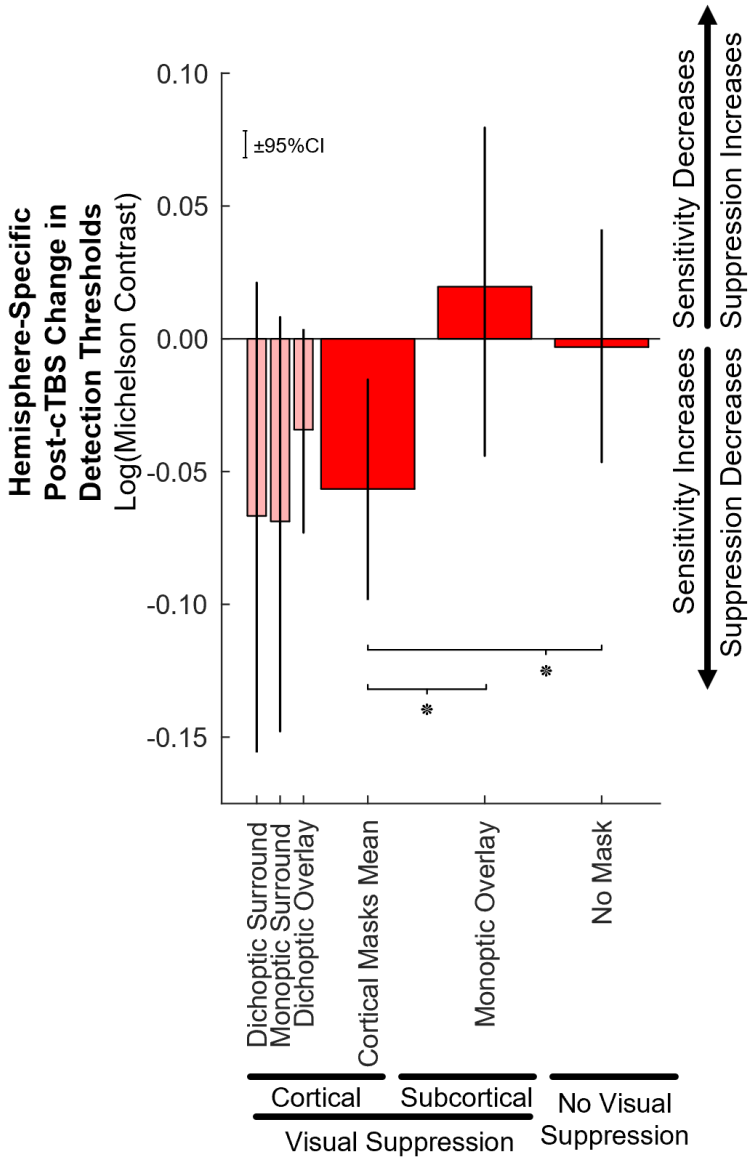

Figure 2.5 Hemisphere-Specific Effect of Unilateral Occipital Pole cTBS. Changes in contrast detection thresholds in the occipital pole targeted by cTBS are controlled for non-specific changes by subtracting changes simultaneously measured in the control unstimulated contralateral hemisphere. Decreased thresholds indicate facilitated liminal perception of visual contrasts, which can result either from increased contrast sensitivity or decreased visual suppression. :* BF>3, moderate (significant) evidence against the null hypothesis; Error bars: bootstrapped 95% C.I.

Finally, cTBS spared the detection of unmasked test stimulus (Figure 2.5, no mask condition; BF_{01}=3.54, moderate evidence). This confirms the increased performances described above do not reflect changes in sensitivity to contrast *per se* but rather result from reduced intracortical visual suppression (Figure 2.5, average of cortical masks vs no mask; BF_{-0}=9.02, moderate evidence). The hemisphere-specific reduction in cortical visual suppression (threshold elevation) amounts to ~10%. The breakdown of results in each hemisphere is reported in Supplementary Figure 2.3.

2.5 DISCUSSION

We found support for occipital rTMS modulating cortical suppression in a way similar to observations in the motor cortex. Specifically, standard cTBS similarly decreased the three cortical types of visual suppression tested. Our phosphene-guided approach ensured that an individually titrated dose of cTBS reached a single occipital pole in all selected participants, and that it generally co-localized with the patch of retinotopic cortex from which the psychophysical measures were taken. Furthermore, baseline behavioral performances confirmed that our consistent set of visual stimuli evoked and sensitively measured the well-characterized phenomena of visual suppression. Finally, three psychophysical controls ruled out effects of time, a modulation of contrast perception *per se* and a general effect on suppression non-specific to intracortical processes. We demonstrated the potential of visual psychophysics to dissect the intracortical circuits modulated by rTMS and assess generalizability across cortices.

2.5.1 Probing rTMS Modulation of Intracortical Processes in Motor and Visual Cortices

Our results suggest cTBS may reduce cortical visual suppression the same way it reduces SICI in the motor cortex (Bradnam et al., 2010; Chung et al., 2016; Huang et al., 2005). Motor cortex investigation of the effect of various brain modulation protocols heavily relies on paired-pulse TMS protocols. Single-pulse TMS of the motor cortex triggers a contraction of the target muscle, a physiological effect quantifiable as motor evoked potentials (MEP). In paired-pulse protocols, a conditioning pulse triggers intracortical excitatory and inhibitory circuit activity, which modulates the corticospinal response to a second test pulse. Intervals <=5ms and low conditioning pulse and high test pulse intensities favor GABAergic synaptic activity on

corticomotoneurons, reducing test pulse MEPs (Di Lazzaro et al., 2006; Ilic et al., 2002) and thereby providing an index of intracortical inhibition that is extensively used to dissect the physiology of rTMS brain modulation of the motor cortex.

The overt output of the visual cortex upon single-pulse TMS is the perception of phosphenes (Marg & Rudiak, 1994). Paired-pulse TMS in the visual cortex has been investigated from phosphene thresholds (Sparing et al., 2005) and sizes (Khammash et al., 2019a, 2019b), showing an inhibitory effect on phosphene size generally compatible with motor cortex phenomenology. Although of value, the lack of an objective measure of phosphene perception—it is an internal subjective criterion that guides observer's response—limits the reliability and internal validity of this approach to the investigation of intracortical processes. Measurement of perception of visual stimuli, on the other hand, is objective through validated psychophysical methods—the subjective criteria confound is removed through a forced choice between target and null stimuli. We argue that visual psychophysics provides a means to dissect and quantify physiological processes of the visual cortex that can be as precise and valid as MEP investigation of motor cortex processes.

Visual psychophysics enjoys a more flexible experimental space compared to TMS that is limited to stimulus strength and timing. Here we exploit the space of a visual masking protocol with stimuli well-known to evoke and quantify interactions between early visual cortex neural populations tuned to the mask and test stimuli. The visual mask stimulus is analogous to the conditioning stimulus in paired-pulse TMS–it triggers modulatory activity in intracortical excitatory and inhibitory circuits. In this perspective, the modulatory effects measured by MEPs in motor cortex studies is analogous to the modulatory effects of perceptual thresholds measured with visual psychophysics, both putatively representing underlying intracortical interactions.

Guided by an extensive body of literature on visual psychophysics, brain imaging and electrophysiology of visual suppression, one can alter various stimulus parameters for probing different early intracortical circuits. Here we chose to focus on inhibitory circuits generally most active with high-intensity masks. A large array of masking and other validated psychophysics

paradigms is, however, available for further dissecting intracortical processes and characterizing rTMS effects beyond modulation of the excitability of the targeted brain tissue.

2.5.2 Cortical and Subcortical Visual Suppression

One of our controls relied on a distinction between visual suppression of cortical vs subcortical origin. Electrophysiology, pharmacological, imaging and psychophysical data showed both surround and overlay masking to be orientation-tuned (Busse et al., 2009; Cavanaugh et al., 2002; Chen, 2014; Deangelis et al., 1992; Petrov et al., 2005), adaptable (Baker et al., 2007; Sengpiel & Vorobyov, 2005; Webb et al., 2005) and transferable between eyes (Baker et al., 2007; Jakobsson, 1985; Li et al., 2005; Moradi & Heeger, 2009; Petrov & Mckee, 2009; Webb et al., 2005)—three mostly cortical phenomenon (Kohn, 2007; Werner & Chalupa, 2004).

Subcortical mechanisms, however, contribute to at least some of the masking effects (Busse et al., 2009; Freeman et al., 2002; Li et al., 2005; Spiegel et al., 2012) and can entirely account for suppression in the case of monoptic cross-orientated overlay masking (Priebe & Ferster, 2006). Indeed, driving lateral geniculate nucleus (LGN) neurons with monoptic masks that flicker too fast to trigger cortical spikes nevertheless strongly suppress cortical neurons that respond to the test stimulus (Freeman et al., 2002) and such suppression was unaffected by local antagonisms of V1 $GABA_A$ receptors (Katzner et al., 2011). Human psychophysics showed monoptic overlay masks are immune to adaptation and carry a faster suppressive signal compared to dichoptic presentation (Baker et al., 2007). Finally, tDCS of the human occipital cortex showed a polarity-dependent modulation of monoptic surround masking but left monoptic overlay masking unaffected (Spiegel et al., 2012). It is therefore reasonable to consider that our occipital pole treatment should *a priori* have no direct effect on subcortically driven monoptic overlay suppression, and therefore constitute an appropriate control for non-specific visual suppression effects.

Our pattern of visual suppression at baseline is consistent with this cortical-subcortical distinction. Reliance on different brain areas for monoptic and dichoptic overlay suppression can account for the observed difference in potency, whereas the absence of difference for the

surround masks implies cortical binocular neurons indiscriminately support monoptic and dichoptic surround suppression (Figure 2.2; but see Petrov and Mckee (2009)).

The possibility of indirect effects of cTBS through subcortical feedback connections cannot be excluded. Indeed, rTMS of the early visual cortex can affect dLGN spiking responses to visual stimulation, as shown during rTMS in anesthetized cats (de Labra et al., 2007) and after rTMS in awake monkeys (Ortuno et al., 2014). However, if these phenomena—observed using high contrast visual stimuli—had any effect in humans on the detection of liminal visual stimuli or its suppression, it went undetected in our experiment.

2.5.3 Relation to Previous Findings

There are two other reports on visual masking after 1-Hz low-frequency rTMS (LF-rTMS), a brain modulation protocol classified along with cTBS as generally excitability reducing. Consistent with our findings, Maniglia et al. (2019) found increased sensitivity for contrast stimuli flanked by facilitatory collinear masks. On the other hand, Ling et al. (2009) found decreased sensitivity for contrast stimuli embedded in suppressive noise masks. Confounding effects on contrast perception alone cannot be firmly excluded due to the lack of no-mask control conditions in both studies. Discrepancies could also arise from the use of different masking stimuli, or from LF-rTMS and cTBS differently affecting intracortical processes despite similarly reducing excitability (Di Lazzaro et al., 2010). Interestingly, Ling et al. (2009) also reported a diminished tilt-repulsion illusion. This phenomenon being understood as the consequence of functional inhibition between neuron pools tuned to different orientations, its reduction could be interpreted as reduced suppression, consistent with our own findings. The two excitability reducing treatments—LF-rTMS and cTBS—may therefore similarly reduce occipital intracortical suppression, but a direct comparison is lacking.

Sensitivity to liminal contrast was left unaffected by occipital pole cTBS in our study. This seems at odds with evidence of generally decreased visually-evoked potentials after excitability-reducing LF-rTMS (Bocci et al., 2011; Bocci et al., 2016; Bohotin et al., 2002; Fumal et al., 2003), which should lead to decreased contrast sensitivity as found by others in healthy humans after cTBS (Ling et al., 2009) and in the healthy fellow-fixing eye of amblyopic patients

after cTBS (Clavagnier et al., 2013) and LF-rTMS (Thompson et al., 2008). Comparison is complicated by several protocol discrepancies, including pulse patterns (cTBS vs LF-rTMS), disease states and time scales (measures interleaved with rTMS every 5-6min in Ling et al. (2009)). One study by Kaderali et al. (2015) closely follows ours and measured contrast detection threshold of unmasked (but moving) stimuli up to 60min after cTBS of the occipital pole, and found no difference relative to a no stimulation control and stimulation of other cortical areas.

2.5.4 Limitations

A limitation of our approach lies in the TMS most certainly reaching both the neural populations tuned to the test and the mask stimuli—cortical columns representing the overlaid stimuli intermingle at the millimeter scale and representations of center and surround are close neighbors. As mentioned above, excitability-reducing LF-rTMS depresses visual evoked potentials (VEP) (Bocci et al., 2011; Bocci et al., 2016; Bohotin et al., 2002; Fumal et al., 2003). It is conceivable that excitability reductions are observable only with the high-contrast stimuli typically used for VEPs, but as observed here and by Kaderali et al. (2015), not in low-contrast perception, which could even be facilitated (Allen et al., 2014; Waterston & Pack, 2010). In this scenario, the effect of cTBS reported here may not result from decreased potency of inhibitory circuits *per se*, but from a reduced drive to these inhibitory circuits by mask stimulation. This possibility is supported by weaker effects of LF-rTMS on VEP measured with lower-contrast stimuli (Bocci et al., 2011) and no effect of cTBS on VEP from liminal stimuli (Allen et al., 2014), but requires further validation.

Another limitation is the significant interindividual variability of the visual field position of phosphenes relative to the psychophysical test stimulus (Supplementary Figure 2.1)—or of the cortical tissue targeted by TMS vs psychophysically characterized. Similarly, although V2 was identified in one participant (Figure 2.3), TMS likely targeted any of V1, V2 or V3 in other participants (Kammer, 1999; Kammer, Puls, Erb, et al., 2005; Kammer, Puls, Strasburger, et al., 2005; Kastner et al., 1998; Schaeffner & Welchman, 2017). These sources of variability could be characterized through some parameterization of the overlap between the phosphenes and the test stimulus, and with brain imaging data for identifying the targeted visual area (Figure 2.3) in

each participant. Included as between-subject factors in a better powered repetition of our protocol, these sources of variability could be leveraged to further dissect how TMS affect different cortical tissues.

2.6 Conclusion

Visual suppression can be modulated in a hemisphere-specific fashion with occipital pole cTBS. This modulation is similar to the decreased intracortical inhibition repeatedly observed in the motor cortex. Our findings provide a physiological interpretation of cTBS likely generalizable across cortices. Our approach highlights the potential of psychophysics of lower visual processes for further dissecting brain modulations at the microcircuit level non-invasively.

2.7 Supplementary Materials

2.7.1 Adaptive Procedure for Optimal Psychophysical Data Collection

Visual performance was evaluated from contrast thresholds for detection of the test. Such threshold needed to be robustly estimated for 10 (5 stimulus x 2 hemisphere) conditions within a potentially limited ~1-hour time window for cTBS effects. We therefore combined a QUEST Bayesian adaptive psychometric method (Kingsmith et al., 1994; Watson & Pelli, 1983) with a 2up-1down staircase to maximize efficiency (collecting data in the steep section of the psychometric function) and robustness (high rate of convergence to reliable estimates within a fixed number of trials).

On most trials, contrast of the test followed a QUEST Bayesian adaptive method (Kingsmith et al., 1994; Watson & Pelli, 1983), which aims at performing trials at threshold, where the psychometric function is steepest (increase efficiency). On each trial, the threshold is estimated from prior knowledge of the expected threshold and available data, and the trial is performed at a test contrast corresponding to that threshold estimate. The response is then used to update the threshold estimate to be used for the next trial. More precisely, the threshold estimate is taken from the mean of the posterior distribution of thresholds, the latter being derived from the combination of a Gaussian prior distribution of the threshold with the likelihood function of thresholds given the available data. Prior distribution of thresholds was

broad (sd=2.00) and centered at -1.71 and -0.75 for the no mask and masking conditions respectively. The likelihood function expressed the likelihood of a Weibull psychometric curve (3.25 slope; 50% guess rate; 5% lapse rate) as a function of threshold of the Weibull. On the first trial, threshold (and decision on the contrast to test) is solely based on prior knowledge. As evidence cumulates with the data the threshold estimate refines and contrasts tested converge to an optimal point at true threshold.

From previous experience in our lab with a similar task, this QUEST method alone was sensitive to lapses occurring early in the procedure, biasing the adaptive procedure toward inefficiently collecting many trials at contrasts well above the actual threshold and leading to failure to converge. As a heuristic approach to alleviate this issue, our combined procedure automatically fall-back to a 2up-1down staircase of 0.4 log unit contrast step size for 8 trials each time the online Quest threshold estimate increased high above the prior distribution center. Simulations showed the incorporation of the staircase fall-back to decrease convergence failure (increase robustness) with minimum cost on data collection efficiency. About 5% of the trials ended being collected in this staircase fall-back mode.

2.7.2 Data Availability

Processed data are available at https://doi.org/10.5281/zenodo.4101627. Raw data are available upon request to the corresponding author.

2.7.3 Supplementary Tables

SubjID	Demographics		TMS							
			Coordinates		Phosphenes		cTBS			
	Age	Sex	hor.	vert.	Thresh.	Qualia	1st Pulse Power			3rd Pulse Roll-Off
	(yrs)	(F/M)	(cm)	(cm)	(%MSO)	(B/G/W/C/T)	(%MSO)	(A/µsec)	(%phos. thresh.)	(%power of 1st pulse)
sp01	33	M			76	B	61		80.3 %	
sw01	22	F			76	G	61	92	80.3 %	97 %
af04	32	F			60		48	72	80.0 %	100 %
az10	25	F	-1.0	0.0	64	W	51	79	79.7 %	100 %
kc11	23	F	0.5	1.0	74	G	59	89	79.7 %	98 %
js12	28	F	0.0	-1.0	68	B	54	80	79.4 %	100 %
gv14	18	M	0.5	0.0	91	W	73	110	80.2 %	88 %
lb16	35	F			70		56	84	80.0 %	100 %
sb17	28	F	1.0	-1.0	66	WB	53	79	80.3 %	100 %
mk18	24	F	-1.0	1.0	83		66	99	79.5 %	94 %
ks19	25	F			67	GCT	54		80.6 %	
jn22	23	M	0.0	-2.0	84	C	67		79.8 %	
ca24	20	F	-1.0	-1.0	64	G	51	76	79.7 %	100 %
min	18		-1.0	-2.0	60		48	72	79.4 %	88 %
max	35		1.0	1.0	91		73	110	80.6 %	100 %
mean (count)	25.8	(10/3)	-0.13	-0.38	72.5	(3/4/3/2/1)	58.0	86.0	79.96%	97.7%

Supplementary Table 2.1 Demographics and Experimental Parameters. TMS cranial coordinates are centered 2cm above the inion. String code for phosphene qualia: B→Black (or darker than the dark background); G→Gray (or faint grayish); W→White (or bright); C→Colored; T→Textured; more than one letter indicates variable or combined qualia. Roll-off of cTBS refers to the power decrease from the first to the last pulse of triple-pulse theta bursts, a hardware limitation only at high power. %MSO: % of maximum stimulator output.

2.7.4 Supplementary Figures

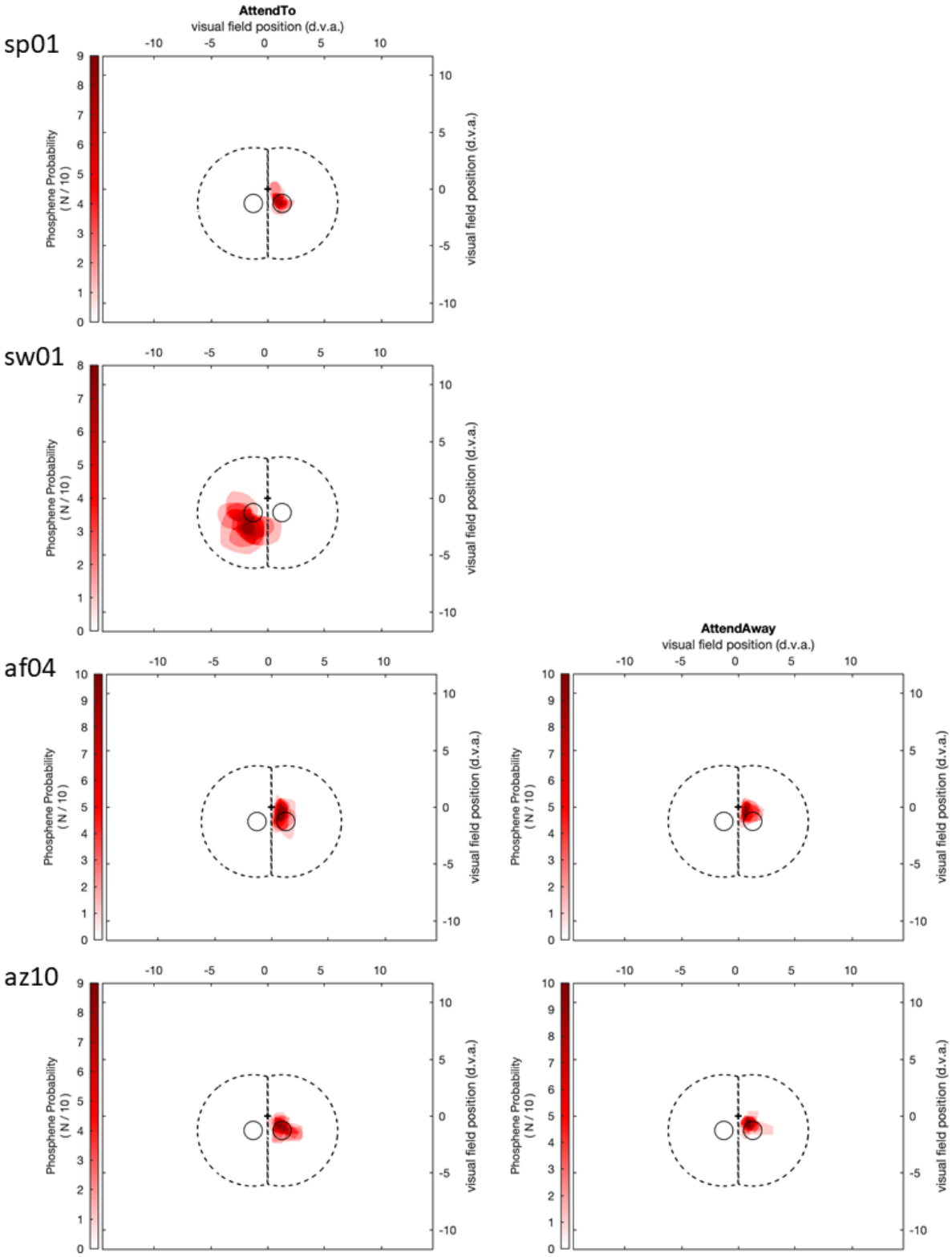

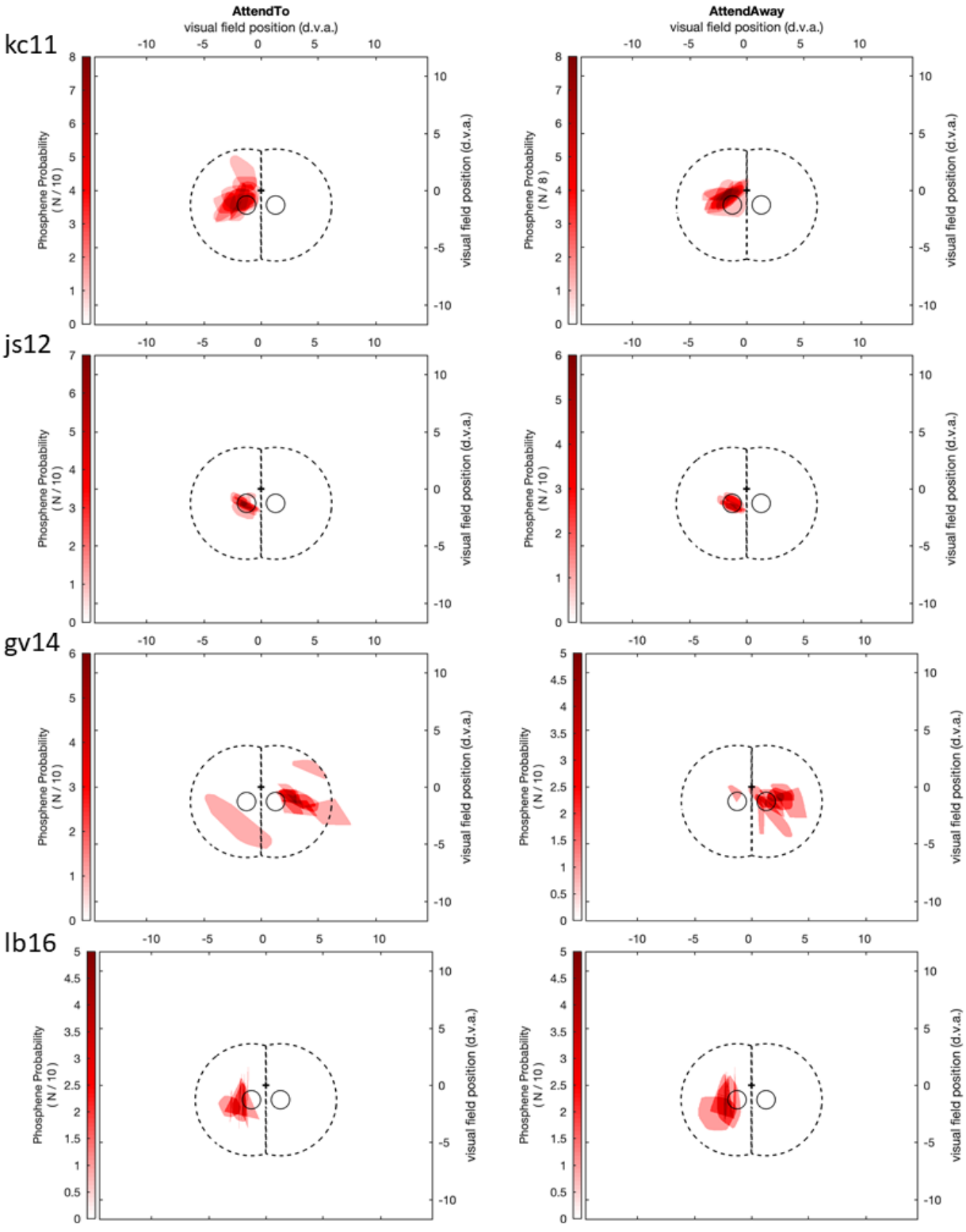
AttendTo
visual field position (d.v.a.)
AttendAway
visual field position (d.v.a.)
kc11
js12
gv14
lb16
Phosphene Probability (N / 10)
Phosphene Probability (N / 8)
visual field position (d.v.a.)

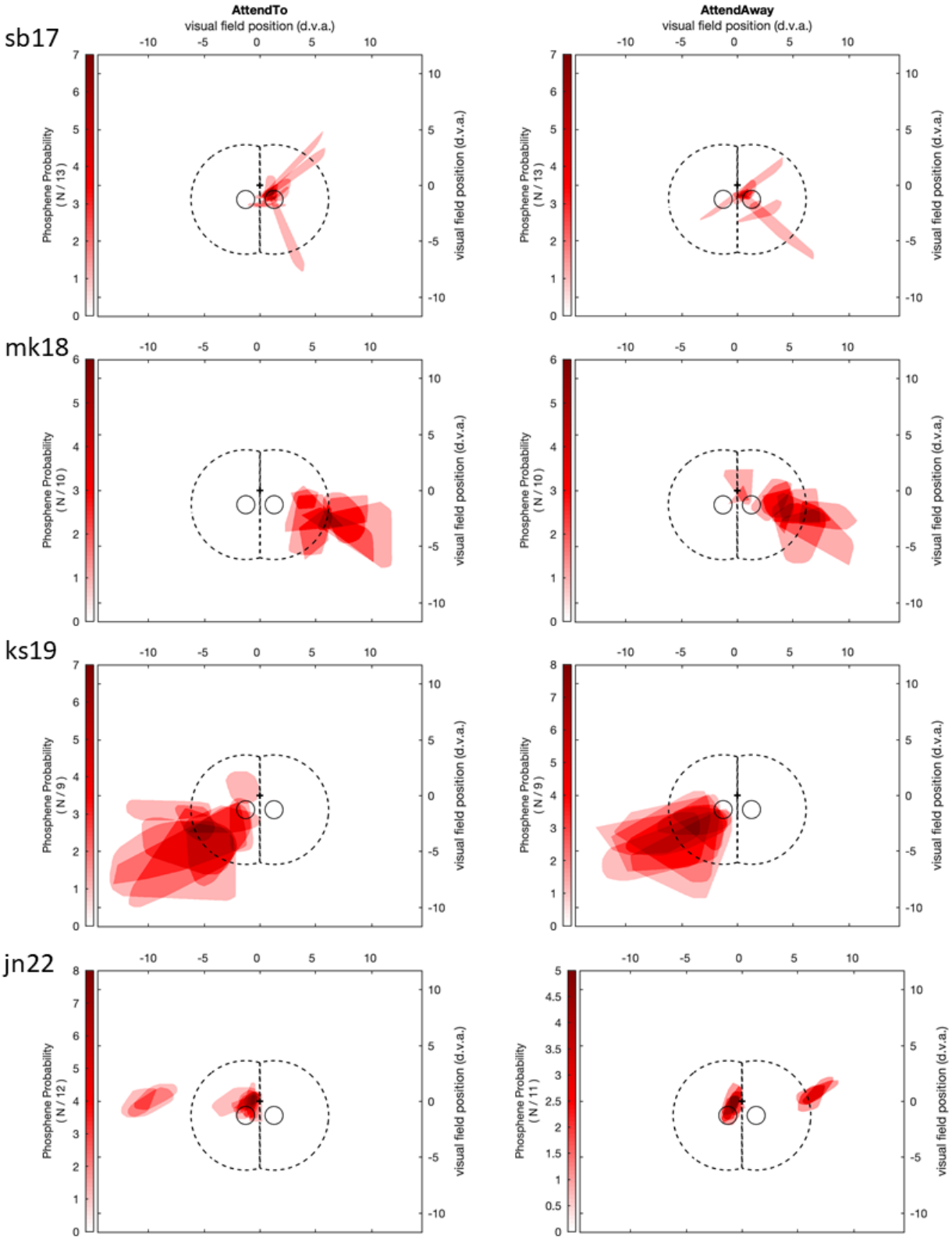
AttendTo
visual field position (d.v.a.)
AttendAway
visual field position (d.v.a.)
sb17
mk18
ks19
jn22
Phosphene Probability (N / 13)
Phosphene Probability (N / 10)
Phosphene Probability (N / 9)
Phosphene Probability (N / 12)
Phosphene Probability (N / 11)
visual field position (d.v.a.)

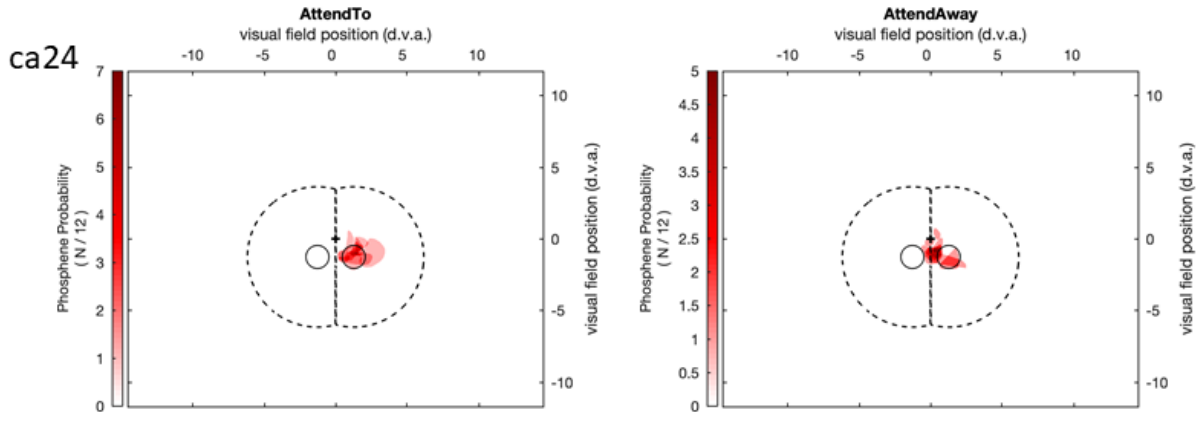

Supplementary Figure 2.1 Phosphene Count Maps of Individual Participants. Rows show data from different participants and columns show data collected while participants attended to the lower quadrant of the phosphene (left column) or the contralateral lower quadrant (right column). Levels of red at a given visual field position indicates how many times (N) it was covered by the phosphene, out of a number of perceived phosphene indicated in the denominator of the color bar unit.

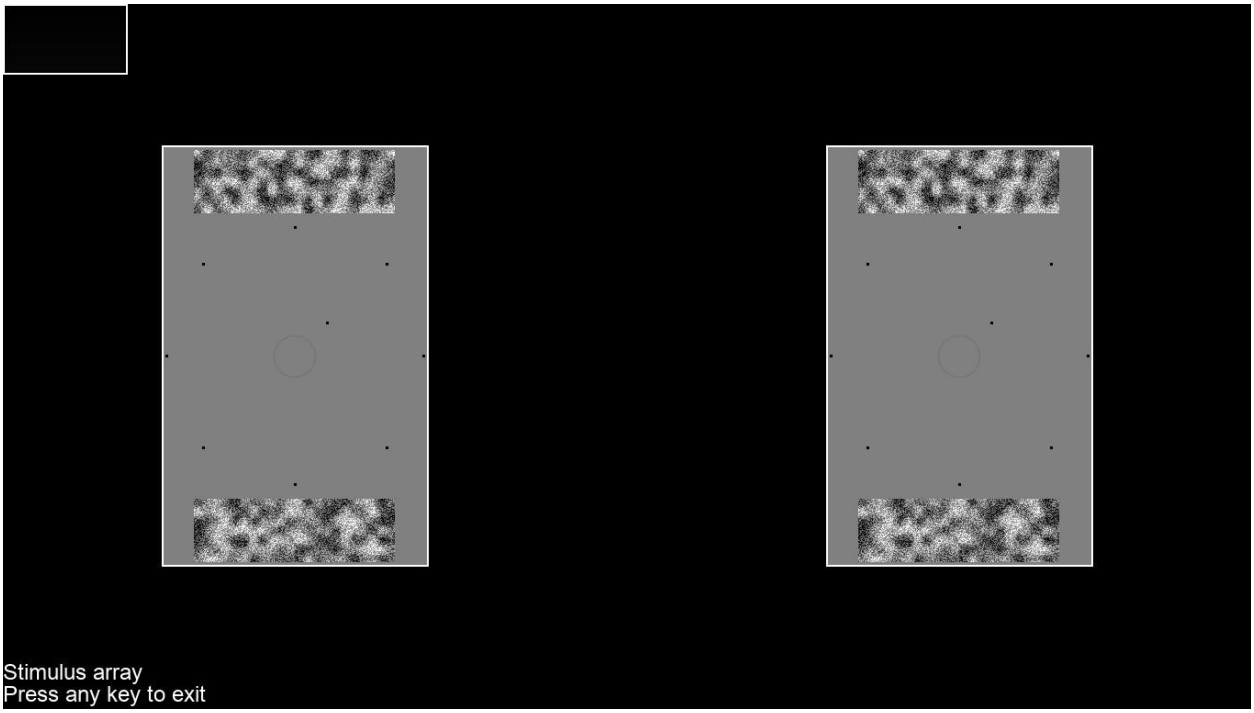

Supplementary Figure 2.2 Screenshot of the display for psychophysics. Through the stereoscope, participants could only see the two stimulus arrays (white-surrounded, gray background area), one in each eye. All elements of the stimulus array are binocular (same in each eye) to aid proper binocular fusion of the psychophysical stimuli (not shown here). The central faint circle indicates the test area. The black dot closest to the faint test stimulus area is the fixation dot. The circular array of black dots are positioned just outside the surround mask stimulus area and, with the noise bands, further aid binocular fusion. All these elements are fixed throughout an acquisition bloc, except the fixation dot that blinks to indicate a change in stimulus condition (see main text). Other elements outside of the two stimulus array are intended to the experimenter.

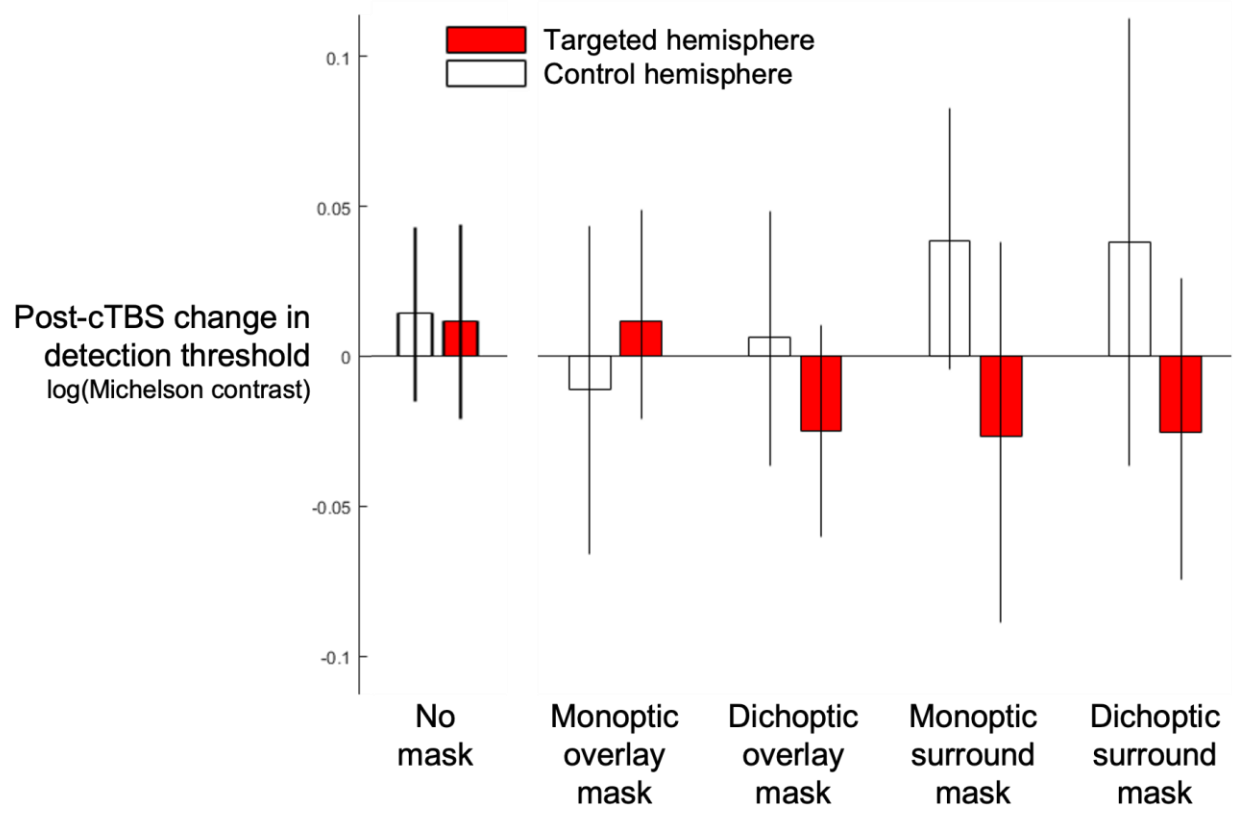

Supplementary Figure 2.3: Results for each stimulus and hemisphere condition. Same data as in Figure 2.5 of main text. Error bar: bootstrapped 95%CI.

2.8 BIBLIOGRAPHY

Allen, C. P. G., Dunkley, B. T., Muthukumaraswamy, S. D., Edden, R., Evans, C. J., Sumner, P., Singh, K. D., & Chambers, C. D. (2014). Enhanced Awareness Followed Reversible Inhibition of Human Visual Cortex: A Combined TMS, MRS and MEG Study. *Plos One*, *9*(6), Article e100350. https://doi.org/10.1371/journal.pone.0100350

Allen, E. A., Pasley, B. N., Duong, T., & Freeman, R. D. (2007). Transcranial magnetic stimulation elicits coupled neural and hemodynamic consequences [Article]. *Science*, *317*(5846), 1918-1921. https://doi.org/10.1126/science.1146426

Angelucci, A., Bijanzadeh, M., Nurminen, L., Federer, F., Merlin, S., & Bressloff, P. C. (2017). Circuits and Mechanisms for Surround Modulation in Visual Cortex. In H. Y. Zoghbi (Ed.), *Annual Review of Neuroscience, Vol 40* (Vol. 40, pp. 425-451). Annual Reviews. https://doi.org/10.1146/annurev-neuro-072116-031418

Angelucci, A., & Bressloff, P. C. (2006). Contribution of feedforward, lateral and feedback connections to the classical receptive field center and extra-classical receptive field surround of primate V1 neurons. *Acetylcholine in the Cerebral Cortex*, *154*, 93-120. https://doi.org/10.1016/S0079-6123(06)54005-1

Antal, A., Kincses, T. Z., Nitsche, M. A., Bartfai, O., Demmer, I., Sommer, M., & Paulus, W. (2002). Pulse configuration-dependent effects of repetitive transcranial magnetic stimulation on visual perception. *Neuroreport*, *13*(17), 2229-2233. https://doi.org/10.1097/01.wnr.0000044216.09266.64

Bair, W., Cavanaugh, J. R., & Movshon, J. A. (2003). Time course and time-distance relationships for surround suppression in macaque V1 neurons. *Journal of Neuroscience*, *23*(20), 7690-7701. https://doi.org/10.1523/JNEUROSCI.23-20-07690.2003

Baker, D. H., Meese, T. S., & Summers, R. J. (2007). Psychophysical evidence for two routes to suppression before binocular summation of signals in human vision. *Neuroscience*, *146*(1), 435-448. https://doi.org/10.1016/j.neuroscience.2007.01.030

Benson, N. C., Butt, O. H., Datta, R., Radoeva, P. D., Brainard, D. H., & Aguirre, G. K. (2012). The Retinotopic Organization of Striate Cortex Is Well Predicted by Surface Topology. *Current Biology*, *22*(21), 2081-2085. https://doi.org/10.1016/j.cub.2012.09.014

Benson, N. C., Jamison, K. W., Arcaro, M. J., Vu, A. T., Glasser, M. F., Coalson, T. S., Van Essen, D. C., Yacoub, E., Ugurbil, K., Winawer, J., & Kay, K. (2018). The Human Connectome Project 7 Tesla retinotopy dataset: Description and population receptive field analysis [Article]. *Journal of Vision*, *18*(13), 22, Article 23. https://doi.org/10.1167/18.13.23

Bestmann, S., Ruff, C. C., Blakemore, C., Driver, J., & Thilo, K. V. (2007). Spatial attention changes excitability of human visual cortex to direct stimulation [Article]. *Current Biology*, *17*(2), 134-139. https://doi.org/10.1016/j.cub.2006.11.063

Blakemore, C., & Tobin, E. A. (1972). LATERAL INHIBITION BETWEEN ORIENTATION DETECTORS IN CATS VISUAL-CORTEX. *Experimental Brain Research*, *15*(4), 439-+. https://doi.org/10.1007/BF00234129

Bocci, T., Caleo, M., Giorli, E., Barloscio, D., Maffei, L., Rossi, S., & Sartucci, F. (2011). TRANSCALLOSAL INHIBITION DAMPENS NEURAL RESPONSES TO HIGH CONTRAST STIMULI IN HUMAN VISUAL CORTEX [Article]. *Neuroscience*, *187*, 43-51. https://doi.org/10.1016/j.neuroscience.2011.04.050

Bocci, T., Caleo, M., Restani, L., Barloscio, D., Rossi, S., & Sartucci, F. (2016). Altered recovery from inhibitory repetitive transcranial magnetic stimulation (rTMS) in subjects with photosensitive epilepsy [Article]. *Clinical Neurophysiology*, *127*(10), 3353-3361. https://doi.org/10.1016/j.clinph.2016.06.013

Bohotin, V., Fumal, A., Vandenheede, M., Gerard, P., Bohotin, C., de Noordhout, A. M., & Schoenen, J. (2002). Effects of repetitive transcranial magnetic stimulation on visual evoked potentials in migraine [Article]. *Brain*, *125*, 912-922. https://doi.org/10.1093/brain/awf081

Bradnam, L. V., Stinear, C. M., & Byblow, W. D. (2010). Theta Burst Stimulation of Human Primary Motor Cortex Degrades Selective Muscle Activation in the Ipsilateral Arm [Article]. *Journal of Neurophysiology*, *104*(5), 2594-2602. https://doi.org/10.1152/jn.00365.2010

Brainard, D. H. (1997). The psychophysics toolbox. *Spatial Vision*, *10*(4), 433-436. https://doi.org/10.1163/156856897x00357

Busse, L., Wade, A. R., & Carandini, M. (2009). Representation of Concurrent Stimuli by Population Activity in Visual Cortex. *Neuron*, *64*(6), 931-942. https://doi.org/10.1016/j.neuron.2009.11.004

Carandini, M., & Heeger, D. J. (2012). Normalization as a canonical neural computation [Review]. *Nature Reviews Neuroscience*, *13*(1), 51-62. https://doi.org/10.1038/nrn3136

Cavanaugh, J. R., Bair, W., & Movshon, J. A. (2002). Nature and interaction of signals from the receptive field center and surround in macaque V1 neurons. *Journal of Neurophysiology*, *88*(5), 2530-2546. https://doi.org/10.1152/jn.00692.2001

Chen, C. C. (2014). Partitioning two components of BOLD activation suppression in flanker effects. *Frontiers in Neuroscience*, *8*. https://doi.org/10.3389/fnins.2014.00149

Chen, R., Classen, J., Gerloff, C., Celnik, P., Wassermann, E. M., Hallett, M., & Cohen, L. G. (1997). Depression of motor cortex excitability by low-frequency transcranial magnetic stimulation [Article; Proceedings Paper]. *Neurology*, *48*(5), 1398-1403. https://doi.org/10.1212/wnl.48.5.1398

Chung, S. W., Hill, A. T., Rogasch, N. C., Hoy, K. E., & Fitzgerald, P. B. (2016). Use of theta-burst stimulation in changing excitability of motor cortex: A systematic review and meta-analysis [Review]. *Neuroscience and Biobehavioral Reviews*, *63*, 43-64. https://doi.org/10.1016/j.neubiorev.2016.01.008

Clavagnier, S., Thompson, B., & Hess, R. F. (2013). Long Lasting Effects of Daily Theta Burst rTMS Sessions in the Human Amblyopic Cortex [Article]. *Brain Stimulation*, *6*(6), 860-867. https://doi.org/10.1016/j.brs.2013.04.002

Cook, E., Hammett, S. T., & Larsson, J. (2016). GABA predicts visual intelligence [Article]. *Neurosci Lett*, *632*, 50-54. https://doi.org/10.1016/j.neulet.2016.07.053

de Labra, C., Rivadulla, C., Grieve, K., Marino, J., Espinosa, N., & Cudeiro, J. (2007). Changes in visual responses in the feline dLGN: Selective thalamic suppression induced by transcranial magnetic stimulation of V1 [Article]. *Cerebral Cortex*, *17*(6), 1376-1385. https://doi.org/10.1093/cercor/bhl048

Deangelis, G. C., Freeman, R. D., & Ohzawa, I. (1994). LENGTH AND WIDTH TUNING OF NEURONS IN THE CATS PRIMARY VISUAL-CORTEX. *Journal of Neurophysiology*, *71*(1), 347-374. https://doi.org/10.1152/jn.1994.71.1.347

Deangelis, G. C., Robson, J. G., Ohzawa, I., & Freeman, R. D. (1992). ORGANIZATION OF SUPPRESSION IN RECEPTIVE-FIELDS OF NEURONS IN CAT VISUAL-CORTEX. *Journal of Neurophysiology*, *68*(1), 144-163. https://doi.org/10.1152/jn.1992.68.1.144

Di Lazzaro, V., Pilato, F., Dileone, M., Ranieri, F., Ricci, V., Profice, P., Bria, P., Tonali, P. A., & Ziemann, U. (2006). GABA(A) receptor subtype specific enhancement of inhibition in human motor cortex [Article]. *Journal of Physiology-London*, *575*(3), 721-726. https://doi.org/10.1113/jphysiol.2006.114694

Di Lazzaro, V., Profice, P., Pilato, F., Dileone, M., Oliviero, A., & Ziemann, U. (2010). The effects of motor cortex rTMS on corticospinal descending activity. *Clinical Neurophysiology*, *121*(4), 464-473. https://doi.org/10.1016/j.clinph.2009.11.007

Dieter, K. C., Sy, J. L., & Blake, R. (2017). Individual differences in sensory eye dominance reflected in the dynamics of binocular rivalry [Article]. *Vision Research*, *141*, 40-50. https://doi.org/10.1016/j.visres.2016.09.014

Douglas, R. J., Koch, C., Mahowald, M., Martin, K. A. C., & Suarez, H. H. (1995). RECURRENT EXCITATION IN NEOCORTICAL CIRCUITS [Article]. *Science*, *269*(5226), 981-985. https://doi.org/10.1126/science.7638624

Fitzgerald, P. B., Fountain, S., & Daskalakis, Z. J. (2006). A comprehensive review of the effects of rTMS on motor cortical excitability and inhibition. *Clinical Neurophysiology*, *117*(12), 2584-2596. https://doi.org/10.1016/j.clinph.2006.06.712

Foley, J. M. (1994). HUMAN LUMINANCE PATTERN-VISION MECHANISMS - MASKING EXPERIMENTS REQUIRE A NEW MODEL [Article]. *Journal of the Optical Society of America a-Optics Image Science and Vision*, *11*(6), 1710-1719. https://doi.org/10.1364/josaa.11.001710

Freeman, T. C. B., Durand, S., Kiper, D. C., & Carandini, M. (2002). Suppression without inhibition in visual cortex. *Neuron*, *35*(4), 759-771. https://doi.org/10.1016/s0896-6273(02)00819-x

Fumal, A., Bohotin, V., Vandenheede, M., Seidel, L., De Pasqua, V., de Noordhout, A. M., & Schoenen, J. (2003). Effects of repetitive transcranial magnetic stimulation on visual evoked potentials: new insights in healthy subjects [Article]. *Experimental Brain Research*, *150*(3), 332-340. https://doi.org/10.1007/s00221-003-1423-7

Gilbert, C. D., & Wiesel, T. N. (1989). COLUMNAR SPECIFICITY OF INTRINSIC HORIZONTAL AND CORTICOCORTICAL CONNECTIONS IN CAT VISUAL-CORTEX [Article]. *Journal of Neuroscience*, *9*(7), 2432-2442. https://doi.org/10.1523/JNEUROSCI.09-07-02432.1989

Huang, Y. Z., Edwards, M. J., Rounis, E., Bhatia, K. P., & Rothwell, J. C. (2005). Theta burst stimulation of the human motor cortex. *Neuron*, *45*(2), 201-206. https://doi.org/10.1016/j.neuron.2004.12.033

Ilic, T. V., Meintzschel, F., Cleff, U., Ruge, D., Kessler, K. R., & Ziemann, U. (2002). Short-interval paired-pulse inhibition and facilitation of human motor cortex: the dimension of stimulus intensity [Article]. *Journal of Physiology-London*, *545*(1), 153-167. https://doi.org/10.1113/jphysiol.2002.030122

Jakobsson, P. (1985). BINOCULAR INTERACTION IN THE VEP TO GRATING STIMULATION .1. ORIENTATIONAL EFFECTS. *Acta Ophthalmologica*, *63*(2), 183-191. https://doi.org/10.1111/j.1755-3768.1985.tb01532.x

Kaderali, S., Kim, Y. J., Reynaud, A., & Mullen, K. T. (2015). The Role of Human Brain Area hMT plus in the Perception of Global Motion Investigated With Repetitive Transcranial Magnetic Stimulation (rTMS) [Article]. *Brain Stimulation*, *8*(2), 200-207. https://doi.org/10.1016/j.brs.2014.11.001

Kammer, T. (1999). Phosphenes and transient scotomas induced by magnetic stimulation of the occipital lobe: their topographic relationship [Article]. *Neuropsychologia*, *37*(2), 191-198. https://doi.org/10.1016/S0028-3932(98)00093-1

Kammer, T., Puls, K., Erb, M., & Grodd, W. (2005). Transcranial magnetic stimulation in the visual system. II. Characterization of induced phosphenes and scotomas [Article]. *Experimental Brain Research*, *160*(1), 129-140. https://doi.org/10.1007/s00221-004-1992-0

Kammer, T., Puls, K., Strasburger, H., Hill, N. J., & Wichmann, F. A. (2005). Transcranial magnetic stimulation in the visual system. I. The psychophysics of visual suppression [Article]. *Experimental Brain Research*, *160*(1), 118-128. https://doi.org/10.1007/s00221-004-1991-1

Kastner, S., Demmer, I., & Ziemann, U. (1998). Transient visual field defects induced by transcranial magnetic stimulation over human occipital pole [Article]. *Experimental Brain Research*, *118*(1), 19-26. https://doi.org/10.1007/s002210050251

Katzner, S., Busse, L., & Carandini, M. (2011). GABA(A) Inhibition Controls Response Gain in Visual Cortex [Article]. *Journal of Neuroscience*, *31*(16), 5931-5941. https://doi.org/10.1523/jneurosci.5753-10.2011

Khammash, D., Simmonite, M., Polk, T. A., Taylor, S. F., & Meehan, S. K. (2019a). Probing short-latency cortical inhibition in the visual cortex with transcranial magnetic stimulation: A reliability study [Article]. *Brain Stimulation*, *12*(3), 702-704. https://doi.org/10.1016/j.brs.2019.01.013

Khammash, D., Simmonite, M., Polk, T. A., Taylor, S. F., & Meehan, S. K. (2019b). Temporal Dynamics of Corticocortical Inhibition in Human Visual Cortex: A TMS Study [Article]. *Neuroscience*, *421*, 31-38. https://doi.org/10.1016/j.neuroscience.2019.10.003

Kim, Y. J., & Mullen, K. T. (2015). The dynamics of cross-orientation masking at monocular and interocular sites [Article]. *Vision Research*, *116*, 80-91. https://doi.org/10.1016/j.visres.2015.09.008

Kingsmith, P. E., Grigsby, S. S., Vingrys, A. J., Benes, S. C., & Supowit, A. (1994). EFFICIENT AND UNBIASED MODIFICATIONS OF THE QUEST THRESHOLD METHOD - THEORY, SIMULATIONS, EXPERIMENTAL EVALUATION AND PRACTICAL IMPLEMENTATION [Article]. *Vision Research*, *34*(7), 885-912. https://doi.org/10.1016/0042-6989(94)90039-6

Kleiner, M., Brainard, D., & Pelli, D. (2007). What's new in Psychtoolbox-3? [Meeting Abstract]. *Perception*, *36*, 14-14.

Kohn, A. (2007). Visual adaptation: Physiology, mechanisms, and functional benefits [Review]. *Journal of Neurophysiology*, *97*(5), 3155-3164. https://doi.org/10.1152/jn.00086.2007

Kozyrev, V., Eysel, U. T., & Jancke, D. (2014). Voltage-sensitive dye imaging of transcranial magnetic stimulation-induced intracortical dynamics. *Proceedings of the National Academy of Sciences of the United States of America*, *111*(37), 13553-13558. https://doi.org/10.1073/pnas.1405508111

Kozyrev, V., Staadt, R., Eysel, U. T., & Jancke, D. (2018). TMS-induced neuronal plasticity enables targeted remodeling of visual cortical maps [Article]. *Proceedings of the National Academy of Sciences of the United States of America*, *115*(25), 6476-6481. https://doi.org/10.1073/pnas.1802798115

Li, B. W., Peterson, M. R., Thompson, J. K., Duong, T., & Freeman, R. D. (2005). Cross-orientation suppression: Monoptic and dichoptic mechanisms are different. *Journal of Neurophysiology*, *94*(2), 1645-1650. https://doi.org/10.1152/jn.00203.2005

Ling, S., Pearson, J., & Blake, R. (2009). Dissociation of Neural Mechanisms Underlying Orientation Processing in Humans. *Current Biology*, *19*(17), 1458-1462. https://doi.org/10.1016/j.cub.2009.06.069

Maniglia, M., Trotter, Y., & Aedo-Jury, F. (2019). TMS reveals inhibitory extrastriate cortico-cortical feedback modulation of V1 activity in humans [Article; Early Access]. *Brain Struct Funct*, *224*(9), 3399-3408. https://doi.org/10.1007/s00429-019-01964-z

Marg, E., & Rudiak, D. (1994). PHOSPHENES INDUCED BY MAGNETIC STIMULATION OVER THE OCCIPITAL BRAIN - DESCRIPTION AND PROBABLE SITE OF STIMULATION [Article]. *Optometry and Vision Science*, *71*(5), 301-311. https://doi.org/10.1097/00006324-199405000-00001

McKeefry, D. J., Gouws, A., Burton, M. P., & Morland, A. B. (2009). The Noninvasive Dissection of the Human Visual Cortex: Using fMRI and TMS to Study the Organization of the Visual Brain. *Neuroscientist*, *15*(5), 489-506. https://doi.org/10.1177/1073858409334424

Meese, T. S., & Holmes, D. J. (2007). Spatial and temporal dependencies of cross-orientation suppression in human vision. *Proceedings of the Royal Society B-Biological Sciences*, *274*(1606), 127-136. https://doi.org/10.1098/rspb.2006.3697

Meese, T. S., Summers, R. J., Holmes, D. J., & Wallis, S. A. (2007). Contextual modulation involves suppression and facilitation from the center and the surround [Review]. *Journal of Vision*, *7*(4), 21, Article 7. https://doi.org/10.1167/7.4.7

Moradi, F., & Heeger, D. J. (2009). Inter-ocular contrast normalization in human visual cortex. *Journal of Vision*, *9*(3), Article 13. https://doi.org/10.1167/9.3.13

Morrone, M. C., Burr, D. C., & Maffei, L. (1982). FUNCTIONAL IMPLICATIONS OF CROSS-ORIENTATION INHIBITION OF CORTICAL VISUAL CELLS .1. NEUROPHYSIOLOGICAL EVIDENCE. *Proceedings of the Royal Society Series B-Biological Sciences*, *216*(1204), 335-354. https://doi.org/10.1098/rspb.1982.0078

Nassi, J. J., Lomber, S. G., & Born, R. T. (2013). Corticocortical Feedback Contributes to Surround Suppression in V1 of the Alert Primate. *Journal of Neuroscience*, *33*(19), 8504-U8440. https://doi.org/10.1523/jneurosci.5124-12.2013

Nurminen, L., Peromaa, T., & Laurinen, P. (2010). Surround suppression and facilitation in the fovea: Very long-range spatial interactions in contrast perception. *Journal of Vision*, *10*(13), Article 9. https://doi.org/10.1167/10.13.9

Ortuno, T., Grieve, K. L., Cao, R., Cudeiro, J., & Rivadulla, C. (2014). Bursting thalamic responses in awake monkey contribute to visual detection and are modulated by corticofugal feedback. *Frontiers in Behavioral Neuroscience*, *8*, 198, Article 198. https://doi.org/10.3389/fnbeh.2014.00198

Ozeki, H., Finn, I. M., Schaffer, E. S., Miller, K. D., & Ferster, D. (2009). Inhibitory stabilization of the cortical network underlies visual surround suppression. *Neuron*, *62*(4), 578-592. https://doi.org/10.1016/j.neuron.2009.03.028

Ozeki, H., Sadakane, O., Akasaki, T., Naito, T., Shimegi, S., & Sato, H. (2004). Relationship between excitation and inhibition underlying size tuning and contextual response modulation in the cat primary visual cortex. *Journal of Neuroscience*, *24*(6), 1428-1438. https://doi.org/10.1523/jneurosci.3852-03.2004

Parkin, B. L., Ekhtiari, H., & Walsh, V. F. (2015). Non-invasive Human Brain Stimulation in Cognitive Neuroscience: A Primer [Review]. *Neuron*, *87*(5), 932-945. https://doi.org/10.1016/j.neuron.2015.07.032

Pascualleone, A., Vallssole, J., Wassermann, E. M., & Hallett, M. (1994). RESPONSES TO RAPID-RATE TRANSCRANIAL MAGNETIC STIMULATION OF THE HUMAN MOTOR CORTEX [Article]. *Brain*, *117*, 847-858. https://doi.org/10.1093/brain/117.4.847

Pasley, B. N., Allen, E. A., & Freeman, R. D. (2009). State-Dependent Variability of Neuronal Responses to Transcranial Magnetic Stimulation of the Visual Cortex [Article]. *Neuron*, *62*(2), 291-303. https://doi.org/10.1016/j.neuron.2009.03.012

Pelli, D. G. (1997). The VideoToolbox software for visual psychophysics: Transforming numbers into movies [Article]. *Spatial Vision*, *10*(4), 437-442. https://doi.org/10.1163/156856897x00366

Petrov, Y., Carandini, M., & McKee, S. (2005). Two distinct mechanisms of suppression in human vision. *Journal of Neuroscience*, *25*(38), 8704-8707. https://doi.org/10.1523/Jneurosci.2871-05.2005

Petrov, Y., & Mckee, S. P. (2009). The time course of contrast masking reveals two distinct mechanisms of human surround suppression. *Journal of Vision*, *9*(1), 21 21-11. https://doi.org/10.1167/9.1.21

Priebe, N. J., & Ferster, D. (2006). Mechanisms underlying cross-orientation suppression in cat visual cortex. *Nature Neuroscience*, *9*(4), 552-561. https://doi.org/10.1038/nn1660

Proulx, S., McLellan, A., Yu, H., & Farivar, F. (2020). *Inhibitory rTMS Modulation of the Occipital Pole Decreases Cortical Suppression of Liminal Contrast Perception* Version 1). https://doi.org/10.5281/zenodo.4101627

Rangelov, D., Muller, H. J., & Taylor, P. C. J. (2015). Occipital TMS at phosphene detection threshold captures attention automatically. *Neuroimage*, *109*, 199-205. https://doi.org/10.1016/j.neuroimage.2015.01.035

Ross, J., & Speed, H. D. (1991). CONTRAST ADAPTATION AND CONTRAST MASKING IN HUMAN VISION. *Proceedings of the Royal Society B-Biological Sciences*, *246*(1315), 61-69. https://doi.org/10.1098/rspb.1991.0125

Rouder, J. N., Morey, R. D., Speckman, P. L., & Province, J. M. (2012). Default Bayes factors for ANOVA designs [Article]. *Journal of Mathematical Psychology*, *56*(5), 356-374. https://doi.org/10.1016/j.jmp.2012.08.001

Salminen-Vaparanta, N., Noreika, V., Revonsuo, A., Koivisto, M., & Vanni, S. (2012). Is selective primary visual cortex stimulation achievable with TMS? *Human Brain Mapping*, *33*(3), 652-665. https://doi.org/10.1002/hbm.21237

Salminen-Vaparanta, N., Vanni, S., Noreika, V., Valiulis, V., Moro, L., & Revonsuo, A. (2014). Subjective Characteristics of TMS-Induced Phosphenes Originating in Human V1 and V2. *Cerebral Cortex*, *24*(10), 2751-2760. https://doi.org/10.1093/cercor/bht131

Schaeffner, L. F., & Welchman, A. E. (2017). Mapping the visual brain areas susceptible to phosphene induction through brain stimulation. *Experimental Brain Research*, *235*(1), 205-217. https://doi.org/10.1007/s00221-016-4784-4

Sengpiel, F., Baddeley, R. J., Freeman, T. C. B., Harrad, R., & Blakemore, C. (1998). Different mechanisms underlie three inhibitory phenomena in cat area 17. *Vision Research*, *38*(14), 2067-2080. https://doi.org/10.1016/S0042-6989(97)00413-6

Sengpiel, F., & Vorobyov, V. (2005). Intracortical origins of interocular suppression in the visual cortex. *Journal of Neuroscience*, *25*(27), 6394-6400. https://doi.org/10.1523/jneurosci.0862-05.2005

Sparing, R., Dambeck, N., Stock, K., Meister, I. G., Huetter, D., & Boroojerdi, B. (2005). Investigation of the primary visual cortex using short-interval paired-pulse transcranial magnetic stimulation (TMS) [Article]. *Neuroscience Letters*, *382*(3), 312-316. https://doi.org/10.1016/j.neulet.2005.03.036

Spiegel, D. P., Hansen, B. C., Byblow, W. D., & Thompson, B. (2012). Anodal Transcranial Direct Current Stimulation Reduces Psychophysically Measured Surround Suppression in the Human Visual Cortex [Article]. *Plos One*, *7*(5), 9, Article e36220. https://doi.org/10.1371/journal.pone.0036220

Stagg, C. J., Wylezinska, M., Matthews, P. M., Johansen-Berg, H., Jezzard, P., Rothwell, J. C., & Bestmann, S. (2009). Neurochemical Effects of Theta Burst Stimulation as Assessed by Magnetic Resonance Spectroscopy. *Journal of Neurophysiology*, *101*(6), 2872-2877. https://doi.org/10.1152/jn.91060.2008

Stokes, M. G., Barker, A. T., Dervinis, M., Verbruggen, F., Maizey, L., Adams, R. C., & Chambers, C. D. (2013). Biophysical determinants of transcranial magnetic stimulation: effects of excitability and depth of targeted area [Article]. *Journal of Neurophysiology*, *109*(2), 437-444. https://doi.org/10.1152/jn.00510.2012

Tajima, S., Watanabe, M., Imai, C., Ueno, K., Asamizuya, T., Sun, P., Tanaka, K., & Cheng, K. (2010). Opposing Effects of Contextual Surround in Human Early Visual Cortex Revealed by Functional Magnetic Resonance Imaging with Continuously Modulated Visual Stimuli. *Journal of Neuroscience*, *30*(9), 3264-3270. https://doi.org/10.1523/jneurosci.4473-09.2010

Thompson, B., Mansouri, B., Koski, L., & Hess, R. F. (2008). Brain plasticity in the adult: Modulation of function in amblyopia with rTMS. *Current Biology*, *18*(14), 1067-1071. https://doi.org/10.1016/j.cub.2008.06.052

Tolhurst, D. J., & Thompson, P. G. (1975). Orientation illusions and after-effects: inhibition between channels. *Vision Res*, *15*, 967-972. https://doi.org/10.1016/0042-6989(75)90238-2

Verhagen, J., & Wagenmakers, E. J. (2014). Bayesian Tests to Quantify the Result of a Replication Attempt. *Journal of Experimental Psychology-General*, *143*(4), 1457-1475. https://doi.org/10.1037/a0036731

Wagenmakers, E. J., Love, J., Marsman, M., Jamil, T., Ly, A., Verhagen, J., Selker, R., Gronau, Q. F., Dropmann, D., Boutin, B., Meerhoff, F., Knight, P., Raj, A., van Kesteren, E. J., van Doorn, J., Smira, M., Epskamp, S., Etz, A., Matzke, D., . . . Morey, R. D. (2018). Bayesian inference for psychology. Part II: Example applications with JASP [Article]. *Psychonomic Bulletin & Review*, *25*(1), 58-76. https://doi.org/10.3758/s13423-017-1323-7

Wagenmakers, E. J., Verhagen, J., & Ly, A. (2016). How to quantify the evidence for the absence of a correlation [Article]. *Behavior Research Methods*, *48*(2), 413-426. https://doi.org/10.3758/s13428-015-0593-0

Waterston, M. L., & Pack, C. C. (2010). Improved Discrimination of Visual Stimuli Following Repetitive Transcranial Magnetic Stimulation. *Plos One*, *5*(4). https://doi.org/10.1371/journal.pone.0010354

Watson, A. B., & Pelli, D. G. (1983). QUEST - A BAYESIAN ADAPTIVE PSYCHOMETRIC METHOD [Article]. *Perception & Psychophysics*, *33*(2), 113-120. https://doi.org/10.3758/bf03202828

Webb, B. S., Dhruv, N. T., Solomon, S. G., Tailby, C., & Lennie, P. (2005). Early and late mechanisms of surround suppression in striate cortex of macaque. *Journal of Neuroscience*, *25*(50), 11666-11675. https://doi.org/10.1523/Jneurosci.3414-05.2005

Werner, J. S., & Chalupa, L. M. (2004). *The visual neurosciences*. MIT Press.

Wilson, M. T., Fulcher, B. D., Fung, P. K., Robinson, P. A., Fornito, A., & Rogasch, N. C. (2018). Biophysical modeling of neural plasticity induced by transcranial magnetic stimulation [Review]. *Clinical Neurophysiology*, *129*(6), 1230-1241. https://doi.org/10.1016/j.clinph.2018.03.018

Wischnewski, M., & Schutter, D. (2015). Efficacy and Time Course of Theta Burst Stimulation in Healthy Humans [Review]. *Brain Stimulation*, *8*(4), 685-692. https://doi.org/10.1016/j.brs.2015.03.004

Xing, J., & Heeger, D. J. (2001). Measurement and modeling of center-surround suppression and enhancement. *Vision Research*, *41*(5), 571-583. https://doi.org/10.1016/s0042-6989(00)00270-4

Yoon, J. H., Maddock, R. J., Rokem, A., Silver, M. A., Minzenberg, M. J., Ragland, J. D., & Carter, C. S. (2010). GABA Concentration Is Reduced in Visual Cortex in Schizophrenia and Correlates with Orientation-Specific Surround Suppression. *Journal of Neuroscience*, *30*(10), 3777-3781. https://doi.org/10.1523/Jneurosci.6158-09.2010

Zenger-Landolt, B., & Heeger, D. J. (2003). Response suppression in V1 agrees with psychophysics of surround masking. *Journal of Neuroscience*, *23*(17), 6884-6893. https://doi.org/10.1523/JNEUROSCI.23-17-06884.2003

Ziemann, U., Lonnecker, S., Steinhoff, B. J., & Paulus, W. (1996). The effect of lorazepam on the motor cortical excitability in man [Article]. *Exp Brain Res*, *109*(1), 127-135. https://doi.org/10.1007/BF00228633

Chapter 3: Plasticity Modulation of Interocular GABA Inhibition

Preamble

The MR spectroscopy measurement of the GABA neurotransmitter concentrations, and its interpretational challenges described in Section 1.4.2, is of obvious interest for a thesis on non-invasive investigation of intracortical processes. The very first experiment I performed aimed at detecting MR GABA signal changes in relation to the then recently discovered adult-form of visual plasticity induced by an hour or two of monocular deprivation (MD)—GABA inhibition was expected to decrease either to support the boosted sensitivity of the deprived eye or, following the concept of metaplasticity, to allow plastic changes to take place. However, the reverse trend was emerging from the first five data points and the project was paused to limit costs.

A later conference abstract report by Lunghi et al. (2014) however showed the expected MR GABA decrease with seemingly the same plasticity protocol that in our hands had failed. This chapter's manuscript, under preparation for resubmission, reports the re-evaluation or our MR spectroscopy data in the light of more thorough measurements from the same participants. Concluding that they unlikely expressed the same visual plasticity as Lunghi et al. (2014)'s participants did, it prompted us to directly compare the types of eye patches used by us and Lunghi et al. (2014) for MD. This factor turned out crucial in determining which circuits undergoes plasticity with MD, an original finding of importance for our understanding of binocular vision plasticity, as discussed in the manuscript.

The manuscript's pattern of findings is further speculatively interpreted in Section 5.2.2 in the light of *in silico* experiments on modeled neural dynamics (Annex B). This offers a novel perspective on the interpretation of neurotransmitter MR signals.

Manuscript Title: GABA Plasticity Rules Depend on the Nature of Deprivation in Human Early Visual Cortex

Authors

Sébastien Proulx[1] and Reza Farivar[1]

Affiliation

[1]Ophthalmology and Visual Sciences Department, McGill University

[1]Research Institute of McGill University Health Centre

Keywords

GABA; GABAergic; visual plasticity; homeostatic plasticity; ocular dominance plasticity; monocular deprivation; eye patching; human; adult; MR spectroscopy; MRS; magnetoencephalography; MEG; frequency tagging; binocular rivalry; binocular phase combination; sensory eye dominance; SED; visual psychophysics

Acknowledgments

Thanks to Alexandre Reynaud and Eva Chadnova for their contributions with MEG data acquisitions. Thanks to Jiawei Zhou for his help with psychophysical data acquisitions. Thanks to Jiawei Zhou, Yasha Sheynin and Robert F. Hess for their intellectual contributions to the project.

Funding

MR spectroscopy and MEG data acquisition were funded from a CIHR grant # Mt108-18 awarded to Robert F. Hess. Psychophysical data acquisition was funded from a NSERC discovery grant # RGPIN 419235-2013 awarded to Reza Farivar. Sébastien Proulx was supported by NSERC and FRSQ PhD scholarships.

3.1 ABSTRACT

Depriving one eye for a few hours increases its influence on perception, an adult-form of ocular dominance plasticity attributed to homeostatic disinhibition in the early visual cortex. The residual neural activity in the deprived-eye pathway is known from animal studies to determine different mechanisms through which visual networks adapt, often leading to similar behavioral consequences. Here we investigated the potential plurality of GABA-related mechanisms underlying ocular dominance plasticity in healthy adults across two experiments including non-invasive MR spectroscopy measures of occipital GABA, MEG measures of cortical eye dominance and two measures of perceptual eye dominance. We found in Exp1 that 3h of monocular deprivation with an opaque patch produced GABA-related changes opposite of those previously observed with a diffuser patch, despite robust replication of the behavioural and physiological eye dominance effect. In Exp2 we directly compared the two treatments in a within-subject cross-over design and found dissociable effects, where ocular dominance shifted either through increased deprived-eye dominance *or* decreased non-deprived-eye dominance. Homeostatic disinhibition alone cannot account for all available data, implying multiple ocular dominance plasticity mechanisms in human adults, which we propose to depend on interocular correlation of the deprived pathway residual activity.

3.2 INTRODUCTION

Homeostatic plasticity stabilizes neural circuits for optimal functioning in constantly changing environments, and cortical disinhibition following input deprivation is an important example of this process (Gainey & Feldman, 2017)—e.g. removal of GABA synapses contacting pyramidal neurons restores normal average firing rates in the primary visual cortex (V1) of adult mice within 1 day of monocular deprivation (van Versendaal et al., 2012). Non-invasive measurements of GABA levels in the occipital cortex of human adults have shown a similar trend (Lunghi et al., 2015), suggesting a general mechanism for adult visual plasticity.

Mechanisms of ocular dominance (OD) plasticity have long been known to depend on how deprivation is achieved, particularly with respect to residual activity in the deprived-eye pathway (reviewed in Nys et al., 2015). For example, during the critical period in mice,

monocular deprivation with lid suture—which maintains uncorrelated spontaneous retinal activity—shifted OD by potentiating deprived-eye responses, while tetrodotoxin silencing of the retina did so by depressing non-deprived-eye responses (Frenkel & Bear, 2004). On the other hand, recent human MR spectroscopy measures of GABA plasticity showed an exquisite dependence on the requirements of the tasks performed on otherwise similar stimuli. Training on a visual detection or discrimination task triggered occipito-temporal GABA modulations of opposite sign (Frangou et al., 2019) and related to performance improvements in opposite directions (Frangou et al., 2018). Doubling training time on a visual detection task to 32min similarly flipped the sign of occipital GABA modulations (Shibata et al., 2017). GABA—repeatedly linked in the occipital cortex to human OD (Ip et al., 2021; Lunghi et al., 2015; van Loon et al., 2013)—can therefore be very plastic, and the rules of both GABA and OD plasticity are context dependent.

Establishing GABA plasticity rules in humans requires challenging multimodal assessments to link different scales. Here, we tackled that challenge through extensive behavioral, electrophysiological and MR spectroscopy investigations of the same individuals (Exp1) and in a separate cohort by directly comparing the perceptual consequences of monocular deprivation (MD) with opaque or diffuser eye patches (Exp2). Our results challenge the generality of a homeostatic disinhibitory mechanism in human adults, as both decreases or increases in GABAergic inhibition—of respectively deprived (DE) and non-deprived eye (NDE) responses—could lead to a similar behavioral expression of OD plasticity.

3.3 Results and Discussion

Using an opaque eye patch for 3h of MD (Figure 3.1A), we failed to replicate the GABA decrease obtained by Lunghi et al. (2015) with a diffuser patch (Figure 3.1G, y-axis; Bayesian Factor Analysis: BF_{0r}=6.1, moderate (significant) evidence against replication). Our MR spectroscopy measurements of GABA averaged 30-min worth of data in each of two sessions, and ensured the same occipital cortical tissue was sampled in the pre- and post-MD sessions through an automatic registration routine (Figure 3.1E). This attempt at replicating the GABA effect failed despite all five participants showing the characteristic effect of MD on

perception—i.e. a shifted sensory eye dominance (SED) that biased binocular vision toward the DE (Figure 3.1F). This bias was evident during tasks (Lunghi et al., 2015; Zhou et al., 2013) involving either binocular combination (BC in Figure 3.1B; BF_{-0}=11.0, strong evidence for the expected effect) or binocular rivalry (BR in Figure 3.1C; BF_{-0}=11.0, strong evidence for the expected effect). The latter task being similar to that of Lunghi et al. (2015), we directly replicated their behavioral effect (BF_{r0}=21.1, strong evidence) but in the absence their GABA effect.

While all our participants expressed the expected shift in SED after opaque MD, it did not relate to GABA changes as expected—bootstrapping Lunghi et al. (2015)'s diffuser MD data and our opaque MD data in sets of 5 samples showed GABA-to-SED relations with orthogonal 95% confidence intervals (Figure 3.1G). More specifically, we failed to directly replicate Lunghi et al. (2015)'s correlation of GABA changes with SED shifts derived from binocular rivalry data (Supplementary Figure 3.1C; BF_{0r}=5.8, moderate evidence against replication). In contrast, we found anecdotal evidence that larger SED shifts measured behaviorally might relate to GABA *increases* instead (Supplementary Figure 3.1B; BF_{10}=1.1 for BC; Supplementary Figure 3.1C, BF_{10}=1.4 for BR). To corroborate with objective neurophysiological measures of SED, we recorded steady state visually evoked MEG responses to the dichoptic presentation of binocularly competing visual noise patterns, modulating each eye at different temporal frequencies to estimate eye-specific—frequency-tagged—neural activity (Chadnova et al., 2017) (Figure 3.1D). Again, all participants showed the expected SED shift (Figure 3.1F and Figure 3.1G, x-axis; BF_{-0}=5.7, moderate evidence), here directly and twice more precisely estimated from neurophysiological responses (Supplementary Figure 3.1D versus Supplementary Figure 3.1B and Supplementary Figure 3.1C). Crucially, larger SED shifts correlated with GABA *increases* (Figure 3.1G: BF_{10}=9.5, moderate evidence), confirming the finding from our behavioural SED measures.

In other words, with an opaque patch we found the opposite of Lunghi et al. (2015)'s observation using a diffuser patch (Figure 3.1G). A parsimonious explanation is that diffuser MD does disinhibit DE responses (Lunghi et al., 2015) but that opaque MD instead increases GABA inhibition of NDE responses, thereby producing similar SED shifts but through independent

GABA-related mechanisms. In rodents, comparable MD treatments can lead to distinct functional reorganizations of V1 circuits (Nys et al., 2015), including increased inhibition (Maffei et al., 2006). In 14 additional participants, we found that opaque and diffuser MD treatments are indeed indistinguishable from their effect on SED (Figure 3.1H; repeated measures: rmANOVA: $F_{1,12}$=0.0, p=0.904). They however differed on their *pattern* of effects on eye-specific responses estimated from the duration of exclusive monocular percepts (Sheynin et al., 2019) during binocular rivalry (Figure 3.1I; rmMANOVA: $F_{2,11}$=6.7, p=0.013), suggesting treatment-specific plasticity mechanisms—diffuser MD shifted SED through increased DE responses (Figure 3.1I; diffuser versus opaque: t_{13}=3.1, p=0.008), as predicted from homeostatic disinhibition (Lunghi et al., 2015), but opaque MD did the same by decreasing NDE responses (Figure 3.1I; diffuser vs opaque: t_{13}=3.0, p=0.010), compatible with increased GABA inhibition and corroborating our GABA measures[6].

Through our two studies using independent samples and an array of behavioral and physiological measures, we found equivocal support for a monocular homeostatic disinhibition mechanism—indeed, further analysis suggests the involvement of binocular circuits. Diffuser MD favoured binocularly integrated or mixed perception during rivalry—longer perception of binocular overlays or piecemeal combinations of the dichoptic stimuli (Riesen et al., 2019)—as we previously reported (Sheynin et al., 2019), but opaque MD did not (Figure 3.1J, y-axis; rmANCOVA with covariate NDE: $F_{1,10.9}$=5.8, p=0.035; diffuser: t_{13}=2.7, p=0.018; opaque: t_{13}=-0.5, p=0.653). These binocular changes were independent from monocular changes in the DE (Supplementary Figure 3.2B; diffuser: R=0.11, p=0.712; opaque: R=0.32, p=0.261). They were, however, strongly related to NDE changes (Figure 3.1J), and in opposite directions for diffuser and opaque MD (diffuser: R=-0.68, p=0.008; opaque: R=0.78, p=0.001; diffuser versus opaque: rmANCOVA with covariate NDE, $F=_{1,21.3}$12.4, p=0.002). This again supports separate mechanisms for the two MD treatments and importantly provides insight into their nature: the

[6] The patch-type effect was interestingly only observed in naïve participants—when both performed a second time in the same participants, the opaque and diffuser MD treatments produced indistinguishable effects. This warrants caution during recruitment in future MD studies (see Online Methods and Supplementary Results and Discussion, Experiment II).

DE effect that dominates after diffuser MD is strictly monocular, whereas the NDE effect involves changes in binocular circuits.

Why would an opaque or diffuser eye patch trigger different plastic changes? An opaque patch blocks all visual information, with only spontaneous retinal activity reaching the cortex. A diffuser patch does not block light—spatial contrast is eliminated but temporal variations in luminance are still congruent with the unpatched eye. We speculate that this correlated neural activity is the essential factor in determining which plasticity regime will occur (Maffei & Turrigiano, 2008). Increased inhibition—through long-term potentiation of inhibitory synapses (LTPi)—has been shown to be a major component of critical period OD plasticity in rodents (Maffei et al., 2006). This presynaptic form of LTPi requires subthreshold post-synaptic depolarization of cortical neurons but is blocked by correlated pre- and post-synaptic firing (Maffei et al., 2006). Binocularly uncorrelated spontaneous retinal activity from the opaque-patched eye could provide this necessary subthreshold depolarization of binocular neurons for the system to cascade toward neural adaptations dominated by LTPi-related GABA increases. In contrast, the interocular correlations allowed by a diffuser patch could block that LTPi on binocular neurons, favoring the mechanism of homeostatic disinhibition of deprived monocular neurons.

Homeostatic disinhibition, generally at play in neural circuits deprived of their input (Gainey & Feldman, 2017), is insufficient to explain all plastic changes observed here and by Lunghi et al. (2015) in the mature human binocular system. We propose that altered levels of interocularly correlated neural activity—from high (natural vision) to only temporal correlation (diffuser MD) to no correlation (opaque MD)—play a critical role in dictating circuit reconfigurations for maintaining homeostasis. We predict that modulating interocular correlation while keeping overall stimulation equal in each eye—e.g. by alternating the patched eye every few seconds—would affect both V1 GABA and binocular function and balance, consistent with theory (Klink et al., 2010; Said & Heeger, 2013) and preliminary observations (Proulx, 2020) and potentially opening new therapeutic options for amblyopia.

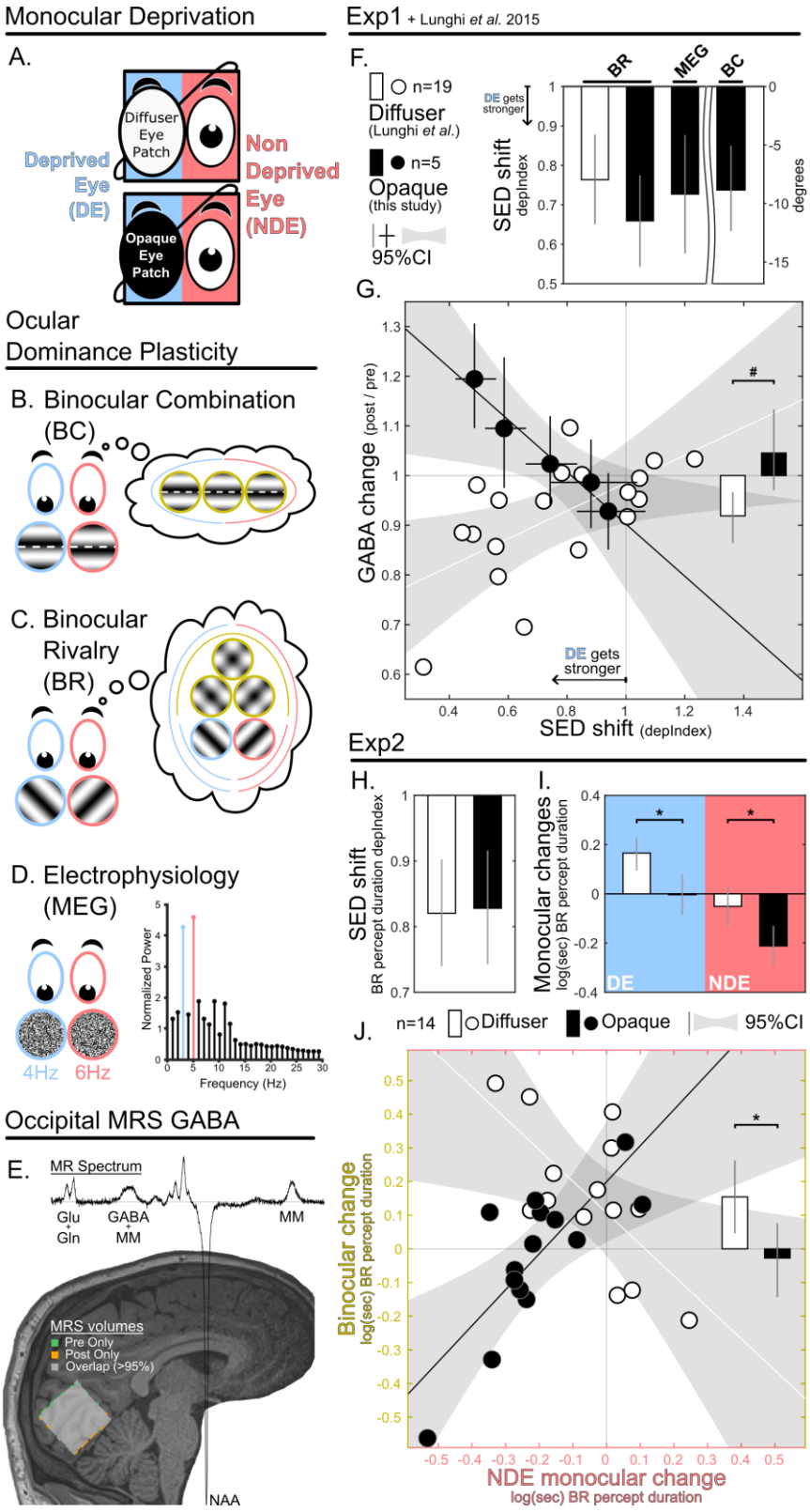

Figure 3.1 A. For monocular deprivation (MD), the deprived and non-deprived eyes were respectively occluded and left open (DE and NDE respectively in blue and red graphics used throughout this figure) while participants freely behaved during the 2 to 3-hour treatment. Occlusion used either an opaque or diffuser eye patch (white and black graphics throughout this figure), effectively blocking all visual inputs (opaque) or filtering out specifically the spatial structure inputs (diffuser). **B, C and D.** Representation of visual stimuli (below the cartoon eyes) and perceptual (in the thought bubbles) or evoked responses (inset graph) used for measuring sensory eye dominance and binocular function. **B.** In the Binocular Combination task (BC), slightly phase-offset gratings in each eye were perceived as binocularly fused (yellow graphics used throughout this figure) into a single grating showing a phase biased toward the dominant eye. **C.** In the Binocular Rivalry (BR) task, gratings with wide orientation offsets competed, creating alternating percepts, i.e. 1 to 10-second periods of left monocular, right monocular and binocular perception. **D.** During magnetoencephalography (MEG), passive viewing of dichoptic noise patterns flickering at different frequencies tagged the cortical neural activity driven by each eye at the corresponding frequencies. **E.** MR spectroscopy data from one participant. GABA-edited spectra (black trace) acquisition used MEGA-PRESS at 3T (Siemens Tim Trio; Tx: body coil; Rx: 20 back channels of Siemens' 32-channel head coil; TR=3s; TE=68ms; center frequency=3ppm; editON editing pulses=1.9 and 4.7ppm; editOff editing pulses=7.5 and 4.7ppm; editing pulse bandwidth=70Hz; VAPOR water suppression; OVS; 32avg per run) and a 3x3x3cm^3 single voxel (grey box) manually prescribed bilaterally over the occipital cortex. Overlap of macromolecular signal with the GABA peak was

accounted for by including an empirically derived macromolecular baseline model during LCModel spectral quantification. Pre- and post-MD spectra each averaged ~30min of data collected eyes open but over a period half overlapping the beginning (pre-MD) or the end (post-MD) of the MD treatment, when the deprived eye was occluded. The post-MD voxel prescription was automatically aligned to the pre-MD voxel using Siemens' AutoAlign™ routine, resulting in over 95% volume overlap (gray; non-overlapping volume in green and orange). **F and G.** Results of the multimodal *Exp1*. **F.** Opaque MD robustly shifted all SED measures, as in Lunghi et al. (2015)'s data using a diffuser patch. **G.** Opaque MD did not decrease GABA as diffuser MD did in Lunghi et al. (2015)'s data. Larger SED shifts related to GABA increases after opaque MD but GABA decreases after diffuser MD in Lunghi et al. (2015)'s data. Note that for the purpose of concise visualization only, diffuser MD SED shifts were derived from Lunghi et al. (2015)'s BR task whereas opaque MD SED shifts were from our MEG frequency tagging protocol. **H and G.** Results of the behavioral *Exp2*. **H.** Diffuser and opaque MD produced equivalent SED shifts. **I** SED shifts were driven by the lengthening of DE monocular percept durations after diffuser MD, but by the shortening of NDE percepts after opaque MD. **J.** Binocularly mixed percept durations lengthened only after diffuser MD (bars), which related to shortening NDE percepts (scatter). The opposite relation was observed with opaque MD, reminiscent of the dissociation observed in *Exp1*. DE: deprived eye; NDE non deprived eye; Glu: glutamate; MM: macromolecules; NAA: N-Acetyl aspartate; SED: sensory eye dominance; Error bars: bootstrapped 95% confidence intervals. Shaded areas: bootstrapped 95% confidence intervals of the fits. * $p<0.05$; # BF>3. All data available at https://doi.org/10.5281/zenodo.4095913 for Exp1 and https://doi.org/10.5281/zenodo.4095828 for Exp2, and individual data are visualized in Supplementary Figure 3.1 and 3.2.

3.4 Online Methods and Supplementary Results and Discussion

3.4.1 Experiment I: Opaque-Patch Monocular Deprivation Induces Ocular Dominance Plasticity Related to Increased Occipital GABA Concentrations

3.4.1.1 Participants

Five healthy adult volunteers (1F; mean age 27; age range: 24-30) with normal or corrected-to-normal vision completed this experiment. Informed consent was obtained from all participants and the protocol NEU-13-043 was approved by the Research Ethics Board of the Montreal Neurological Institute.

3.4.1.2 Procedure

3.4.1.2.1 Monocular Deprivation

Participants underwent three monocular deprivation (MD) treatment sessions separated by at least a month. Each session consisted of wearing an opaque eye patch over the dominant eye (Miles' sighting eye dominance (Miles, 1929; Valle-Inclan et al., 2008)). Treatment lasted ~170min during which participants stayed in the vicinity of our lab but with no specific instructions other than to keep the patch on. Different pre-post measures were performed on each session to assess treatment effects. They consisted of magnetic resonance (MR)

spectroscopy measures of occipital GABA concentrations, as well as 3 different measures of sensory eye dominance (SED) derived from (1) binocular combination and (2) binocular rivalry behavioral tasks and from (3) magnetoencephalography (MEG) neurophysiological data.

3.4.1.2.2 First MD Session—GABA Measures & Binocular Combination Behavioral Measures

A 15-min GABA measure was obtained in-between two 2-min binocular combination behavioral measures performed in the MR scanner. Then the MR table was moved out of the MR bore to initiate MD with an opaque cloth occluding the eye to be deprived. The table was moved back in position for another 15-min GABA measure, after which the participant was taken out. The occluding cloth was replaced with an eye patch, with care to avoid interruption of MD (2:30 hours outside of the scanner). Participants came back shortly before the end of the MD treatment for the reverse measurement sequence: one 15-min GABA measure, followed by removal of the patch (i.e. termination of 3 hours of MD—15 min patched in the scanner, 2:30 patched outside of the scanner, and another 15 min patched inside the scanner), one 2-min behavioral measure, another 15-min GABA measure and a final 2-min behavioral measure. During all GABA measurements, participants performed a simple attentional task, i.e. detecting color changes of a small central fixation dot displayed over a gray background.

3.4.1.2.3 Second MD Session—Binocular Rivalry Behavioral Measures

The timing of the participants' experience (i.e., the experimental procedure) in the first session was reproduced in the second, where 3-min binocular rivalry behavioral measures replaced the binocular combination measures and where the binocular rivalry and attentional tasks were performed seated in our lab instead of lying in the MR bore.

3.4.1.2.4 Third MD Session—Magnetoencephalography Measures

Participants were included in Chadnova et al. (2017)'s MEG frequency tagging protocol, where 3 consecutive 8-min MEG measures were performed before and after MD, approximately matching the timing of measures in Session 1 and Session 2. An additional MEG measure was performed 45min after MD but not included in our analysis.

3.4.1.3 MR Spectroscopy Measures of Occipital GABA

3.4.1.3.1 MR Acquisitions

MR imaging (MRI) and spectroscopy were performed on a 3T scanner (Siemens Tim Trio) at the Brain Imaging Center of the Montreal Neurological Institute, using Siemens body coil for RF transmission and Siemens 32-channel head coil (only the back 20 channels were used as to not obstruct access to the eyes) for RF reception. Participants wore ear plugs and their head was padded to minimize movement.

All exam prescriptions used Siemens's proprietary procedure for automatic online head registration from a localizer scan (AutoAlign™, head basis). TRUFISP localizer (TR=4.6ms, TE=2.3ms, FA=37º, matrix size=256×256, voxel size=1mm×1mm, 23 sagittal 4-mm slices, distance factor 20%, BW=558 Hz/Px) and high-resolution MPRAGE (TR=2.3s, TE=2.98ms, TI=900ms, FA=9º, GRAPPA accel. fact. 2, matrix size=256×256, voxel size=1mm×1mm, 176 sagittal 1-mm slices, BW=240 Hz/Px) anatomical scans were performed to guide the manual prescription of a 3×3×3cm^3 occipital spectroscopy voxel centered on the calcarine and on the two hemispheres, as posterior as possible while avoiding the inclusion of ventricles and sagittal sinus. Shimming of the magnetic field within the MRS volume used the FASTESTMAP procedure (Gruetter & Tkac, 2000) and ensured <10Hz water linewidth before GABA data acquisition begun.

A MEGA-PRESS single-voxel spectroscopy sequence (Mescher et al., 1998) was used (TR=3s, TE=68ms, center frequency on the γ-CH_2 GABA resonance at 3ppm, double banded editing pulse position: 1.9 and 4.7ppm for editON and 7.5 and 4.7ppm for editOff scans; editing pulse bandwidth=70Hz) for simultaneous GABA editing and water suppression. Additional water suppression, using variable power with optimized relaxation delays (VAPOR), and outer volume suppression (OVS) techniques (Tkac et al., 1999) were incorporated prior to the MEGA-PRESS. The polarity of the gradients for intra-voxel signal selection was optimized to minimize contaminating lipid signals from the scalp. Spectra were acquired from the prescribed voxel in series of 32 editOn and 32 editOff interleaved single-scan repetitions, i.e. 32 averages, to minimize reduction in editing efficiency with scanner drift. Four series, i.e. 4×32=128 averages,

were obtained for one GABA measure. FIDs were stored separately in memory for individual frequency and phase correction using a spectral range covering the 3.2-ppm choline-containing compounds (tCho) peak and the 3.0-ppm creatine and phosphocreatine peak ($tCrCH_3$) and performed with custom Matlab scripts.

GABA-edited difference spectra were obtained by subtracting editOff from editOn spectra. No immediate effect of eye occlusion or occlusion removal was observed (data not shown), such that averages from two consecutive GABA measures were pooled (pre-MD with early-MD and late-MD with post-MD) for a single measure (2×128=256 averages) of pre- and a single measure (2×128=256 averages) of post-MD GABA concentrations.

3.4.1.3.2 MR Spectra Quantification

Spectral quantification used LCModel 6.3-1H (Provencher, 1993, 2001), which fits a linear combination of model spectra to an average experimental GABA-edited difference spectrum. The basis set of model spectra included an experimentally-measured *in vivo* metabolite-nulled macromolecular spectrum (previously acquired from the occipital region of 11 participants (Tremblay et al., 2013)) and NAA, GABA, Glu and Gln spectra experimentally-measured at 37ºC from 100-mM phantoms. LCModel's default modeling of the lipid and macromolecule baseline was disabled (no spline NOBASE=T and no simulated lipid or macromolecule allowed NSIMUL=0) to accommodate the use of our own macromolecule model and the virtually absent lipid contamination. Fitting was performed over the 0.5-4.0ppm range. GABA concentrations were expressed as ratios to NAA and the effect of MD as post/pre deprivation ratios.

Within-subject 95% confidence intervals were obtained from 12,000 bootstrap resamples of 256 pre- and 256 post-deprivation averages, with replacement. Group-level 95% confidence intervals were obtained from 12,000 bootstrap resamples of 5 participants, with replacement.

3.4.1.3.3 Colocalization of MR Spectroscopy Voxel Within-Subject

Several TRUFISP localizers confirmed stable head position within the pre- and post-MD MR sessions. Prescription of a post-MD voxel co-localized with the pre-MD voxel relied on AutoAlign. To assess proper colocalization, intensity-corrected and brain-masked TRUFISP anatomicals from the pre- and post-deprivation MR sessions were coregistered using

normalized mutual information minimisation as implemented in the SPM8 toolbox (https://www.fil.ion.ucl.ac.uk/spm/software/spm8/). The obtained post-to-pre spatial transformation was applied to the post-deprivation MRS voxel prescription in scanner space. The pre- and coregistered post-deprivation MRS voxels were drawn as high-resolution masks using the MarsBaR toolbox (http://marsbar.sourceforge.net/ (Brett et al., 2002)). These were overlaid on the pre-deprivation MPRAGE anatomicals for visualization, and volumetric percent voxel mask overlap was computed.

3.4.1.4 Behavioral Measures of Sensory Eye Dominance

3.4.1.4.1 From Perception of Binocularly Combined Stimuli

One eye usually exerts a relatively stronger influence on cortical activity and perception—this is sensory eye dominance (SED) (Dieter et al., 2017; Huang et al., 2009). This is manifest in the process of combining compatible stimuli from the two eyes, i.e. identical or very similar stimuli. We used a version of the standard Binocular Phase Combination task (Ding & Sperling, 2006; Huang et al., 2009; Zhou et al., 2013), where dichoptic gratings with a small between-eye phase offset are binocularly combined into the 'cyclopean' perception of a single grating showing a phase-bias toward the dominant eye.

3.4.1.4.1.1 Apparatus and Stimuli

The dichoptic stimuli were spatially overlaid, maximal contrast, horizontal 0.3 cpd sine-wave gratings, spanning 6.6dva (two cycles) horizontally and vertically, one presented in each eye and differing only in their phase being respectively shifted by -22.5° and +22.5°. A high-contrast binocular frame aided binocular fusion and proper binocular alignment was ensured through the adjustment of nonius lines before each measure.

Stimulus presentation and response recordings used the Psychophysics Toolbox extensions (Brainard, 1997) in Matlab. Dichoptic stimulus presentation was achieved with a linearized MR-compatible polarizer LCD screen (BOLDscreen, Cambridge Research Systems; circularly polarized interleaved lines) placed at the back of the MR scanner bore and viewed through polarized filters and a mirror at an effective distance of 1.15m.

3.4.1.4.1.2 Task

On a given trial, participants had unlimited time to indicate the phase of the perceived grating by adjusting the position of a reference line to the center of the middle dark stripe. One behavioral measurement contained 16 trials, where response bias was removed by randomly picking the initial position of the reference line and by inverting the polarity of the physical dichoptic phase shifts on a randomly chosen half of the trials. After few training trials prior to the experiment, one behavioral measure typically completed within 2 minutes.

3.4.1.4.1.3 Analysis

The perceived phase reported on single trials was pooled across measures and averaged to compute the post-pre MD-induced perceived phase shift in degrees. A 0-value indicates no effect of MD and negative or positive values indicate SED shifted toward the deprived (DE) or non-deprived (NDE) eye, respectively. Within-subject 95% confidence intervals were obtained from 12,000 bootstrap resamples of 2×16 pre- and 2×16 post-deprivation trials, with replacement. Group-level 95% confidence intervals were obtained from 12,000 bootstrap resamples of 5 participants, with replacement.

3.4.1.4.2 From Perception of Binocularly Competing Stimuli

SED is also manifest during the process of binocular competition, or rivalry, between incompatible (i.e. very different) dichoptic stimuli. We used a version of the standard Binocular Rivalry task (Lunghi et al., 2011; Lunghi et al., 2015; Sheynin et al., 2019; Skerswetat et al., 2016, 2018), where two gratings differently oriented in each eye compete for conscious awareness. Despite unchanging physical stimuli, conscious perception continuously changes, alternating every ~1-10 seconds between (1) exclusively perceiving the stimulus from one eye, (2) exclusively perceiving the stimulus from the other eye and (3) perceiving a piecemeal or overlay binocular mixture in varying proportions of the two eye's stimuli (Skerswetat et al., 2016, 2018). SED is evident from longer durations of perceptual periods, or percepts, driven by the dominant eye.

3.4.1.4.2.1 Apparatus and Stimuli

Stimulus presentation and response recording used the Psychophysics Toolbox extensions (Brainard, 1997) in Matlab. Dichoptic stimulus presentation was achieved with a linearized MR-compatible polarizer LCD screen (BOLDscreen, Cambridge Research Systems; circularly polarized interleaved lines) placed at the back of the MR scanner bore and viewed through polarized filters and a mirror at an effective distance of 1.15m.

The binocularly rivalrous dichoptic stimuli consisted of two static achromatic sine-wave gratings (3-cpd; 50%-contrast) spanning 3.5×3.5 dva of the central visual field, differing only in orientation (-26.6˚ and +26.6˚ relative to vertical respectively in one and the other eye). A high contrast surrounding binocular frame aided binocular fusion.

3.4.1.4.2.2 Task

After nonius line adjustment for binocular alignment, subjects initiated the presentation of stimuli. In a continuous version of a two-alternative forced-choice task, they continuously reported their rivaling perception by pressing and holding down either one of two keys depending, at any moment, on the most clearly perceived of two stimulus orientations. They were specifically instructed to fixate the center of the stimulus, to hold one key down at a time and to always be holding a key down, even when one orientation did not clearly stand-out during periods of mixed perception (forced-choice). Assignment of grating orientation to each eye was randomly chosen at the beginning of each 90-sec rivalry trial, with two consecutive trials per ~3-min rivalry measurement.

Stable performance on the task was ensured by several practice measurements performed on a day prior to the experiment.

3.4.1.4.2.3 Analysis

A given eye's response strength was inferred from the duration of percepts where the corresponding stimulus orientation dominated perception. Percepts shorter than 180ms were discarded (Skerswetat et al., 2016, 2018), as well as percepts interrupted by termination of stimulus presentation. The gamma distributed durations were normalized by taking their natural logarithm, then averaged within each ~3-min measurement. The two pre- and the two

post-MD measurements were further averaged into single measures of pre- and post-MD percept duration.

A deprivation index (depIndex) was derived as in Lunghi et al. (2015), following:

$$\text{depIndex} = \frac{x_{deprived\ eye}^{pre\ deprivation}}{x_{deprived\ eye}^{post\ deprivation}} \times \frac{x_{non\ deprived\ eye}^{post\ deprivation}}{x_{non\ deprived\ eye}^{pre\ deprivation}} \quad 3.1$$

where x refers to the average dominant percept duration (exponentiated back in linear units of seconds) from the DE or NDE (subscripts) and measured before and after MD (superscripts). It summarizes the effect of MD on SED, where a value of 1 means no change, <1 is the expected shift toward the DE and >1 is a shift toward the NDE.

Within-subject 95% confidence intervals were obtained from 12,000 bootstrap resamples of the same number of percepts contained within a ~3-min measure, with replacement. Group-level 95% confidence intervals were obtained from 12,000 bootstrap resamples of 5 participants, with replacement.

3.4.1.5 Neurophysiological Measure of Sensory Eye Dominance from Neural Activity Driven by Frequency-Tagging Dichoptic Stimuli

Measurement of frequency-tagged steady-state visually evoked MEG potentials was described in Chadnova et al. (2017), where dichoptic visual noise patterns flickering at different frequencies in each eye are driving neural activity at the corresponding frequencies. The MEG signal at these "tagged" frequency bands therefore allowed us to isolate the contribution of each eye to cortical neural activity (Norcia et al., 2015).

3.4.1.5.1 Apparatus and Stimuli

Stimuli were generated and controlled using the Psychophysics toolbox (Brainard, 1997; Pelli, 1997) in Matlab, displayed in the dimly-illuminated, magnetically-shielded MEG room on a linearized 3D polarizer monitor (LG 23", 1920 × 1080, 60Hz refresh rate), and viewed through polarized filters at a 170-cm viewing distance. The stimuli in each eye consisted of a different binary noise pattern presented within a soft-edge circular aperture of 8° in diameter over a mean luminance gray background and surrounded by a binocular frame to aid fusion.

Tagging of MEG signal driven by each eye was achieved through cyclical onset/offset modulation (sinusoidal modulation between 32% contrast and mean luminance) of the noise pattern stimuli at 4 and 6Hz, respectively for the non-dominant and the dominant eye. These stimuli were presented in 4-second trials with a 1.5-second delay between trials. One measure lasted ~8-min and contained a single block of 80 trials, randomly interleaving 20 repetitions of 4 stimulus conditions. Participants were instructed to passively view the stimuli while fixating a black cross overlaying the center of the stimulus field.

The 4 stimulus conditions included (1) non-dominant and (2) dominant eye monocular stimulation, (3) dichoptic stimulation and (4) null 0%-contrast stimulation. Only the dichoptic stimulation condition is considered here as it revealed the strongest SED shift after monocular deprivation in the full cohort in Chadnova et al. (2017).

3.4.1.5.2 MEG Recordings and Processing

MEG data were collected at 2.4kHz using a CTF OMEGA System with 275 gradiometers located in a 3-layer magnetically shielded room. Prior to each session, a 2-minute recording captured the daily environmental noise statistics (sample data covariance across MEG channels) for later use in MEG source modeling. Participants' head position within the MEG system was localized at the beginning of each recording block using three indicator coils registered to head landmarks and cranial shape previously digitized using a Polhemus Isotrak system. Eye blinks and movements and electrocardiographic signals were recorded from two electrodes above and below the left eye and two others across the plane of the chest.

Data preprocessing, source reconstruction and analysis used Brainstorm. Preprocessing removed heartbeats and eye blinks/movements artifacts (Gross et al., 2013; Uusitalo & Ilmoniemi, 1997) and resampled MEG signal to 1kHz with no band-pass filtering. Multi-channel MEG signals were reconstructed into source space time series at 15,000 vertices of individual participant's cortical surface using the empty-room noise statistics and the depth-weighted L2-minimum norm estimator (Baillet et al., 2001). Time-resolved power spectral density was obtained for each 4-sec trial (1000-ms window; 50% overlap) and at each vertex of a V1 ROI derived from standard functional MR imaging retinotopic mapping (Clavagnier et al., 2015;

Dumoulin & Wandell, 2008; Engel et al., 1994) obtained from other studies. Time points covering the first 500ms of a trial were discarded to ensure steady-state. Signals were averaged over time and V1 vertices within trials. Trials from consecutive measures (acquisition blocs) were pooled, separately for pre- and post-deprivation measures and stimulus conditions.

3.4.1.5.3 Analysis

Power spectra were normalized within acquisition blocs by dividing by the power spectrum averaged from null non-stimulated trials. The contribution of the non-deprived (dominant) eye to V1 neural activity was then estimated from the normalized power at the tagged 4Hz frequency band, averaged over trials and separately for pre- and post-deprivation trials. The contribution of the deprived (non-dominant) eye was estimated the same way using the tagged 6Hz frequency. Calculation of the deprivation index followed Eq1, where x is now the normalized frequency-tagged MEG signal power density described above. Within-subject 95% confidence intervals were obtained from 12,000 bootstrap resamples of 3×20 pre- and 3×20 post-deprivation trials, with replacement. Group-level 95% confidence intervals were obtained from 12,000 bootstrap resamples of 5 participants.

3.4.1.6 Statistical Analysis

3.4.1.6.1 Bayesian Statistics

Formal comparison to existing studies—in our case Lunghi et al. (2015)'s—is best achieved within the Bayesian Framework (Wagenmakers, Marsman, et al., 2018), which fundamentally relies on the effect of evidence (newly acquired data) on our belief (null and alternate hypotheses). This belief can be generic (i.e. using a general-purpose prior distribution of possible effect sizes) or informed (i.e. using a prior distribution of expected effect sizes derived from a previous study). Bayesian Factor (BF) hypothesis testing consists in 1) formalizing the hypotheses (H_0 and H_1) into a prior distribution, 2) updating it with evidence, i.e. newly acquired data, and 3) quantifying how our belief in H_1 *and* the null hypothesis (H_0) changed to finally 4) compute the desired BF (e.g. BF_{10}), i.e. the ratio of change in these beliefs (e.g. H_1/H_0).

The logic underlying BF analysis more closely follows the process of empirical knowledge validation. This makes BF analysis superior to frequentist hypothesis testing especially when a

quantitative judgment on the H_0 is needed. With a frequentist approach, failure to reject H_0 is inconclusive—formally, a p-value can only indicate either 1) support for H_1 from the exclusion of H_0 or 2) inconclusive results, as judgment on acceptation of H_0 is ill-defined. The formalization of prior beliefs within the calculation of a BF allows for a third possible conclusion: 3) support for the H_0. Otherwise said, from a BF one *can* conclude the hypothesis is wrong.

This comes in particularly handy when one attempts to replicate a previous study. Frequentist summary statistics do not formally allow to conclude failure of replication. In the Bayesian framework, deriving the priors from the results of a previous study turns H_1 into the hypothesis of replication (H_r). Computing a BF_{r0} then formally allows to conclude whether the new experiment replicated the previous one (support for H_r), failed to replicate it (support for H_0) or is statistically inconclusive (requires more data). From choosing differently shaped prior distribution of possible effect sizes, more specific hypothesis like that of a negative or positive one-sided effect (H_- or H_+, respectively) can be weighed against H_0 (yielding BF_{-0} BF_{+0}, respectively).

Finally, the BF is designed to allow, when properly visualized on a logarithmic scale, for a *graded* judgement on the collected evidence (Wagenmakers, Love, et al., 2018)—from perfectly ambiguous (BF_{10} = 1) or inconclusive (BF_{10} = 1 to 3: *anecdotal* support for the H_1; $BF_{10} = \frac{1}{3}$ to 1: *anecdotal* support for H_0) to conclusive, i.e. providing *moderate*, *strong* or *very strong* support for H_1 (BF_{10} > 3, BF > 10 or BF > 100, respectively) or H_0 ($BF_{10} < \frac{1}{3}$, BF < $\frac{1}{10}$ or BF < $\frac{1}{100}$, respectively). Note that support for H_0 can also be expressed as the reciprocal of support for H_1 ($BF_{01} = \frac{1}{BF_{10}}$).

BF analyses being more appropriate for replication test, it was chosen for Exp I as it is mostly concerned with replicating Lunghi et al. (2015)'s findings. For statistics not concerned with replication, we used BF versions of T-tests and Kendall's correlation (Verhagen & Wagenmakers, 2014; Wagenmakers et al., 2016) for consistency and for taking the full benefit of graded judgment on instances of ambiguous results.

BF T-tests used the default Cauchy prior with scale 0.707 and BF Kendall's correlation tests used the default flat prior. For BF replication tests, priors were derived from Lunghi et al. (2015). All Bayesian analysis followed (Verhagen & Wagenmakers, 2014; Wagenmakers et al., 2016) implemented in R 3.4.0 and JASP 0.11.1.

3.4.1.6.2 Multi-Level Bootstrapping for Correlation Coefficient Confidence Intervals Robust to Within-Subject Measurement Error

To further evaluate the robustness of correlations between GABA changes and the three estimates of SED shift, we used a multi-level bootstrapping approach to take into account the effect of within-subject measurement error on the estimates of the precision (confidence intervals) of between-subject correlations. The multi-level bootstrapping scheme combines the single-subject and group-level bootstrapping procedures described above, by nesting *within-subject* resamples within each *group-level* resample. More explicitly, to perform *one* multi-level resample, we first perform a group-level resample—i.e. we resample 5 subjects with replacement. Then, for each resampled subject, we perform a *within-subject* resample—i.e. we resample *n* data points with replacement, *n* being the number acquired data points within a given subject. Finally, we average the *n* data points within each resampled subject and compute between-subject correlation, yielding the correlation coefficient of *the* multi-level resample. By repeating this multi-level resampling 12,000 times, we empirically build a bootstrapped estimate of the distribution of correlation coefficients that accounts for the uncertainty of single-subject measures. We reported the 95% confidence interval of both this distribution of correlation coefficients and of the similarly constructed distribution of regression lines. In-house permutation tests and simulations revealed this multi-level approach to be conservative relative to parametric or simpler group-level bootstrap estimates of confidence intervals—as expected from taking into account within-subject measurement error when computing between-subject correlation in a small sample.

3.4.1.7 Data Availability

Processed data are available at https://doi.org/10.5281/zenodo.4095913. Raw data are available upon request to the corresponding author.

3.4.1.8 Supplementary Results

Volume overlap between pre- and post-MD MRS voxels ranged between 94.5% and 99.2%. Acquired spectra showed minimal lipid contamination, high SNRs and narrow linewidths, and LCModel metrics of reliability of the fits were all below the recommended 20% for NAA and GABA (**Supplementary Figure 3.1**A).

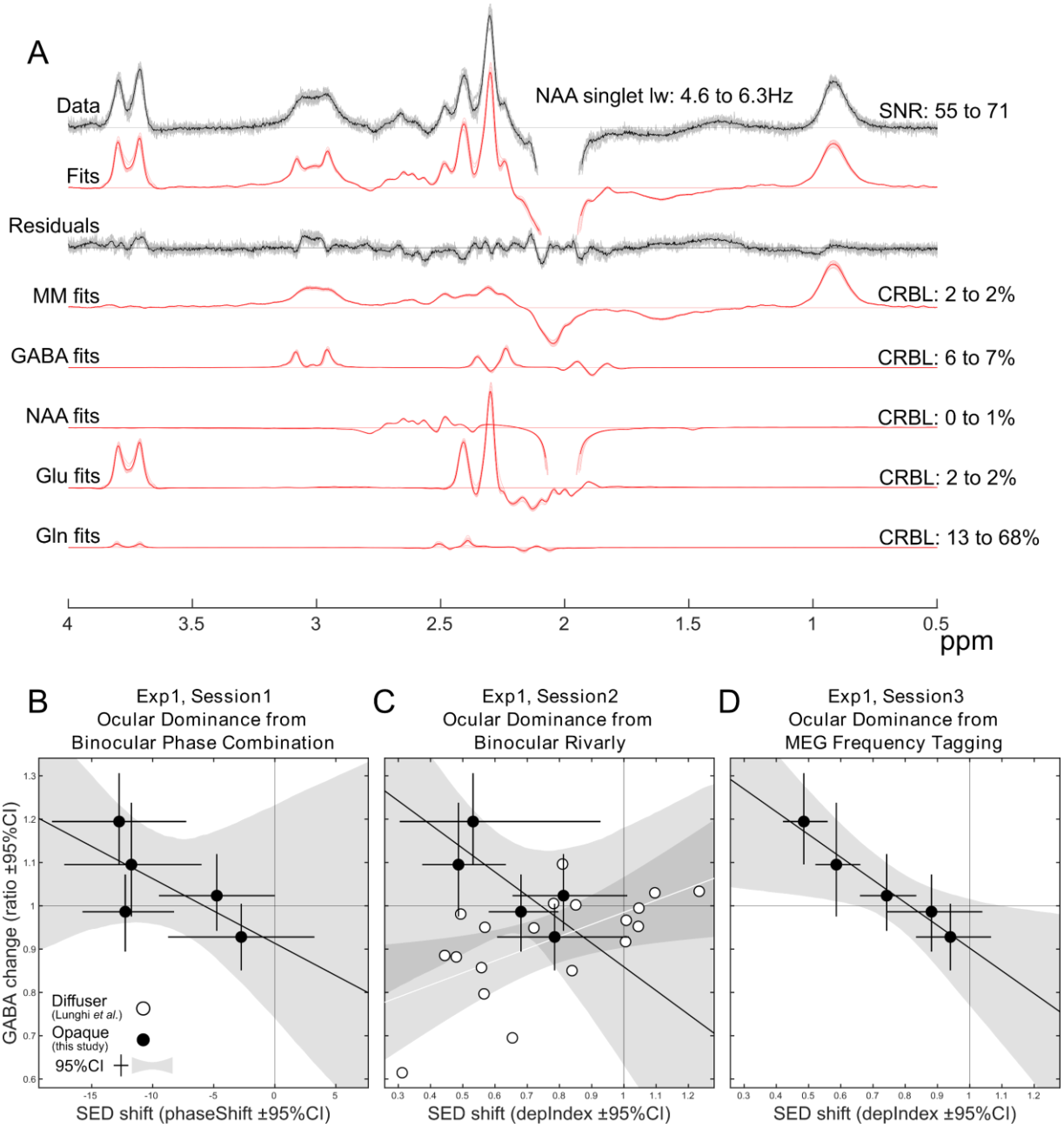

Supplementary Figure 3.1 All data from Experiment I. A. All GABA-edited MR spectra (black traces) and their fits (red traces). Heavy black and red traces represent cross-subject averages. Light black and red traces represent

single measures, one pre- and one post-MD measure per each subject. Heavy traces represent the group average. A fit is composed of the combination of five model spectra, modeling the contribution of different metabolites to the measured spectrum—namely GABA, NAA, glutamate and glutamine—as well as the contribution of the baseline of macromolecules (MM). The main NAA resonance at 1.9ppm was truncated for visualization purposes only, and its linewidth was measured as the full width at half maximum of its fit. Metrics of spectral signal-to-noise (SNR) ratio and reliability of single metabolite fits (CRLB for Cramer-Rao Lower Bound) are provided by the spectral fitting LCModel software. **B, C and D.** MRS GABA data as a function of SED shift measured behaviorally from the phase combination task (B) and the binocular rivalry task (C), and measured electrophysiologically from frequency-tagged MEG signals (D). The three graph share the same y-axis. Values above the horizontal null line indicate increases after MD and values to the left of the vertical null line indicate SED shifts toward the DE. Black lines are the linear fit to data from this study and their surrounding shaded areas the multilevel bootstrapped 95% confidence intervals (see text for details). The white line of C is the fit to the data from Lunghi et al. (2015) and its surrounding shaded area the group-level bootstrapped 95% confidence interval. Data from D are the same as in **Figure 3.1** of the main text. Error bars represent measurement error estimated from within-subject bootstrapped 95% confidence intervals.

3.4.1.9 Supplementary Discussion

The lack of a control for a potential time of day effect constitute a limitation of this study. Indeed, a no-MD group included in Lunghi's orginal study suggested GABA can increase in V1 with the passage of time only. This was based on an underpower trend (GABA:tNAA: $t(6) = 1.7$, $p = 0.14$) that nevertheless warrants caution in interpreting our GABA findings. It is important to note that our observation of increased GABA after deprivation is also an underpowered trend, and that our argument for a role of GABA in opaque MD rests on the correlation with MEG SED measures—which although also underpowered is significant—as well as on indirect evidence from Exp II. The potential time-of-day confound in our correlation between GABA and SED changes could be controlled for by comparing it data from Lunghi's no-MD group. SED data from the latter were unfortunately not reported.

3.4.2 Experiment II: Dissociable Mechanisms of Ocular Dominance Plasticity Induced by Opaque- vs Diffuser-Patch Monocular Deprivation

3.4.2.1 Participants

Fourteen healthy human adults (Four females; mean age 28.5, range 20-40 years) with normal or corrected-to-normal vision participated after providing informed consent for the protocol, approved by the research ethics board of the Montreal Neurological Institute. They had experience in performing various psychophysical tasks but were naïve to the purpose of the experiment, except the two authors (SP and YS).

3.4.2.2 Study Design

We used a within-subject controlled cross-over design to compare the effects of MD treatments using a diffuser or an opaque eye patch. Participants were subjected to 4 weekly MD sessions (inter-session delay: median 9d, range 3-43d), alternating patch type on successive sessions and counter-balancing order across participants. Each participant therefore experienced, for the first time, one treatment type on session 1 and the other on session 2. They then experienced the same treatments a second time and in the same order on session 3 and 4.

For simplicity, statistical analysis was performed on dependent variables corresponding to the post-pre effect of MD. Within-subject factors included Treatment Cross-Over (one treatment type in sessions 1 and 3 VS the other treatment type in sessions 2 and 4) and Treatment Repetition ('early' repetition in sessions 1 and 2 VS 'late' repetition in sessions 3 and 4). A between-subject factor accounted for Treatment Order (diffuser patch treatment in sessions 1 and 3 and opaque patch treatment in session 2 and 4 VS opaque patch treatment in sessions 1 and 3 and diffuser patch treatment in session 2 and 4). The effect of interest therefore corresponds to a Treatment Cross-Over × Treatment Order interaction, which we will refer to as a Treatment Type factor for simplicity. Properly accounting for the extra degrees of freedom of the cross-over design, this statistical analysis is conservative compared to one ignoring Treatment Order by out sessions according to Treatment Type.

Results reported in the main text exclusively concern the two early sessions. Late sessions interestingly differed from early ones, as reported here in the Supplementary Results section.

3.4.2.3 Monocular Deprivation

Similar to Exp I, the dominant eye (Miles' sighting eye dominanceMiles, 1929; Valle-Inclan et al., 2008) was occluded, this time for 120min during which the participants were asked to stay in the vicinity of our laboratory but with no specific instructions other than to keep the patch in place. Diffuser-patch MD used mylar paper (~20% mean luminance reduction) mounted on goggles and opaque-patch MD used a standard wearable medical occluder made of opaque black fabric. Both patches were tight fitted around the orbit using opaque tape on top of

medical tape. Diffuser MD effectively blinded the eye to spatial information while allowing temporal changes in mean luminance to reach the retina. Opaque MD prevented all light from reaching the retina.

3.4.2.4 Binocular Rivalry Task

Binocular rivalry behavioral measurements used rivaling stimuli (different orientation presented in each eye) only slightly different from experiment one. Task instructions however allowed to infer monocular response strength from the duration of exclusively monocular percepts (i.e. when only the stimulus from one eye is perceived) and binocular response strength from the duration of binocularly mixed percepts (i.e. when a piecemeal or overlay mixture of the two stimuli, in any proportion, is perceived) (Riesen et al., 2019).

3.4.2.4.1 Apparatus and Stimuli

Stimulus presentation and response recording used the Psychophysics Toolbox extensions (Brainard, 1997) in Matlab. Dichoptic stimulus presentation was achieved with a linearized 3-D monitor (HP 2311gt; circularly polarized interleaved lines) viewed through polarized filters at a 30.5-cm viewing distance.

The binocularly rivalrous stimuli were two static, continuously presented and orthogonally-oriented achromatic sine-wave gratings ($\pm$45˚ orientation, 3cpd spatial frequency) seen through a Gaussian aperture (σ=0.75 degree of visual angle; visible range of ~1.5dva) with 50% contrast. They were dichoptically presented with a different orientation in eye and surrounded by a high contrast binocular square frame (~4.75dva away from the visible range of the test stimuli) to aid binocular fusion.

3.4.2.4.2 Task

Participants initiated stimulus presentation and reported their perception through key presses. They were instructed to fixate the center of the stimuli and to hold down a key when they exclusively perceived one grating, and another key when they exclusively perceived the other grating. Whenever they perceived any mixture in any proportion of the two gratings, whether in the form of a transparent overlay or a piecemeal mixture, they were instructed to

release and not press any key. This therefore corresponded to a continuous version of a three-alternative forced choice task.

Examples of exclusive and overlay/piecemeal mixed percepts were shown on a printout and, on a day prior to actual data collection, participants familiarized with the task until stable performance was achieved. A rivalry measurement lasted 180 seconds, divided in two halves between which the assignment of the two grating orientations to each eyes was flipped to counter-balance a potential response bias. Short breaks were allowed between half-trials and trials. Two-consecutive ~3-min measurements were performed immediately before and after MD.

3.4.2.4.3 Analysis

Analysis was the same as in Exp I, with the addition a third percept type which was defined as the periods when no key was pressed. Too short percepts and those interrupted by the end of a half-trial or a trial were discarded. The natural logarithm of percept durations were averaged within then across consecutive measurements to yield normally-distributed single measures of pre- and post-MD percept (DE exclusively monocular, NDE exclusively monocular and binocularly mixed) durations. Most statistics used these averaged log percept duration measures. The deprivation index was however also computed, using Eq. 1 where x now refers to the average exclusively monocular percept duration exponentiated back in linear units of seconds.

Single-subject 95% confidence intervals were obtained from 12,000 bootstrap resamples of the same number of percepts contained within a ~3-min measure, with replacement. Group-level 95% confidence intervals were obtained from 12,000 bootstrap resamples of 5 participants.

3.4.2.5 Frequentist Statistical Analysis

We performed most statistical tests using functions from the Matlab R2017a Statistical Toolbox (rmANOVAs, Pearson's correlations and paired T-tests) or an in-house modification of the function (rmMANOVAs). The rmANCOVAs were performed with the *mixed* function of the IBM SPSS Statistics 23 software, using compound symmetry covariance structure and

continuous time-varying covariates z-scored cell-wise. See Study Design section for statistical designs and Supplementary Results section for more details and supplementary results.

3.4.2.6 Data Availability

Processed data are available at https://doi.org/10.5281/zenodo.4095828. Raw data are available upon request to the corresponding author.

3.4.2.7 Supplementary Results and Discussion

Supplementary Figure 3.2 shows the full dataset, i.e. data from the first two 'early' sessions (Supplementary Figure 3.2A and B; same data as Figure 3.1 of the main text) and from the following two 'late' sessions (where each participant experienced the same two treatments a second time and in the same order; Supplementary Figure 3.2C and D). Analysis of this full dataset revealed a third mechanism for OD plasticity that operates in 'late' sessions (rmMANOVA on the three dependent variables of DE and NDE exclusively monocular and binocularly mixed percept duration changes: Treatment Repetition × Treatment Type interaction, $F_{3,10}$=4.1, p=0.038). 'Late'-session MD is as potent as 'early'-session MD in shifting SED (left subpanel; rmANOVA on SED shifts: no main of or interaction effect with Treatment Repetition). It however now operates similarly for both treatment types (Supplementary Figure 3.2C; rmMANOVA: no main effect of Treatment Type in late sessions, $F_{3,10}$=0.7, p=0.571), i.e. through decreased NDE percept durations (rmANOVA: main effect, $F_{1,12}$=12.5, p=0.004; no interaction with Treatment Type, $F_{1,12}$=1.7, p=0.220) and marginally significant DE increases (rmANOVA: main effect, $F_{1,12}$=3.5, p=0.086; no interaction with Treatment Type, $F_{1,12}$=0.1, p=0.738).

Also, binocular vision during rivalry was not affected in 'late' sessions (Supplementary Figure 3.2C; rmANOVA: no treatment effect on mixed percepts evidenced by a null intercept, $F_{1,12}$=0.0, p=0.855) where, contrary to 'early' sessions, diffuser MD did not increase durations of binocularly mixed percepts ('late': t_{13}=-0.0, p=0.981; 'early' vs 'late': t_{13}=1.9, one-sided p=0.041). The inconsistent 'late'-session changes in binocular percepts did not anymore—as compared to 'early' sessions—predict NDE monocular changes (rmANCOVA on mixed percept

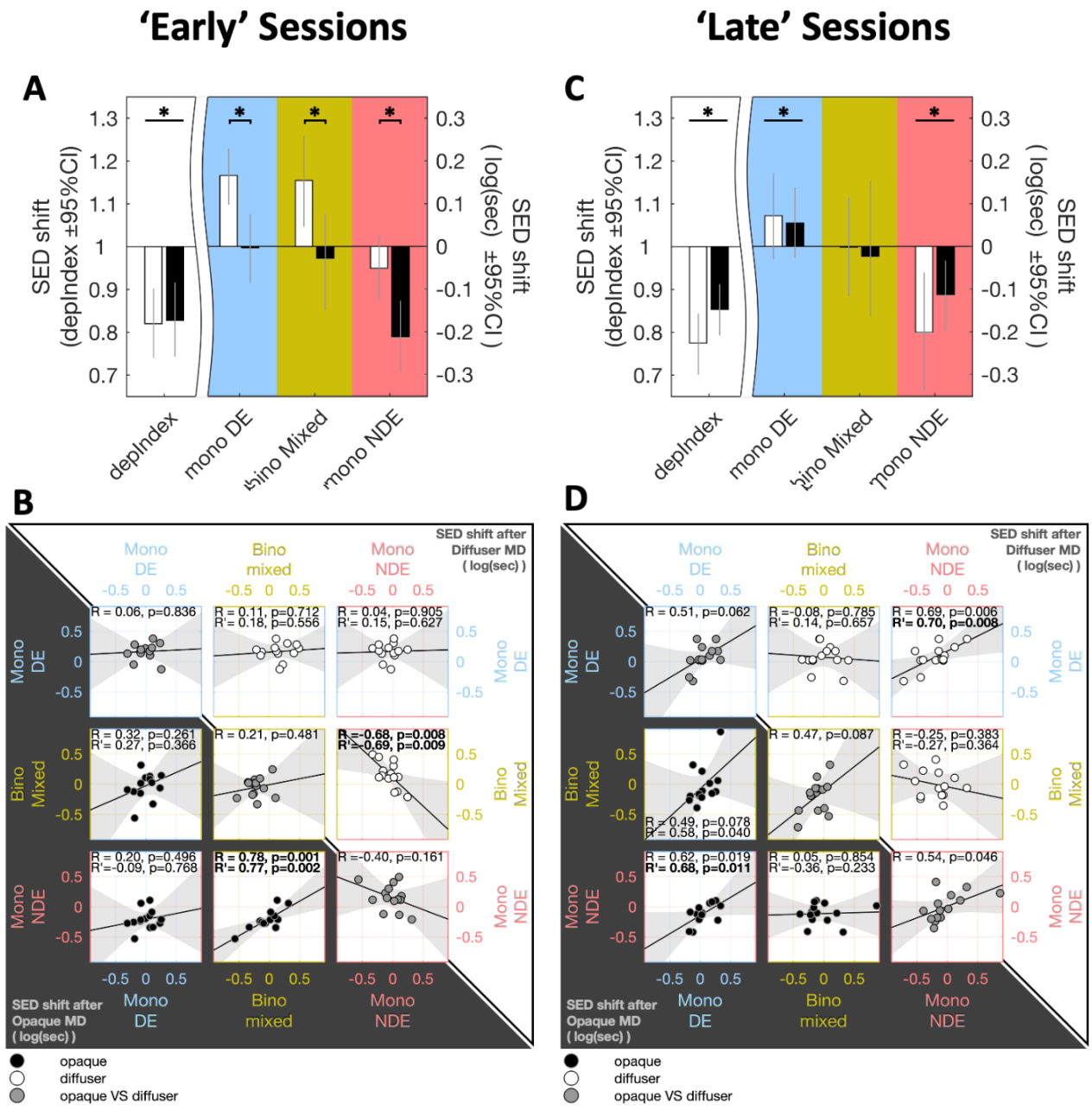

Supplementary Figure 3.2. All data from Experiment II, from the first two 'early' (A and B) and the following two 'late' (C and D) sessions of MD and pre/post binocular rivalry measures. **A and B.** Group averages of the MD effect on SED (left sub-panels) and on durations of monocular (mono) and binocular (bino) percepts. **C and D.** Correlation matrices showing the relation between MD-induced changes in monocular and binocular percept duration. Lower and upper triangle scatter plots show these relations within opaque and diffuser MD sessions, respectively. Diagonal scatter plots show the relation between changes in duration of percept of the same type but induced by different treatment types. Displayed on each plot is the Pearson's correlation coefficient (R) as well as the partial Pearson's correlation coefficient (R') accounting for covariation of the third percept type (e.g. lower left plot shows the correlation between DE and NDE monocular changes after opaque MD and the partial correlation accounts for the covariate of changes in binocularly mixed percept). Bolded statistics showed significance that survived false-discovery rate correction applied over all performed correlations, but separately for each treatment repetition and regular vs partial correlations. Data in A are the same as the bars in Figure 3.1 H, I and J. Data from B, middle row/right column and bottom row/middle column, are the same as the scatter in Figure 3.1 J.

with NDE percept covariate: Treatment Repetition × Treatment Type × NDE covariate interaction, $F_{1,45.2}$=4.9, p=0.032; 'late'-session mixed VS NDE percept correlations: R=0.05, p=0.854 for opaque and R=-0.25, p=0.383 for diffuser patches; compare lower row/middle column and middle/right column plots between Supplementary Figure 3.2B and D). Instead, 'late'-session DE and NDE monocular changes related to one another (Supplementary Figure 3.2C, lower row/left column and upper row/right column plots; R=0.62, p=0.019 for opaque and R=0.69, p=0.006 for diffuser patches). See Supplementary Figure 3.2B and D for all correlations.

These results suggest that—at least in our protocol interleaving diffuser and opaque MD treatments across consecutive weeks—the visual system stores a "memory" trace of the experienced MD adaptations for at least one week, allowing a different response to subsequent adaptation challenges. Indeed, newly formed GABA synapses in the binocular cortex of adult mice are maintained for at least 2 weeks during post-MD recovery and support faster adaptation on a 2nd MD treatment (Hofer et al., 2009). Interestingly, the neural substrate of visual adaptation overlaps with those of learning: e.g. successfully learning to perform better in a given adapted state comes at the cost of degraded performance in other adapted states (McGovern et al., 2012). Our pattern of results therefore suggests that the visual system can face repeated and varying short-term sensory alterations with a variety of plastic mechanisms. These might be best understood in terms of gain-control and homeostatic mechanisms that automatically maintain individual neurons around an optimal response range; with the addition of perceptual learning and memory mechanisms that refine the population response of the adapted neurons for optimal perceptual performances under the learnt adapted states.

Importantly, this effect of repeating interleaved MD treatments warrants caution in future studies for recruiting naïve participants, as is common in studies on learning and memory.

3.5 Bibliography

Baillet, S., Mosher, J. C., & Leahy, R. M. (2001). Electromagnetic brain mapping [Article]. *Ieee Signal Processing Magazine*, *18*(6), 14-30. https://doi.org/10.1109/79.962275

Brainard, D. H. (1997). The psychophysics toolbox. *Spatial Vision*, *10*(4), 433-436. https://doi.org/10.1163/156856897x00357

Brett, M., Anton, J.-L., Valabregue, R., & Poline, J.-B. (2002, June 2-6). Region of interest analysis using an SPM toolbox. 8th International Conference on Functional Mapping of the Human Brain, Sendai, Japan.

Chadnova, E., Reynaud, A., Clavagnier, S., & Hess, R. F. (2017). Short-term monocular occlusion produces changes in ocular dominance by a reciprocal modulation of interocular inhibition [Article]. *Scientific Reports*, *7*, 6, Article 41747. https://doi.org/10.1038/srep41747

Clavagnier, S., Dumoulin, S. O., & Hess, R. F. (2015). Is the Cortical Deficit in Amblyopia Due to Reduced Cortical Magnification, Loss of Neural Resolution, or Neural Disorganization? [Article]. *Journal of Neuroscience*, *35*(44), 14740-14755. https://doi.org/10.1523/jneurosci.1101-15.2015

Dieter, K. C., Sy, J. L., & Blake, R. (2017). Individual differences in sensory eye dominance reflected in the dynamics of binocular rivalry [Article]. *Vision Research*, *141*, 40-50. https://doi.org/10.1016/j.visres.2016.09.014

Ding, J., & Sperling, G. (2006). A gain-control theory of binocular combination [Article]. *Proceedings of the National Academy of Sciences of the United States of America*, *103*(4), 1141-1146. https://doi.org/10.1073/pnas.0509629103

Dumoulin, S. O., & Wandell, B. A. (2008). Population receptive field estimates in human visual cortex [Article]. *Neuroimage*, *39*(2), 647-660. https://doi.org/10.1016/j.neuroimage.2007.09.034

Engel, S. A., Rumelhart, D. E., Wandell, B. A., Lee, A. T., Glover, G. H., Chichilnisky, E. J., & Shadlen, M. N. (1994). FMRI OF HUMAN VISUAL-CORTEX [Letter]. *Nature*, *369*(6481), 525-525. https://doi.org/10.1038/369525a0

Frangou, P., Correia, M., & Kourtzi, Z. (2018). GABA, not BOLD, reveals dissociable learning-dependent plasticity mechanisms in the human brain [Article]. *Elife*, *7*, 22, Article e35854. https://doi.org/10.7554/eLife.35854

Frangou, P., Emir, U. E., Karlaftis, V. M., Nettekoven, C., Hinson, E. L., Larcombe, S., Bridge, H., Stagg, C. J., & Kourtzi, Z. (2019). Learning to optimize perceptual decisions through suppressive interactions in the human brain [Article]. *Nature Communications*, *10*, 12, Article 474. https://doi.org/10.1038/s41467-019-08313-y

Frenkel, M. Y., & Bear, M. F. (2004). How monocular deprivation shifts ocular dominance in visual cortex of young mice. *Neuron*, *44*(6), 917-923. https://doi.org/10.1016/j.neuron.2004.12.003

Gainey, M. A., & Feldman, D. E. (2017). Multiple shared mechanisms for homeostatic plasticity in rodent somatosensory and visual cortex [Review]. *Philosophical Transactions of the Royal Society B-Biological Sciences*, *372*(1715), 7, Article 20160157. https://doi.org/10.1098/rstb.2016.0157

Gross, J., Baillet, S., Barnes, G. R., Henson, R. N., Hillebrand, A., Jensen, O., Jerbi, K., Litvak, V., Maess, B., Oostenveld, R., Parkkonen, L., Taylor, J. R., van Wassenhove, V., Wibral, M., & Schoffelen, J. M. (2013). Good practice for conducting and reporting MEG research [Article]. *Neuroimage*, *65*, 349-363. https://doi.org/10.1016/j.neuroimage.2012.10.001

Gruetter, R., & Tkac, I. (2000). Field mapping without reference scan using asymmetric echo-planar techniques [Article]. *Magnetic Resonance in Medicine*, *43*(2), 319-323. https://doi.org/10.1002/(sici)1522-2594(200002)43:2<319::aid-mrm22>3.0.co;2-1

Hofer, S. B., Mrsic-Flogel, T. D., Bonhoeffer, T., & Hubener, M. (2009). Experience leaves a lasting structural trace in cortical circuits [Article]. *Nature*, *457*(7227), 313-U314. https://doi.org/10.1038/nature07487

Huang, C. B., Zhou, J. W., Lu, Z. L., Feng, L. X., & Zhou, Y. F. (2009). Binocular combination in anisometropic amblyopia [Article]. *Journal of Vision*, *9*(3), 16, Article 17. https://doi.org/10.1167/9.3.17

Ip, I. B., Emir, U. E., Lunghi, C., Parker, A. J., & Bridge, H. (2021). GABAergic inhibition in the human visual cortex relates to eye dominance. *Scientific Reports*, *11*(1), Article 17022. https://doi.org/10.1038/s41598-021-95685-1

Klink, P. C., Brascamp, J. W., Blake, R., & van Wezel, R. J. A. (2010). Experience-Driven Plasticity in Binocular Vision. *Current Biology*, *20*(16), 1464-1469. https://doi.org/10.1016/j.cub.2010.06.057

Lunghi, C., Burr, D. C., & Morrone, C. (2011). Brief periods of monocular deprivation disrupt ocular balance in human adult visual cortex. *Current Biology*, *21*(14), R538-R539. https://doi.org/10.1016/j.cub.2011.06.004

Lunghi, C., Emir, U., Morrone, M. C., Burr, D. C., & Bridge, H. (2014). Transient monocular deprivation affects binocular rivalry and GABA concentrations in adult human visual cortex. *Journal of Vision*, *14*(10), 378-378. https://doi.org/10.1167/14.10.378

Lunghi, C., Emir, U. E., Morrone, M. C., & Bridge, H. (2015). Short-Term Monocular Deprivation Alters GABA in the Adult Human Visual Cortex [Article]. *Current Biology*, *25*(11), 1496-1501. https://doi.org/10.1016/j.cub.2015.04.021

Maffei, A., Nataraj, K., Nelson, S. B., & Turrigiano, G. G. (2006). Potentiation of cortical inhibition by visual deprivation [Article]. *Nature*, *443*(7107), 81-84. https://doi.org/10.1038/nature05079

Maffei, A., & Turrigiano, G. G. (2008). Multiple modes of network homeostasis in visual cortical layer 2/3 [Article]. *Journal of Neuroscience*, *28*(17), 4377-4384. https://doi.org/10.1523/jneurosci.5298-07.2008

McGovern, D. P., Roach, N. W., & Webb, B. S. (2012). Perceptual Learning Reconfigures the Effects of Visual Adaptation. *Journal of Neuroscience*, *32*(39), 13621-13629. https://doi.org/10.1523/jneurosci.1363-12.2012
Mescher, M., Merkle, H., Kirsch, J., Garwood, M., & Gruetter, R. (1998). Simultaneous in vivo spectral editing and water suppression. *Nmr in Biomedicine*, *11*(6), 266-272. https://doi.org/10.1002/(sici)1099-1492(199810)11:6<266::aid-nbm530>3.0.co;2-j
Miles, W. (1929). Ocular dominance demonstrated by unconscious sighting [Article]. *Journal of Experimental Psychology*, *12*, 113-126. https://doi.org/10.1037/h0075694
Norcia, A. M., Appelbaum, L. G., Ales, J. M., Cottereau, B. R., & Rossion, B. (2015). The steady-state visual evoked potential in vision research: A review [Article]. *Journal of Vision*, *15*(6), 46, Article 4. https://doi.org/10.1167/15.6.4
Nys, J., Scheyltjens, I., & Arckens, L. (2015). Visual system plasticity in mammals: the story of monocular enucleation-induced vision loss. *Front Syst Neurosci*, *9*, 60. https://doi.org/10.3389/fnsys.2015.00060
Pelli, D. G. (1997). The VideoToolbox software for visual psychophysics: Transforming numbers into movies [Article]. *Spatial Vision*, *10*(4), 437-442. https://doi.org/10.1163/156856897x00366
Proulx, S., Sheynin, Y., Hess, R., Farivar, R. (2020, June 23 to July 3). What Can MR Spectroscopy Measures of Occipital GABA tell about Visual Plasticity in Human Adult? 26th Annual Meeting of the Organization for Human Brain Mapping, Canada. https://doi.org/10.5281/zenodo.4034898
Provencher, S. W. (1993). ESTIMATION OF METABOLITE CONCENTRATIONS FROM LOCALIZED IN-VIVO PROTON NMR-SPECTRA. *Magnetic Resonance in Medicine*, *30*(6), 672-679. https://doi.org/10.1002/mrm.1910300604
Provencher, S. W. (2001). Automatic quantitation of localized in vivo H-1 spectra with LCModel. *Nmr in Biomedicine*, *14*(4), 260-264. https://doi.org/10.1002/nbm.698
Riesen, G., Norcia, A. M., & Gardner, J. L. (2019). Humans Perceive Binocular Rivalry and Fusion in a Tristable Dynamic State [Article]. *Journal of Neuroscience*, *39*(43), 8527-8537. https://doi.org/10.1523/jneurosci.0713-19.2019
Said, C. P., & Heeger, D. J. (2013). A Model of Binocular Rivalry and Cross-orientation Suppression. *Plos Computational Biology*, *9*(3), Article e1002991. https://doi.org/10.1371/journal.pcbi.1002991
Sheynin, Y., Proulx, S., & Hess, R. F. (2019). Temporary monocular occlusion facilitates binocular fusion during rivalry [Article]. *Journal of Vision*, *19*(5), 17, Article 23. https://doi.org/10.1167/19.5.23
Shibata, K., Sasaki, Y., Bang, J. W., Walsh, E. G., Machizawa, M. G., Tamaki, M., Chang, L. H., & Watanabe, T. (2017). Overlearning hyperstabilizes a skill by rapidly making neurochemical processing inhibitory-dominant [Article]. *Nature Neuroscience*, *20*(3), 470-475. https://doi.org/10.1038/nn.4490
Skerswetat, J., Formankiewicz, M. A., & Waugh, S. J. (2016). Very few exclusive percepts for contrast-modulated stimuli during binocular rivalry. *Vision Research*, *121*, 10-22. https://doi.org/10.1016/j.visres.2016.01.002
Skerswetat, J., Formankiewicz, M. A., & Waugh, S. J. (2018). More superimposition for contrast-modulated than luminance-modulated stimuli during binocular rivalry [Article]. *Vision Research*, *142*, 40-51. https://doi.org/10.1016/j.visres.2017.10.002
Tkac, I., Starcuk, Z., Choi, I. Y., & Gruetter, R. (1999). In vivo H-1 NMR spectroscopy of rat brain at 1 ms echo time. *Magnetic Resonance in Medicine*, *41*(4), 649-656. https://doi.org/10.1002/(sici)1522-2594(199904)41:4<649::aid-mrm2>3.0.co;2-g
Tremblay, S., Beaule, V., Proulx, S., de Beaumont, L., Marjanska, M., Doyon, J., Pascual-Leone, A., Lassonde, M., & Theoret, H. (2013). Relationship between transcranial magnetic stimulation measures of intracortical inhibition and spectroscopy measures of GABA and glutamate plus glutamine [Article]. *Journal of Neurophysiology*, *109*(5), 1343-1349. https://doi.org/10.1152/jn.00704.2012
Uusitalo, M. A., & Ilmoniemi, R. J. (1997). Signal-space projection method for separating MEG or EEG into components [Article]. *Medical & Biological Engineering & Computing*, *35*(2), 135-140. https://doi.org/10.1007/bf02534144
Valle-Inclan, F., Blanco, M. J., Soto, D., & Leiros, L. (2008). A new method to assess eye dominance [Article]. *Psicologica*, *29*(1), 55-64.
van Loon, A. M., Knapen, T., Scholte, H. S., St John-Saaltink, E., Donner, T. H., & Lamme, V. A. F. (2013). GABA Shapes the Dynamics of Bistable Perception [Article]. *Current Biology*, *23*(9), 823-827. https://doi.org/10.1016/j.cub.2013.03.067

van Versendaal, D., Rajendran, R., Saiepour, M. H., Klooster, J., Smit-Rigter, L., Sommeijer, J. P., De Zeeuw, C. I., Hofer, S. B., Heimel, J. A., & Levelt, C. N. (2012). Elimination of Inhibitory Synapses Is a Major Component of Adult Ocular Dominance Plasticity [Article]. *Neuron*, *74*(2), 374-383. https://doi.org/10.1016/j.neuron.2012.03.015

Verhagen, J., & Wagenmakers, E. J. (2014). Bayesian Tests to Quantify the Result of a Replication Attempt. *Journal of Experimental Psychology-General*, *143*(4), 1457-1475. https://doi.org/10.1037/a0036731

Wagenmakers, E. J., Love, J., Marsman, M., Jamil, T., Ly, A., Verhagen, J., Selker, R., Gronau, Q. F., Dropmann, D., Boutin, B., Meerhoff, F., Knight, P., Raj, A., van Kesteren, E. J., van Doorn, J., Smira, M., Epskamp, S., Etz, A., Matzke, D., . . . Morey, R. D. (2018). Bayesian inference for psychology. Part II: Example applications with JASP [Article]. *Psychonomic Bulletin & Review*, *25*(1), 58-76. https://doi.org/10.3758/s13423-017-1323-7

Wagenmakers, E. J., Marsman, M., Jamil, T., Ly, A., Verhagen, J., Love, J., Selker, R., Gronau, Q. F., Smira, M., Epskamp, S., Matzke, D., Rouder, J. N., & Morey, R. D. (2018). Bayesian inference for psychology. Part I: Theoretical advantages and practical ramifications [Article]. *Psychonomic Bulletin & Review*, *25*(1), 35-57. https://doi.org/10.3758/s13423-017-1343-3

Wagenmakers, E. J., Verhagen, J., & Ly, A. (2016). How to quantify the evidence for the absence of a correlation [Article]. *Behavior Research Methods*, *48*(2), 413-426. https://doi.org/10.3758/s13428-015-0593-0

Zhou, J. W., Clavagnier, S., & Hess, R. F. (2013). Short-term monocular deprivation strengthens the patched eye's contribution to binocular combination. *Journal of Vision*, *13*(5), 1-10. https://doi.org/10.1167/13.5.12

Chapter 4: MEASURING THE EXCITATION-TO-INHIBITION BALANCE WITH FMRI

PREAMBLE

The mapping of human brain functions has taken a huge leap with the advent of fMRI. However today, the detection of fMRI activations sometimes feels like "blobology"—a caricatural reference to the long debunked discipline of phrenology—where one attempts to interpret collections of blobs displayed on MR images. Those are of undisputable value for studying network-level computations—e.g. with connectivity or representational similarity analysis—but the value of a blob in itself is limited due to an ill-defined relation to microcircuit-level computational work. Caricaturally, a blob merely indicates where to point other investigational tools.

Yet, with data cumulating from now widely available clinical MR systems, functional maps are being refined at a pace that appears faster than our ability to characterize the underlying microcircuit dynamics through other methods. As described in Section 1.4.3.3, significant efforts are being deployed to clarify how hemodynamics relate to cell-type-specific activity and extract more computationally relevant information from fMRI data alone.

This chapter's manuscript takes a purely empirical approach and linked a single computationally relevant aspect of a neural activation, its EI balance, to a single aspect of hemodynamics, the delay of the BOLD response. Inspired by seminal work by Farivar et al. (2011) in amblyopia—a pathological model of altered EI balance—the approach is here for the first time applied to healthy human vision and is in stark contrast to other approaches that rely on less readily available non-BOLD fMRI methods and advanced modeling. Results support the notion that, within a given patch of cortical tissue, a longer BOLD delay indicates a stronger involvement of inhibitory circuits.

Manuscript Title: BOLD Response Delays Represent Local Cortical Processing

Authors

Sébastien Proulx[1*] and Reza Farivar[1*]

Affiliation

[1]Department of Ophthalmology & Visual Sciences, McGill University, Montreal, Canada

* sebastien.proulx2@mail.mcgill.ca; reza.farivar@mcgill.ca

Montreal General Hospital, 1650 Avenue Cedar L11.409

Montréal, Québec, H3G 1A4, Canada

Tel: +1(514)-934-1934-44508

Keywords

fMRI, BOLD, hemodynamic response function, V1, cross-orientation suppression

Conflict of Interest

There are no known conflicts of interest associated with this publication and there has been no significant financial support for this work that could have influenced its outcome.

Funding

This work was supported by the Natural Sciences and Engineering Research Council (NSERC) Discovery grant (NSERC RGPIN 419235-2013) and NSERC and Fonds de la recherche en santé du Québec (FRSQ) PhD scholarships.

Acknowledgment

Thanks to Kendrick Kay for the inspiration his GLM denoise code (http://kendrickkay.net/GLMdenoise/) provided for the first iterations of the custom analysis code used here.

4.1 ABSTRACT

A number of studies showed that stimulus or task conditions can alter the shape of the hemodynamic response (HR). Contrary to variations across brains and brain regions, vascular factors alone cannot account for within-voxel HR waveform variations. Instead, various neuron types and subvoxel functional domains may differently contribute in shaping the HR, suggesting that beyond levels of neurometabolic activity, measurements of stimulus- or task-specific HRs could inform on the nature of underlying neural processes. To assess this hypothesis, we measured HR delays to oriented visual stimuli with 1-mm and 1-sec resolution BOLD fMRI in healthy humans. As expected, decoding V1 patterns of HR amplitudes allowed robust cross-validated predictions of stimulus conditions, i.e. two orthogonal gratings and an overlay of the two. More interestingly, this was also true using patterns of HR delays alone, and predictions using both delay and amplitude information outperformed those using amplitude alone. Finally, while all stimuli evoked similar V1-averaged HR amplitudes, responses peaked ~160ms later for the overlay compared to the grating stimuli. We interpret this increased HR delay as reflecting different neural computations, here more cross-orientation inhibition with overlay stimuli, and conclude that neurally-relevant information can be obtained from condition-specific temporal characteristics of the HR.

4.2 INTRODUCTION

In functional MR (fMRI) and optical imaging, the amplitude of the hemodynamic response (HR) to local neuroelectric and neurometabolic activity (Kim & Ogawa, 2012; Logothetis, 2002) is used to identify 0.1 to 10-mm patches of active brain tissue and to map brain functions (Yacoub et al., 2008). These indirect non-invasive estimates of neural activity are, however, largely blind to the interplay between heterogenous intermingled neural populations—e.g. potent vasodilation can be triggered by optogenetic activation of either excitatory pyramidal neurons *or* inhibitory interneurons (Anenberg et al., 2015; Uhlirova, Kılıç, Tian, Thunemann, et al., 2016). The temporal waveform of the HR unfolds over 10-20 seconds, obeying complex dynamics between vasomotion and flow, volume and oxygenation of blood (Buxton et al., 1998; Kim & Ogawa, 2012). Small variations in this waveform are usually ignored or modeled out at

the analysis stage (Boynton et al., 1996). A few lines of evidence (Bartolo et al., 2011; Farivar et al., 2011; Havlicek, Ivanov, Roebroeck, et al., 2017; Uhlirova, Kılıç, Tian, Sakadžić, et al., 2016; Uhlirova, Kılıç, Tian, Thunemann, et al., 2016) however suggest that interactions between active sub-populations of neurons can affect the shape of the HR, meaning that careful time-resolved measurements could yield important information on the nature of ongoing neural processes, e.g. the ratio between excitatory and inhibitory activity.

There are a few reports of variations of the HR to short stimulus presentations beyond its mere scaling by the overall level of neurometabolic activity. HRs triggered by visual stimuli of varying contrast (J. E. Chen et al., 2021; Thompson et al., 2014) or presented alone vs spatially overlaid (Bartolo et al., 2011; Farivar et al., 2011) showed varying delays despite being measured within the same piece of brain tissue—where the effect of purely vascular dynamics is removed. Upon visual presentation of a plaid overlay of orthogonal gratings compared to gratings presented alone in non-human primates, Bartolo et al. (2011) observed larger HR delays accompanied by reduced γ-LFP and increased spiking activity. Farivar et al. (2011) showed in amblyopic patients that HRs to visual stimulation of pathologically suppressed eyes exhibit unusually delayed HRs compared to stimulation of the normal eye, which were delayed even further when using dichoptic stimuli designed to maximize interocular suppression. Finally, features of a visual stimulus (e.g. its flicker frequency) were early on shown to alter features of the response to longer presentation times—e.g. transients, response adaptation and undershoot (Bandettini et al., 1997; Griffeth et al., 2015; Hoge et al., 1999c; Sadaghiani et al., 2009)—which recent modeling work attributes to different temporal profile of subpopulations of excitatory and inhibitory neurons (Havlicek, Ivanov, Roebroeck, et al., 2017).

Non-invasively measurable variations in the shape of HRs may therefore not solely depend on the mechanical properties of the vascular bed. They may additionally reflect different intermingled sub-populations of neurons contributing via different neurovascular coupling mechanisms to macroscopically measured responses (Farivar et al., 2011; Uhlirova, Kılıç, Tian, Sakadžić, et al., 2016). Inhibitory interneurons directly stimulated optogenetically by Anenberg et al. (2015) triggered surprisingly large blood flow responses that did not depend on glutamatergic or GABAergic ionotropic neurotransmission. With a similar optogenetic

approach, Uhlirova, Kılıç, Tian, Sakadžić, et al. (2016) showed that pyramidal neurons and GABAergic interneurons produced clearly distinct temporal profile of single-vessel dilation and constriction. Direct measurements in cats' striate cortex by Li and Freeman (2011) of local tissue oxygenation (down to 60μm resolution) also revealed clearly distinct temporal profiles in response to visual stimuli within and beyond the receptive field (surround suppression) and overlaying different orientations (cross-orientation overlay suppression).

The above series of experiments overall suggests inhibitory processes in the early visual cortex can affect temporal characteristics of macroscopic hemodynamics. This relation may also generalize across the cortex, given another report by Peck et al. (2001) of delayed motor cortex HRs in a task requiring inhibitory control of finger isometric force production. Given the interest in bringing fMRI measurements beyond the mere identification of active brain areas (Buxton et al., 2014; Uhlirova, Kılıç, Tian, Sakadžić, et al., 2016), further evaluating the sensitivity of the HR shape to the nature of the underlying neural processes appears relevant.

In this study, we sought to test if non-invasive BOLD measures of the HR shape—specifically, its delay—are sensitive to neural processes associated with different stimuli. We optimized the sensitivity of high-resolution (1mm) fMRI measures at 3T over the early visual cortex of healthy adults, which we stimulated visually with oriented grating and cross-oriented plaid overlay stimuli to evoke different levels of inhibitory interactions between cortical orientation columns/channels (Angelucci & Bressloff, 2006; Deangelis et al., 1992; Hubel & Wiesel, 1974; Meese & Baker, 2013; Morrone et al., 1987; Sengpiel & Vorobyov, 2005). We timed the presentation of stimuli so that the complex HR waveform—more typically estimated with event-related stimulus designs—reduces to a simple sinusoid, maximizing sensitivity for estimation of the HR delay. We adopted a cross-validated multivariate approach to decode cortical patterns of HR delays (Haynes & Rees, 2005; Kamitani & Tong, 2005), pooling relevant signals across voxels and maximizing sensitivity.

Results showed that HR delays are sufficient—independently of HR amplitudes—to discriminate BOLD responses evoked by the plaid overlay stimuli from those evoked by single gratings. Moreover, different stimulus orientation produced different cortical patterns of

response amplitude, whereas inducing cross-orientation inhibition with overlaid stimuli (Angelucci & Bressloff, 2006) overall increased the V1 response delay but left amplitude unaffected. We conclude that different neural processes in brain tissue showing similar levels of neurometabolic activity can affect the shape of the BOLD HR. This opens a novel way to investigate the computational function of active brain tissues, non-invasively with widely available MRI scanners.

4.3 Materials and Methods

4.3.1 Participants

Six (including author SP) healthy human adults (1F, 5M; mean age: 30.8yrs; age range: 19-47) with normal or corrected-to-normal vision participated in this study. Informed consent was obtained from all participants and the protocol NEU-13-043 approved by the Research Ethics Board of the Montreal Neurological Institute.

4.3.2 Stimuli

Stimuli used are shown in Figure 4.1A. Sinusoidal grating and plaid stimuli were displayed to participants against a mean luminance gray background through a coil-mounted mirror using a gamma-calibrated MRI-compatible LCD monitor (3-D BOLD Screen, Cambridge Research Systems Ltd) positioned at the back of the MRI bore.

Stimuli in the ON periods of the fMRI stimulus design consisted in stationary sinusoidal gratings or a plaid overlay (2-cpd spatial frequency) with contrast reversal following a square-wave function (8Hz temporal frequency). Participants viewed the stimuli over a mean luminance background, through an annular aperture centered on fixation (0.7dva-diameter concentric pattern) and spanning from 0.75 to 7dva eccentricity. Grating stimuli were full contrast and orthogonally oriented at $\pm 45°$ relative to vertical. The plaid stimulus was composed of an overlay of the half-contrast orthogonal gratings, matching RMS contrast between grating and plaid stimuli. During the OFF periods of the fMRI stimulus design, only fixation over the mean luminance gray background was presented.

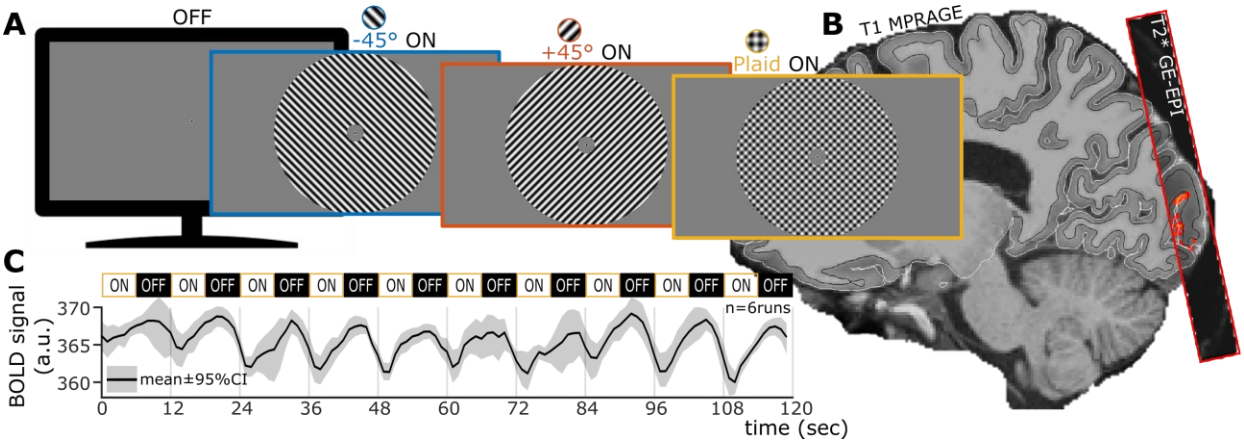

Figure 4.1 Experiment overview. A. Stimuli presented during OFF (fixation only) and ON (fixation + contrast-reversing grating or plaid overlay) periods. **B.** Example BOLD functional (T2*-weighted) and anatomical (T1-weighted) images, coregistered using boundary-based registration. Gray matter inner and outer boundaries respectively outlined in dark and white. **C.** Example BOLD timeseries averaged across the V1 gray matter ROI and across runs of the plaid stimulus condition. Data from participant 03sk. Confidence intervals derived from 8,192 bootstrap resamples with replacement.

4.3.3 MR Imaging

We sought to acquire very high-resolution functional images (i.e., 1-mm isotropic voxels) to minimize partial volumes—unresolved veins and tissue boundaries decreases the neural specificity of a voxel's signal. Increased resolution comes at a cost to SNR, increased transient (TR) acquisition time and increased echo-planar imaging (EPI) distortions in the phase-encode direction. We mitigated the SNR loss by using a custom 32-channel posterior-only RF coil that doubles the SNR in the occipital region (Farivar et al., 2016). We maintained acquisition time within our target TR=1s by focusing on a small stack of imaging slices over the occipital pole (Figure 4.1B). We acquired extra EPI images with the phase-encoding direction reversed to allow for off-line correction of EPI distortions using the up-down method (Andersson et al., 2003; Holland et al., 2010).

Each MR session lasted ~1 hour in a 3T Siemens Tim Trio scanner using the body coil for RF transmission. RF signal reception used the Siemens 32-channel full-head coil for whole-head T1-weighted anatomical scans (MPRAGE or MEMPRAGE; $1\times1\times1mm^3$ voxel size) and a custom-built, occipital-cortex dedicated, 32-channel coil array (Farivar et al., 2016) for all other acquisitions, including TRUFISP localizer scans (31 sagittal slices; 1.3×1.0mm in-plane resolution; FOV 250mm; 4mm slice thickness with 20% gap; TR 4.6ms; TE 2.3ms; FA 37°). Functional acquisitions

consisted of 15 to 21 runs of 120 BOLD fMRI high-resolution volumes ($1\times1\times1mm^3$ GE-EPI; 13 oblique coronal slices; 10% gap; 128mm FOV; TR 1,000ms; TE 33ms; Echo spacing 1.05ms; Left-Right phase-encoding direction; GRAPPA=3 with 126 reference lines; FA=33°; first 4 volumes discarded before image reconstruction). Additional shorter 10-volume functional runs were acquired in the reversed phase-encoding direction at the beginning and end of each session for correction of EPI spatial distortions. To minimize head motion, a bite bar was used for three participants and foam padding for the other three. The slice prescription—perpendicular rather than parallel to the calcarine sulcus—further minimized through-plane head motion and therefore limited issues related to separately performed movement and slice timing corrections (Parker & Razlighi, 2019).

Each subject underwent two MRI sessions separated by a ~1 hour break. In the first session, functional runs were manually prescribed to cover the tip of and ~0.5mm beyond the occipital pole with slices perpendicular to the calcarine sulcus (see Figure 4.1B), based on the anatomical localizers. In the second session, functional runs' prescription was matched to that of the first session using Siemens' auto-align routine with visual confirmation.

4.3.4 Functional MRI Design

During each 120-sec functional run, stimuli were presented in 10 consecutive 6sec-ON – 6sec-OFF cycles (Figure 4.1C). Only one of the three stimulus conditions, namely -45° grating, +45° grating or plaid, was presented per run, in an order randomized within three consecutive runs. This three-run sequence was repeated 5 to 7 times per session per participant, with ~10s to 30s rests between each run.

Throughout each run, participants performed a simple attentional fixation task, producing button-press reports of contrast reversals of the concentric fixation pattern (Figure 4.1A; random reversal delays drawn from a flat distribution between 1s and 9s).

4.3.5 MRI preprocessing

4.3.5.1 Functional Volume Preprocessing

Functional volumes preprocessing used AFNI tools (https://afni.nimh.nih.gov/), starting with slice timing correction and followed by a series of spatial transformations that were combined and applied in one interpolation step to minimize spurious spatial smoothing. These spatial transformations included, chronologically, (1) within-session motion correction, (2) EPI distortion correction and (3) between-session registration.

Within- and between-session registration used AFNI's 3dvolreg function. EPI spatial distortion correction used the up-down non-linear registration method (AFNI's 3dQWarp function; Andersson et al., 2003; Holland et al., 2010), aligning EPI images and reversed phase-encoding EPI images only along the phase-encoding axis. Distortions were estimated as such for each separate fMRI session after manually masking out non-brain voxels. Finally, we used the distortion corrected images, again masking out non-brain voxels, to estimate the between-session registration. All spatial correction estimates (i.e., motion and distortion corrections and between-session registration) were combined and applied to the slice timing corrected images in one interpolation step using 3dNwarpApply. No spatial smoothing was applied.

Each run timeseries was expressed as %BOLD relative to the run mean and all further analyses performed on %BOLD.

4.3.5.2 Retinotopic Atlas Registration and V1 ROI

We obtained estimates of retinotopy for individual subjects through the registration of a probabilistic retinotopic atlas (Benson et al., 2012) to each participants' own functional volume space. Brain surface reconstruction from T1-weighted anatomical scans used Freesurfer's analysis pipeline (http://surfer.nmr.mgh.harvard.edu/). The atlas' brain surface was registered to each participant's brain surface using Freesurfer's tools for non-linear surface-based registration, following Benson et al. (2012; https://cfn.upenn.edu/aguirre/wiki/public:retinotopy_template).

We then estimated each participant's functional-to-anatomical registration using boundary-based volume registration (Greve & Fischl, 2009). Using the reverse of the estimated functional-to-anatomical registration, we projected the atlas-based retinotopy from each participant's own surface-based anatomy to their functional volume space.

This allowed the definition of a V1 gray-matter ROI in the native acquisition space of the functional images. This ROI excluded voxels from the first and last slice to avoid partial volumes, after motion correction, with regions out of the imaging field-of-view. The atlas-based retinotopy also served as priors for the empirical estimation of the cortical representation of the visual stimuli (see section A. Cortical Representation of the Visual Stimuli).

4.3.6 Analysis

4.3.6.1 Sinusoidal Response Vector Estimation

The ON–OFF cyclical pattern of visual stimulation was designed to reduce the BOLD response to a simple sinusoidal shape that could be described with only two parameters: response amplitude and delay. Those parameters are conveniently estimated through the linear fit of a pair of sine and cosine regressor functions (Figure 4.2C) matching the 12-sec stimulus cycle length. The fit coefficients form a *response vector* best represented in a 2D complex plane (Figure 4.2A), where the real (x-axis) and imaginary (y-axis) coordinates correspond respectively to the sine and cosine fits. The length and angle of vectors (single dots and circles in Figure 4.2A) correspond respectively to the amplitude and delay of the represented stimulus driven responses.

In a linear model of a voxel's single-run BOLD timeseries (Figure 4.2C), we included sine and cosine regressors of interest along with constant baseline and linear drift nuisance regressors. Fitting used ordinary least-squares regression (OLS), censoring the first 24 timepoints corresponding to the first two stimulus cycles (top gray section in Figure 4.2C).

4.3.6.2 Model-Free Hemodynamic Response Estimation

For visualization purposes only, the actual shape of the BOLD response to the ON–OFF stimulus cycle was also estimated (Figure 4.2B). The sine and cosine regressors in the linear

model described above were replaced with 11 delta function regressors modeling signal amplitude from the 2nd (t_{0+1}) to the 12th (t_{0+11}) functional volume into the 12-sec stimulus cycle (Figure 4.2C). Constant baseline and linear drift regressors were left unchanged. Signal at the 1st (t_0) volume was implicitly modeled by the baseline. We reconstructed the hemodynamic responses (HR; Figure 4.2B) from t_0 to t_{0+11} into the stimulus cycle using the fit coefficients (Figure 4.2C).

For display purpose only, the interindividual variability in HR amplitude and delay was removed, thereby highlighting stimulus condition effects (Figure 5B) and interindividual variation in waveform (Figure S2). Dividing the zero-centered HRs of each participant by the length of their respective condition-averaged sinusoidal response vector and multiplying by the length of the group average response vector effectively removed HR amplitude variations. Delay variations were removed by cubic interpolation of each participant's HRs on time axes shifted according to the angle difference of the particpant's response vector relative to the group.

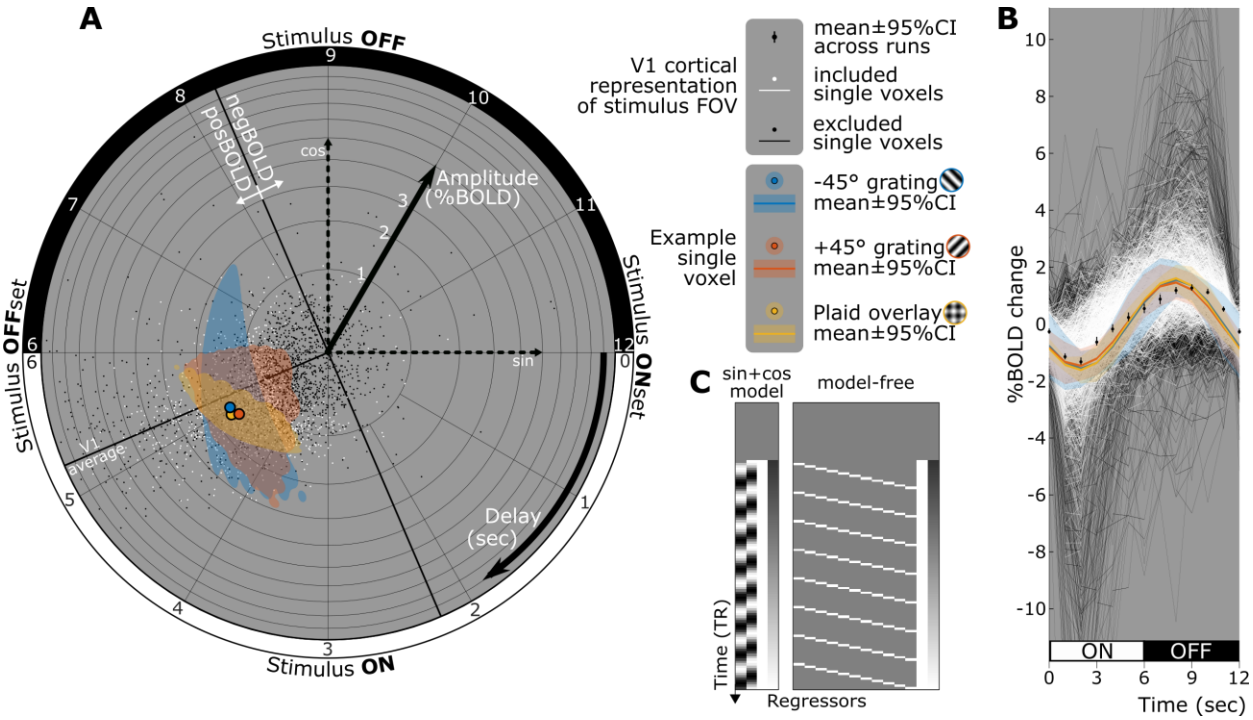

Figure 4.2 Stimulus-driven BOLD response overview. A. Two-dimensional representation of sinusoidal response vectors (sin+cos model). Each dot or circle represents the tip of a vector with an origin at coordinate [0,0] of the [sin,cos] Cartesian plane (dashed arrows). In a polar representation, vector length and angle respectively reflect the BOLD response amplitude and delay relative to stimulus onset (thick arrows). Also shown is the delay of the ROI-averaged response (thin radial dark line) and, orthogonal to that delay, the limit between positive (posBOLD) and negative BOLD (negBOLD) responses. Excluded/included voxels relate to spatial feature selection (see section Spatial Feature Selection). **B.** Same data as in A, now expressed as signal change across time through the stimulus cycle, i.e. the hemodynamic response (HR). The model-free HR is shown for single voxels (thin white and dark traces) and the sinusoidal fit of the HR is shown for the example single voxel (coloured traces). **C.** Design matrices used for fitting BOLD timeseries. For the sin+cos model, the first pair of regressors are the sine and cosine regressors of interest, and the second pair the baseline and signal drift nuisance regressors. For the model-free matrix, the regressors of interest are the first 11. The gray zone corresponds to the censored time points from the first two stimulus cycles. Data from participant 03sk. Confidence intervals derived from 8,192 bootstrap resamples with replacement.

4.3.6.3 Spatial Feature Selection

4.3.6.3.1 A. Cortical Representation of the Visual Stimuli

We used the probabilistic estimate of each participant's retinotopy (see section Retinotopic Atlas Registration and V1 ROI) to project data from the functional space to a visual field space (Figure 4.3A). To account for cortical magnification and better visualize boundaries across eccentricities, we uniformized the voxel density across each hemisphere's visual field space through non-linear scaling of the eccentricity axis (Figure 4.3C, see Supplementary Figure 1 for details).

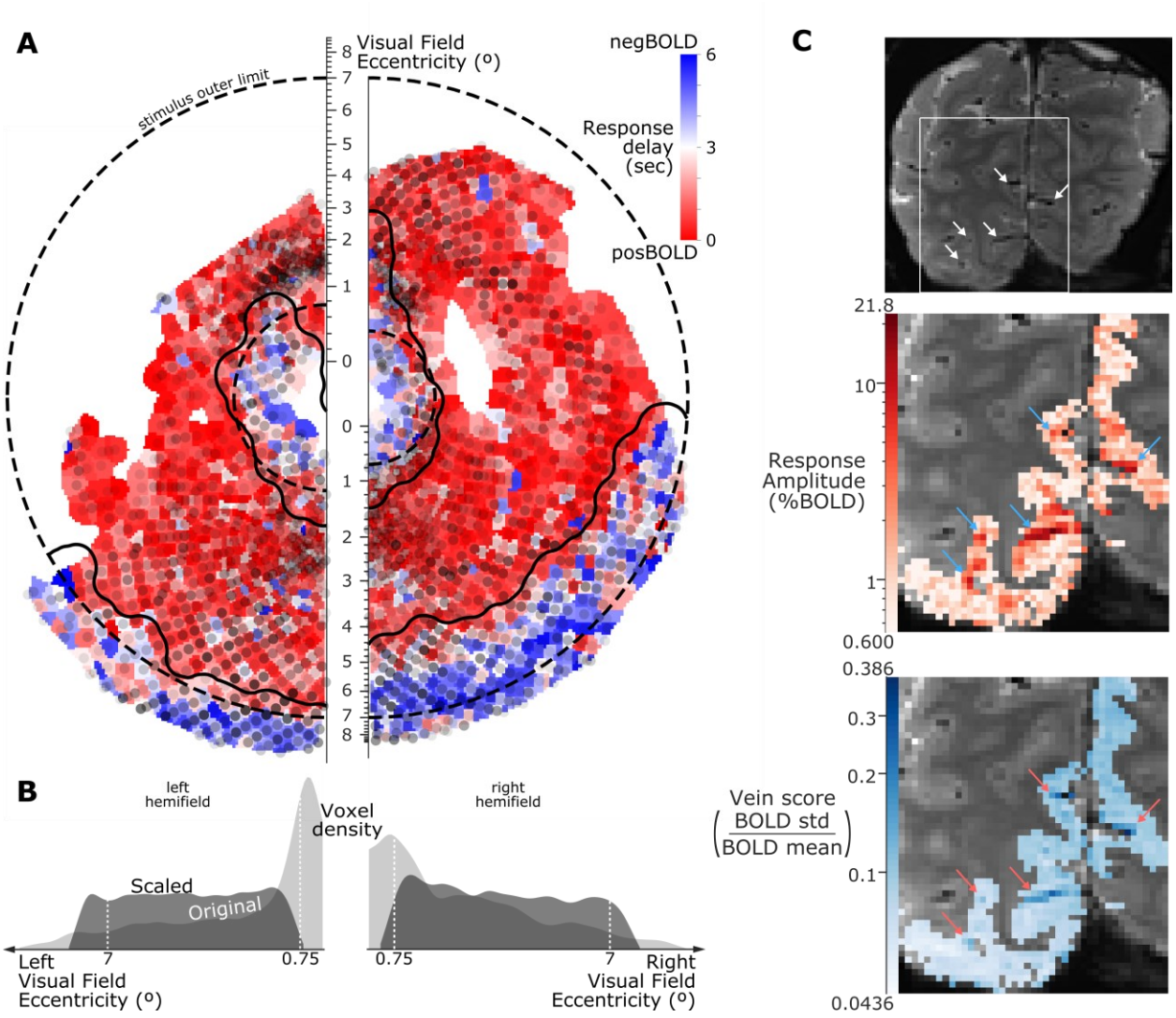

Figure 4.3 Overview of spatial feature selection. A. Voxel's response polarity mapped on a scaled visual field space. Inner and outer dashed lines show the inner and outer limit of the stimulus field-of-view. Solid lines show the limit of the cortical representation of the stimulus field-of-view as conservatively estimated from the positive to negative BOLD response transition zones. The transparent dark overlay shows the density of voxels representing units of the scaled visual field space. **B.** Density of voxel representation (# of voxels per unit visual space area) as a function of eccentricity in the original (darker overlay) and non-linearly scaled (lighter overlay) visual field space. **C.** BOLD signal characteristics of large veins. White arrows in top panel show large veins resolved as low signal points or streaks in our 1x1x1mm^2-resolution images. The same veins are shown magnified with the blue and red arrows in the middle and lower panel, as regions of large BOLD responses and signal variability. Data from participant 03sk.

Regions of positive (posBOLD) and negative (negBOLD) BOLD responses (see Figure 4.2A) are expected respectively within and surrounding the stimulus' cortical representation (Shmuel et al., 2006; Smith et al., 2004; Wade & Rowland, 2010). We computed the absolute deviation of each voxel's response delay, relative to the delay of the ROI-averaged response (see Figure

4.2A), and produced response polarity maps in the visual field space to highlight posBOLD and negBOLD regions (Figure 4.3A).

We finally leveraged the posBOLD/negBOLD boundaries to functionally delineate the cortical representation of the stimulus, using the probabilistic retinotopic atlas as prior (Figure 4.3A). This followed a heuristic approach based on successive iterations of contour extraction from smoothed polarity maps and contour inflation, merging and selection (see Supplementary Figure 1 for details), culminating in a conservative selection of voxels representing the stimulus' field-of-view.

4.3.6.3.2 B. Stimulus Driven Voxels

We identified stimulus-driven voxels as those showing non-random response vectors across runs. The 2D coordinates of response vectors were entered as two dependent variables in a multivariate ANOVA for repeated measures implemented in an adaptation of the manova.m function from MATLAB's Statistical Toolbox. The statistical model included the repeated-measure factor of stimulus condition and the intercept, the latter effectively testing whether the mean response vector differed from the 0-length null vector. Voxels with a significant main effect of the intercept (α=0.05) were selected without correction for multiple comparison.

4.3.6.3.3 C. Non-Vein Voxels

Large vein voxels are known to show low mean signals (Figure 4.3C, white arrows in the top panel), large stimulus driven BOLD responses (Figure 4.3C, blue arrows in the middle panel) and high signal variability (Kay et al., 2019; Olman et al., 2007). We therefore computed the ratio of the standard deviation of a voxel's detrended absolute BOLD (not %BOLD) timeseries over its baseline (Figure 4.3C, bottom panel) as a commonly used metric of the likeliness of a voxel containing a large vein. A threshold was defined as the vein likeliness metric at the 80^{th} percentile of voxels having passed feature selection steps A and B. Voxels below this vein likeliness threshold were selected.

4.3.6.3.4 D. Most Discriminant Voxels

The sensitivity of a voxel to stimulus conditions was evaluated as the Hotelling's T^2 statistics of the main effect of stimulus condition in the multivariate ANOVA described in feature

selection step B. A threshold was defined as the T^2 at the 20^{th} percentile of voxels having passed feature selection steps A through C. Voxels above this T^2 threshold were selected.

4.3.6.4 Support Vector Machine Training

We used the spatial patterns of BOLD responses delay, amplitude or both to train a Support Vector Machine (SVM) algorithm for the pairwise classification of stimulus conditions, independently for each participant, session and stimulus condition pair. The training data consisted of a $n \times p$ complex-valued matrix containing the sinusoidal response vectors, with n runs as samples and p voxels as features. Mainly to minimise phase wrap, the matrix was first normalized by rotating and scaling response vectors voxel-by-voxel to a mean of 0-angle and length 1.

For classification based on response delay only, we replaced response vectors in the data matrix by their angle. For classification based on response amplitude only, we replaced the response vectors by their length. For classification based on both response delay and amplitude, we concatenated the real and imaginary parts of the complex-valued $n \times p$ matrix of response vectors into a real-valued $n \times 2p$ matrix. This latter approach was inspired by 2011); Bouboulis et al. (2015) to allow the training of standard algorithms with complex-valued data.

After further z-scoring voxel-by-voxel, all model training used the linear C-SVM classifier algorithm from the LiBSVM-3.24 library with default parameters (Chang & Lin, 2011).

4.3.6.5 Cross-Validation Between Sessions

We leveraged our two-repeated-session design to avoid circular inference. Only anatomical information bridged the two sessions: through registration of the functional spaces and of the probabilistic retinotopic atlas. Response vector estimation, spatial feature selection and SVM training in one session were strictly independent of the other session. Only the trained models crossed from the *train* session to the other *test* session for computing the classification performance metric that was then averaged across sessions for group-level inference statistics. Similarly, when averaging response vectors and time courses across voxels, each session used the voxel selection derived from the other session.

We used the Area Under the ROC Curve (AUC) to assess classification performance. It is interpreted in the same way as a percent correct accuracy estimate, i.e. ranging between 0 and 1 with chance level at 0.5, but has the advantage of being threshold-insensitive.

4.3.7 Statistics

Significance of AUC was determined against a null distribution empirically derived from 8,192 permutations of condition labels within each 3-run repetition. We applied this permutation of labels at an early stage, before response vector estimation. An actual AUC larger than 95% of its corresponding permuted AUCs was deemed significantly (uncorrected one-sided $p<0.05$) above the 0.5 chance level. Repeated-measures ANOVAs and t-tests used $\alpha=0.05$.

We derived all confidence intervals from 8,192 bootstrap resamples with replacement. For single-participant statistics, each resample contained the same number of runs as the original sample. For group statistics, each resample contained n=6 participants. Bivariate confidence intervals used the probability density map, based on a normal kernel function, of resampled means. We lowered a probability density threshold until 95% of resamples passed it (p=0.05). That threshold defined a contour on the probability density map. The contour was taken as the credible interval, as termed in Bayesian statistics, but here referred to as the confidence interval for simplicity.

4.4 RESULTS

4.4.1 Data Overview And Voxel Selection

Figure 4.1, Figure 4.2 and Figure 4.3 summarize data from one representative participant, sk03. The HRs (Figure 4.2B) extracted from voxels within the V1 gray matter ROI (Section 4.3.6.3.2) did follow the expected sinusoidal shape, albeit with a positive lobe appearing wider than the negative one (see Supplementary Figure 4.2 for the HR of each participant). The compact representation of the participant's HRs as sinusoidal response vectors on a polar plot (Figure 4.2A) showed an ROI-averaged hemodynamic delay of 5.2-sec (Figure 4.2A, dark line in lower left quadrant; phase delay between the sinusoidal function fit and the stimulus presentation's square-wave function). This delay ranged from 3.6s to 5.6s across sessions and

participants (mean 4.9s), consistent with an expected long and variable hemodynamic delay of vascular origin (Handwerker et al., 2004; Proulx et al., 2014).

Several voxels showed a phase opposite to the main hemodynamic delay (responses above the solid dark diagonal in Figure 4.2A). In our example participant, 33% of ROI voxels showed this characteristic consistent with negative BOLD responses (35% on average across sessions and participants, ranging from 25% to 41%). Projecting each voxel's absolute phase offset on our representation of the visual field-of-view revealed opposite-phase voxels clustering outside or close to the edge of the stimulus field-of-view (Figure 4.3A), in patterns that reproduced across sessions (Supplementary Figure 1). This is consistent with previously observed negative BOLD responses in cortical tissue neighboring stimulus-driven fMRI activations (Shmuel et al., 2006; Smith et al., 2004; Wade & Rowland, 2010). The solid dark outlines in Figure 4.3A outline our estimate of the cortical representation of the stimulus field-of-view, which leveraged these physiological negBOLD/posBOLD boundaries to refine estimates initially obtained from the surface-based registration of a retinotopic atlas (dashed dark circular outlines in Figure 4.3A).

Large veins were clearly resolved in our 1-mm resolution maps of vein likeliness (red arrows in Figure 4.3C's bottom panel). They expectedly (Olman et al., 2007) colocalized with voxels with low baseline BOLD signal (white arrows in Figure 4.3C's top panel), high temporal variability (data not shown) and large stimulus-driven modulation (blue arrows in Figure 3C's middle panel).

The dimensionality (number of voxels) of participants functional datasets was reduced independently within each of the two fMRI session repeats. In our example participant, selection for voxels (A) representing the stimulus's field-of-view, (B) significantly responding to the stimulus presentation, (C) unlikely to contain veins and (D) most sensitive to stimulus orientation reduced the 4,697 gray matter V1 voxel ROI to 1,111 in one session and 1,415 in the other. Across participants and sessions, the initial ROI contained 3,419 to 5,410 voxels and reduced to 570 to 1,415 voxels after feature selection (see Supplementary Table 1 for details).

4.4.2 Decoding Patterns of BOLD Response Delays and Amplitudes

To assess whether different oriented visual gratings or plaid could produce different delays of individual voxels' BOLD response, we used the following logic: if we can predict the orientation profile of visual stimuli from the pattern of BOLD delay that they generate across the V1 cortical sheet, then these orientation profiles must modulate BOLD response delays in individual voxels. Importantly, to avoid circularity in predicting/classifying stimulus orientation (Kriegeskorte et al., 2009), both selection of relevant voxels (dimensionality reduction) and training of decoding spatial (SVM classifier) models relied on functional data from one *train* session while strictly reserving data from the other *test* session for cross-validation of decoding performances (see section "Cross-Validation Between Sessions").

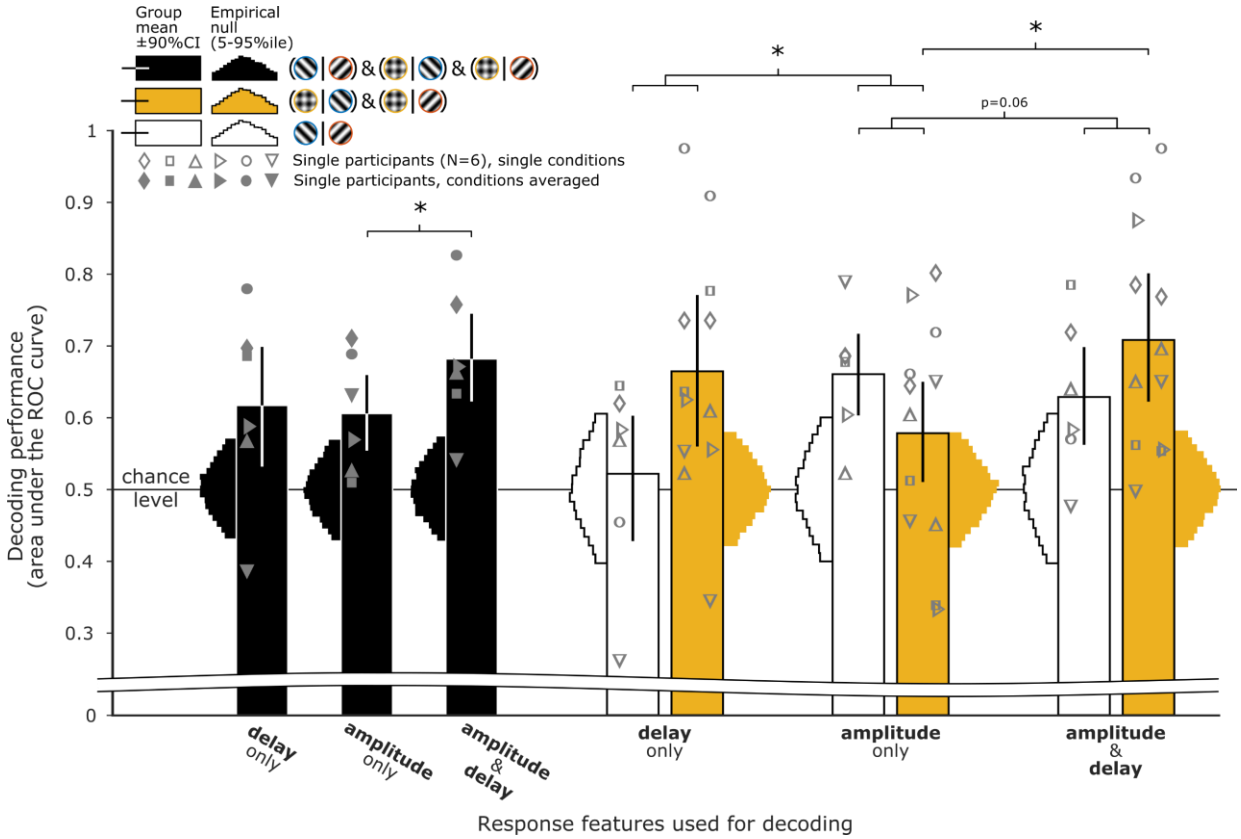

Figure 4.4 Decoding of V1 patterns of BOLD response amplitudes and delays for pair-wise predictions of stimulus conditions. Dark bars average prediction performances across all pairs of stimulus conditions. White bars show predictions of the orientation of the two gratings. Yellow bars average prediction performance across pairs comparing the plaid overlay stimulus to either grating. Sideway histograms show null distributions (5^{th} to 95^{th} percentiles) empirically derived from 8,192 random permutations of stimulus condition labels. Out of all decoding performances shown, only prediction of grating orientation from delay-only information did not significantly rise above chance (bar below the null distribution's 95^{th} percentile and error bar overlapping chance level). Error bars: 90% confidence intervals derived from 8,192 bootstrap resamples of n=6 participants with replacement. ∗: p<0.05.

Both amplitude and delay of BOLD responses could *alone* support accurate two-class prediction of stimulus conditions. Averaged across all pairs of stimulus conditions, AUC measures of decoding performance (Figure 4.4, solid dark bars) respectively rose to 0.62 (delay-only: t_5=2.1, one-sided p=0.045; permutation test one-sided p=0.003) and 0.61 (amplitude-only t_5=3.1, one-sided p=0.014; permutation test one-sided p=0.006), significantly above chance (H_0: AUC=0.50). Interestingly, prediction using the cartesian representation of response vectors—carrying both delay and amplitude information—offered the best performance, with an AUC of 0.68 (t_5=4.5, one-sided p=0.003; permutation test, one-sided p=0). Adding delay information increased prediction performances (delay+amplitude vs amplitude only: t=-2.1117, one-sided p=0.044). Cortical BOLD response delays therefore *do* carry relevant information, which may inform on underlying neural processes.

4.4.3 Stimulus-Related Modulation of the BOLD Response Delay

Converging evidence tend to associate neurally-related BOLD delays with intra-cortical inhibitory processes (Farivar et al., 2011; Muthukumaraswamy et al., 2009; Muthukumaraswamy et al., 2012; Uhlirova, Kılıç, Tian, Sakadžić, et al., 2016). We therefore tested whether single-voxel's delay modulations in our experiment were more specifically driven by the neural suppression at play during the simultaneous processing of two orientations, i.e. during presentation of the plaid overlay stimulus. We found evidence for that in AUC decoding performances showing a significant interaction ($F_{1,5}$=7.0, p=0.046) between the type of stimulus prediction (plaid|grating vs -45°|+45°) and the type of information it relied on (delay-only vs amplitude-only)—amplitude information supported the prediction of any type of stimulus whereas delay information supported only predictions involving plaid overlay stimuli, the condition putatively engaging higher levels of intracortical inhibition (Figure 4.4, delay- and amplitude-only white and yellow bars). Finally, adding delay information to decoding based on amplitude information increased performance when plaids were involved (Figure 4.4; trend for a type of information × type of stimulus interaction: $F_{1,5}$=5.9, p=0.060; amplitude-only vs delay+amplitude for predictions involving plaids: t=3.693, p=0.014).

Interestingly, when averaged across all selected voxels, responses to grating and plaid overlay stimuli were similarly distinct (Figure 4.5): responses driven by the plaid overlay showed a delay 156ms longer (range: 81 to 327ms) than those driven by gratings (plaid vs gratings: t_5=3.9, p=0.012; plaid vs -45° vs +45°: $F_{(2,10)}$ = 5.7, p=0.022), but all responses showed similar amplitudes (plaid vs gratings: Δ=0.04%BOLD, t_5=1.1, p=0.311; plaid vs -45° vs +45°: $F_{(2,10)}$ = 1.1, p=0.366).

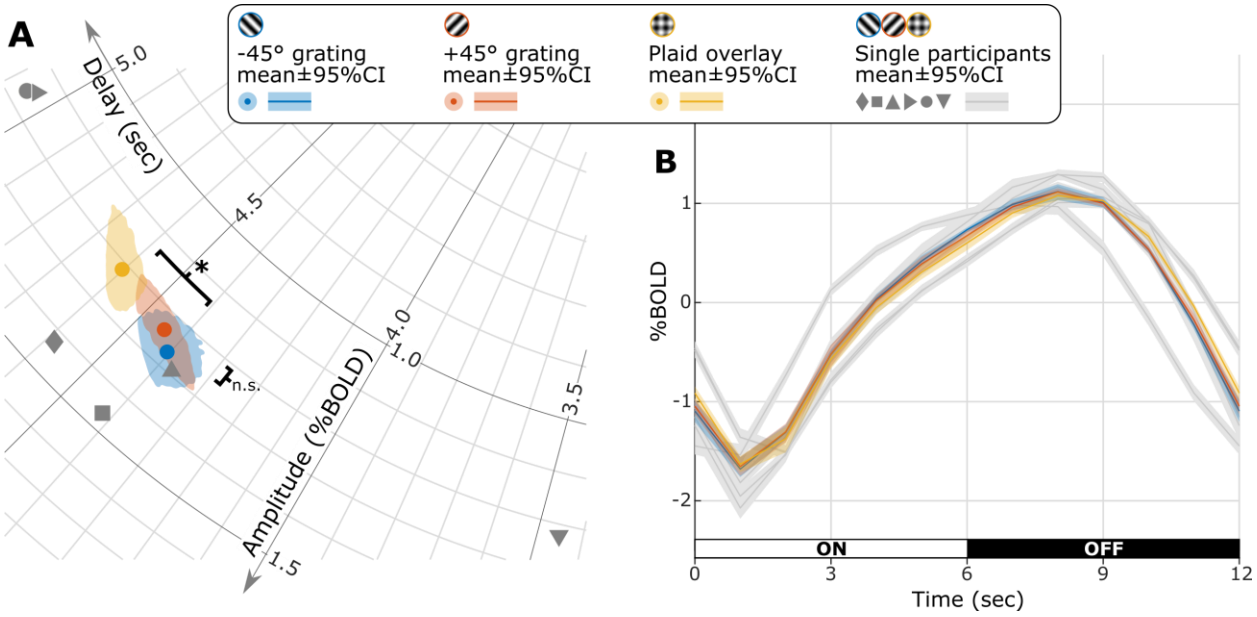

Figure 4.5 Effect of stimulus condition on the hemodynamic response shape. A. Polar representation (as in Figure 4.2A) of sinusoidal response vectors in V1, spatially averaged across selected voxels (feature selection steps A-C). Gray markers show individual participant's response averaged across stimulus conditions. Colored markers show the response to each stimulus conditions averaged across participants. Between-participant error is excluded from the error area to exclusively show the more relevant within-subject error. **B.** Same data as in A., represented as the average BOLD time course through the ON-OFF stimulus cycle. Gray traces show actual time courses for individual participants. For the condition-specific average responses (colored traces), the sinusoidal fit is shown for more clarity, again with the error area showing the within-subject error only.

Together with the decoding results, this suggests that the orientation profile of visual stimuli affects the cortical pattern of BOLD response amplitudes. Importantly, increasing cross-orientation inhibition by overlaying different orientations increases response delays across the V1 cortex.

4.5 Discussion

Using optimized fMRI measures of BOLD response delays in the human early visual cortex, we found that V1 voxel patterns of delays are alone sufficient for predicting features of the driving

visual stimuli, here the stimuli's orientation profile. This challenges the common belief that temporal characteristics of fMRI responses are pure vascular artefacts. Instead, incorporating delay information in a decoding analysis of response patterns outperformed decoding based only on response amplitude. Moreover, response amplitudes and delays showed different characteristics. Overall V1 response amplitudes were stable across all stimuli—both orthogonally-oriented gratings and the plaid overlay of the two—but patterns of amplitudes differed. This is consistent with matched overall levels of neurometabolic activity across V1 that however differently distributes across cortical columns representing the stimuli's orientation content (Brouwer & Heeger, 2011; Haynes & Rees, 2005; Kamitani & Tong, 2005; O'Herron et al., 2016). For delays, the cortical patterns were indistinguishable across orientations when presented alone but presenting them as a cross-oriented plaid overlay delayed the overall V1 response by ~160ms. Together, our findings suggest that neurally-relevant information lies in the delay of hemodynamic signals. We propose this information relates to decreased cortical excitation/inhibition ratios, such as during binocular cross-orientation suppression (Morrone et al., 1987; Sengpiel & Vorobyov, 2005; Suarez et al., 1995). This has important implications for use of non-invasive fMRI beyond the localisation of neurometabolically active cortical tissues, opening the possibility of investigating the underlying neural computations with widely-available clinical-grade MRI systems.

To the best of our knowledge, five previous studies in humans (Bartolo et al., 2011; J. E. Chen et al., 2021; Farivar et al., 2011; Peck et al., 2001; Thompson et al., 2014) reported changes in the shape of the hemodynamic response—within a given piece of brain tissue—upon different stimuli or task requirements not meaningfully expected to affect neural activity timing. The earliest of these studies, by Peck et al. (2001), found the BOLD HR in the supplementary motor area to show increasing delay with increasing level of the inhibitory control required for production of isometric forces with the fingers. Bartolo et al. (2011) reported increased early visual cortex BOLD delays in two macaque monkeys using stimuli like ours, along with different profiles of evoked spiking and local field potentials.

Farivar et al. (2011) more specifically investigated the impact of intracortical inhibition on the BOLD HR in the context of pathological inter-ocular inhibition in amblyopia (Sengpiel et al.,

2005; Sengpiel & Vorobyov, 2005). Here the inhibited amblyopic eye, compared to the inhibiting normal eye, showed longer delays upon brief monocular stimulations. Pathological alterations of the cortical microvasculature may have confounded this result. However, boosting functional inhibition with a dichoptic mask, continuously presented to the inhibiting normal eye, further lengthen the delay, arguing against a purely vascular effect.

The above studies and ours support the hypothesis that different computations performed within the same piece of cortical tissue can lead to differently shaped HRs, and that those involving more intracortical inhibition specifically increase the HR delay. Indeed, optogenetics studies have shown activation of inhibitory interneuron alone can drive large hemodynamic responses (Anenberg et al., 2015; Uhlirova, Kılıç, Tian, Thunemann, et al., 2016) with time courses not matching that driven by pyramidal neuron (Uhlirova, Kılıç, Tian, Sakadžić, et al., 2016). This is further supported by human individuals showing high levels of the GABA neurotransmitter, as measured in the early visual cortex with MR spectroscopy, also showing longer BOLD delays (Muthukumaraswamy et al., 2009; Muthukumaraswamy et al., 2012). However, the functional significance of MR spectroscopy measures of neurotransmitters is still unclear (Ip & Bridge, 2021; Stagg, 2014). Evidence reported here and previously (Farivar et al., 2011; Peck et al., 2001) that link HR delays with inhibition in humans remain scarce and indirect. More complete studies incorporating modulations of the neural substrate of inhibition, e.g. through brain modulation techniques (Allen et al., 2014; Stagg et al., 2009) or plasticity paradigms (Lunghi et al., 2015), are needed.

The suppressive effects of cross-oriented masks can begin sub-cortically (Freeman et al., 2002; Priebe & Ferster, 2006) with contrast saturation in non-oriented thalamic neurons (Priebe & Ferster, 2006). This was likely at play during the binocular presentation of our plaid stimulus. However, sub-cortical suppression is usually demonstrated using monocular stimulation (Freeman et al., 2002). On the other hand, dichoptic stimulation produces cross-orientation that, given its susceptibility to adaptation, *is* of cortical origin (Li et al., 2005). Suppression during our binocular stimulation therefore likely began sub-cortically and deepened in V1 cortex (Baker et al., 2007; Li et al., 2005; Walker et al., 1998).

It is interesting to note that Peck et al. (2001), Bartolo et al. (2011) and Farivar et al. (2011) all observed decreased response amplitudes accompanying the longer delays, and that this relation was even evident across participants in Muthukumaraswamy et al.'s studies (Muthukumaraswamy et al., 2009; Muthukumaraswamy et al., 2012). This at first sight suites the increased inhibition interpretation: inhibited tissues show smaller BOLD responses. However, Thompson et al. (2014) showed increased BOLD delays in human V1 with decreasing contrast of grating visual stimuli (but see J. E. Chen et al., 2021). Should inhibitory drive change with decreasing stimulus energy, it would most likely decrease, following decreasing need for divisive normalization or gain control (Carandini & Heeger, 2012; Heeger, 1992; Katzner et al., 2011). Yet, longer delays came with smaller amplitudes, just as previously reported (Bartolo et al., 2011; Farivar et al., 2011; Muthukumaraswamy et al., 2009; Muthukumaraswamy et al., 2012; Peck et al., 2001). Thompson et al. (2014) would consequently contradict the hypothesis of inhibition causing longer delays, but their results were not reproduced in J. E. Chen et al. (2021) who showed the reversed pattern in a similar experiment performed at higher magnetic field, suggesting that Thompson et al. (2014)'s effect may stem from a methodology that confounded interindividual correlations (Muthukumaraswamy et al., 2012). Moreover, our results argue against the inhibition-related delay effect being mediated through amplitude in the following two ways. First, when cortical patterns of amplitude are decodable, patterns of delay should be as well. That was not the case when comparing the two grating orientations (Figure 4.4). Second, we should have observed smaller amplitudes along with longer delays in response to our plaid stimulus, which we did not either (Figure 4.5). Our results rather show a novel dissociation between HR delay and amplitude, strengthening the excitation/inhibition ratio hypothesis.

One limitation of this study is the lack of specificity to the temporal feature of the HR that is affected by stimulus condition. Indeed, stimuli can drive fast—up to 0.75Hz—BOLD responses (Lewis et al., 2016) such that response transients often observed with long stimulation blocs (Gonzalez-Castillo et al., 2012) may have contributed to our measurements—e.g. broader positive lobe of the response relative to the negative one (Figure 1C and Figure S2). The delayed sinusoidal fit of the response to the plaid stimulus could therefore stem, for example, from a

smaller onset transient and/or a larger offset transient. Those and other features of responses to short stimulus presentations—onset time, slopes and peak time—are however not resolved *by design* in our experiment. Further dissecting these stimulus-dependencies of HRs will require a combination of shorter and longer stimulation durations, which will importantly help disambiguating modulations of the measured time course related to different neural subpopulations showing (1) different activity time courses with prolonged stimulations or (2) different neurovascular transfer functions.

4.6 Conclusion

Evidence is accumulating to show that temporal characteristics of hemodynamic signals such as their delay, when carefully measured and analyzed, can provide relevant information on the neural computations underlying fMRI activations. If a causal link were demonstrated, e.g. with the excitation/inhibition ratio, it would mean the latter could be non-invasively measured with widely available 3T fMRI scanners.

4.7 Supplementary Materials

4.7.1 Supplementary Table

	Number of voxels after successive dimensionality reduction steps, averaged across sessions (feature selection steps)				
Participants	Initial ROI	& within cortical representation (A)	& stimulus driven (B)	& non-vein (C)	& sensitive to stimulus condition (D)
02jp	3,419	2,565.5	1,833.5	1,467.0	1,173.5
03sk	4,697	2,945.0	1,973.5	1,579.0	1,263.0
04sp	4,747	1,891.5	1,257.5	1,006.0	804.5
05bm	5,410	2,801.0	1,735.0	1,388.0	1,110.5
06sb	4,057	2,370.0	1,683.5	1,346.5	1,077.0
07bj	3,793	2,233.5	952.5	762.0	609.5
Average	4,354	2,468.8	1,573.6	1,258.1	1,006.3

Supplementary Table 1. Summary of dimensionality reduction, from feature selection steps A to D. From left to right, the number of selected voxels diminishes as successive feature selection steps are applied

4.7.2 Supplementary Figure

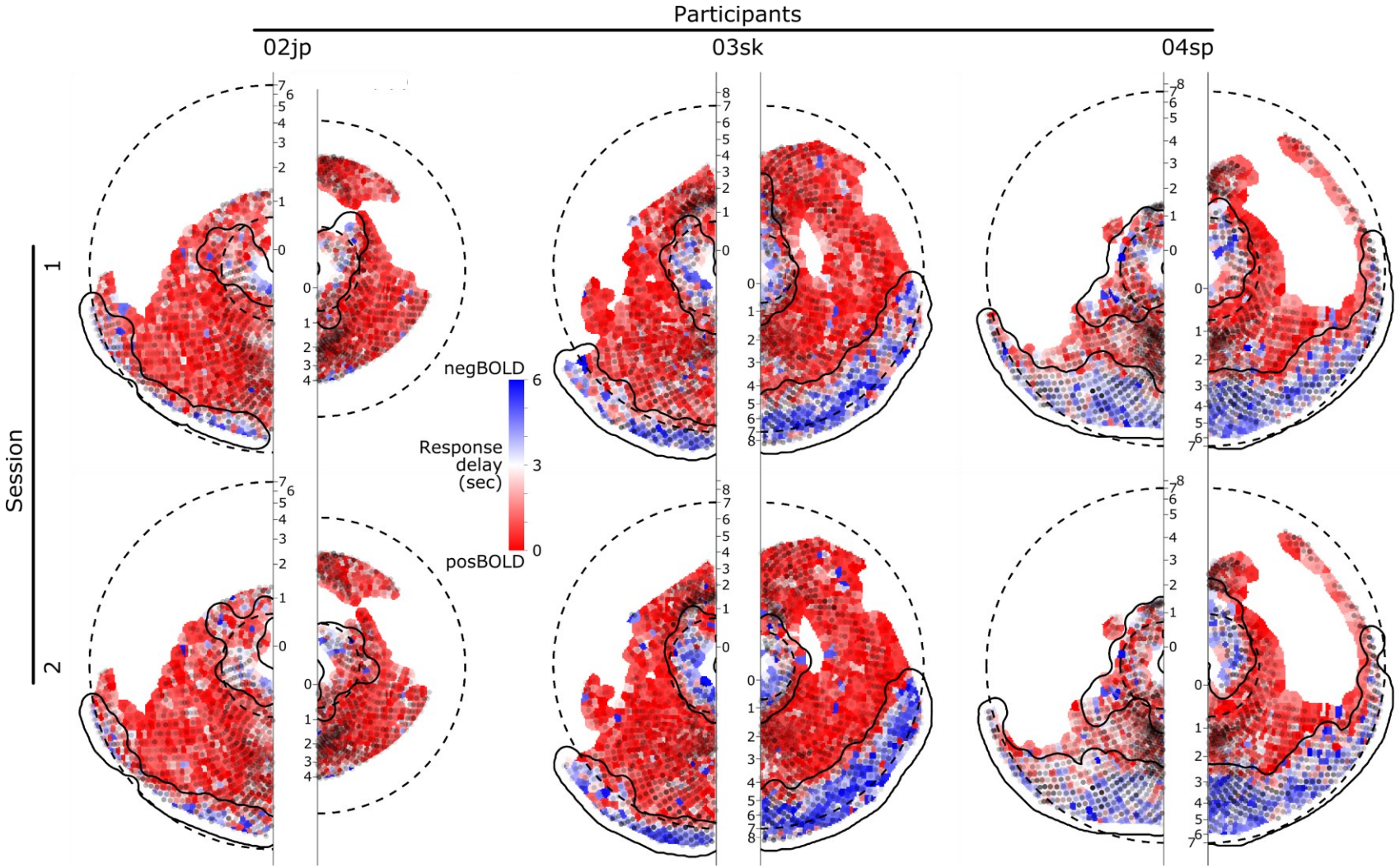

Supplementary Figure 4.1. BOLD response polarity mapped to the scaled visual field for each hemisphere, participant and session. Same convention as Figure 3 of the main text. Scaling of the visual field affected only the radial axis, relying on linearization of the…

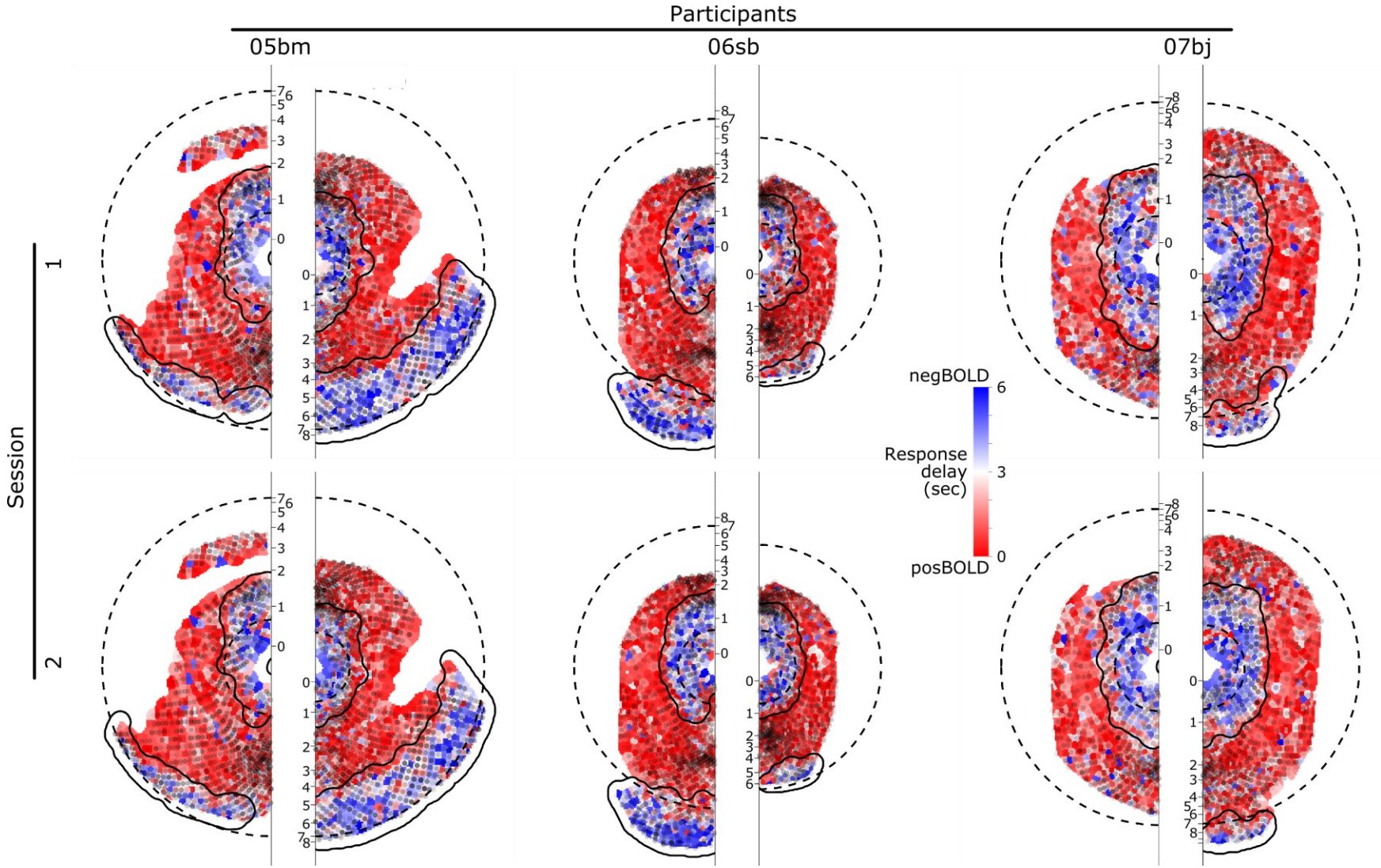

Supplementary Figure 4.1. *cont.* …cumulative distribution function of ROI voxel's eccentricities to counteract cortical magnification and allow visualization on a more homogeneously represented (uniform voxel density) visual field. Scaling was performed…

Supplementary Figure 4.1. *cont.* …independently for each participant's hemisphere. It was however the same across sessions since it ultimately depended on the geometry of the fMRI imaging grid, which was very similar by design across session and made the same after preprocessing. Note that polarity maps, on the other hand, are based on independent data across sessions and yet show remarkable similarities within all participants. The heuristic algorithmic approach aimed at outlining the negBOLD regions surrounding the cortical representation of the annular stimulus field-of-view. It began with extracting the contours of the smoothed polarity map at a value mid-way between negBOLD and posBOLD. It selected the contours that, after slight inflation, overlaps the outside of the visual stimulus field-of-view as defined from the probabilistic retinotopic atlas (dashed outlines). The selected contours generally outlined multiple small areas of negBOLD, which were merged into generally two areas (one for the inner surround and the other for the outer surround of the stimulus field-of-view) by successive inflation and deflation. The resulting contours were inflated again such the non-negBOLD area now constitutes a conservative estimate of the region responding with posBOLD to the stimulus, the latter being taken as a functional estimate of the cortical representation of the stimulus field-of-view. As this did not catch all clearly negBOLD areas, the process was repeated using heavier smoothing of the map and replacing the retinotopic estimate of the representation of the stimulus' field-of-view by that provided by the first iteration. This second pass provided an even more conservative definition of the stimulus' representation by incorporating more negBOLD speckled areas that tended to neighbor the clearly negBOLD areas

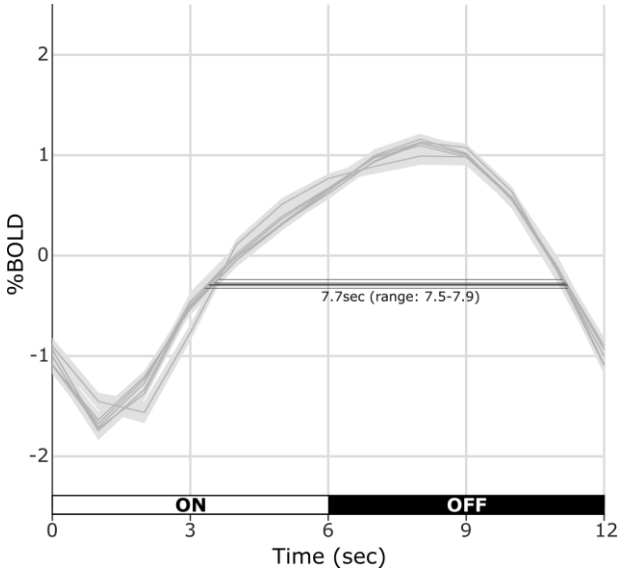

Supplementary Figure 4.2. Model-free estimate of stimulus responses, averaged across V1 voxels representing the stimulus FOV (feature selection step A) in each participant. Same data as in Figure 5B but normalized to the same sinusoidal response delay and amplitude. Horizontal lines indicate the width of the positive lobes at half the peak-to-peak amplitudes. Shaded areas: 95% CI bootstrapped across all runs.

4.8 BIBLIOGRAPHY

Allen, C. P. G., Dunkley, B. T., Muthukumaraswamy, S. D., Edden, R., Evans, C. J., Sumner, P., Singh, K. D., & Chambers, C. D. (2014). Enhanced Awareness Followed Reversible Inhibition of Human Visual Cortex: A Combined TMS, MRS and MEG Study. *Plos One*, *9*(6), Article e100350. https://doi.org/10.1371/journal.pone.0100350

Andersson, J. L. R., Skare, S., & Ashburner, J. (2003). How to correct susceptibility distortions in spin-echo echo-planar images: application to diffusion tensor imaging [Article]. *Neuroimage*, *20*(2), 870-888. https://doi.org/10.1016/s1053-8119(03)00336-7

Anenberg, E., Chan, A. W., Xie, Y. C., LeDue, J. M., & Murphy, T. H. (2015). Optogenetic stimulation of GABA neurons can decrease local neuronal activity while increasing cortical blood flow. *Journal of Cerebral Blood Flow and Metabolism*, *35*(10), 1579-1586. https://doi.org/10.1038/jcbfm.2015.140

Angelucci, A., & Bressloff, P. C. (2006). Contribution of feedforward, lateral and feedback connections to the classical receptive field center and extra-classical receptive field surround of primate V1 neurons. *Acetylcholine in the Cerebral Cortex*, *154*, 93-120. https://doi.org/10.1016/S0079-6123(06)54005-1

Baker, D. H., Meese, T. S., & Summers, R. J. (2007). Psychophysical evidence for two routes to suppression before binocular summation of signals in human vision. *Neuroscience*, *146*(1), 435-448. https://doi.org/10.1016/j.neuroscience.2007.01.030

Bandettini, P. A., Kwong, K. K., Davis, T. L., Tootell, R. B. H., Wong, E. C., Fox, P. T., Belliveau, J. W., Weisskoff, R. M., & Rosen, B. R. (1997). Characterization of cerebral blood oxygenation and flow changes during prolonged brain activation. *Human Brain Mapping*, *5*(2), 93-109.

Bartolo, M. J., Gieselmann, M. A., Vuksanovic, V., Hunter, D., Sun, L., Chen, X., Delicato, L. S., & Thiele, A. (2011). Stimulus-induced dissociation of neuronal firing rates and local field potential gamma power and its relationship to the resonance blood oxygen level-dependent signal in macaque primary visual cortex. *European Journal of Neuroscience*, *34*(11), 1857-1870. https://doi.org/10.1111/j.1460-9568.2011.07877.x

Benson, N. C., Butt, O. H., Datta, R., Radoeva, P. D., Brainard, D. H., & Aguirre, G. K. (2012). The Retinotopic Organization of Striate Cortex Is Well Predicted by Surface Topology. *Current Biology*, *22*(21), 2081-2085. https://doi.org/10.1016/j.cub.2012.09.014

Bouboulis, P., & Theodoridis, S. (2011). Extension of Wirtinger's Calculus to Reproducing Kernel Hilbert Spaces and the Complex Kernel LMS [Article]. *Ieee Transactions on Signal Processing*, *59*(3), 964-978. https://doi.org/10.1109/tsp.2010.2096420

Bouboulis, P., Theodoridis, S., Mavroforakis, C., & Evaggelatou-Dalla, L. (2015). Complex Support Vector Machines for Regression and Quaternary Classification [Article]. *Ieee Transactions on Neural Networks and Learning Systems*, *26*(6), 1260-1274. https://doi.org/10.1109/tnnls.2014.2336679

Boynton, G. M., Engel, S. A., Glover, G. H., & Heeger, D. J. (1996). Linear systems analysis of functional magnetic resonance imaging in human V1. *Journal of Neuroscience*, *16*(13), 4207-4221. https://doi.org/10.1523/JNEUROSCI.16-13-04207.1996

Brouwer, G. J., & Heeger, D. J. (2011). Cross-orientation suppression in human visual cortex. *Journal of Neurophysiology*, *106*(5), 2108-2119. https://doi.org/10.1152/jn.00540.2011

Buxton, R. B., Griffeth, V. E. M., Simon, A. B., Moradi, F., & Shmuel, A. (2014). Variability of the coupling of blood flow and oxygen metabolism responses in the brain: a problem for interpreting BOLD studies but potentially a new window on the underlying neural activity (vol 8, pg 139, 2014) [Correction]. *Frontiers in Neuroscience*, *8*, 1, Article 241. https://doi.org/10.3389/fnins.2014.00241

Buxton, R. B., Wong, E. C., & Frank, L. R. (1998). Dynamics of blood flow and oxygenation changes during brain activation: The balloon model. *Magnetic Resonance in Medicine*, *39*(6), 855-864. https://doi.org/10.1002/mrm.1910390602

Carandini, M., & Heeger, D. J. (2012). Normalization as a canonical neural computation [Review]. *Nature Reviews Neuroscience*, *13*(1), 51-62. https://doi.org/10.1038/nrn3136

Chang, C. C., & Lin, C. J. (2011). LIBSVM: A Library for Support Vector Machines [Article]. *Acm Transactions on Intelligent Systems and Technology*, *2*(3), 27, Article 27. https://doi.org/10.1145/1961189.1961199

Chen, J. E., Glover, G. H., Fultz, N. E., Rosen, B. R., Polimeni, J. R., & Lewis, L. D. (2021). Investigating mechanisms of fast BOLD responses: The effects of stimulus intensity and of spatial heterogeneity of hemodynamics. *Neuroimage*, *245*, Article 118658. https://doi.org/10.1016/j.neuroimage.2021.118658

Deangelis, G. C., Robson, J. G., Ohzawa, I., & Freeman, R. D. (1992). ORGANIZATION OF SUPPRESSION IN RECEPTIVE-FIELDS OF NEURONS IN CAT VISUAL-CORTEX. *Journal of Neurophysiology*, *68*(1), 144-163. https://doi.org/10.1152/jn.1992.68.1.144

Farivar, R., Grigorov, F., van der Kouwe, A. J., Wald, L. L., & Keil, B. (2016). Dense, Shape-Optimized Posterior 32-Channel Coil for Submillimeter Functional Imaging of Visual Cortex at 3T. *Magnetic Resonance in Medicine*, *76*(1), 321-328. https://doi.org/10.1002/mrm.25815

Farivar, R., Thompson, B., Mansouri, B., & Hess, R. F. (2011). Interocular suppression in strabismic amblyopia results in an attenuated and delayed hemodynamic response function in early visual cortex. *Journal of Vision*, *11*(14), Article 16. https://doi.org/10.1167/11.14.16

Freeman, T. C. B., Durand, S., Kiper, D. C., & Carandini, M. (2002). Suppression without inhibition in visual cortex. *Neuron*, *35*(4), 759-771. https://doi.org/10.1016/s0896-6273(02)00819-x

Gonzalez-Castillo, J., Saad, Z. S., Handwerker, D. A., Inati, S. J., Brenowitz, N., & Bandettini, P. A. (2012). Whole-brain, time-locked activation with simple tasks revealed using massive averaging and model-free analysis. *Proc Natl Acad Sci U S A*, *109*(14), 5487-5492. https://doi.org/10.1073/pnas.1121049109

Greve, D. N., & Fischl, B. (2009). Accurate and robust brain image alignment using boundary-based registration [Article]. *Neuroimage*, *48*(1), 63-72. https://doi.org/10.1016/j.neuroimage.2009.06.060

Griffeth, V. E. M., Simon, A. B., & Buxton, R. B. (2015). The coupling of cerebral blood flow and oxygen metabolism with brain activation is similar for simple and complex stimuli in human primary visual cortex. *Neuroimage*, *104*, 156-162. https://doi.org/10.1016/j.neuroimage.2014.10.003

Handwerker, D. A., Ollinger, J. M., & D'Esposito, M. (2004). Variation of BOLD hemodynamic responses across subjects and brain regions and their effects on statistical analyses. *Neuroimage*, *21*(4), 1639-1651. https://doi.org/10.1016/j.neuroimage.2003.11.029

Havlicek, M., Ivanov, D., Roebroeck, A., & Uludag, K. (2017). Determining Excitatory and Inhibitory Neuronal Activity from Multimodal fMRI Data Using a Generative Hemodynamic Model [Article]. *Frontiers in Neuroscience*, *11*, 20, Article 616. https://doi.org/10.3389/fnins.2017.00616

Haynes, J. D., & Rees, G. (2005). Predicting the orientation of invisible stimuli from activity in human primary visual cortex. *Nature Neuroscience*, *8*(5), 686-691. https://doi.org/10.1038/nn1445

Heeger, D. J. (1992). NORMALIZATION OF CELL RESPONSES IN CAT STRIATE CORTEX [Review]. *Visual Neuroscience*, *9*(2), 181-197. https://doi.org/10.1017/s0952523800009640

Hoge, R. D., Atkinson, J., Gill, B., Crelier, G. R., Marrett, S., & Pike, G. B. (1999c). Stimulus-dependent BOLD and perfusion dynamics in human V1. *Neuroimage*, *9*(6), 573-585. https://doi.org/10.1006/nimg.1999.0443

Holland, D., Kuperman, J. M., & Dale, A. M. (2010). Efficient correction of inhomogeneous static magnetic field-induced distortion in Echo Planar Imaging [Article]. *Neuroimage*, *50*(1), 175-183. https://doi.org/10.1016/j.neuroimage.2009.11.044

Hubel, D. H., & Wiesel, T. N. (1974). SEQUENCE REGULARITY AND GEOMETRY OF ORIENTATION COLUMNS IN MONKEY STRIATE CORTEX. *Journal of Comparative Neurology*, *158*(3), 267-294. https://doi.org/10.1002/cne.901580304

Ip, I. B., & Bridge, H. (2021). Investigating the neurochemistry of the human visual system using magnetic resonance spectroscopy [Review; Early Access]. *Brain Struct Funct*, 15. https://doi.org/10.1007/s00429-021-02273-0

Kamitani, Y., & Tong, F. (2005). Decoding the visual and subjective contents of the human brain. *Nature Neuroscience*, *8*(5), 679-685. https://doi.org/10.1038/nn1444

Katzner, S., Busse, L., & Carandini, M. (2011). GABA(A) Inhibition Controls Response Gain in Visual Cortex [Article]. *Journal of Neuroscience*, *31*(16), 5931-5941. https://doi.org/10.1523/jneurosci.5753-10.2011

Kay, K., Jamison, K. W., Vizioli, L., Zhang, R. Y., Margalit, E., & Ugurbil, K. (2019). A critical assessment of data quality and venous effects in sub-millimeter fMRI [Article]. *Neuroimage*, *189*, 847-869. https://doi.org/10.1016/j.neuroimage.2019.02.006

Kim, S. G., & Ogawa, S. (2012). Biophysical and physiological origins of blood oxygenation level-dependent fMRI signals. *Journal of Cerebral Blood Flow and Metabolism*, *32*(7), 1188-1206. https://doi.org/10.1038/jcbfm.2012.23

Kriegeskorte, N., Simmons, W. K., Bellgowan, P. S. F., & Baker, C. I. (2009). Circular analysis in systems neuroscience: the dangers of double dipping. *Nature Neuroscience*, *12*(5), 535-540. https://doi.org/10.1038/nn.2303

Lewis, L. D., Setsompop, K., Rosen, B. R., & Polimeni, J. R. (2016). Fast fMRI can detect oscillatory neural activity in humans. *Proceedings of the National Academy of Sciences of the United States of America*, *113*(43), E6679-E6685. https://doi.org/10.1073/pnas.1608117113

Li, B. W., & Freeman, R. D. (2011). Neurometabolic coupling differs for suppression within and beyond the classical receptive field in visual cortex. *Journal of Physiology-London*, *589*(13), 3175-3190. https://doi.org/10.1113/jphysiol.2011.205039

Li, B. W., Peterson, M. R., Thompson, J. K., Duong, T., & Freeman, R. D. (2005). Cross-orientation suppression: Monoptic and dichoptic mechanisms are different. *Journal of Neurophysiology*, *94*(2), 1645-1650. https://doi.org/10.1152/jn.00203.2005

Logothetis, N. K. (2002). The neural basis of the blood-oxygen-level-dependent functional magnetic resonance imaging signal. *Philosophical Transactions of the Royal Society of London Series B-Biological Sciences*, *357*(1424), 1003-1037. https://doi.org/10.1098/rstb.2002.1114

Lunghi, C., Emir, U. E., Morrone, M. C., & Bridge, H. (2015). Short-Term Monocular Deprivation Alters GABA in the Adult Human Visual Cortex [Article]. *Current Biology*, *25*(11), 1496-1501. https://doi.org/10.1016/j.cub.2015.04.021

Meese, T. S., & Baker, D. H. (2013). A common rule for integration and suppression of luminance contrast across eyes, space, time, and pattern. *I-Perception*, *4*(1), 1-16. https://doi.org/10.1068/i0556

Morrone, M. C., Burr, D. C., & Speed, H. D. (1987). CROSS-ORIENTATION INHIBITION IN CAT IS GABA MEDIATED. *Experimental Brain Research*, *67*(3), 635-644. https://doi.org/10.1007/BF00247294

Muthukumaraswamy, S. D., Edden, R. A. E., Jones, D. K., Swettenham, J. B., & Singh, K. D. (2009). Resting GABA concentration predicts peak gamma frequency and fMRI amplitude in response to visual stimulation in humans. *Proceedings of the National Academy of Sciences of the United States of America*, *106*(20), 8356-8361. https://doi.org/10.1073/pnas.0900728106

Muthukumaraswamy, S. D., Evans, C. J., Edden, R. A. E., Wise, R. G., & Singh, K. D. (2012). Individual variability in the shape and amplitude of the BOLD-HRF correlates with endogenous GABAergic inhibition. *Human Brain Mapping*, *33*(2), 455-465. https://doi.org/10.1002/hbm.21223

O'Herron, P., Chhatbar, P. Y., Levy, M., Shen, Z. M., Schramm, A. E., Lu, Z. Y., & Kara, P. (2016). Neural correlates of single-vessel haemodynamic responses in vivo. *Nature*, *534*(7607), 378-+. https://doi.org/10.1038/nature17965

Olman, C. A., Inati, S., & Heeger, D. J. (2007). The effect of large veins on spatial localization with GE BOLD at 3 T: Displacement, not blurring [Article]. *Neuroimage*, *34*(3), 1126-1135. https://doi.org/10.1016/j.neuroimage.2006.08.045

Parker, D. B., & Razlighi, Q. R. (2019). The Benefit of Slice Timing Correction in Common fMRI Preprocessing Pipelines. *Frontiers in Neuroscience*, *13*, Article 821. https://doi.org/10.3389/fnins.2019.00821

Peck, K. K., Sunderland, A., Peters, A. M., Butterworth, S., Clark, P., & Gowland, P. A. (2001). Cerebral activation during a simple force production task: changes in the time course of the haemodynamic response. *Neuroreport*, *12*(13), 2813-2816. https://doi.org/10.1097/00001756-200109170-00012

Priebe, N. J., & Ferster, D. (2006). Mechanisms underlying cross-orientation suppression in cat visual cortex. *Nature Neuroscience*, *9*(4), 552-561. https://doi.org/10.1038/nn1660

Proulx, S., Safi-Harb, M., LeVan, P., An, D., Watanabe, S., & Gotman, J. (2014). Increased sensitivity of fast BOLD fMRI with a subject-specific hemodynamic response function and application to epilepsy [Article]. *Neuroimage*, *93*, 59-73. https://doi.org/10.1016/j.neuroimage.2014.02.018

Sadaghiani, S., Ugurbil, K., & Uludag, K. (2009). Neural activity-induced modulation of BOLD poststimulus undershoot independent of the positive signal. *Magn Reson Imaging*, *27*(8), 1030-1038. https://doi.org/10.1016/j.mri.2009.04.003

Sengpiel, F., Jirmann, K.-U., Vorobyov, V., & Eysel, U. T. (2005). Strabismic Suppression Is Mediated by Inhibitory Interactions in the Primary Visual Cortex. *Cerebral Cortex*, *16*(12), 1750-1758. https://doi.org/10.1093/cercor/bhj110

Sengpiel, F., & Vorobyov, V. (2005). Intracortical origins of interocular suppression in the visual cortex. *Journal of Neuroscience*, *25*(27), 6394-6400. https://doi.org/10.1523/jneurosci.0862-05.2005

Shmuel, A., Augath, M., Oeltermann, A., & Logothetis, N. K. (2006). Negative functional MRI response correlates with decreases in neuronal activity in monkey visual area V1. *Nature Neuroscience*, *9*(4), 569-577. https://doi.org/10.1038/nn1675

Smith, A. T., Williams, A. L., & Singh, K. D. (2004). Negative BOLD in the visual cortex: evidence against blood stealing. *Human Brain Mapping*, *21*(4), 213-220. https://doi.org/10.1002/hbm.20017

Stagg, C. J. (2014). Magnetic Resonance Spectroscopy as a tool to study the role of GABA in motor-cortical plasticity [Review]. *Neuroimage*, *86*, 19-27. https://doi.org/10.1016/j.neuroimage.2013.01.009

Stagg, C. J., Wylezinska, M., Matthews, P. M., Johansen-Berg, H., Jezzard, P., Rothwell, J. C., & Bestmann, S. (2009). Neurochemical Effects of Theta Burst Stimulation as Assessed by Magnetic Resonance Spectroscopy. *Journal of Neurophysiology*, *101*(6), 2872-2877. https://doi.org/10.1152/jn.91060.2008

Suarez, H., Koch, C., & Douglas, R. (1995). MODELING DIRECTION SELECTIVITY OF SIMPLE CELLS IN STRIATE VISUAL-CORTEX WITHIN THE FRAMEWORK OF THE CANONICAL MICROCIRCUIT. *Journal of Neuroscience*, *15*(10), 6700-6719. https://doi.org/10.1523/JNEUROSCI.15-10-06700.1995

Thompson, S. K., Engel, S. A., & Olman, C. A. (2014). Larger neural responses produce BOLD signals that begin earlier in time. *Frontiers in Neuroscience*, *8*, 159. https://doi.org/10.3389/fnins.2014.00159

Uhlirova, H., Kılıç, K., Tian, P., Sakadžić, S., Gagnon, L., Thunemann, M., Desjardins, M., Saisan, P. A., Nizar, K., Yaseen, M. A., Hagler, D. J., Vandenberghe, M., Djurovic, S., Andreassen, O. A., Silva, G. A., Masliah, E., Kleinfeld, D., Vinogradov, S., Buxton, R. B., . . . Devor, A. (2016). The roadmap for estimation of cell-type-specific neuronal activity from non-invasive measurements. *Philosophical Transactions of the Royal Society B: Biological Sciences*, *371*(1705), 20150356. https://doi.org/10.1098/rstb.2015.0356

Uhlirova, H., Kılıç, K., Tian, P. F., Thunemann, M., Desjardins, M., Saisan, P. A., Sakadzic, S., Nese, T. V., Mateo, C., Cheng, Q., Weldy, K. L., Razoux, F., Vandenberghe, M., Cremonesi, J. A., Ferri, C. G. L., Nizar, K., Sridhar, V. B., Steed, T. C., Abashin, M., . . . Devor, A. (2016). Cell type specificity of neurovascular coupling in cerebral cortex. *Elife*, *5*. https://doi.org/10.7554/elife.14315

Wade, A. R., & Rowland, J. (2010). Early Suppressive Mechanisms and the Negative Blood Oxygenation Level-Dependent Response in Human Visual Cortex. *Journal of Neuroscience*, *30*(14), 5008-5019. https://doi.org/10.1523/Jneurosci.6260-09.2010

Walker, G. A., Ohzawa, I., & Freeman, R. D. (1998). Binocular cross-orientation suppression in the cat's striate cortex. *Journal of Neurophysiology*, *79*(1), 227-239. https://doi.org/10.1152/jn.1998.79.1.227

Yacoub, E., Harel, N., & Ugurbil, K. (2008). High-field fMRI unveils orientation columns in humans. *Proceedings of the National Academy of Sciences of the United States of America*, *105*(30), 10607-10612. https://doi.org/10.1073/pnas.0804110105

Chapter 5: General Discussion and Conclusion

This thesis set out to better characterize how available non-invasive investigational tools relate to computationally relevant aspects of neural activity. I pointed psychophysics, TMS, MRS and fMRI methods on well-known occipital intracortical processes. Carefully interpreted in the light of more detailed knowledge developed from previous theoretical and invasive animal studies, results provided new insights on non-invasively accessible biophysical processes and related low-level visual computations. Below I elaborate on these opportunities to solidify the interpretational framework for non-invasive brain signals and on their limitations. I conclude with further propositions for extracting computationally relevant information from such non-invasive brain signals.

5.1 Visual Science to Haul the Principled Design of TMS Brain Therapies

The development of safe NIBS tools and particularly TMS is revolutionising cognitive science, psychiatry and neurology. Before TMS, having precisely mapped a cognitive function with fMRI did little for restoring it in a patient, and even when resection or intracranial neurostimulation can be construed as potential cures, the risks often outweigh the benefits. On the other hand, the increasingly demonstrated innocuity of NIBS allows human trials at an unprecedented scale, which may at times feel like a fishing expedition. Indeed, although functional imaging and cross-sectional brain lesion studies allow evidence-based selection of target sites, the selection of other treatment parameters remains an educated guess. The discovery of effective treatments requires a fair bit of trial-and-error on patients.

A more principled approach to brain stimulation treatment discovery would require more basic research to mapping the immense parameter space of NIBM protocols to the also large space of neural computations carried by a given targeted brain tissue. Great progress was made in the motor cortex, thanks to quantifiable motor outputs, but at the expense of unknown generalizability. Chapter 2 addressed this latter issue by emulating a motor cortex protocol in the visual cortex and, for the first time, showing similarly affected inhibitory processes. However, an important additional goal was to experiment with and demonstrate the possibility

to map the parameter space of TMS NIBM with respect to their effect on specific visual cortex microcircuits. Here we will therefore discuss the experimental design opportunities that the visual system offers and how they can overcome limitations of Chapter 2 and motor cortex experiments.

5.1.1 Navigating the Intractably Large Space of NIBM Protocols and Neural Processes

The main challenge of TMS research is the scale of its TMS parameter space. Only exploring D=3 parameter dimensions at N=2 levels each—e.g. two intensities, two train frequencies and two directions of monophasic pulses—in one brain target requires $N^D = 2^3 = 8$ experimental conditions. Adding a control TMS target region doubles that number which grows exponentially with D. Whether in the motor or visual cortex, a systematic "grid search" is impractical, at least in humans.

Such thorough TMS parameter space exploration would require a paradigm where the duration of the experiment and the risk of tissue damage is not a concern. This could be achieved with a chronically head-mounted or implanted magnetic stimulation setup compatible with simultaneous chronic neural recordings in animals (Saha et al., 2022) freely behaving in a monitored environment. Standardized protocols automatically ran daily or weekly could then streamline a systematic exploration of the NIBM parameter space, where promising locations in this space could be characterized further in naïve animals. Despite likely challenging translation to human—accuracy of the E-field modeling will be crucial here—such animal data would be invaluable for designing new NIBM protocols with better informed expectations about their safety and neural effects.

Another challenge to NIBM therapy design in humans is that the expected effects and the appropriate way to measure them may not be *a priori* known—a potent modulation may go undetected if the affected and measured microcircuits don't overlap (Albouy et al., 2017; Lin et al., 2021; Thut et al., 2011). This equally concern both motor and visual cortex study, but the latter has an advantage: visual psychophysics offers a large set of validated stimuli and procedures—along with virtually unlimited freedom to design new ones—for quantifying well-characterized neural processes. The inception of Chapter 2's study is a good example: we

needed a protocol for measuring intracortical inhibition in the early visual cortex and an extensive literature identified visual masking as an appropriate candidate.

In contrast, the view on intracortical processes of the motor cortex is rather narrow. It is based on the phenomenology of paired-pulse protocols—a conditioning single pulse of TMS affects the corticospinal output of a subsequent test pulse through different intracortical microcircuits depending on the pulse strength and time separation (Ilic et al., 2002). Such measures probe a limited set of neural circuits not well aligned to functionally relevant microcircuits. Visual psychophysics therefore compare favorably, as it can probe a virtually unlimited set of naturally driven microcircuits.

Chapter 2's study is one of compromises. Testing five masking conditions ensured coverage of potentially mask-type-specific microcircuits while retaining sensitivity for a general cortical masking effect and controlling for non-cortical masking. At the same time, focussing on a single NIBM protocol and intracortical process comes at the risk of triggering no effect or missing it, which may have happened in the first sail of the project. Indeed, we first used a less powerful TMS system that maxed out at 45% of its maximum output during cTBS in all participants (Figure 5.1)—corresponding to 49% to 63% of individual phosphene thresholds—and failed to produce any effect (unpublished results). This suggests that potent cTBS of the visual cortex sits on the higher end of the TMS intensity dimension, consistent with similar dose-dependency observed in the motor cortex (Sasaki et al., 2018). It also highlights the necessary trade-off, under limited research resources, between exploring a large section of the TMS parameter space or sensitively testing a narrow one.

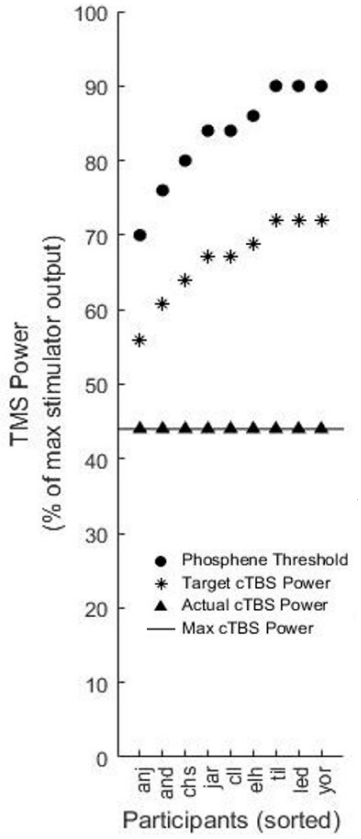

Figure 5.1 Targeted and achieved power of cTBS in an unpublished study that preceded that presented in Chapter 2. The cTBS power maxed out in every participant before reaching the target of 80% of phosphene threshold, possibly explaining null findings.

5.1.2 Leveraging the Retinotopy of the Occipital Pole

The occipital cortex anatomy offers two other advantages over the motor cortex for studying the intracortical effects of NIBM. The first one is its protruding shape (Figure 2.3) that should expose the tip of the occipital pole to the highest E-field. In contrast, the relatively flat outer shape of the brain at the level of the motor cortex makes it virtually impossible to avoid stimulating neighboring gyral crowns with standard coils (Figure 5.2)—some paired-pulse effects (see Section 1.4.1.2.3) are actually thought to involve e.g. S1 to M1 connections (Ziemann, 2020), complicating the distinction between intracortical and corticocortical interactions.

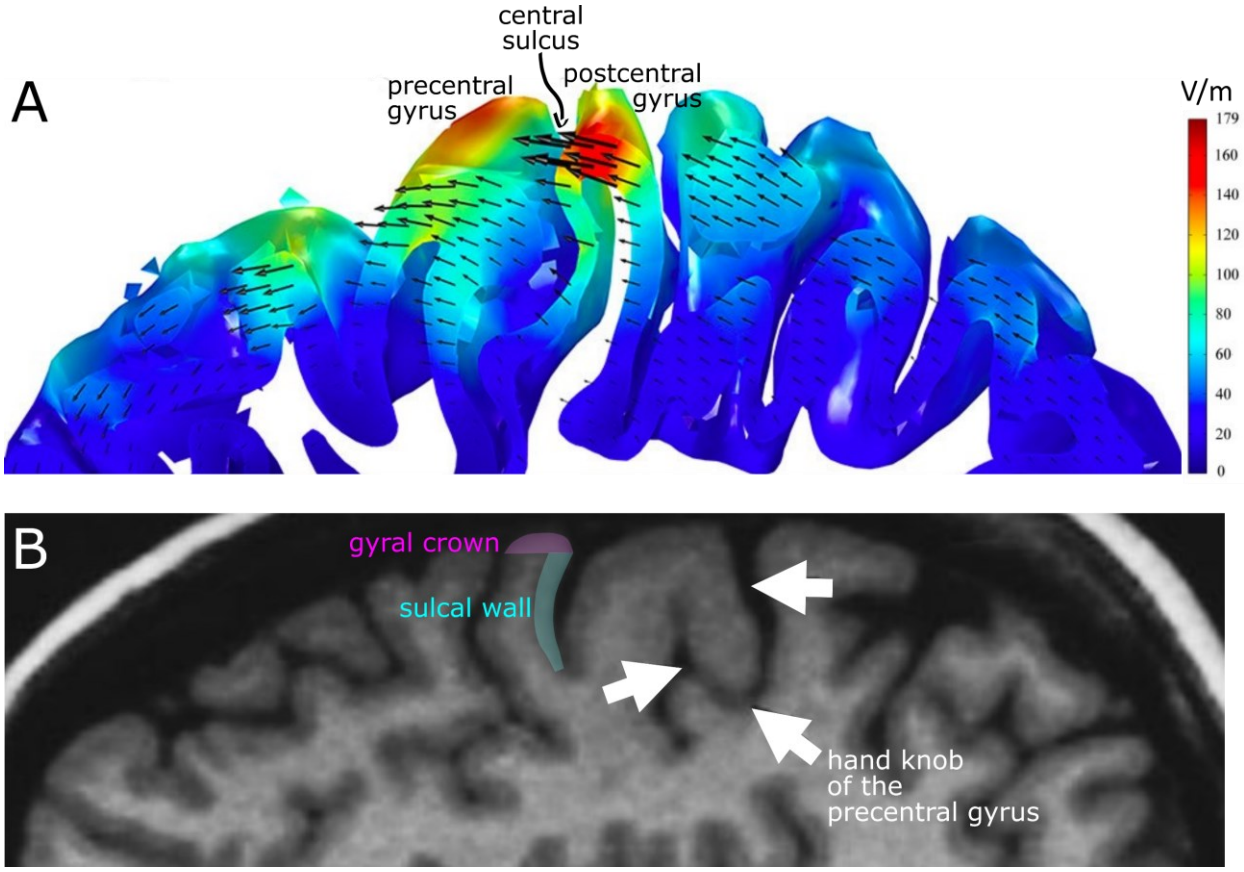

Figure 5.2 TMS of the motor cortex. A. Example biophysical model of the electric field induced by TMS over the motor cortex. Note that the electric field is strongest at the crown of the postcentral and precentral gyri and oriented parallel and perpendicular to the cortical surface in the gyral crown and sulcal wall, respectively. **B.** MRI showing the primary motor representation of the hand, the "hand knob", bulging into the central sulcus. Magenta and cyan colors respectively show an example gyral crown and sulcal wall. Adapted with permission from (A) Salvador et al. (2015) and B Yousry et al. (1997).

Moreover, the gyrification of the hand representation is very convoluted. The “hand-knob” bulges deep into the central sulcus (Figure 5.2B)(Yousry et al., 1997), which greatly complexifies how anatomofunctional idiosyncrasies affect the spatial configuration of brain tissues into the E-field. Indeed, the MEP-generating corticomotoneurons in the hand-knob are buried more or less deep in the sulcus in different participants. This affects the amplitude and relative orientation of the experienced E-field and the consequent pattern of directly depolarized neural fibers (Figure 5.3)(Aberra et al., 2020; Shirinpour et al., 2021). For example, TMS sometime activates corticomotoneurons strictly indirectly through mono and polysynaptic circuits—note the optional presence of a D-wave in Figure 1.11’s subdural spinal volleys. The motor microcircuits activated by TMS and contributing to MEPs therefore significantly vary across participants (Dubbioso et al., 2021; Eichert et al., 2021; Weise et al., 2020), which likely contributes to the notoriously large interindividual variability of NIBM (Valero-Cabre et al., 2017). The simpler shape of the occipital pole reduces the impact of these issues.

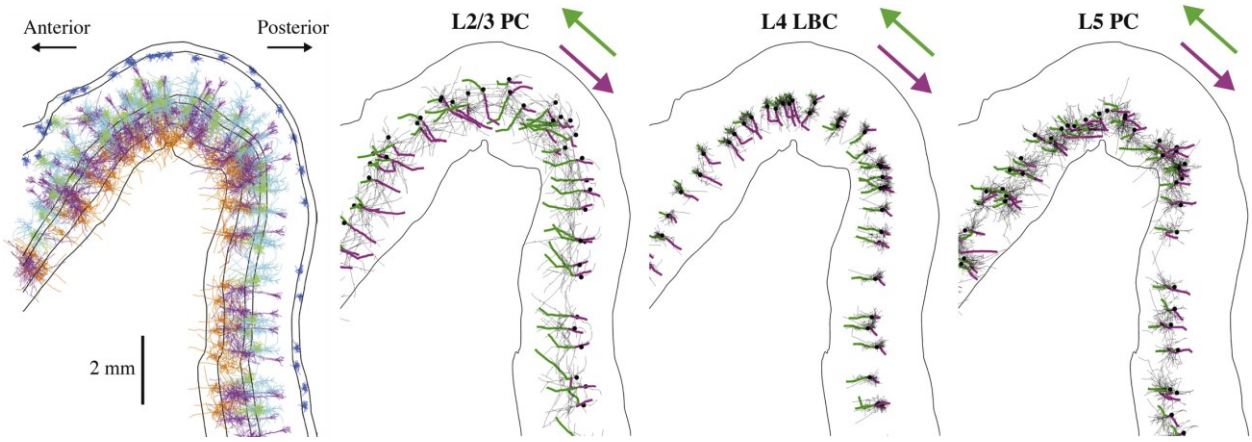

Figure 5.3 Modeling the effect of TMS on an arrangement of morphologically realistic neurons in a cortical gyrus. Leftmost panel shows all modeled neurons. Panels on the right each shows a subset of modeled neurons (dendrite not shown) with directly activated axons colored from the action potential initiation point to the proximal branching point and according to TMS direction (green and magenta arrows). Black dots represent neural somata. PC: principal cells, LBC: large basket cells. *Reproduced with permission from Aberra et al. (2020)*

The second advantage of the visual cortex resides in the nature of its organization. Indeed, retinotopy allows to precisely predict the cortical patch that will process a circumscribed stimulus (Figure 2.3A and C). The visual field location of the psychophysical stimuli can therefore be adjusted to probe the cortical patch that e.g. experienced the strongest E-field. In motor cortex studies, using the same TMS coil position for modulating the brain and measuring

the after-effect may lead to the false belief that the modulated and measured tissues are well-matched. The measured tissue is however largely determined by the muscle from which the MEPs are recorded. Worse, the functional relevance of MEPs is limited since cortical neurons represent limb movements and muscle synergies more than single muscles (Kakei et al., 1999; Shenoy et al., 2013). The latter further means that one can hardly select the cortical patch to be probed by selecting the muscle to record.

The occipital cortex is however not completely immune to the above issues. In Chapter 2 for example, although the phosphene mapping suggested unilateral stimulation, the actual exposition of the contralateral occipital pole remains unknown. In the participant from which structural MRI was available, the cortical projection of the phosphene map suggested a V2 target, but it could very well be V1 or V3 in other participants (Kammer, Puls, Erb, et al., 2005; Salminen-Vaparanta et al., 2014; Schaeffner & Welchman, 2017). Finally, we did not adjust to visual field position of our psychophysical stimuli on an individual basis because of the tight field-of-view of our dichoptic stimulation apparatus (Supplementary Figure 2.1). According to individual phosphene maps (Supplementary Figure 2.2), the cortical patch receiving the highest cTBS dose represented the center stimulus area in some participants but another area falling on the surround stimulus in others.

Now that our approach focusing on the tip of the occipital pole for dissecting NIBM microcircuit effects has shown a detectable effect, it should be refined by incorporating modern E-field modeling, more precise retinotopic mapping and robotized neuronavigation. Indeed, planning the coil positioning in advance using each participant's structural MRI and E-field simulations would allow an optimally focal stimulation of the occipital pole tip. Less than five minutes of fMRI can improve the retinotopic atlas registration used in Chapter 2 by ~20% (Benson & Winawer, 2018) and allow the prescription of psychophysical stimuli that would precisely match the TMS target. Robotized neuronavigation would speedup manipulation time, reduce participants' fatigue and increase targeting precision (Harquel et al., 2016). Phosphene mapping would remain relevant as a confirmatory measure, but also as an object of study on its own rights—the origin of phosphenes is still not clear and an interesting approach to the origin of MEPs by Weise et al. (2020) could be applied here. Importantly, unavoidable but now

precisely identified idiosyncrasies would no longer contribute to NIBM outcome variability and could instead be leveraged. For example, whether the target fell in V1, V2 or V3 could be entered as a cofactor at the analysis stage. Moreover, as each visual field position maps to a cortical patch experiencing a different E-field vector, mapping NIBM effects across the visual field with perimetric psychophysical measures would be an efficient way to investigate the impact of E-field amplitude and orientation in a multivariate statistical design. Brought to its full potential, such individualized precision TMS of the occipital pole could streamline the investigation of microcircuit mechanisms of NIBM.

5.1.3 Toward a Computational Description of Local Brain Modulations

Contrary to what the term 'masking' may suggest, a visual mask does not always suppress perception. Indeed, Meese et al. (2007) showed that the detection of a test grating is suppressed by cross-oriented masks (blue in Figure 5.4) but facilitated in a scaled-down version of the test and mask arrangement (purple in Figure 5.4). In fact, masking is thought to involve both excitatory and inhibitory circuits onto the neurons tuned to the test stimuli (Huang & Chen, 2016; Meese et al., 2007). It is their balance that determines the net facilitatory or inhibitory effect.

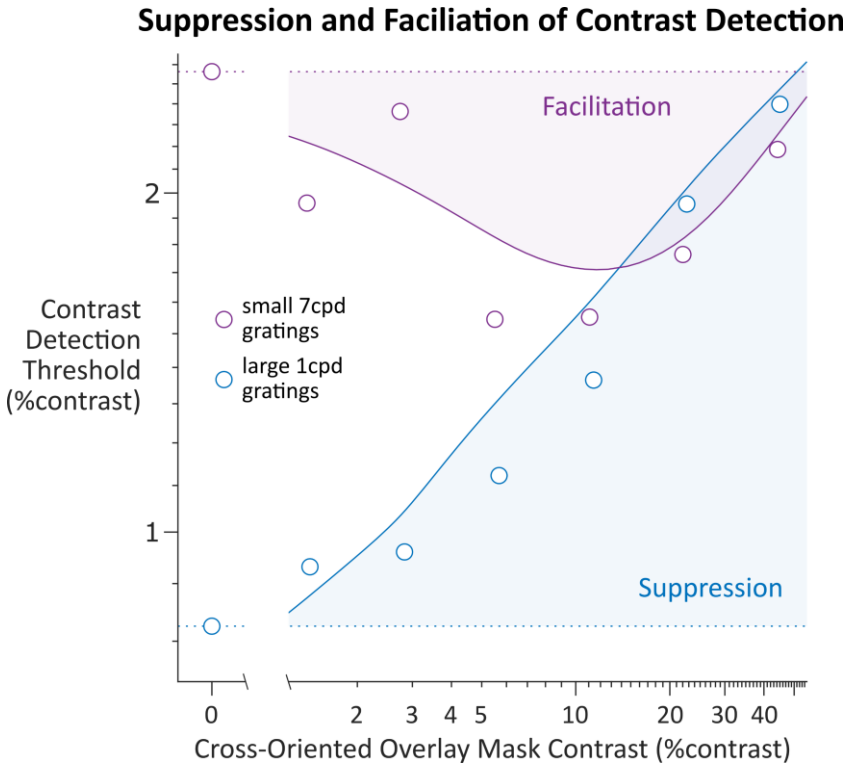

Figure 5.4 Inhibitory and excitatory effects of visual masks. A cross-oriented overlay mask can either suppress (blue) or facilitate (purple) perception of contrast at threshold. The low threshold for a small ~2° patch showing 2 cycles of a grating (1cpd) is increasingly elevated with increasing mask contrasts, consistent with inhibition-dominated interactions. The high threshold for the same stimuli scaled down by a factor of 7 (to 0.29° and 7cpd) are however lowered by the mask, consistent with excitation-dominated interactions. The facilitatory effect dies off at the highest mask contrasts, consistent with an excitation-to-inhibition balance that gradually shifts from excitatory to inhibitory with increasing stimulus energy. cpd: cycle-per-degree. *Data and fits replotted from Meese et al. (2007) (observer DHB and DJH). Code available at https://github.com/farivarlab/psychoCRFdemo.*

This may limit the specificity of simple visual masking protocols—altered masking effects can either result from a change in excitation or an opposite change in inhibition. Chapter 2 addressed this issue with high-contrast masks on a low-threshold test stimulus that minimize the contribution of excitation. When desired, sensitivity to excitatory microcircuits can be tuned up with simple parameter teaks, e.g. by using mild-contrast masks on a high-threshold test (see Figure 5.4 and its caption).

A more interesting avenue would be to estimate the strength of both inhibitory and excitatory circuits using threshold data acquired over the full range of mask contrast. This can be achieved using well-validated psychophysical models of the contrast response function of visual channels and signal detection theory (SDT) (Baker et al., 2013; Foley, 1994; Huang & Chen, 2016; Meese & Baker, 2013; Meese et al., 2007). In Meese et al. (2007) for example,

$$r(c_{test}, c_{mask}) = \frac{c_{test}^{p}(1 + a \cdot c_{mask})}{z + c_{test}^{q}(1 + b \cdot c_{mask})} \quad [5.1]$$

defines the signal or response r within the visual channel of the test stimulus—an abstraction of neural detector mechanisms sensitive to the test stimulus (see Section 1.4.1.1)—as a function of the contrast of the test c_{test} and mask c_{mask} stimuli. The parameters p, q and z define the shape of the contrast response function when $c_{mask} = 0$ (see Figure C.1). Importantly here, a and b control the influence of the mask stimulus on signal in the test stimulus channel: on the numerator, a models facilitatory influences while b on the denominator models suppressive influences. Finally, thanks to SDT (see Annex C), detection thresholds can be predicted from any contrast response function model $r(c_{test}, c_{mask})$, allowing to fit actual threshold data as in Figure 5.4 and, most interestingly here, estimate the strength of cross-channel (mask to test) excitatory and inhibitory interactions respectively through the value of a and b. Such estimates are data hungry—over a thousand trials—but could be achieved within reasonable time after NIBM by trading off on the number of mask conditions and using extensions of adaptive psychophysics method (Lesmes et al., 2006; Watson, 2017).

Interestingly, the above modeling approach could resolve another limitation raised in Chapter 2: the possibility of an undetected within-channel effect of cTBS. Indeed, both Chapter

2's empirical and the above model-based approaches focus on cross-channel/intercolumnar interactions, but cTBS could also affect intra-channel/intracolumnar mechanisms. Luckily, excitation and inhibition can also be estimated within-channel by using a mask identical to the test stimulus—the detection task becomes a contrast increment detection task—and a now simpler model of the contrast response function (Meese et al., 2007):

$$r(c_{test}, c_{mask}) = \frac{(c_{test} + c_{mask})^p}{z + (c_{test} + c_{mask})^q} \quad [5.2].$$

Here again thresholds are collected over a range of mask contrasts and fitted to the contrast response function using SDT, but now p are q are of interest. The exponent p amplifies the effect of contrast on the numerator and is therefore construed as reflecting within-channel excitation (intracolumnar recurrent amplification). The exponent q doing the same on the denominator, it reflects within-channel suppression (feedforward or feedback inhibition). Under the alternate interpretation of Chapter 2's findings—decreased signal only at the high contrasts shown to the mask channel—a smaller p, larger q or both are expected after cTBS. The absence of such change in p or q would confirm the interpretation favored in Chapter 2 of decreased intercolumnar suppression after cTBS.

Ideally, both within- and between-channel effects would be accounted for in a single model. Equation [5.1] appears fit for that, but extrapolating Meese et al. (2007)'s fit to a higher-contrast cross-oriented mask (Figure C.2) failed to predict the suppression of low-contrast tests observed in Chapter 2 and by others (Huang & Chen, 2016). Adaptation of other models may more appropriately account for both within- and between-channel interactions (Baker et al., 2007; Kim et al., 2013; Said & Heeger, 2013).

In summary, the unique anatomy and functional organization of the occipital pole makes it particularly suited for individualized precision TMS of a well characterized patch of cortex. Advanced visual psychophysics empower a detailed non-invasive characterization of computational processes relying on different intracortical microcircuits within the cortical patch targeted by TMS. Brought to its full potential, the approach proposed in Chapter 2 and further

elaborated in this section has the potential to streamline the investigation of the microcircuit-level mechanism of NIBM and foster the principled design of novel brain therapies.

5.2 Interpreting Neurotransmitter MR Signals

By exploiting the spectral properties of the MR signal, MR spectroscopy promised the first MR measure with a direct biologically relevant interpretation—concentrations of specific chemicals. However, applied to the study neurotransmitter function, MR spectroscopy has yet to deliver. Indeed, although rapidly evolving, the field still suffers from poorly interpretable MR-derived neurotransmitter concentrations. This is due on one hand to complex subcellular compartmentation with different MR-visibility and multiple biological roles of neurotransmitters, and on the other hand to the lack of a coherent and empirically demonstrated understanding of how these factors relate to measured MR spectroscopy signals. In Chapter 1, I described the three main paradigms used for investigating neurotransmitters with MRS: (1) correlating baseline—constitutive—concentrations measured in a single sMRS session to interindividual differences in brain function, (2) tracking slow—hours to months—signal changes across mMRS sessions and (3) tracking fast—fraction of a second to minutes—neural activity-related fMRS changes. Drawing conclusions on neurotransmission from MR spectroscopy data requires to consider the various hypothetical and somewhat overlapping biophysical mechanisms at play at these different time scales.

5.2.1 Biocellular Determinants of MR GABA Signals Across Time Scales

On the slow end of the temporal spectrum, constitutive concentrations from sMRS protocols provide a snapshot of MR-visible neurotransmitters from all subcellular compartments, but mostly from the non-synaptic intra-cellular compartment (Section 1.4.2.1). Most of the detected neurotransmitters are therefore not readily available for activating neurotransmitter receptors—they either need to reach the synapse or the extracellular space to participate in respectively synaptic and non-synaptic transmission. In that context, MR neurotransmitter signals probably most accurately reflect the extent of the cellular machinery (e.g. neuron density) supporting the potential for neurotransmission, which would at best relate indirectly to actual neurotransmission. Given the shear number of functionally different but interrelated

circuits within a typically large MRS voxel, sMRS protocols are at high risk of uncovering epiphenomenal correlations.

As chemical synapses evolve during brain development and remain plastic in mature brains, so should their supporting cellular machinery—neural somata, synaptic terminals, astroglial processes, membrane transporters, and catabolic and anabolic enzymes. Indeed, to support a developmental or training-induced increase in e.g. GABA synapse density, one could expect the whole GABAergic system to scale up, with glutamic acid decarboxylase (GAD) activation (Chattopadhyaya et al., 2007) leading to net *de novo* GABA production and overall increased concentrations. Changes in largely MR-invisible synaptic neurotransmitters would therefore be indirectly detectable in mMRS protocols through corresponding changes in related MR-visible pools (Section 1.4.2.4). Note that the time scale of those MR changes would follow that of associated plastic changes or adaptations: days to months for axonal sprouting, hours for new synapse formation or silent synapse unmasking, tens of minutes for synaptic enlargement, and potentially less if neurotransmitters synthesized *de novo* simply overflow into the extracellular space (Caroni et al., 2012; Forrest et al., 2018).

Finally, the activity of chemical synapses may directly influence the MR-visibility of neurotransmitters, and therefore the measured MR signal. With relatively slow vesicular repackaging, increased synaptic release could push the neurotransmitter cycling dynamics to a new equilibrium that exhibits a smaller fraction of intravesicular—invisible—neurotransmitter. This compartment shift mechanism implies fMRS changes time-locked to synaptic activity in the millisecond range (Section 1.4.2.2).

Interestingly, the above mechanisms hypothesised to link MR neurotransmitter signals to neurotransmission likely overlap across sMRS, mMRS and fMRS. Indeed, a trait is necessarily the cumulation of a series of developmental and experience-dependent changes and, vice versa, adaptation and plasticity induce state changes that can become permanent. Compared to correlating traits across individuals, manipulating states—e.g. with specific training regiments, brain modulation treatments or, as in Chapter 3, sensorial regime modifications—appears as a more sound experimental strategy to investigate neurotransmission functions.

Indeed, only a subset of the many microcircuits sampled in an MRS voxel should be affected and the influence of unrelated circuits should subtract out, giving mMRS approaches superior specificity and robustness to epiphenomenological relations.

The more directly synaptic mechanisms underlying fMRS also potentially overlap with the plasticity-related mechanisms involved in mMRS. The perisynaptic astrocytic processes (PAP) that ensheath synapses and recycle neurotransmitters show high motility (Oliet et al., 2001; Rusakov & Stewart, 2021). For example, 24-hour of continuous single-whisker stimulation led to a more extensive astrocytic coverage of glutamatergic synapses and increased expression of astrocytic glutamate transporters that lasted 4 days (Genoud et al., 2006). Conversely, PAP retracted immediately and for at least 30min after a 2-min LTP-inducing whisker stimulation protocol, which was associated with increased synaptic spillover of glutamate to the extracellular space in hippocampal slice preparations (Henneberger et al., 2020). Interestingly, at some axon terminals lacking post-synaptic partners, neurotransmitters are not spilled over but directly released into the extracellular space in an activity-dependent fashion (Olah et al., 2007; Olah et al., 2009). Whether spilled over or directly released, these neurotransmitters slowly diffuse through the extracellular space to activate distant extrasynaptic receptors, supporting a non-synaptic form of neurotransmission coined ‘volume transmission’ (Agnati et al., 2010; Moroz et al., 2021; Vizi et al., 2010). By determining neurotransmitter spillover, PAP gates how much “wired transmission” at the synapse also contributes to volume transmission.

Consistent with the role of astrocytes in regulating excitatory and inhibitory synaptic plasticity (Bernardinelli et al., 2014; Heller & Rusakov, 2015; Kaczor & Mozrzymas, 2017; Rusakov & Stewart, 2021; Sipe et al., 2021), information processing (Nagai et al., 2021; Perea et al., 2014) and the EI balance (Sears & Hewett, 2021), leaky synapses can have profound consequences on neural circuits through heterosynaptic activation (Zhang & Sulzer, 2003) and through the activation of extrasynaptic glutamate (Best et al., 2005; Chalifoux & Carter, 2011b; Chokshi et al., 2019; Hires et al., 2008; Oliet et al., 2001; Zhang & Sulzer, 2003) and GABA receptors (Dittman & Regehr, 1997; Semyanov et al., 2004; Wang et al., 2019; Wang & Maffei, 2014). Interestingly, astrocytic process motility could impact both mMRS and fMRS signals as their retraction can be expected to both (1) produce a stable leak from the MR-invisible

presynaptic compartment and (2) amplify the temporary compartment shift associated with increased synaptic activity.

Equipped with the above-described interpretational framework, below I deepen the discussion of Chapter 3's findings in the light of further modeling work.

5.2.2 Modeling the Binocular Rivalry Dynamics to Better Interpret Related MR GABA Signals

The challenge of interpreting MR neurotransmitter signals is double. On one hand, firm neurotransmission-related conclusions can hardly be made given the many and poorly studied biophysical mechanisms described above and in Chapter 1. On the other hand, even if the neurotransmission aspect is resolved, microcircuit-level questions remain: Which inhibitory circuits are involved? and how are they affecting downstream circuits? Otherwise said, little can be said from MR neurotransmitter signals alone.

Meaningful interpretation of MR neurotransmitter findings requires narrow constraints. For Chapter 3, the mMRS paradigm restricted the set of possibly involved microcircuits to those possibly affected by the plasticity manipulation. This was not sufficient to deliver an interpretation of MR neurotransmitter findings beyond face validity: GABA were tentatively associated to monocular percept duration during binocular rivalry with no mechanistic explanation. Further constraints can however come from good prior knowledge of related neural dynamics, ideally embodied in a formal model. Luckily, binocular rivalry is a heavily studied phenomenon for which relatively consensual dynamic models exists (Brascamp et al., 2015; Devia et al., 2022). Below I therefore attempt to deepen the interpretation of Chapter 3 findings by casting them into the simplest yet powerful instance of those models (Figure 5.5A). In a nutshell, possibly GABA-related mechanisms are identified from the model's structure and then manipulated *in silico* (Figure 5.5B). From the model's behavior, clear predictions are made and challenged against available data (Figure 5.5C), leading to a now mechanistic and hopefully less equivocal interpretation, or at least new and clear testable predictions. Simulations were performed as part of a class work reported in full in Annex B.

5.2.2.1 Selected Model

The chosen model (Figure 5.5A), by Noest et al. (2007), implements the key ingredients common to most models proposed to date (Brascamp et al., 2015; Devia et al., 2022) for simulating the rivalry dynamics (Figure 5.5B, Model Time Course). At its core are two mutually inhibiting (γ connections in Figure 5.5A) monocular neural representations (X units in Figure 5.5A), each independently driven by constant inputs (I connections in Figure 5.5A) from their corresponding eye. High activity levels in both representations ($\mathrm{X_L} \approx \mathrm{X_R}$; diagonal in Figure 5.5B, Model Phase Space) constitute an unstable state of the system. The slightest activity imbalance allows one representation to suppress the other and establish perceptual dominance—the $\mathrm{X_L} >> \mathrm{X_R}$ or $\mathrm{X_L} << \mathrm{X_R}$ attractor states (Pastukhov et al., 2013) in Figure 5.5B, Model Phase Space. Dominance is limited to few seconds (percept duration in Figure 5.5B, Model Time Course) by slow activity-dependent adaptation (α connections in Figure 5.5A)—activity of the dominant representation gradually tapers off, relieving suppression on the dominated representation. When nearing balanced activity across the two representations again, the system eventually swings rapidly toward dominance of the previously dominated representation (Figure 5.5B, Model Time Course). The cycle then repeats and the model alternates between dominance states, the hallmark of binocular rivalry (Brascamp et al., 2015; Levelt, 1966).

How can such model provide insight into the actual rivalry phenomenon? The best example lies in van Loon et al. (2013)'s inspirational work leveraging Noest et al. (2007)'s model to test the long-hypothesized role of interocular inhibition in rivalry dynamics. They observed that *in silico* manipulations of the strength of mutual inhibition (γ_L and γ_R in Figure 5.5A) impacted dominance durations in numerical simulations (Figure 5.5B, Model Time Course panel)—stronger mutual inhibition allowed a representation to maintain its dominance for longer periods (Figure 5.5C, left section, *in silico* in gray). Importantly, *in vivo* observations (Figure 5.5C, left section, *in vivo* in dark) concurred: in sMRS protocols, high occipital MR GABA signals also related to longer dominance durations (Ip et al., 2021; Robertson et al., 2016; van Loon et al., 2013) (but see Brascamp et al., 2018; Sandberg et al., 2016). By linking dominance durations to both interocular inhibition *in silico* and GABA concentrations *in vivo*, van Loon et al. (2013)

interestingly but indirectly linked MR GABA signals to a specific synaptic inhibitory process. As discussed above, this synaptic interpretation of an sMRS finding is susceptible to confounds, but it here finds support in further experiments where pharmacological activation of inotropic $GABA_A$ (Mentch et al., 2019; van Loon et al., 2013) or metabotropic $GABA_B$ (Mentch et al., 2019) receptors had consistent effects on the rivalry dynamics.

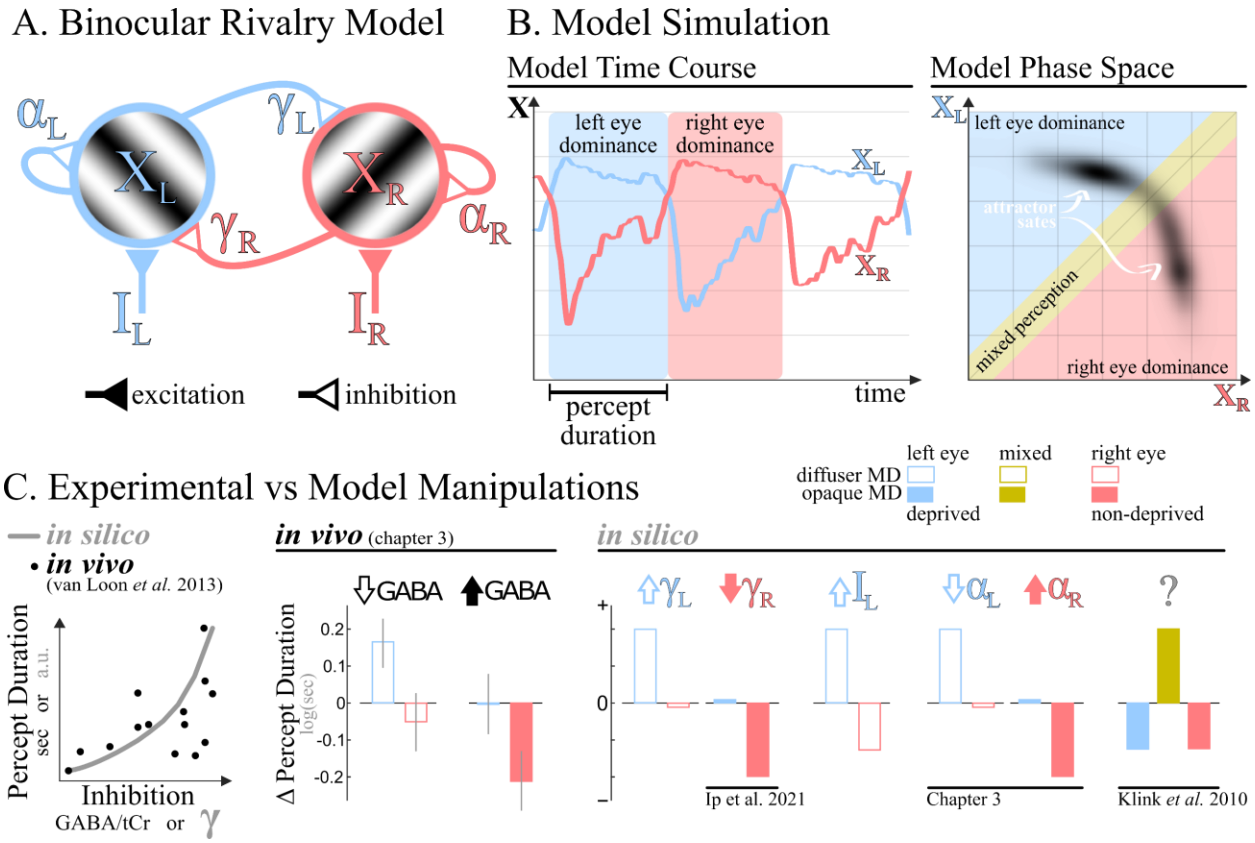

Figure 5.5 Manipulation of *in silico* rivalry dynamics and comparison to *in vivo* binocular rivalry findings. A. Two units (circles) model the activity (X) of neurons tuned to incompatible stimuli (gratings) presented as constant input (I) to the left (L) and right (R) eyes. The units inhibit each other with gain γ. They also self adapt with gain α on a two-orders-of-magnitude slower time scale. **B.** Example numerical simulation of the dynamic model. The system alternates between two attractor states corresponding to dominance of one or the other unit. These dominance states are characterized by their duration. A dominance state corresponds to the percept from one eye, while transition periods would correspond to the perception of a binocular mixture of the two stimuli. **C.** The 1st section from the left shows the relation between mutual inhibition and percept duration, as observed *in silico* from symmetrical modulations of γ and *in vivo* from occipital GABA measurements with MRS. The 2nd section summarizes Chapter 3 *in vivo* findings. The 3rd section shows attempts at recapitulating *in vivo* findings (Ip et al. (2021) and Chapter 3) with selected *in silico* manipulations (arrows). The last panel illustrate the need for a model that would also account for changes in mixed perception.

5.2.2.2 In Silico Manipulations

All simulations are available online (Proulx, 2022) and described in detail in Annex B. Here we are looking for those that can recapitulate key features of the *vivo* manipulations and

observations (Figure 5.5C, *in vivo* section and Chapter 3). These key features go as follow. (1) The *in silico* manipulations should reflect the asymmetric nature of the *in vivo* MD manipulation. (2) Given that eye-specific changes are dissociable *in vivo*—specific to deprived eye dominance durations after diffuser MD but to non-deprived-eye durations after opaque MD—*in silico* manipulations should also be able to leave one of the two eyes unaffected. (3) The effect of two *in silico* manipulations on dominance durations should together match *in vivo* observations, and the manipulations themselves should be reasonably interpretable as underlying the observed MR GABA signal changes.

Let's first address the most obvious hypothesis that MD affects the strength of interocular inhibition (Chadnova et al., 2017; Han et al., 2020; Kim et al., 2017; Wang et al., 2020). For that I strengthened interocular inhibition *in silico* as in van Loon et al. (2013), but only from the left to the right eye (γ_L in Figure 5.5A). Conversely in a second simulation, I weakened inhibition in the other direction (γ_R). Comparing *in silico* results (Figure 5.5C, 1st and 2nd panels of *in silico* section) to *in vivo* observations (Figure 5.5C, *in vivo* section) reveals that—presuming γ can be assimilated to the MR GABA signal—the two patterns are the reverse of one another. A MD mechanism based on altered interocular inhibition is therefore incompatible with available data.

A side note unrelated to MD should be made here concerning an interesting hybrid sMRS-fMRS dataset by Ip et al. (2021). Early visual cortex MR GABA signals were measured during monocular stimulation of either eye or with both eyes closed (fMRS) and compared to interindividual differences in binocular rivalry measures of SED (sMRS). Larger SED imbalances related to lower early visual cortex MR GABA signals, but only during non-dominant-eye stimulation. The authors' interpretation of a failure of interocular inhibition from the non-dominant-eye is compatible with the *in silico* reduction of γ_R in Figure 5.5C, 2nd panels of *in silico* section. This interestingly suggests that monocular stimulation may, through the compartment shift mechanism, unmask MR GABA signals from active interocular-inhibition-mediating synapses. Otherwise said, the specificity of sMRS paradigms may be increased simply by performing neurotransmitter measurements during tasks that activate the brain function under investigation.

Let's now come back to another mechanism proposed for MD: monocular gain modulations (Atallah et al., 2012; Ferguson & Cardin, 2020; Han et al., 2020; Lunghi et al., 2011; Wilson et al., 2012). Strengthening—increasing the gain of—inputs from the left eye (I_L in Figure 5.5A) lengthened left eye dominances together with a reciprocally shortening of right eye dominances (Figure 5.5C, *in silico* section, 3rd panel), violating the requirement of dissociable eye-specific effects. Monocular gain mechanisms are also ruled out under the chosen model.

The remaining candidate mechanism concerns activity-dependent adaptation. Unilaterally modulating its gain (α_L or α_R connections in Figure 5.5A) did produce dissociable eye-specific effects: strengthening or weakening adaptation in one eye respectively lengthened or shortened its own dominance. Importantly, these *in silico* manipulations could fully recapitulate the *in vivo* pattern *if* MR GABA signals can be likened to activity-dependent adaptation—in Figure 5.5C, compare *in vivo* section -vs- 4th and 5th panels of *in silico* section.

In summary, under Noest et al. (2007)'s model, available human data are compatible with synaptic interocular inhibition underlying MR GABA signals in sMRS (van Loon et al., 2013) and fMRS (Ip et al., 2021) protocols. This is however not the case for MR GABA signals from Lunghi et al. (2015)'s and Chapter 3's mMRS protocols. My *in silico* experiments instead highlight the intriguing possibility that MD-related MR GABA signal modulations relate to fast activity-dependent neural adaptation dynamics, an original hypothesis further discussed below.

5.2.3 Fast and Slow GABA-Related Adaptation During Binocular Rivalry and Monocular Deprivation

Neurons are continuously adjusting their sensitivity according to their synaptic drive and fire rate history (Adibi & Lampl, 2021; Kohn, 2007; Weber et al., 2019; Whitmire & Stanley, 2016). This computation is caried by various mechanisms operating across a continuum of time scales. At the shorter time scale of the binocular rivalry dynamics, adaptation builds-up with activity within the perceptually dominant neural units (Section 5.2.2.1)(Alais et al., 2010)—a phenomenon likened to fast contrast adaptation, where exposure to luminance contrast for seconds to minutes reduces sensitivity within the channel of the adaptor stimulus also for seconds to minutes (Kohn, 2007; Weber et al., 2019; Whitmire & Stanley, 2016). Indeed,

moving rivaling stimuli across the visual field to recruit fresh unadapted brain tissue lengthens perceptual dominance, while traversing a preadapted location triggers dominance switch (Blake et al., 2003).

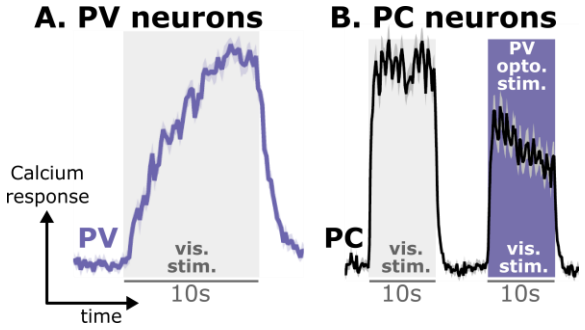

Figure 5.6 Example involvement of GABA inhibition in fast circuit-level adaptation. A. The calcium response of PV interneurons in the rodent EVC, showed a facilitating type of fast adaptation during visual stimulation. **B.** PC neurons showed both facilitating and depressing types of adaptation (not shown) which averaged to a stable population response during visual stimulation (left half of the trace). Optogenetic activation of PV neurons however biased the adaptation of PCs toward the depressing type (right half of the trace), suggesting inheritance of adaptation patterns from PV to PC. *Reproduced with permission from Heintz et al. (2020)*

Interestingly, inhibitory microcircuits have recently been identified to underly contrast adaptation of PC responses (Chen et al., 2015; Hamm & Yuste, 2016; Heintz et al., 2020; Keller & Martin, 2015; Natan et al., 2015; Natan et al., 2017). For example, V1 PV interneurons showed a paradoxical facilitating type of adaptation (Figure 5.6A)—their calcium responses ramped up over a 10-s visual stimulation periods (Heintz et al., 2020; Keller & Martin, 2015). Importantly, PC responses appeared to inherit their adaptation pattern from inhibitory interneurons (Heintz et al., 2020). Indeed, optogenetic overactivation of PVs increased PCs' expression of depressing adaptation (Figure 5.6B), consistent with similar manipulations in the auditory cortex (Natan et al., 2015; Natan et al., 2017). Central to most recent mechanistic accounts of circuit-level cortical adaptation (Ross & Hamm, 2020; Schulz et al., 2021; Seay et al., 2020; Solomon & Kohn, 2014; Whitmire & Stanley, 2016), rapid modulations of GABAergic inhibition are likely to also underly the adaptation dynamics involved during rivalry.

Equally interesting is a few lines of evidence suggesting that fast GABA-mediated cortical adaptation may specifically operate through volume transmission, a phenomenon to which MR neurotransmitter signals should be particularly sensitive to (Section 5.2.1). For one, cortical adaptation was repeatedly shown to not depend on the function of the mostly synaptic $GABA_A$ receptor (Debruyn & Bonds, 1986; Heistek et al., 2010; Kuravi & Vogels, 2018; McLean & Palmer, 1996; Rosburg et al., 2004; Vidyasagar, 1990). This suggests that GABA-mediated adaptation instead relies on exclusively extrasynaptic—volume transmission activated (Del Arco

et al., 2003; Scanziani, 2000)—$GABA_B$ receptors, which were indeed associated with adaptation outside the cortex (Binns & Salt, 1997; Stange et al., 2013; Yang et al., 2003) and surprisingly only ever tested on three cells in the cortex (McLean & Palmer, 1996). Also, $GABA_B$ receptors are involved in various forms of synaptic and post-synaptic forms of plasticity that are compatible with depressing adaptation (Chalifoux & Carter, 2011a), including LTD of excitatory synapses (Jia et al., 2004; Wang & Maffei, 2014), LTP of inhibitory synapses (Wang & Maffei, 2014) and inhibition of dendritic calcium spikes (Perez-Garci et al., 2013). Finally, microdialysate in the hippocampus directly linked extrasynaptic GABA concentrations to depressing adaptation of auditory evoked potentials (Garcia-Garcia et al., 2020).

Now, can GABA-volume-transmission-mediated adaptation during binocular rivalry be linked to MR GABA signals? In theory yes, MR GABA signals would—at the columnar scale—track PV to PC synaptic activity through the synaptically leaked and MR visible GABA, producing fMRS-like modulations time-locked to the perceptual dominance of one eye. In practice however, these modulations would cancel out across unresolved ocular dominance columns in an MR spectroscopy voxel, as the same phenomenon will happen in antiphase in each eye. Intercolumnar inhibition could also lead to fMRS signals as in Ip et al. (2021), but here again antiphase time courses across ocular columns would cancel each other.

Could MD induce slower, perhaps structural adaptations that would both (1) affect MR GABA signals in a measurable way and (2) impact GABA-mediated adaptation? We have seen in Section 5.2.1 that different brain plasticity protocols can alter the ensheathing of synapses by astrocytic processes and consequently modulate synaptic spillover, which should affect the MR visibility of neurotransmitters. Here I would tentatively propose that PAP motility can underly MD-related modulations of MR GABA signals and binocular rivalry dynamics as observed in Chapter 3. Under this scenario, the PAP coverage of GABA synapses on deprived-eye PCs—putatively originating from PV interneurons—would tighten after diffuser MD. Reduced synaptic spillover would keep more GABA in the MR-invisible compartment, supporting the observed MR GABA signal reductions. Reduced synaptic spillover would also reduce $GABA_B$-dependent adaptation of perceptually dominant representations and, according to binocular rivalry simulations (Section 5.2.2.2), underly the observed lengthening of deprived-eye percepts

only. Opaque MD would do the reverse: PAP would retract from GABA synapses on the non-deprived-eye PCs and GABA spillover would increase, which would consequently increase both GABA MR visibility and activity-dependent adaptation, ultimately shortening the duration of non-deprived-eye percepts. The above view finds some support in Wang and Maffei (2014), who showed a $GABA_B$-dependent type of LTP at PV-to-PC synapses that appeared to saturate in the cortex of monocularly deprived (eye lid sutured) rats.

Finally, although mostly based on conjectural evidence, the above speculation could bridge the explanatory gap in Chapter 3 between mMRS findings and their related behavioral consequences. At the same time, it offers an interesting new perspective on the interpretation MR neurotransmitter signals, one that emphasizes volume transmission.

5.2.4 Limitations and Predictions

An important limitation of this interpretational framework centered on volume transmission is that it is built on hypothesized roles for fast GABA-dependent adaptation dynamics. Past work did linked rapid depressing adaptation to both dominance durations in binocular rivalry (Alais et al., 2010; Blake et al., 2003) and the inhibitory action of GABA (Chen et al., 2015; Hamm & Yuste, 2016; Heintz et al., 2020; Keller & Martin, 2015; Natan et al., 2015; Natan et al., 2017), and the plasticity induced by MD can reasonably be understood as a medium-term—hours—adaptation phenomenon that is likely to interact with faster—seconds to minutes—adaptation mechanisms (Adibi & Lampl, 2021; Bao & Engel, 2012; Bao et al., 2013; Weber et al., 2019). This three-way conjecture is however solely based on simulations performed on a single, likely oversimplified model of binocular rivalry (Section 5.2.2). Indeed, a large body of literature involves a much richer phenomenology and associated brain mechanisms not addressed in Noest et al. (2007)'s model, including eye-independent rivalry (Kovacs et al., 1996; Logothetis et al., 1996), deepening multi-level rivalry (Freeman, 2005; Nguyen et al., 2003; Wilson, 2003), cognitive influences (Dieter & Tadin, 2011; Hohwy et al., 2008; Tong et al., 2006) and subcortical and cortical network dynamics (Baker et al., 2015; Bock et al., 2019; Buckthought et al., 2011; Song et al., 2021; Wunderlich et al., 2005). It is therefore conceivable that the *in silico* behavior of a more comprehensive computational model could instead indicate e.g. interocular inhibition mechanisms as best accounting for *in vivo* findings.

Another important aspect of binocular rivalry neglected in Noest et al. (2007)'s model is the complex spatiotemporal dynamics unfolding across the stimulated visual field (Blake, 1989; Blake et al., 1992; Kang et al., 2010; Oshea et al., 1997), where incomplete dominance often allows the otherwise rivaling stimuli to binocularly combine and produce the perception of an overlay (Blake, 1989; Hupe et al., 2019; Skerswetat et al., 2016, 2018). Such periods of binocularly combined perception may bear previously unsuspected importance given the striking patch-type specificity of their relation to non-deprived-eye percepts (Figure 3.1J). The model of Riesen et al. (2019)—elegantly casting binocularly combined perception as a third attractor sate that itself rivals with the two monocular states—would be worthwhile experimenting with *in silico*. Equally interesting are models by Said and Heeger (2013) or Rideaux and Welchman (2018) where mutual inhibition is driven by interocular conflict detector neurons (Katyal et al., 2016) which themselves can adapt (Kingdom et al., 2018), thereby momentarily giving way to binocularly combined perception. More importantly, any future MD experiment should strive to record binocular percepts during rivalry—this was not done in Lunghi et al. (2015)' mMRS experiment and neither in ours.

At the same time binocular combination may not be causally related to monocular dominance—the correlation between the two disappeared in the later sessions of our weekly repetition of the MD treatment (Supplementary Figure 3.2) and several protocols were able to modulate binocular combination during rivalry without biasing monocular dominance to one eye or the other (Abuleil et al., 2021; Cao et al., 2016; Hollins & Hudnell, 1980; Klink et al., 2010; Proulx, 2020; Said & Heeger, 2013). This led us to predict in Chapter 3 that alternating the patched eye every minute or so during MD would both potentiate binocular combination during rivalry—as preliminary data suggested (Proulx, 2020)—and proportionally reduce V1 MR GABA signals.

Finally, the hypothesis of a GABA-volume-transmission-mediated fast adaptation for bridging the explanatory gap of Chapter 3 leads to other clear testable predictions. The most important and easily testable would be that hours of diffuser MD should reduce fast sensory adaptation of evoked responses and perception from the deprived eye, while opaque MD will have the reverse effect on the non-deprived eye. Relying on modulations of GABA volume transmission,

both effects should relate to modulations of V1 MR GABA signal changes. Finally, increased PAP motility should be observed in association with animal models of MD, though extracellular GABA may not necessarily be spilled from synapses and could instead be non-synaptically released by the axon terminal varicosities from neurogliaform neurons (Olah et al., 2007; Olah et al., 2009) or transporter reversal (Wu et al., 2007).

5.3 Computationally Relevant Hemodynamic Signals

In Chapter 1, I reviewed current understandings of the main non-invasive fMRI signals: BOLD, CBF, CBV and—derived from the first three—$CMRO_2$. Neural activity influences these signals through two related but independent mechanism: (1) neurovascular coupling, where various multicellular signalling pathways within the neurovascular unit transmit feedforward signals from active neurons to contractile mural cells, which physically control blood vessel diameters and measurably affect blood volume and flow, and (2) neurometabolic coupling, where the oxidative metabolism required by neural membrane computations draws oxygen from the blood, measurably altering its magnetic and optical properties. Importantly, both neurovascular and neurometabolic coupling exhibit cell-type specificity (Buxton, 2021; Howarth et al., 2021; Iadecola, 2017; Lourenco & Laranjinha, 2021; Schaeffer & Iadecola, 2021). This latter property complicates quantitative estimations of neural activity from fMRI signals, but it could at the same time empower more meaningful interpretations of "brain activations"—away from vaguely defined levels of neurometabolic activity and closer to computationally relevant interactions between a voxel's subpopulations of neurons. Chapter 4 contributed to pioneering work (Buxton, 2021; Buxton et al., 2014; Havlicek, Ivanov, Roebroeck, et al., 2017; Havlicek et al., 2015; Uhlirova, Kılıç, Tian, Sakadžić, et al., 2016) by demonstrating that information on the nature of a voxel's activation can be extracted from the BOLD signal alone, specifically from its response delay. Here I will discuss the potential of this approach to inform on a cardinal feature of neural activations, the excitation-inhibition balance.

Our approach, as those of Havlicek, Ivanov, Roebroeck, et al. (2017) and Buxton et al. (2014), relies on the following logic. Within an fMRI voxel, different types of neurons—with different connectivity and neurotransmission mode—flexibly assemble into various functional

microcircuits for performing specific computational tasks. For example, both visual stimulation and mental imagery involve the early visual cortex (Kosslyn et al., 1999; Pearson et al., 2015) but most certainly recruit local microcircuits differently—e.g. through a thalamocortical drive for the former and feedback signals for the latter. With different cell types driving hemodynamics through different mechanisms, different fMRI patterns—in space, in time and across measurable biophysiological signals—can potentially be related to different local computations. Discriminating such patterns is useful for dissociating computations (Chapter 4), but more relevant information would be obtained if—through appropriate knowledge of cell-type-specific hemodynamics—these fMRI patterns could be mapped to the activation of specific microcircuits. Such knowledge is building up (Anenberg et al., 2015; Dahlqvist et al., 2020; Echagarruga et al., 2020; Krawchuk et al., 2020; Lee et al., 2010; Lee et al., 2021; Lee et al., 2020; Moon et al., 2021; Poplawsky et al., 2021; Uhlirova, Kılıç, Tian, Thunemann, et al., 2016; Urban et al., 2012; Vazquez et al., 2018) and has the potential to unlock a new age of non-invasive investigation of computationally relevant human brain processes.

5.3.1 Neurovascular and Neurometabolic Coupling: Toward Computationally Relevant fMRI Patterns

Recent advances are most remarkably revealing a dissociation, or at best a loose connection between the neural processes engaging the largest energy expenditure and those exerting the strongest influence on blood supplies (Buxton, 2021; Howarth et al., 2021). The ion flow that enacts glutamatergic excitation is the costliest process (Howarth et al., 2012) as it requires the continuous replenishment of large transmembrane ionic gradients; and indeed, the neurovascular unit appears responsive to related metabolic feedback signals such as K^+ ions concentrations and by-products of energy metabolism like adenosine (Ido et al., 2004; Raichle & Mintun, 2006). However, glutamate release also triggers vasodilation more directly—in a feedforward fashion—through transcellular signaling pathways involving various diffusible arachidonic acid metabolites (AAM), which can mediate up to 80% of the vasodilation response (Nippert et al., 2018) (Figure 5.7).

Even more striking is the strong influence of GABAergic interneurons on vascular responses despite their comparatively small energy requirements—GABA receptor activation has little

effect on ionic gradients due to a near equilibrium reversal potential, and consequently represents only ⅙ of neuronal glucose consumption (Duarte & Gruetter, 2013). Indeed, interneuron axons can directly target vessels (Cauli et al., 2004; Takado et al., 2022; Tricoire & Vitalis, 2012) and optogenetic activation of GABAergic neurons alone can produce large vascular responses that easily reach the magnitude of sensory-driven responses (Anenberg et al., 2015; Uhlirova, Kılıç, Tian, Thunemann, et al., 2016; Vazquez et al., 2018). This neurovascular coupling largely do not require glutamate and GABA neurotransmission (Anenberg et al., 2015; Dahlqvist et al., 2020; Poplawsky et al., 2021; Vazquez et al., 2018) and instead relies on NO (Echagarruga et al., 2020; Krawchuk et al., 2020; Lee et al., 2020). This potent diffusible vasodilator is synthesized by nNOS, an enzyme specifically expressed by ~20% of cortical interneurons (Lourenco & Laranjinha, 2021; Tricoire & Vitalis, 2012). Blocking nNOS reduces vascular responses by ⅔ (Hosford & Gourine, 2019). Most remarkably and in contrast to pyramidal neurons, vascular responses driven by optogenetic activation of interneurons are accompanied by little or negative electrophysiological changes (Echagarruga et al., 2020; Lee et al., 2020). Together, the above properties interestingly place inhibitory circuits in a position to anticipate neurometabolic needs, and to both limit demand and ensure supply respectively by limiting the amplification of excitatory activity and sending dedicated feedforward vasodilatory signals to nearby blood vessels (Buxton et al., 2014; Lourenco & Laranjinha, 2021).

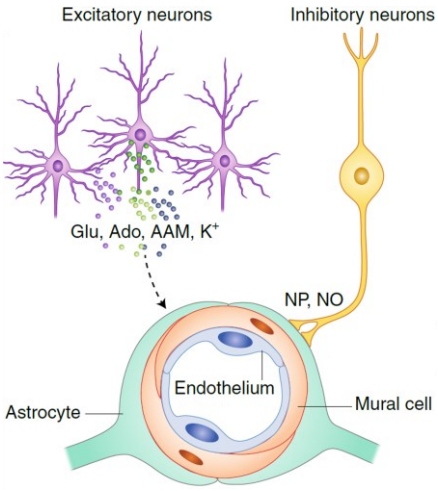

Figure 5.7 Cell-type-specific neurovascular signaling pathways. *Glu: glutamate, Ado: adenosine, AAM: arachidonic acid metabolites, K^+: potassium ion, NP: neuropeptide, NO: nitric oxide. Reproduced with permission from Schaeffer and Iadecola (2021).*

Finally, subtypes of interneuron can also trigger vasoconstriction through vasoactive neuropeptides like NPY and SOM (Cauli & Hamel, 2010; Cauli et al., 2004). Optogenetic studies are revealing that specific interneurons trigger a rich repertoire spatiotemporal patterns of dilation and constriction (Lee et al., 2010; Lee et al., 2020; Moon et al., 2021; Uhlirova, Kılıç,

Tian, Thunemann, et al., 2016), interestingly suggesting that inhibitory circuits shape hemodynamics just as much as they shape neural activity patterns (Isaacson & Scanziani, 2011).

Now, can the above recent progresses actually help linking fMRI patterns to specific microcircuit activity patterns? Optogenetically driving specific neuron types did show dissociated vascular and metabolic responses (Dahlqvist et al., 2020; Lee et al., 2021; Vazquez et al., 2018), consistent with Buxton et al. (2014)'s view that vascular responses are driven by both excitatory and inhibitory neurons while metabolic responses chiefly result from the activity of excitatory neurons (Section 1.4.3.3). So, yes, estimating both the vascular and metabolic response may allow relevant characterization of the underlying neural activation, with grounds for interpreting the ratio as reflecting the EI balance. On the other hand, while the complexity of neurovascular signaling pathways clearly supports a rich diversity of spatiotemporal dilation and constriction responses, consistent relations to specific neural motifs have yet to emerge. The use of vasoactive anesthetics (C. Chen et al., 2021; Lee et al., 2021) and potentially area-specific microcircuit effects (Moon et al., 2021) are likely muddying the waters. For example, optogenetic activation of PV neurons under 1.5% isoflurane increased blood volumes but decreased it awake animals (Lee et al., 2021). Not to mention that the latter effect likely resulted from PV neurons suppressing the activity of connected neurons rather than directly signaling to vessels, highlighting the challenge of isolating the behavior of deeply interconnected neurons. Moreover, the ecological validity of strong synchronous optogenetic activation is limited as the genetic markers used show limited correspondence to functional circuits (Tremblay et al., 2016). So, for interpreting fMRI spatiotemporal patterns, the answer is no, the current understanding of neurovascular coupling mechanisms remains of limited use. More helpful would be experiments aiming at slightly perturbing functionally relevant neural dynamics in awake animals. For example, weakly upregulating optogenetically targeted neural populations could influence the processing of sensorial stimuli within physiological limits and consequently better reveal signature hemodynamic perturbations. I propose that such an approach is the most likely to establish mechanistic links for interpretating spatiotemporal fMRI patterns in terms of computationally relevant neural processes.

5.3.2 Subvoxel Summation of Negative and Positive BOLD responses: A Working Model

Chapter 4 discussed the two lines of evidence relating the observed BOLD delay to functional inhibition. The first one relies on the inhibitory mechanisms expected to support task- or stimulus-related processing: normalization at higher sensory stimulus energy (J. E. Chen et al., 2021; but see Thompson et al., 2014), intercolumnar inhibition with stimulus overlays (Bartolo et al., 2011; Farivar et al., 2011) and inhibitory control of motor responses (Peck et al., 2001). In all these, increased inhibition produced longer BOLD delays. The second line arises from sMRS data, where higher EVC GABA concentrations related to longer BOLD delays across participants (Donahue et al., 2010; Muthukumaraswamy et al., 2009; Muthukumaraswamy et al., 2012).

A third line of evidence however relates to the interesting mechanistic model proposed by Farivar et al. (2011), where inhibition and excitation respectively drive negative BOLD (negBOLD) and *slightly delayed* positive BOLD (posBOLD) response components, which sum within a voxel—the subvoxel summation model (Figure 5.8). Indeed, negBOLD responses were associated with suppressed neural activity (Boorman et al., 2015; Boorman et al., 2010; Devor et al., 2007; Harel et al., 2002; Kastrup et al., 2008; Shmuel et al., 2006) and suppressed perceptual performances (Blankenburg et al., 2003; Kastrup et al., 2008), and to larger concentrations of GABA in an sMRS protocol (Northoff et al., 2007). Moreover, negBOLD may

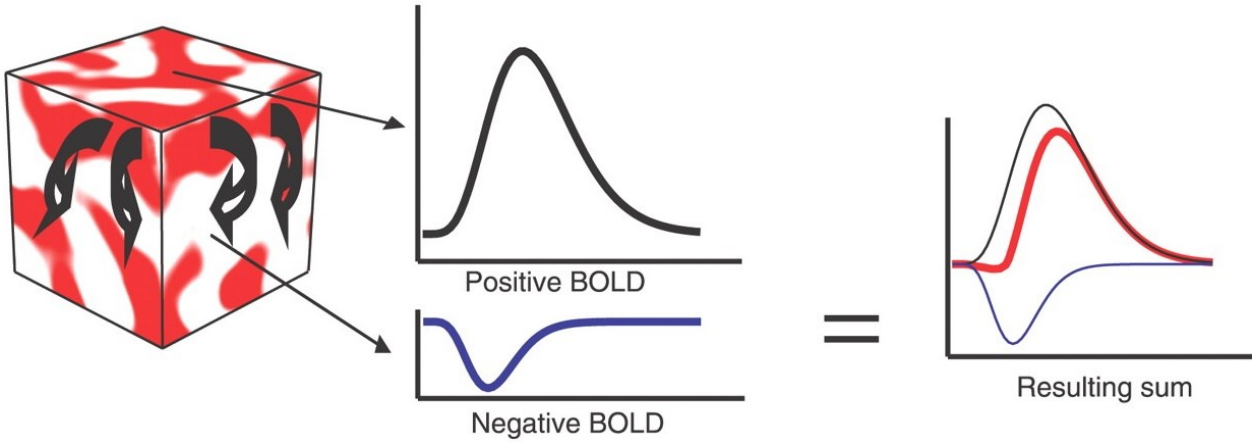

Figure 5.8 Subvoxel summation model of for an inhibition-related BOLD delay. Spatial domains within a voxel (left) are hypothesized to separately drive positive and negative BOLD response components (middle) that sum to give the measured response (right). Given a slightly shorter delay for the negative component, a larger—presumably inhibition-related—negative component translates into a longer delay for the voxel's response. *From Farivar et al. (2011)*

stem from PV interneuron inhibition, as PV optogenetic activation did produce large negative CBV, CBF and $CMRO_2$ responses (Lee et al., 2021).

Measuring BOLD in and around the retinotopic representation of visual stimuli, Shmuel et al. (2006) did observe the specific timing of posBOLD and negBOLD responses predicted by the subvoxel summation model (Figure 5.9). However, visual inspection of time courses reported by others suggests they can sum in ways that either (1) support the proposed relation between inhibition and BOLD delay (Bressler et al., 2007; Goense et al., 2012; Huber et al., 2014), (2) support the relation but through features related to response offset rather than onset (Kastrup

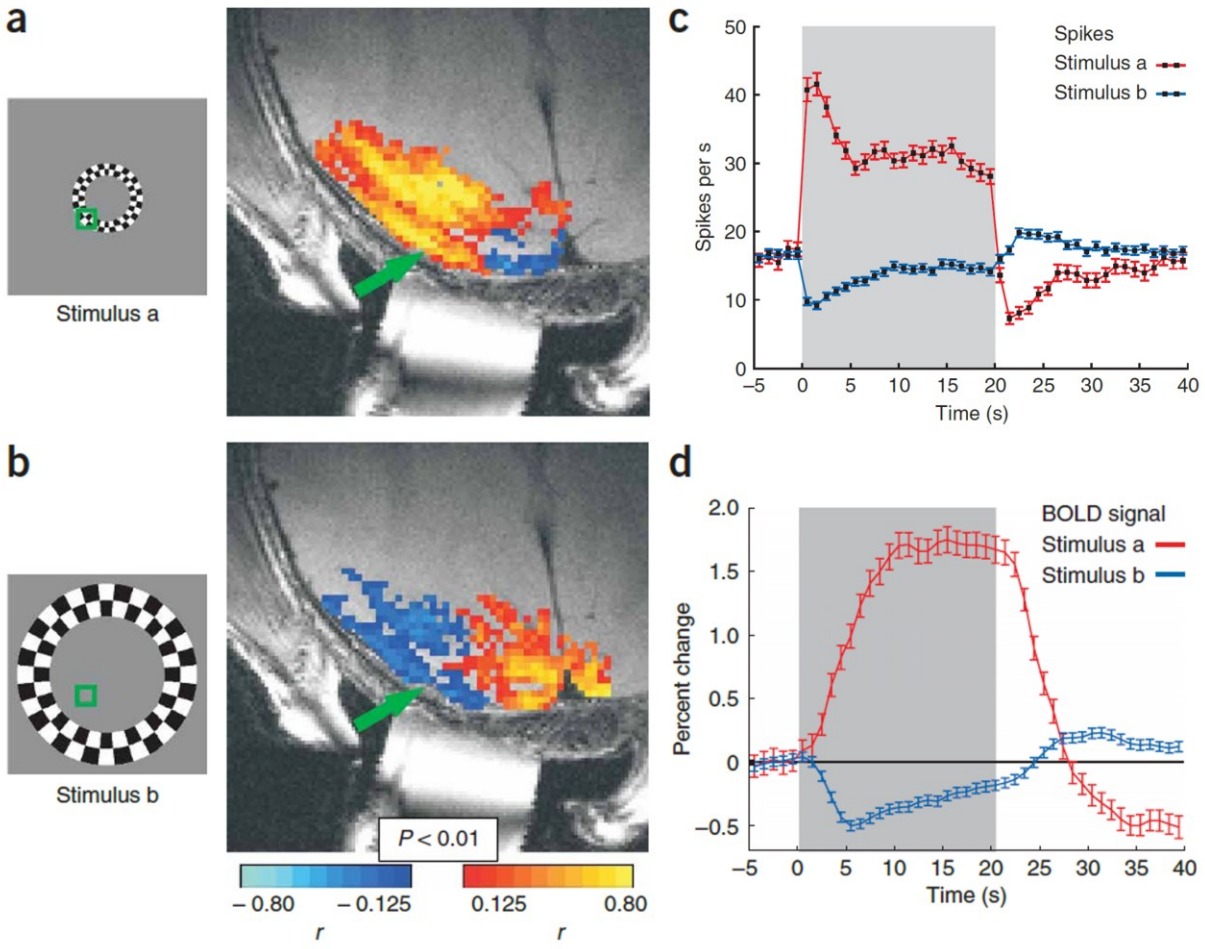

Figure 5.9 Positive and negative BOLD responses. A. Stimulus *a* evoked a positive BOLD response in a cortical patch of the anaesthetized monkey visual cortex (green arrow) representing a stimulated portion of the visual field (green square). **B.** Another stimulus *b* over a neighboring section of the visual field produced a negative response in the same cortical patch (green arrow and square). **C.** Spiking activity within the cortical patch showed a similar pattern of stimulus-dependant activation and deactivation, the time course of which were the mirror image of one another. **D.** The time courses of the stimulus-dependent positive and negative BOLD responses were also similar, but note the earlier peaking time of the negative response. *Modified with permission from Shmuel et al. (2006)*

et al., 2008; Shmuel et al., 2002), (3) support no relation (Boorman et al., 2010) or (4) support the reverse relation (Boorman et al., 2015; Devor et al., 2007; Stefanovic et al., 2004). However, purely vascular factors may have confounded the comparison of posBOLD and negBOLD time courses since they were estimated from different patches of cortical tissue—interestingly, only Shmuel et al. (2006) compared posBOLD and negBOLD recorded from the same tissue (Figure 5.9).

Although the time course and even the number of hemodynamic components is unclear, the subvoxel summation model remains a useful framework for predicting the impact cell-type-specific drivers of hemodynamics could have on fMRI signals. The most useful insights will probably come from studies—like that of (Moon et al., 2021)—striving to characterize, through a deconvolution approach, the multiple hemodynamic components involved during activation of even a single neuron type. At term, it may be possible to identify a set of neural computations, carried by canonical circuit motifs, that translates into specific hemodynamic patterns which—after accounting for vascular distortions—could be reliably identified from non-invasive fMRI signals. Alas, non-invasive brain imaging may inform on truly relevant aspects of neural activity.

5.3.3 Limitations and Predictions

A major limitation in demonstrating that BOLD signals contain cell-type-specific information lies in the space-time inseparability of the highly complex fluid dynamics that govern the flow of blood in networks of vessels. Indeed, the vast majority of analytical approaches to fMRI signals, including ours, wrongly assume space-time separable processes (Aquino et al., 2014; Biessmann et al., 2012; Kriegeskorte et al., 2010)—BOLD responses measured in and outside a hypothetically single activated cortical column are not merely scaled versions of a single temporal kernel and, vice versa, the spatial pattern is changing over time into a response (Kriegeskorte et al., 2010). Hemodynamic signals instead follow the vascular network they arise from—beginning close to the triggering neural event but spreading unevenly along vessels (Section 1.4.3.1)—and are therefore best described as complex spatiotemporal filters. Simply put, responses measured at a given location will exhibit different delays whether it was triggered locally or spread from adjacent regions. In that scenario, even if precautions are

taken—matching stimulus intensities, retinotopy and timing—it is virtually impossible to exclude the possibility that stimulus-specific temporal patterns are resulting from stimulus-specific spatial patterns that wrap into the temporal dimension through spatiotemporal hemodynamic filtering. Ultra-high-field functional imaging paired with detailed charactirizations of the underlying microvascular anatomy may help unwrap these spatiotemporal vascular distorsions.

The above confound may not readily account for Chapter 4's main effect as the observed time course differences mainly concerned an overall—across V1—rather than spatially patterned temporal shift of the BOLD response. However, artefactual stimulus-specific hemodynamics cannot be excluded here either. Indeed, vessels' viscoelastic properties governing CBF-to-CBV uncoupling and BOLD time courses are not stationary. They depend on baseline flow (Behzadi & Liu, 2005; Cohen et al., 2002), strength and duration of a neural activation (Polimeni & Lewis, 2021) and post-stimulus activation vs deactivation phases (Havlicek, Ivanov, Roebroeck, et al., 2017). Spatiotemporal responses to adjacent neural activations therefore most likely interact non-linearly and non-neurally through their partly overlapping vascular networks (Havlicek & Uludag, 2020). For example, whether two cortical columns draining to the same ascending vein are active simultaneously (Chapter 4's plaid stimulus condition) or one at a time (Chapter 4's grating stimulus condition) could affect downstream pressure and, consequently, overall hemodynamics (Krieger et al., 2012). Importantly, since this mechanism would play out the same across voxels, its potential role in generating the longer BOLD delay with our plaid stimulus cannot be ruled out.

5.4 Conclusion and Future Directions

This thesis achieved its overall objective of better characterizing non-invasive brain signals in terms of relevant neural computations. More specifically, Chapter 2 did showcased the advantages of occipital pole TMS—with the idea of individualized precision TMS and psychophysical quantification of intracortical processes further developed in Section 5.1.2 and 5.1.3—by showing the generalization of a cTBS effect from the motor to the visual cortex. Chapter 3 showed that the effect of MD on interocular inhibitory interactions do not generalize

across treatment modalities, and a deeper interpretation of the GABA modulation findings in Section 5.2.2 interestingly suggested that the inhibitory effects of MD may not concern interocular interactions but activity-dependent adaptation. Finally, Chapter 4 did show significantly longer BOLD delay in a stimulus condition thought to involved stronger intracortical inhibitory interactions.

Interesting avenues for further studies have been proposed along the discussion of each investigational tool used. A few more opportunities for combining them, although more technically and logistically challenging, are worth mentioning here as concluding remarks. Indeed, neural sources should be more tractable when they overlap across simultaneously acquired signal modalities, as the latter are affected by likely non-overlapping distortions and epiphenomenal biophysical processes (Sui et al., 2012). Such multimodal approach however allows to also characterize these modality-specific distortions and artifacts—the 'measurement model' (Kriegeskorte & Diedrichsen, 2016)—less equivocally; and this in turn would inform more relevant interpretations or more accurate generative models of unimodal signals. In my opinion, that endeavor would benefit more from dense multimodal sampling of fewer brains than from brute force averaging of idiosyncrasies, which are known to be large in human brains (Gratton et al., 2018; Singh et al., 2020).

This above view is probably best exemplified with Section 5.1.2 proposition of individualized precision occipital pole TMS, where TMS E-field vector strength and orientation across the cortical sheet would be related to modulations of computations psychophysically mapped across the visual field. With fMRI or EEG/MEG data acquired before and after NIBM of the same occipital pole target, the impact of the modulated computations on those non-invasive brain signals could be assessed in a similarly efficient fashion.

Chapter 3's brain plasticity approach for causally relating computations to brain signals can also be pushed further. First the plasticity modulation could be restricted to a narrower band of the visual feature space—e.g. by depriving a single orientation using a head-mounted altered visual reality system (Zhang et al., 2009)—to increase the specificity of the modulation to a smaller set of computations. Then a hybrid mMRS/fMRS protocol—i.e. performing fMRS before

and after the brain modulation—could further challenge the volume transmission hypothesis, as the proposed PAP motility mechanism predicts that both time averaged (mMRS) and task-modulated (fMRS) MR neurotransmitter signals would be affected in the same directions. Even more interestingly, the empirically modulated MR neurotransmitter signals would constitute an excellent paradigm for demonstrating a causal link between the BOLD delay and intracortical inhibition.

Finally, there are cTBS, MRS, visual masking and binocular rivalry findings that appear contradictory and would deserve clarification. While sMRS protocols related occipital GABA to stronger visual surround masking (Yoon et al., 2010) and longer dominance during binocular rivalry (Ip et al., 2021; Robertson et al., 2016; van Loon et al., 2013) (but see Brascamp et al., 2018; Sandberg et al., 2016), occipital pole cTBS increased occipital GABA in an mMRS protocol (Allen et al., 2014) but shortened dominance (Abuleil et al., 2021) and decreased visual masking (Chapter 2). Incorporating MRS measures to a study like that of Chapter 2 could potentially highlight a dissociation between the computational processes associated with sMRS vs mMRS GABA signals.

To conclude, more experiments should be specifically designed to leveraging prior knowledge of neural phenomena to better characterize the computational relevance of non-invasive brain signals and empower further non-invasive studies of less known human neural processes. This thesis demonstrated that this can be done directly in humans.

GENERAL BIBLIOGRAPHY

Aberra, A. S., Wang, B. S., Grill, W. M., & Peterchev, A. V. (2020). Simulation of transcranial magnetic stimulation in head model with morphologically-realistic cortical neurons [Article]. *Brain Stimulation*, *13*(1), 175-189. https://doi.org/10.1016/j.brs.2019.10.002

Abuleil, D., McCulloch, D., & Thompson, B. (2021). Visual cortex cTBS increases mixed percept duration while a-tDCS has no effect on binocular rivalry [Article]. *Plos One*, *16*(2), 12, Article e0239349. https://doi.org/10.1371/journal.pone.0239349

Adesnik, H., Bruns, W., Taniguchi, H., Huang, Z. J., & Scanziani, M. (2012). A neural circuit for spatial summation in visual cortex. *Nature*, *490*(7419), 226-231. https://doi.org/10.1038/nature11526

Adibi, M., & Lampl, I. (2021). Sensory Adaptation in the Whisker-Mediated Tactile System: Physiology, Theory, and Function. *Frontiers in Neuroscience*, *15*, Article 770011. https://doi.org/10.3389/fnins.2021.770011

Agnati, L. F., Guidolin, D., Guescini, M., Genedani, S., & Fuxe, K. (2010). Understanding wiring and volume transmission. *Brain Research Reviews*, *64*(1), 137-159. https://doi.org/10.1016/j.brainresrev.2010.03.003

Alais, D., Cass, J., O'Shea, R. P., & Blake, R. (2010). Visual Sensitivity Underlying Changes in Visual Consciousness. *Current Biology*, *20*(15), 1362-1367. https://doi.org/10.1016/j.cub.2010.06.015

Albouy, P., Weiss, A., Baillet, S., & Zatorre, R. J. (2017). Selective Entrainment of Theta Oscillations in the Dorsal Stream Causally Enhances Auditory Working Memory Performance. *Neuron*, *94*(1), 193-+. https://doi.org/10.1016/j.neuron.2017.03.015

Allen, C. P. G., Dunkley, B. T., Muthukumaraswamy, S. D., Edden, R., Evans, C. J., Sumner, P., Singh, K. D., & Chambers, C. D. (2014). Enhanced Awareness Followed Reversible Inhibition of Human Visual Cortex: A Combined TMS, MRS and MEG Study. *Plos One*, *9*(6), Article e100350. https://doi.org/10.1371/journal.pone.0100350

Allen, E. A., Pasley, B. N., Duong, T., & Freeman, R. D. (2007). Transcranial magnetic stimulation elicits coupled neural and hemodynamic consequences [Article]. *Science*, *317*(5846), 1918-1921. https://doi.org/10.1126/science.1146426

Andersen, J. V., McNair, L. F., Schousboe, A., & Waagepetersen, H. S. (2017). Specificity of exogenous acetate and glutamate as astrocyte substrates examined in acute brain slices from female mice using methionine sulfoximine (MSO) to inhibit glutamine synthesis. *J Neurosci Res*, *95*(11), 2207-2216. https://doi.org/10.1002/jnr.24038

Andersson, J. L. R., Skare, S., & Ashburner, J. (2003). How to correct susceptibility distortions in spin-echo echo-planar images: application to diffusion tensor imaging [Article]. *Neuroimage*, *20*(2), 870-888. https://doi.org/10.1016/s1053-8119(03)00336-7

Anenberg, E., Chan, A. W., Xie, Y. C., LeDue, J. M., & Murphy, T. H. (2015). Optogenetic stimulation of GABA neurons can decrease local neuronal activity while increasing cortical blood flow. *Journal of Cerebral Blood Flow and Metabolism*, *35*(10), 1579-1586. https://doi.org/10.1038/jcbfm.2015.140

Angelucci, A., Bijanzadeh, M., Nurminen, L., Federer, F., Merlin, S., & Bressloff, P. C. (2017). Circuits and Mechanisms for Surround Modulation in Visual Cortex. In H. Y. Zoghbi (Ed.), *Annual Review of Neuroscience, Vol 40* (Vol. 40, pp. 425-451). Annual Reviews. https://doi.org/10.1146/annurev-neuro-072116-031418

Angelucci, A., & Bressloff, P. C. (2006). Contribution of feedforward, lateral and feedback connections to the classical receptive field center and extra-classical receptive field surround of primate V1 neurons. *Acetylcholine in the Cerebral Cortex*, *154*, 93-120. https://doi.org/10.1016/S0079-6123(06)54005-1

Antal, A., Kincses, T. Z., Nitsche, M. A., Bartfai, O., Demmer, I., Sommer, M., & Paulus, W. (2002). Pulse configuration-dependent effects of repetitive transcranial magnetic stimulation on visual perception. *Neuroreport*, *13*(17), 2229-2233. https://doi.org/10.1097/01.wnr.0000044216.09266.64

Aquino, K. M., Robinson, P. A., Schira, M. M., & Breakspear, M. (2014). Deconvolution of neural dynamics from fMRI data using a spatiotemporal hemodynamic response function. *Neuroimage*, *94*, 203-215. https://doi.org/10.1016/j.neuroimage.2014.03.001

Archibald, J., MacMillan, E. L., Enzler, A., Jutzeler, C. R., Schweinhardt, P., & Kramer, J. L. K. (2020). Excitatory and inhibitory responses in the brain to experimental pain: A systematic review of MR spectroscopy studies [Review]. *Neuroimage*, *215*, 14, Article 116794. https://doi.org/10.1016/j.neuroimage.2020.116794

Atallah, B. V., Bruns, W., Carandini, M., & Scanziani, M. (2012). Parvalbumin-Expressing Interneurons Linearly Transform Cortical Responses to Visual Stimuli. *Neuron*, *73*(1), 159-170. https://doi.org/10.1016/j.neuron.2011.12.013

Attwell, D., Mishra, A., Hall, C. N., O'Farrell, F. M., & Dalkara, T. (2016). What is a pericyte? *Journal of Cerebral Blood Flow & Metabolism*, *36*(2), 451-455. https://doi.org/10.1177/0271678x15610340

Bachtiar, V., Johnstone, A., Berrington, A., Lemke, C., Johansen-Berg, H., Emir, U., & Stagg, C. J. (2018). Modulating Regional Motor Cortical Excitability with Noninvasive Brain Stimulation Results in Neurochemical Changes in Bilateral Motor Cortices. *J Neurosci*, *38*(33), 7327-7336. https://doi.org/10.1523/JNEUROSCI.2853-17.2018

Baillet, S., Mosher, J. C., & Leahy, R. M. (2001). Electromagnetic brain mapping [Article]. *Ieee Signal Processing Magazine*, *18*(6), 14-30. https://doi.org/10.1109/79.962275

Bair, W., Cavanaugh, J. R., & Movshon, J. A. (2003). Time course and time-distance relationships for surround suppression in macaque V1 neurons. *Journal of Neuroscience*, *23*(20), 7690-7701. https://doi.org/10.1523/JNEUROSCI.23-20-07690.2003

Bak, L. K., Schousboe, A., & Waagepetersen, H. S. (2006). The glutamate/GABA-glutamine cycle: aspects of transport, neurotransmitter homeostasis and ammonia transfer [Review]. *Journal of Neurochemistry*, *98*(3), 641-653. https://doi.org/10.1111/j.1471-4159.2006.03913.x

Baker, D. H., Karapanagiotidis, T., Coggan, D. D., Wailes-Newson, K., & Smallwood, J. (2015). Brain networks underlying bistable perception [Article]. *Neuroimage*, *119*, 229-234. https://doi.org/10.1016/j.neuroimage.2015.06.053

Baker, D. H., Meese, T. S., & Georgeson, M. A. (2013). Paradoxical psychometric functions ("swan functions") are explained by dilution masking in four stimulus dimensions. *I-Perception*, *4*(1), 17-35. https://doi.org/10.1068/i0552

Baker, D. H., Meese, T. S., & Summers, R. J. (2007). Psychophysical evidence for two routes to suppression before binocular summation of signals in human vision. *Neuroscience*, *146*(1), 435-448. https://doi.org/10.1016/j.neuroscience.2007.01.030

Bandettini, P. A., Kwong, K. K., Davis, T. L., Tootell, R. B. H., Wong, E. C., Fox, P. T., Belliveau, J. W., Weisskoff, R. M., & Rosen, B. R. (1997). Characterization of cerebral blood oxygenation and flow changes during prolonged brain activation. *Human Brain Mapping*, *5*(2), 93-109.

Bao, M., & Engel, S. A. (2012). Distinct mechanism for long-term contrast adaptation [Article]. *Proceedings of the National Academy of Sciences of the United States of America*, *109*(15), 5898-5903. https://doi.org/10.1073/pnas.1113503109

Bao, M., Fast, E., Mesik, J., & Engel, S. (2013). Distinct mechanisms control contrast adaptation over different timescales [Article]. *Journal of Vision*, *13*(10), 11, Article Unsp 14. https://doi.org/10.1167/13.10.14

Bartolo, M. J., Gieselmann, M. A., Vuksanovic, V., Hunter, D., Sun, L., Chen, X., Delicato, L. S., & Thiele, A. (2011). Stimulus-induced dissociation of neuronal firing rates and local field potential gamma power and its relationship to the resonance blood oxygen level-dependent signal in macaque primary visual cortex. *European Journal of Neuroscience*, *34*(11), 1857-1870. https://doi.org/10.1111/j.1460-9568.2011.07877.x

Befroy, D. E., & Shulman, G. I. (2011). Magnetic resonance spectroscopy studies of human metabolism. *Diabetes*, *60*(5), 1361-1369. https://doi.org/10.2337/db09-0916

Behzadi, Y., & Liu, T. T. (2005). An arteriolar compliance model of the cerebral blood flow response to neural stimulus. *Neuroimage*, *25*(4), 1100-1111. https://doi.org/10.1016/j.neuroimage.2004.12.057

Benson, N. C., Butt, O. H., Datta, R., Radoeva, P. D., Brainard, D. H., & Aguirre, G. K. (2012). The Retinotopic Organization of Striate Cortex Is Well Predicted by Surface Topology. *Current Biology*, *22*(21), 2081-2085. https://doi.org/10.1016/j.cub.2012.09.014

Benson, N. C., Jamison, K. W., Arcaro, M. J., Vu, A. T., Glasser, M. F., Coalson, T. S., Van Essen, D. C., Yacoub, E., Ugurbil, K., Winawer, J., & Kay, K. (2018). The Human Connectome Project 7 Tesla retinotopy dataset: Description and population receptive field analysis [Article]. *Journal of Vision*, *18*(13), 22, Article 23. https://doi.org/10.1167/18.13.23

Benson, N. C., & Winawer, J. (2018). Bayesian analysis of retinotopic maps [Article]. *Elife*, *7*, 29, Article e40224. https://doi.org/10.7554/eLife.40224.001

Bergmann, T. O., & Hartwigsen, G. (2021). Inferring Causality from Noninvasive Brain Stimulation in Cognitive Neuroscience. *Journal of Cognitive Neuroscience*, *33*(2), 195-225. https://doi.org/10.1162/jocn_a_01591

Bergmann, T. O., Karabanov, A., Hartwigsen, G., Thielscher, A., & Siebner, H. R. (2016). Combining non-invasive transcranial brain stimulation with neuroimaging and electrophysiology: Current approaches and future perspectives. *Neuroimage*, *140*, 4-19. https://doi.org/10.1016/j.neuroimage.2016.02.012

Bernardinelli, Y., Randall, J., Janett, E., Nikonenko, I., Konig, S., Jones, E. V., Flores, C. E., Murai, K. K., Bochet, C. G., Holtmaat, A., & Muller, D. (2014). Activity-Dependent Structural Plasticity of Perisynaptic Astrocytic Domains Promotes Excitatory Synapse Stability. *Current Biology*, *24*(15), 1679-1688. https://doi.org/10.1016/j.cub.2014.06.025

Best, A. R., Thompson, J. V., Fletcher, M. L., & Wilson, D. A. (2005). Cortical metabotropic glutamate receptors contribute to habituation of a simple odor-evoked behavior. *Journal of Neuroscience*, *25*(10), 2513-2517. https://doi.org/10.1523/jneurosci.5298-04.2005

Bestmann, S., Ruff, C. C., Blakemore, C., Driver, J., & Thilo, K. V. (2007). Spatial attention changes excitability of human visual cortex to direct stimulation [Article]. *Current Biology*, *17*(2), 134-139. https://doi.org/10.1016/j.cub.2006.11.063

Biessmann, F., Murayama, Y., Logothetis, N. K., Muller, K. R., & Meinecke, F. C. (2012). Improved decoding of neural activity from fMRI signals using non-separable spatiotemporal deconvolutions. *Neuroimage*, *61*(4), 1031-1042. https://doi.org/10.1016/j.neuroimage.2012.04.015

Binns, K. E., & Salt, T. E. (1997). Different roles for GABA(A) and GABA(B) receptors in visual processing in the rat superior colliculus. *Journal of Physiology-London*, *504*(3), 629-639. https://doi.org/10.1111/j.1469-7793.1997.629bd.x

Blake, R. (1989). A NEURAL THEORY OF BINOCULAR-RIVALRY. *Psychological Review*, *96*(1), 145-167. https://doi.org/10.1037//0033-295x.96.1.145

Blake, R., & Logothetis, N. K. (2002). Visual competition. *Nature Reviews Neuroscience*, *3*(1), 13-23. https://doi.org/10.1038/nrn701

Blake, R., Oshea, R. P., & Mueller, T. J. (1992). SPATIAL ZONES OF BINOCULAR-RIVALRY IN CENTRAL AND PERIPHERAL-VISION. *Visual Neuroscience*, *8*(5), 469-478. https://doi.org/10.1017/s0952523800004971

Blake, R., Sobel, K. V., & Gilroy, L. A. (2003). Visual motion retards alternations between conflicting perceptual interpretations. *Neuron*, *39*(5), 869-878. https://doi.org/10.1016/s0896-6273(03)00495-1

Blake, R., & Wilson, H. (2011). Binocular vision. *Vision Research*, *51*(7), 754-770. https://doi.org/10.1016/j.visres.2010.10.009

Blakemore, C., & Tobin, E. A. (1972). LATERAL INHIBITION BETWEEN ORIENTATION DETECTORS IN CATS VISUAL-CORTEX. *Experimental Brain Research*, *15*(4), 439-+. https://doi.org/10.1007/BF00234129

Blankenburg, F., Taskin, B., Ruben, J., Moosmann, M., Ritter, P., Curio, G., & Villringer, A. (2003). Imperceptible stimuli and sensory processing impediment. *Science*, *299*(5614), 1864-1864. https://doi.org/10.1126/science.1080806

Bocci, T., Caleo, M., Giorli, E., Barloscio, D., Maffei, L., Rossi, S., & Sartucci, F. (2011). TRANSCALLOSAL INHIBITION DAMPENS NEURAL RESPONSES TO HIGH CONTRAST STIMULI IN HUMAN VISUAL CORTEX [Article]. *Neuroscience*, *187*, 43-51. https://doi.org/10.1016/j.neuroscience.2011.04.050

Bocci, T., Caleo, M., Restani, L., Barloscio, D., Rossi, S., & Sartucci, F. (2016). Altered recovery from inhibitory repetitive transcranial magnetic stimulation (rTMS) in subjects with photosensitive epilepsy [Article]. *Clinical Neurophysiology*, *127*(10), 3353-3361. https://doi.org/10.1016/j.clinph.2016.06.013

Bock, D. D., Lee, W. C. A., Kerlin, A. M., Andermann, M. L., Hood, G., Wetzel, A. W., Yurgenson, S., Soucy, E. R., Kim, H. S., & Reid, R. C. (2011). Network anatomy and in vivo physiology of visual cortical neurons. *Nature*, *471*(7337), 177-U159. https://doi.org/10.1038/nature09802

Bock, E. A., Fesi, J. D., Baillet, S., & Mendola, J. D. (2019). Tagged MEG measures binocular rivalry in a cortical network that predicts alternation rate. *Plos One*, *14*(7), Article e0218529. https://doi.org/10.1371/journal.pone.0218529

Bohotin, V., Fumal, A., Vandenheede, M., Gerard, P., Bohotin, C., de Noordhout, A. M., & Schoenen, J. (2002). Effects of repetitive transcranial magnetic stimulation on visual evoked potentials in migraine [Article]. *Brain*, *125*, 912-922. https://doi.org/10.1093/brain/awf081

Boorman, L., Harris, S., Bruyns-Haylett, M., Kennerley, A., Zheng, Y., Martin, C., Jones, M., Redgrave, P., & Berwick, J. (2015). Long-Latency Reductions in Gamma Power Predict Hemodynamic Changes That Underlie the Negative BOLD Signal. *Journal of Neuroscience*, *35*(11), 4641-4656. https://doi.org/10.1523/jneurosci.2339-14.2015

Boorman, L., Kennerley, A. J., Johnston, D., Jones, M., Zheng, Y., Redgrave, P., & Berwick, J. (2010). Negative Blood Oxygen Level Dependence in the Rat: A Model for Investigating the Role of Suppression in Neurovascular Coupling. *Journal of Neuroscience*, *30*(12), 4285-4294. https://doi.org/10.1523/jneurosci.6063-09.2010

Boroojerdi, B., Prager, A., Muellbacher, W., & Cohen, L. G. (2000). Reduction of human visual cortex excitability using 1-Hz transcranial magnetic stimulation. *Neurology*, *54*(7), 1529-1531. https://doi.org/10.1212/wnl.54.7.1529

Bouboulis, P., & Theodoridis, S. (2011). Extension of Wirtinger's Calculus to Reproducing Kernel Hilbert Spaces and the Complex Kernel LMS [Article]. *Ieee Transactions on Signal Processing*, *59*(3), 964-978. https://doi.org/10.1109/tsp.2010.2096420

Bouboulis, P., Theodoridis, S., Mavroforakis, C., & Evaggelatou-Dalla, L. (2015). Complex Support Vector Machines for Regression and Quaternary Classification [Article]. *Ieee Transactions on Neural Networks and Learning Systems*, *26*(6), 1260-1274. https://doi.org/10.1109/tnnls.2014.2336679

Boucsein, C., Nawrot, M. P., Schnepel, P., & Aertsen, A. (2011). Beyond the cortical column: abundance and physiology of horizontal connections imply a strong role for inputs from the surround. *Frontiers in Neuroscience*, *5*, Article 32. https://doi.org/10.3389/fnins.2011.00032

Boynton, G. M., Engel, S. A., Glover, G. H., & Heeger, D. J. (1996). Linear systems analysis of functional magnetic resonance imaging in human V1. *Journal of Neuroscience*, *16*(13), 4207-4221. https://doi.org/10.1523/JNEUROSCI.16-13-04207.1996

Braddick, O., Campbell, F. W., & Atkinson, J. (1978). Channels in Vision: Basic Aspects. In R. Held, H. W. Leibowitz, & H.-L. Teuber (Eds.), *Perception* (pp. 3-38). Springer Berlin Heidelberg. https://doi.org/10.1007/978-3-642-46354-9_1

Bradnam, L. V., Stinear, C. M., & Byblow, W. D. (2010). Theta Burst Stimulation of Human Primary Motor Cortex Degrades Selective Muscle Activation in the Ipsilateral Arm [Article]. *Journal of Neurophysiology*, *104*(5), 2594-2602. https://doi.org/10.1152/jn.00365.2010

Brainard, D. H. (1997). The psychophysics toolbox. *Spatial Vision*, *10*(4), 433-436. https://doi.org/10.1163/156856897x00357

Brascamp, J. W., Becker, M. W., & Hambrick, D. Z. (2018). Revisiting individual differences in the time course of binocular rivalry. *Journal of Vision*, *18*(7), Article 3. https://doi.org/10.1167/18.7.3

Brascamp, J. W., Klink, P. C., & Levelt, W. J. M. (2015). The 'laws' of binocular rivalry: 50 years of Levelt's propositions [Review]. *Vision Research*, *109*, 20-37. https://doi.org/10.1016/j.visres.2015.02.019

Brascamp, J. W., Van Ee, R., Noest, A. J., Jacobs, R., & van den Berg, A. V. (2006). The time course of binocular rivalry reveals a fundamental role of noise. *Journal of Vision*, *6*(11), 1244-1256. https://doi.org/10.1167/6.11.8

Bressler, D., Spotswood, N., & Whitney, D. (2007). Negative BOLD fMRI Response in the Visual Cortex Carries Precise Stimulus-Specific Information. *Plos One*, *2*(5), Article e410. https://doi.org/10.1371/journal.pone.0000410

Brett, M., Anton, J.-L., Valabregue, R., & Poline, J.-B. (2002, June 2-6). Region of interest analysis using an SPM toolbox. 8th International Conference on Functional Mapping of the Human Brain, Sendai, Japan.

Broca, P. (1861). Remarques sur le siege de la faculté du langage articulé; suivies d'une observation d'aphemie (perte de la parole). *Bulletins de La Société Anatomique (Paris)*, *6*, 330-357; 398-407.

Brouwer, G. J., & Heeger, D. J. (2011). Cross-orientation suppression in human visual cortex. *Journal of Neurophysiology*, *106*(5), 2108-2119. https://doi.org/10.1152/jn.00540.2011

Bruhn, H., Frahm, J., Gyngell, M. L., Merboldt, K. D., Hanicke, W., & Sauter, R. (1989). CEREBRAL METABOLISM IN MAN AFTER ACUTE STROKE - NEW OBSERVATIONS USING LOCALIZED PROTON NMR-SPECTROSCOPY [Note]. *Magnetic Resonance in Medicine*, *9*(1), 126-131. https://doi.org/10.1002/mrm.1910090115

Buckthought, A., Jessula, S., & Mendola, J. D. (2011). Bistable Percepts in the Brain: fMRI Contrasts Monocular Pattern Rivalry and Binocular Rivalry. *Plos One*, *6*(5). https://doi.org/10.1371/journal.pone.0020367

Busse, L., Wade, A. R., & Carandini, M. (2009). Representation of Concurrent Stimuli by Population Activity in Visual Cortex. *Neuron*, *64*(6), 931-942. https://doi.org/10.1016/j.neuron.2009.11.004

Buxton, R. B. (2021). The thermodynamics of thinking: connections between neural activity, energy metabolism and blood flow. *Philosophical Transactions of the Royal Society B-Biological Sciences*, *376*(1815), Article 20190624. https://doi.org/10.1098/rstb.2019.0624

Buxton, R. B., Griffeth, V. E. M., Simon, A. B., Moradi, F., & Shmuel, A. (2014). Variability of the coupling of blood flow and oxygen metabolism responses in the brain: a problem for interpreting BOLD studies but potentially a new window on the underlying neural activity (vol 8, pg 139, 2014) [Correction]. *Frontiers in Neuroscience*, *8*, 1, Article 241. https://doi.org/10.3389/fnins.2014.00241

Buxton, R. B., Wong, E. C., & Frank, L. R. (1998). Dynamics of blood flow and oxygenation changes during brain activation: The balloon model. *Magnetic Resonance in Medicine*, *39*(6), 855-864. https://doi.org/10.1002/mrm.1910390602

Calamante, F., Thomas, D. L., Pell, G. S., Wiersma, J., & Turner, R. (1999). Measuring cerebral blood flow using magnetic resonance imaging techniques. *Journal of Cerebral Blood Flow and Metabolism*, *19*(7), 701-735. https://doi.org/10.1097/00004647-199907000-00001

Cali, C., Agus, M., Kare, K., Boges, D. J., Lehvaslaiho, H., Hadwiger, M., & Magistretti, P. J. (2019). 3D cellular reconstruction of cortical glia and parenchymal morphometric analysis from Serial Block-Face Electron Microscopy of juvenile rat. *Prog Neurobiol*, *183*, 101696. https://doi.org/10.1016/j.pneurobio.2019.101696

Cao, D. C., Zhuang, X. H., Kang, P., Hong, S. W., & King, A. C. (2016). Acute Alcohol Drinking Promotes Piecemeal Percepts during Binocular Rivalry [Article]. *Frontiers in Psychology*, *7*, 10, Article 489. https://doi.org/10.3389/fpsyg.2016.00489

Caputi, A., Melzer, S., Michael, M., & Monyer, H. (2013). The long and short of GABAergic neurons. *Current Opinion in Neurobiology*, *23*(2), 179-186. https://doi.org/10.1016/j.conb.2013.01.021

Carandini, M., & Heeger, D. J. (2012). Normalization as a canonical neural computation [Review]. *Nature Reviews Neuroscience*, *13*(1), 51-62. https://doi.org/10.1038/nrn3136

Cardin, J. A. (2019). Functional flexibility in cortical circuits. *Current Opinion in Neurobiology*, *58*, 175-180. https://doi.org/10.1016/j.conb.2019.09.008

Cardin, J. A., Palmer, L. A., & Contreras, D. (2007). Stimulus feature selectivity in excitatory and inhibitory neurons in primary visual cortex. *Journal of Neuroscience*, *27*(39), 10333-10344. https://doi.org/10.1523/jneurosci.1692-07.2007

Caroni, P., Donato, F., & Muller, D. (2012). Structural plasticity upon learning: regulation and functions. *Nature Reviews Neuroscience*, *13*(7), 478-490. https://doi.org/10.1038/nrn3258

Cauli, B., & Hamel, E. (2010). Revisiting the role of neurons in neurovascular coupling. *Frontiers in neuroenergetics*, *2*, 9. https://doi.org/10.3389/fnene.2010.00009

Cauli, B., Tong, X. K., Rancillac, A., Serluca, N., Lambolez, B., Rossier, J., & Hamel, E. (2004). Cortical GABA interneurons in neurovascular coupling: Relays for subcortical vasoactive pathways. *Journal of Neuroscience*, *24*(41), 8940-8949. https://doi.org/10.1523/Jneurosci.3065-04.2004

Cavanaugh, J. R., Bair, W., & Movshon, J. A. (2002). Nature and interaction of signals from the receptive field center and surround in macaque V1 neurons. *Journal of Neurophysiology*, *88*(5), 2530-2546. https://doi.org/10.1152/jn.00692.2001

Chadnova, E., Reynaud, A., Clavagnier, S., & Hess, R. F. (2017). Short-term monocular occlusion produces changes in ocular dominance by a reciprocal modulation of interocular inhibition [Article]. *Scientific Reports*, *7*, 6, Article 41747. https://doi.org/10.1038/srep41747

Chalavi, S., Pauwels, L., Heise, K. F., Adab, H. Z., Maes, C., Puts, N. A. J., Edden, R. A. E., & Swinnen, S. P. (2018). The neurochemical basis of the contextual interference effect. *Neurobiology of Aging*, *66*, 85-96. https://doi.org/10.1016/j.neurobiolaging.2018.02.014

Chalifoux, J. R., & Carter, A. G. (2011a). GABA(B) receptor modulation of synaptic function. *Current Opinion in Neurobiology*, *21*(2), 339-344. https://doi.org/10.1016/j.conb.2011.02.004

Chalifoux, J. R., & Carter, A. G. (2011b). Glutamate Spillover Promotes the Generation of NMDA Spikes. *Journal of Neuroscience*, *31*(45), 16435-16446. https://doi.org/10.1523/jneurosci.2777-11.2011

Chang, C. C., & Lin, C. J. (2011). LIBSVM: A Library for Support Vector Machines [Article]. *Acm Transactions on Intelligent Systems and Technology*, *2*(3), 27, Article 27. https://doi.org/10.1145/1961189.1961199

Chattopadhyaya, B., Di Cristo, G., Wu, C. Z., Knott, G., Kuhlman, S., Fu, Y., Palmiter, R. D., & Huang, Z. J. (2007). GAD67-Mediated GABA synthesis and signaling regulate inhibitory synaptic innervation in the visual cortex. *Neuron*, *54*(6), 889-903. https://doi.org/10.1016/j.neuron.2007.05.015

Chen, C., She, Z., Tang, P., Qin, Z., He, J., & Qu, J. Y. (2021). Study of neurovascular coupling by using mesoscopic and microscopic imaging. *Iscience*, *24*(10), 103176, Article 103176. https://doi.org/10.1016/j.isci.2021.103176

Chen, C. C. (2014). Partitioning two components of BOLD activation suppression in flanker effects. *Frontiers in Neuroscience*, *8*. https://doi.org/10.3389/fnins.2014.00149
Chen, I. W., Helmchen, F., & Lutcke, H. (2015). Specific Early and Late Oddball-Evoked Responses in Excitatory and Inhibitory Neurons of Mouse Auditory Cortex. *J Neurosci*, *35*(36), 12560-12573. https://doi.org/10.1523/JNEUROSCI.2240-15.2015
Chen, J. E., Glover, G. H., Fultz, N. E., Rosen, B. R., Polimeni, J. R., & Lewis, L. D. (2021). Investigating mechanisms of fast BOLD responses: The effects of stimulus intensity and of spatial heterogeneity of hemodynamics. *Neuroimage*, *245*, Article 118658. https://doi.org/10.1016/j.neuroimage.2021.118658
Chen, R., Classen, J., Gerloff, C., Celnik, P., Wassermann, E. M., Hallett, M., & Cohen, L. G. (1997). Depression of motor cortex excitability by low-frequency transcranial magnetic stimulation [Article; Proceedings Paper]. *Neurology*, *48*(5), 1398-1403. https://doi.org/10.1212/wnl.48.5.1398
Chokshi, V., Gao, M., Grier, B. D., Owens, A., Wang, H., Worley, P. F., & Lee, H. K. (2019). Input-Specific Metaplasticity in the Visual Cortex Requires Homer1a-Mediated mGluR5 Signaling. *Neuron*, *104*(4), 736-+. https://doi.org/10.1016/j.neuron.2019.08.017
Chung, S. W., Hill, A. T., Rogasch, N. C., Hoy, K. E., & Fitzgerald, P. B. (2016). Use of theta-burst stimulation in changing excitability of motor cortex: A systematic review and meta-analysis [Review]. *Neuroscience and Biobehavioral Reviews*, *63*, 43-64. https://doi.org/10.1016/j.neubiorev.2016.01.008
Cirillo, G., Di Pino, G., Capone, F., Ranieri, F., Florio, L., Todisco, V., Tedeschi, G., Funke, K., & Di Lazzaro, V. (2017). Neurobiological after-effects of non-invasive brain stimulation [Article]. *Brain Stimulation*, *10*(1), 1-18. https://doi.org/10.1016/j.brs.2016.11.009
Clavagnier, S., Dumoulin, S. O., & Hess, R. F. (2015). Is the Cortical Deficit in Amblyopia Due to Reduced Cortical Magnification, Loss of Neural Resolution, or Neural Disorganization? [Article]. *Journal of Neuroscience*, *35*(44), 14740-14755. https://doi.org/10.1523/jneurosci.1101-15.2015
Clavagnier, S., Thompson, B., & Hess, R. F. (2013). Long Lasting Effects of Daily Theta Burst rTMS Sessions in the Human Amblyopic Cortex [Article]. *Brain Stimulation*, *6*(6), 860-867. https://doi.org/10.1016/j.brs.2013.04.002
Cohen, E. R., Ugurbil, K., & Kim, S. G. (2002). Effect of basal conditions on the magnitude and dynamics of the blood oxygenation level-dependent fMRI response. *Journal of Cerebral Blood Flow and Metabolism*, *22*(9), 1042-1053. https://doi.org/10.1097/00004647-200209000-00002
Cone, J. J., Scantlen, M. D., Histed, M. H., & Maunsell, J. H. R. (2019). Different Inhibitory Interneuron Cell Classes Make Distinct Contributions to Visual Contrast Perception. *eNeuro*, *6*(1), Article 0337-18.2019. https://doi.org/10.1523/eneuro.0337-18.2019
Contreras, D., & Palmer, L. (2003). Response to contrast of electrophysiologically defined cell classes in primary visual cortex. *Journal of Neuroscience*, *23*(17), 6936-6945.
Cook, E., Hammett, S. T., & Larsson, J. (2016). GABA predicts visual intelligence [Article]. *Neurosci Lett*, *632*, 50-54. https://doi.org/10.1016/j.neulet.2016.07.053
da Costa, N. M., & Martin, K. A. C. (2010). Whose cortical column would that be? *Frontiers in Neuroanatomy*, *4*, Article 16. https://doi.org/10.3389/fnana.2010.00016
Dahlqvist, M. K., Thomsen, K. J., Postnov, D. D., & Lauritzen, M. J. (2020). Modification of oxygen consumption and blood flow in mouse somatosensory cortex by cell-type-specific neuronal activity. *Journal of Cerebral Blood Flow and Metabolism*, *40*(10), 2010-2025, Article 0271678x19882787. https://doi.org/10.1177/0271678x19882787
Davis, T. L., Kwong, K. K., Weisskoff, R. M., & Rosen, B. R. (1998). Calibrated functional MRI: Mapping the dynamics of oxidative metabolism. *Proceedings of the National Academy of Sciences of the United States of America*, *95*(4), 1834-1839. https://doi.org/10.1073/pnas.95.4.1834
Dayan, E., Censor, N., Buch, E. R., Sandrini, M., & Cohen, L. G. (2013). Noninvasive brain stimulation: from physiology to network dynamics and back. *Nature Neuroscience*, *16*(7), 838-844. https://doi.org/10.1038/nn.3422
de Graaf, T. A., Koivisto, M., Jacobs, C., & Sack, A. T. (2014). The chronometry of visual perception: Review of occipital TMS masking studies. *Neuroscience and Biobehavioral Reviews*, *45*, 295-304. https://doi.org/10.1016/j.neubiorev.2014.06.017

de Labra, C., Rivadulla, C., Grieve, K., Marino, J., Espinosa, N., & Cudeiro, J. (2007). Changes in visual responses in the feline dLGN: Selective thalamic suppression induced by transcranial magnetic stimulation of V1 [Article]. *Cerebral Cortex*, *17*(6), 1376-1385. https://doi.org/10.1093/cercor/bhl048

Deangelis, G. C., Freeman, R. D., & Ohzawa, I. (1994). LENGTH AND WIDTH TUNING OF NEURONS IN THE CATS PRIMARY VISUAL-CORTEX. *Journal of Neurophysiology*, *71*(1), 347-374. https://doi.org/10.1152/jn.1994.71.1.347

Deangelis, G. C., Robson, J. G., Ohzawa, I., & Freeman, R. D. (1992). ORGANIZATION OF SUPPRESSION IN RECEPTIVE-FIELDS OF NEURONS IN CAT VISUAL-CORTEX. *Journal of Neurophysiology*, *68*(1), 144-163. https://doi.org/10.1152/jn.1992.68.1.144

Debruyn, E. J., & Bonds, A. B. (1986). CONTRAST ADAPTATION IN CAT VISUAL-CORTEX IS NOT MEDIATED BY GABA. *Brain Research*, *383*(1-2), 339-342. https://doi.org/10.1016/0006-8993(86)90036-3

Del Arco, A., Segovia, G., Fuxe, K., & Mora, F. (2003). Changes in dialysate concentrations of glutamate and GABA in the brain: an index of volume transmission mediated actions? *Journal of Neurochemistry*, *85*(1), 23-33. https://doi.org/10.1046/j.1471-4159.2003.01692.x

Devia, C., Concha-Miranda, M., & Rodriguez, E. (2022). Bi-Stable Perception: Self-Coordinating Brain Regions to Make-Up the Mind. *Frontiers in Neuroscience*, *15*, Article 805690. https://doi.org/10.3389/fnins.2021.805690

Devor, A., Dunn, A. K., Andermann, M. L., Ulbert, I., Boas, D. A., & Dale, A. M. (2003). Coupling of total hemoglobin concentration, oxygenation, and neural activity in rat somatosensory cortex. *Neuron*, *39*(2), 353-359. https://doi.org/10.1016/s0896-6273(03)00403-3

Devor, A., Tian, P. F., Nishimura, N., Teng, I. C., Hillman, E. M. C., Narayanan, S. N., Ulbert, I., Boas, D. A., Kleinfeld, D., & Dale, A. M. (2007). Suppressed neuronal activity and concurrent arteriolar vasoconstriction may explain negative blood oxygenation level-dependent signal. *Journal of Neuroscience*, *27*(16), 4452-4459. https://doi.org/10.1523/jneurosci.0134-07.2007

Deyoe, E. A., Bandettini, P., Neitz, J., Miller, D., & Winans, P. (1994). FUNCTIONAL MAGNETIC-RESONANCE-IMAGING (FMRI) OF THE HUMAN BRAIN [Article; Proceedings Paper]. *Journal of Neuroscience Methods*, *54*(2), 171-187. https://doi.org/10.1016/0165-0270(94)90191-0

Di Lazzaro, V., Pilato, F., Dileone, M., Ranieri, F., Ricci, V., Profice, P., Bria, P., Tonali, P. A., & Ziemann, U. (2006). GABA(A) receptor subtype specific enhancement of inhibition in human motor cortex [Article]. *Journal of Physiology-London*, *575*(3), 721-726. https://doi.org/10.1113/jphysiol.2006.114694

Di Lazzaro, V., Profice, P., Pilato, F., Dileone, M., Oliviero, A., & Ziemann, U. (2010). The effects of motor cortex rTMS on corticospinal descending activity. *Clinical Neurophysiology*, *121*(4), 464-473. https://doi.org/10.1016/j.clinph.2009.11.007

Di Lazzaro, V., Restuccia, D., Oliviero, A., Profice, P., Ferrara, L., Insola, A., Mazzone, P., Tonali, P., & Rothwell, J. C. (1998). Magnetic transcranial stimulation at intensities below active motor threshold activates intracortical inhibitory circuits [Article]. *Experimental Brain Research*, *119*(2), 265-268.

Dienel, G. A. (2019). Brain Glucose Metabolism: Integration of Energetics with Function. *Physiol Rev*, *99*(1), 949-1045. https://doi.org/10.1152/physrev.00062.2017

Dieter, K. C., Sy, J. L., & Blake, R. (2017). Individual differences in sensory eye dominance reflected in the dynamics of binocular rivalry [Article]. *Vision Research*, *141*, 40-50. https://doi.org/10.1016/j.visres.2016.09.014

Dieter, K. C., & Tadin, D. (2011). Understanding attentional modulation of binocular rivalry: a framework based on biased competition. *Frontiers in Human Neuroscience*, *5*, Article 155. https://doi.org/10.3389/fnhum.2011.00155

Ding, J., & Sperling, G. (2006). A gain-control theory of binocular combination [Article]. *Proceedings of the National Academy of Sciences of the United States of America*, *103*(4), 1141-1146. https://doi.org/10.1073/pnas.0509629103

Ding, Y., Zheng, Y., Liu, T., Chen, T., Wang, C., Sun, Q., Hua, M., & Hua, T. (2017). Changes in GABAergic markers accompany degradation of neuronal function in the primary visual cortex of senescent rats. *Scientific Reports*, *7*(1), 14897. https://doi.org/10.1038/s41598-017-15006-3

Dittman, J. S., & Regehr, W. G. (1997). Mechanism and kinetics of heterosynaptic depression at a cerebellar synapse. *Journal of Neuroscience*, *17*(23), 9048-9059. https://doi.org/10.1523/JNEUROSCI.17-23-09048.1997

Donahue, M. J., Near, J., Blicher, J. U., & Jezzard, P. (2010). Baseline GABA concentration and fMRI response. *Neuroimage*, *53*(2), 392-398. https://doi.org/10.1016/j.neuroimage.2010.07.017
Douglas, R. J., Koch, C., Mahowald, M., Martin, K. A. C., & Suarez, H. H. (1995). RECURRENT EXCITATION IN NEOCORTICAL CIRCUITS [Article]. *Science*, *269*(5226), 981-985. https://doi.org/10.1126/science.7638624
Drew, P. J. (2019). Vascular and neural basis of the BOLD signal. *Current Opinion in Neurobiology*, *58*, 61-69. https://doi.org/10.1016/j.conb.2019.06.004
Drew, P. J., Shih, A. Y., & Kleinfeld, D. (2011). Fluctuating and sensory-induced vasodynamics in rodent cortex extend arteriole capacity. *Proc Natl Acad Sci U S A*, *108*(20), 8473-8478. https://doi.org/10.1073/pnas.1100428108
Duarte, J. M. N., & Gruetter, R. (2013). Glutamatergic and GABAergic energy metabolism measured in the rat brain by C-13 NMR spectroscopy at 14.1 T. *Journal of Neurochemistry*, *126*(5), 579-590. https://doi.org/10.1111/jnc.12333
Dubbioso, R., Madsen, K. H., Thielscher, A., & Siebner, H. R. (2021). The Myelin Content of the Human Precentral Hand Knob Reflects Interindividual Differences in Manual Motor Control at the Physiological and Behavioral Level. *J Neurosci*, *41*(14), 3163-3179. https://doi.org/10.1523/JNEUROSCI.0390-20.2021
Dumoulin, S. O., & Wandell, B. A. (2008). Population receptive field estimates in human visual cortex [Article]. *Neuroimage*, *39*(2), 647-660. https://doi.org/10.1016/j.neuroimage.2007.09.034
Duvernoy, H. M., Delon, S., & Vannson, J. L. (1981). CORTICAL BLOOD-VESSELS OF THE HUMAN-BRAIN [Article]. *Brain Research Bulletin*, *7*(5), 519-579. https://doi.org/10.1016/0361-9230(81)90007-1
Echagarruga, C. T., Gheres, K. W., Norwood, J. N., & Drew, P. J. (2020). nNOS-expressing interneurons control basal and behaviorally evoked arterial dilation in somatosensory cortex of mice. *Elife*, *9*, Article e60533. https://doi.org/10.7554/eLife.60533
Eichert, N., Watkins, K. E., Mars, R. B., & Petrides, M. (2021). Morphological and functional variability in central and subcentral motor cortex of the human brain. *Brain Struct Funct*, *226*(1), 263-279. https://doi.org/10.1007/s00429-020-02180-w
El-Bouri, W. K., & Payne, S. J. (2016). A statistical model of the penetrating arterioles and venules in the human cerebral cortex [Article]. *Microcirculation*, *23*(7), 580-590. https://doi.org/10.1111/micc.12318
Engel, S. A., Rumelhart, D. E., Wandell, B. A., Lee, A. T., Glover, G. H., Chichilnisky, E. J., & Shadlen, M. N. (1994). FMRI OF HUMAN VISUAL-CORTEX [Letter]. *Nature*, *369*(6481), 525-525. https://doi.org/10.1038/369525a0
Farivar, R., Grigorov, F., van der Kouwe, A. J., Wald, L. L., & Keil, B. (2016). Dense, Shape-Optimized Posterior 32-Channel Coil for Submillimeter Functional Imaging of Visual Cortex at 3T. *Magnetic Resonance in Medicine*, *76*(1), 321-328. https://doi.org/10.1002/mrm.25815
Farivar, R., Thompson, B., Mansouri, B., & Hess, R. F. (2011). Interocular suppression in strabismic amblyopia results in an attenuated and delayed hemodynamic response function in early visual cortex. *Journal of Vision*, *11*(14), Article 16. https://doi.org/10.1167/11.14.16
Farrant, M., & Nusser, Z. (2005). Variations on an inhibitory theme: Phasic and tonic activation of GABA(A) receptors. *Nature Reviews Neuroscience*, *6*(3), 215-229. https://doi.org/10.1038/nrn1625
Fechner, G. T. (1860). *Elemente der psychophysik*. Breitkopf und Härtel.
Feinberg, T. E. (2012). Neuroontology, neurobiological naturalism, and consciousness: A challenge to scientific reduction and a solution [Review]. *Physics of Life Reviews*, *9*(1), 13-34. https://doi.org/10.1016/j.plrev.2011.10.019
Ferguson, K. A., & Cardin, J. A. (2020). Mechanisms underlying gain modulation in the cortex. *Nature Reviews Neuroscience*, *21*(2), 80-92. https://doi.org/10.1038/s41583-019-0253-y
Fitzgerald, P. B., Fountain, S., & Daskalakis, Z. J. (2006). A comprehensive review of the effects of rTMS on motor cortical excitability and inhibition. *Clinical Neurophysiology*, *117*(12), 2584-2596. https://doi.org/10.1016/j.clinph.2006.06.712
Floyer-Lea, A., Wylezinska, M., Kincses, T., & Matthews, P. M. (2006). Rapid modulation of GABA concentration in human sensorimotor cortex during motor learning [Article]. *Journal of Neurophysiology*, *95*(3), 1639-1644. https://doi.org/10.1152/jn.00346.2005
Foley, J. M. (1994). HUMAN LUMINANCE PATTERN-VISION MECHANISMS - MASKING EXPERIMENTS REQUIRE A NEW MODEL [Article]. *Journal of the Optical Society of America a-Optics Image Science and Vision*, *11*(6), 1710-1719. https://doi.org/10.1364/josaa.11.001710

Fonnum, F. (1984). GLUTAMATE - A NEUROTRANSMITTER IN MAMMALIAN BRAIN [Review]. *Journal of Neurochemistry*, *42*(1), 1-11. https://doi.org/10.1111/j.1471-4159.1984.tb09689.x
Forrest, M. P., Parnell, E., & Penzes, P. (2018). Dendritic structural plasticity and neuropsychiatric disease. *Nature Reviews Neuroscience*, *19*(4), 215-234. https://doi.org/10.1038/nrn.2018.16
Frangou, P., Correia, M., & Kourtzi, Z. (2018). GABA, not BOLD, reveals dissociable learning-dependent plasticity mechanisms in the human brain [Article]. *Elife*, *7*, 22, Article e35854. https://doi.org/10.7554/eLife.35854
Frangou, P., Emir, U. E., Karlaftis, V. M., Nettekoven, C., Hinson, E. L., Larcombe, S., Bridge, H., Stagg, C. J., & Kourtzi, Z. (2019). Learning to optimize perceptual decisions through suppressive interactions in the human brain [Article]. *Nature Communications*, *10*, 12, Article 474. https://doi.org/10.1038/s41467-019-08313-y
Freeman, A. W. (2005). Multistage model for binocular rivalry. *Journal of Neurophysiology*, *94*(6), 4412-4420. https://doi.org/10.1152/jn.00557.2005
Freeman, T. C. B., Durand, S., Kiper, D. C., & Carandini, M. (2002). Suppression without inhibition in visual cortex. *Neuron*, *35*(4), 759-771. https://doi.org/10.1016/s0896-6273(02)00819-x
Frenkel, M. Y., & Bear, M. F. (2004). How monocular deprivation shifts ocular dominance in visual cortex of young mice. *Neuron*, *44*(6), 917-923. https://doi.org/10.1016/j.neuron.2004.12.003
Fumal, A., Bohotin, V., Vandenheede, M., Seidel, L., De Pasqua, V., de Noordhout, A. M., & Schoenen, J. (2003). Effects of repetitive transcranial magnetic stimulation on visual evoked potentials: new insights in healthy subjects [Article]. *Experimental Brain Research*, *150*(3), 332-340. https://doi.org/10.1007/s00221-003-1423-7
Gagnon, L., Sakadzic, S., Lesage, F., Musacchia, J. J., Lefebvre, J., Fang, Q., Yucel, M. A., Evans, K. C., Mandeville, E. T., Cohen-Adad, J., Polimeni, J. R., Yaseen, M. A., Lo, E. H., Greve, D. N., Buxton, R. B., Dale, A. M., Devor, A., & Boas, D. A. (2015). Quantifying the microvascular origin of BOLD-fMRI from first principles with two-photon microscopy and an oxygen-sensitive nanoprobe. *J Neurosci*, *35*(8), 3663-3675. https://doi.org/10.1523/JNEUROSCI.3555-14.2015
Gainey, M. A., & Feldman, D. E. (2017). Multiple shared mechanisms for homeostatic plasticity in rodent somatosensory and visual cortex [Review]. *Philosophical Transactions of the Royal Society B-Biological Sciences*, *372*(1715), 7, Article 20160157. https://doi.org/10.1098/rstb.2016.0157
Gao, F., Edden, R. A. E., Li, M. W., Puts, N. A. J., Wang, G. B., Liu, C., Zhao, B., Wang, H. Q., Bai, X., Zhao, C., Wang, X., & Barker, P. B. (2013). Edited magnetic resonance spectroscopy detects an age-related decline in brain GABA levels. *Neuroimage*, *78*, 75-82. https://doi.org/10.1016/j.neuroimage.2013.04.012
Garcia-Garcia, R., Guerrero, J. F., Lavilla-Miyasato, M., Magdalena, J. R., Ordono, J. F., Llansola, M., Montoliu, C., Teruel-Marti, V., & Felipo, V. (2020). Hyperammonemia alters the mismatch negativity in the auditory evoked potential by altering functional connectivity and neurotransmission. *J Neurochem*, *154*(1), 56-70. https://doi.org/10.1111/jnc.14941
Garcia-Marin, V., Kelly, J. G., & Hawken, M. J. (2019). Major Feedforward Thalamic Input Into Layer 4C of Primary Visual Cortex in Primate [Article]. *Cerebral Cortex*, *29*(1), 134-149. https://doi.org/10.1093/cercor/bhx311
Garrett, M., Manavi, S., Roll, K., Ollerenshaw, D. R., Groblewski, P. A., Ponvert, N. D., Kiggins, J. T., Casal, L., Mace, K., Williford, A., Leon, A., Jia, X., Ledochowitsch, P., Buice, M. A., Wakeman, W., Mihalas, S., & Olsen, S. R. (2020). Experience shapes activity dynamics and stimulus coding of VIP inhibitory cells. *Elife*, *9*. https://doi.org/10.7554/eLife.50340
Gauthier, C. J., & Fan, A. P. (2019). BOLD signal physiology: Models and applications. *Neuroimage*, *187*, 116-127. https://doi.org/10.1016/j.neuroimage.2018.03.018
Genoud, C., Quairiaux, C., Steiner, P., Hirling, H., Welker, E., & Knott, G. W. (2006). Plasticity of astrocytic coverage and glutamate transporter expression in adult mouse cortex. *Plos Biology*, *4*(11), 2057-2064, Article e343. https://doi.org/10.1371/journal.pbio.0040343
George, M. S. (2019). Whither TMS: A One-Trick Pony or the Beginning of a Neuroscientific Revolution? [Review]. *American Journal of Psychiatry*, *176*(11), 904-910. https://doi.org/10.1176/appi.ajp.2019.19090957
Gilbert, C. D., Das, A., Ito, M., Kapadia, M., & Westheimer, G. (1996). Spatial integration and cortical dynamics. *Proceedings of the National Academy of Sciences of the United States of America*, *93*(2), 615-622. https://doi.org/10.1073/pnas.93.2.615
Gilbert, C. D., & Li, W. (2013). Top-down influences on visual processing. *Nature Reviews Neuroscience*, *14*(5), 350-363. https://doi.org/10.1038/nrn3476

Gilbert, C. D., & Wiesel, T. N. (1989). COLUMNAR SPECIFICITY OF INTRINSIC HORIZONTAL AND CORTICOCORTICAL CONNECTIONS IN CAT VISUAL-CORTEX [Article]. *Journal of Neuroscience*, *9*(7), 2432-2442. https://doi.org/10.1523/JNEUROSCI.09-07-02432.1989

Godlewska, B. R., Clare, S., Cowen, P. J., & Emir, U. E. (2017). Ultra-High-Field Magnetic Resonance Spectroscopy in Psychiatry. *Front Psychiatry*, *8*, 123. https://doi.org/10.3389/fpsyt.2017.00123

Goense, J., Merkle, H., & Logothetis, N. K. (2012). High-resolution fMRI reveals laminar differences in neurovascular coupling between positive and negative BOLD responses. *Neuron*, *76*(3), 629-639. https://doi.org/10.1016/j.neuron.2012.09.019

Gonzalez-Castillo, J., Saad, Z. S., Handwerker, D. A., Inati, S. J., Brenowitz, N., & Bandettini, P. A. (2012). Whole-brain, time-locked activation with simple tasks revealed using massive averaging and model-free analysis. *Proc Natl Acad Sci U S A*, *109*(14), 5487-5492. https://doi.org/10.1073/pnas.1121049109

Gratton, C., Laumann, T. O., Nielsen, A. N., Greene, D. J., Gordon, E. M., Gilmore, A. W., Nelson, S. M., Coalson, R. S., Snyder, A. Z., Schlaggar, B. L., Dosenbach, N. U. F., & Petersen, S. E. (2018). Functional Brain Networks Are Dominated by Stable Group and Individual Factors, Not Cognitive or Daily Variation. *Neuron*, *98*(2), 439-+. https://doi.org/10.1016/j.neuron.2018.03.035

Greve, D. N., & Fischl, B. (2009). Accurate and robust brain image alignment using boundary-based registration [Article]. *Neuroimage*, *48*(1), 63-72. https://doi.org/10.1016/j.neuroimage.2009.06.060

Griffeth, V. E. M., Perthen, J. E., & Buxton, R. B. (2011). Prospects for quantitative fMRI: Investigating the effects of caffeine on baseline oxygen metabolism and the response to a visual stimulus in humans. *Neuroimage*, *57*(3), 809-816. https://doi.org/10.1016/j.neuroimage.2011.04.064

Griffeth, V. E. M., Simon, A. B., & Buxton, R. B. (2015). The coupling of cerebral blood flow and oxygen metabolism with brain activation is similar for simple and complex stimuli in human primary visual cortex. *Neuroimage*, *104*, 156-162. https://doi.org/10.1016/j.neuroimage.2014.10.003

Gross, J., Baillet, S., Barnes, G. R., Henson, R. N., Hillebrand, A., Jensen, O., Jerbi, K., Litvak, V., Maess, B., Oostenveld, R., Parkkonen, L., Taylor, J. R., van Wassenhove, V., Wibral, M., & Schoffelen, J. M. (2013). Good practice for conducting and reporting MEG research [Article]. *Neuroimage*, *65*, 349-363. https://doi.org/10.1016/j.neuroimage.2012.10.001

Gruetter, R., & Tkac, I. (2000). Field mapping without reference scan using asymmetric echo-planar techniques [Article]. *Magnetic Resonance in Medicine*, *43*(2), 319-323. https://doi.org/10.1002/(sici)1522-2594(200002)43:2<319::aid-mrm22>3.0.co;2-1

Hall, C. N., Reynell, C., Gesslein, B., Hamilton, N. B., Mishra, A., Sutherland, B. A., O'Farrell, F. M., Buchan, A. M., Lauritzen, M., & Attwell, D. (2014). Capillary pericytes regulate cerebral blood flow in health and disease. *Nature*, *508*(7494), 55-+. https://doi.org/10.1038/nature13165

Hamm, J. P., & Yuste, R. (2016). Somatostatin Interneurons Control a Key Component of Mismatch Negativity in Mouse Visual Cortex. *Cell Reports*, *16*(3), 597-604. https://doi.org/10.1016/j.celrep.2016.06.037

Han, S. E., Alais, D., MacDougall, H., & Verstraten, F. A. J. (2020). Brief localised monocular deprivation in adults alters binocular rivalry predominance retinotopically and reduces spatial inhibition [Article]. *Scientific Reports*, *10*(1), 12, Article 18739. https://doi.org/10.1038/s41598-020-75252-w

Handwerker, D. A., Ollinger, J. M., & D'Esposito, M. (2004). Variation of BOLD hemodynamic responses across subjects and brain regions and their effects on statistical analyses. *Neuroimage*, *21*(4), 1639-1651. https://doi.org/10.1016/j.neuroimage.2003.11.029

Harel, N., Lee, S. P., Nagaoka, T., Kim, D. S., & Kim, S. G. (2002). Origin of negative blood oxygenation level-dependent fMRI signals. *Journal of Cerebral Blood Flow and Metabolism*, *22*(8), 908-917. https://doi.org/10.1097/00004647-200208000-00002

Harquel, S., Bacle, T., Beynel, L., Marendaz, C., Chauvin, A., & David, O. (2016). Mapping dynamical properties of cortical microcircuits using robotized TMS and EEG: Towards functional cytoarchitectonics. *Neuroimage*, *135*, 115-124. https://doi.org/10.1016/j.neuroimage.2016.05.009

Hashimoto, T., Volk, D. W., Eggan, S. M., Mirnics, K., Pierri, J. N., Sun, Z., Sampson, A. R., & Lewis, D. A. (2003). Gene expression deficits in a subclass of GABA neurons in the prefrontal cortex of subjects with schizophrenia [Article]. *J Neurosci*, *23*(15), 6315-6326. https://doi.org/10.1523/JNEUROSCI.23-15-06315.2003

Havlicek, M., Ivanov, D., Poser, B. A., & Uludag, K. (2017). Echo-time dependence of the BOLD response transients - A window into brain functional physiology. *Neuroimage*, *159*, 355-370. https://doi.org/10.1016/j.neuroimage.2017.07.034

Havlicek, M., Ivanov, D., Roebroeck, A., & Uludag, K. (2017). Determining Excitatory and Inhibitory Neuronal Activity from Multimodal fMRI Data Using a Generative Hemodynamic Model [Article]. *Frontiers in Neuroscience*, *11*, 20, Article 616. https://doi.org/10.3389/fnins.2017.00616

Havlicek, M., Roebroeck, A., Friston, K., Gardumi, A., Ivanov, D., & Uludag, K. (2015). Physiologically informed dynamic causal modeling of fMRI data [Article]. *Neuroimage*, *122*, 355-372. https://doi.org/10.1016/j.neuroimage.2015.07.078

Havlicek, M., Roebroeck, A., Friston, K. J., Gardumi, A., Ivanov, D., & Uludag, K. (2017). On the importance of modeling fMRI transients when estimating effective connectivity: A dynamic causal modeling study using ASL data [Article]. *Neuroimage*, *155*, 217-233. https://doi.org/10.1016/j.neuroimage.2017.03.017

Havlicek, M., & Uludag, K. (2020). A dynamical model of the laminar BOLD response. *Neuroimage*, *204*, 116209. https://doi.org/10.1016/j.neuroimage.2019.116209

Hayden, M. R. (2019). Hypothesis: Astrocyte Foot Processes Detachment from the Neurovascular Unit in Female Diabetic Mice May Impair Modulation of Information Processing-Six Degrees of Separation. *Brain Sci*, *9*(4). https://doi.org/10.3390/brainsci9040083

Haynes, J. D., & Rees, G. (2005). Predicting the orientation of invisible stimuli from activity in human primary visual cortex. *Nature Neuroscience*, *8*(5), 686-691. https://doi.org/10.1038/nn1445

Heeger, D. J. (1992). NORMALIZATION OF CELL RESPONSES IN CAT STRIATE CORTEX [Review]. *Visual Neuroscience*, *9*(2), 181-197. https://doi.org/10.1017/s0952523800009640

Heintz, T. G., Hinojosa, A. J., & Lagnado, L. (2020). Opposing forms of adaptation in mouse visual cortex are controlled by distinct inhibitory microcircuits and gated by locomotion [Preprint posted online January 17, 2020]. *bioRxiv*. https://doi.org/10.1101/2020.01.16.909788

Heistek, T. S., Lodder, J. C., Brussaard, A. B., Bosman, L. W. J., & Mansvelder, H. D. (2010). GABAergic inhibition shapes frequency adaptation of cortical activity in a frequency-dependent manner. *Brain Research*, *1321*, 31-39. https://doi.org/10.1016/j.brainres.2010.01.047

Heller, J. P., & Rusakov, D. A. (2015). Morphological Plasticity of Astroglia: Understanding Synaptic Microenvironment. *Glia*, *63*(12), 2133-2151. https://doi.org/10.1002/glia.22821

Henneberger, C., Bard, L., Panatier, A., Reynolds, J. P., Kopach, O., Medvedev, N. I., Minge, D., Herde, M. K., Anders, S., Kraev, I., Heller, J. P., Rama, S., Zheng, K. Y., Jensen, T. P., Sanchez-Romero, I., Jackson, C. J., Janovjak, H., Ottersen, O. P., Nagelhus, E. A., . . . Rusakov, D. A. (2020). LTP Induction Boosts Glutamate Spillover by Driving Withdrawal of Perisynaptic Astroglia. *Neuron*, *108*(5), 919-+. https://doi.org/10.1016/j.neuron.2020.08.030

Hetherington, H. P., Newcomer, B. R., & Pan, J. W. (1998). Measurements of human cerebral GABA at 4.1 T using numerically optimized editing pulses [Article]. *Magnetic Resonance in Medicine*, *39*(1), 6-10. https://doi.org/10.1002/mrm.1910390103

Hill, R. A., Tong, L., Yuan, P., Murikinati, S., Gupta, S., & Grutzendler, J. (2015). Regional Blood Flow in the Normal and Ischemic Brain Is Controlled by Arteriolar Smooth Muscle Cell Contractility and Not by Capillary Pericytes. *Neuron*, *87*(1), 95-110. https://doi.org/10.1016/j.neuron.2015.06.001

Hires, S. A., Zhu, Y. L., & Tsien, R. Y. (2008). Optical measurement of synaptic glutamate spillover and reuptake by linker optimized glutamate-sensitive fluorescent reporters. *Proceedings of the National Academy of Sciences of the United States of America*, *105*(11), 4411-4416. https://doi.org/10.1073/pnas.0712008105

Hofer, S. B., Mrsic-Flogel, T. D., Bonhoeffer, T., & Hubener, M. (2009). Experience leaves a lasting structural trace in cortical circuits [Article]. *Nature*, *457*(7227), 313-U314. https://doi.org/10.1038/nature07487

Hoge, R. D. (2012). Calibrated fMRI. *Neuroimage*, *62*(2), 930-937. https://doi.org/10.1016/j.neuroimage.2012.02.022

Hoge, R. D., Atkinson, J., Gill, B., Crelier, G. R., Marrett, S., & Pike, G. B. (1999a). Investigation of BOLD signal dependence on cerebral blood flow and oxygen consumption: The deoxyhemoglobin dilution model. *Magnetic Resonance in Medicine*, *42*(5), 849-863. https://doi.org/10.1002/(sici)1522-2594(199911)42:5<849::Aid-mrm4>3.0.Co;2-z

Hoge, R. D., Atkinson, J., Gill, B., Crelier, G. R., Marrett, S., & Pike, G. B. (1999b). Linear coupling between cerebral blood flow and oxygen consumption in activated human cortex. *Proceedings of the National Academy of Sciences of the United States of America*, *96*(16), 9403-9408. https://doi.org/10.1073/pnas.96.16.9403
Hoge, R. D., Atkinson, J., Gill, B., Crelier, G. R., Marrett, S., & Pike, G. B. (1999c). Stimulus-dependent BOLD and perfusion dynamics in human V1. *Neuroimage*, *9*(6), 573-585. https://doi.org/10.1006/nimg.1999.0443
Hohwy, J., Roepstorff, A., & Friston, K. J. (2008). Predictive coding explains binocular rivalry: An epistemological review. *Cognition*, *108*(3), 687-701. https://doi.org/10.1016/j.cognition.2008.05.010
Holland, D., Kuperman, J. M., & Dale, A. M. (2010). Efficient correction of inhomogeneous static magnetic field-induced distortion in Echo Planar Imaging [Article]. *Neuroimage*, *50*(1), 175-183. https://doi.org/10.1016/j.neuroimage.2009.11.044
Hollins, M., & Hudnell, K. (1980). Adaptation of the binocular rivalry mechanism. *Investigative Ophthalmology & Visual Science*, *19*(9), 1117-1120.
Hosford, P. S., & Gourine, A. V. (2019). What is the key mediator of the neurovascular coupling response? *Neuroscience and Biobehavioral Reviews*, *96*, 174-181. https://doi.org/10.1016/j.neubiorev.2018.11.011
Howarth, C., Gleeson, P., & Attwell, D. (2012). Updated energy budgets for neural computation in the neocortex and cerebellum. *J Cereb Blood Flow Metab*, *32*(7), 1222-1232. https://doi.org/10.1038/jcbfm.2012.35
Howarth, C., Mishra, A., & Hall, C. N. (2021). More than just summed neuronal activity: how multiple cell types shape the BOLD response. *Philos Trans R Soc Lond B Biol Sci*, *376*(1815), 20190630. https://doi.org/10.1098/rstb.2019.0630
Hu, X. P., & Yacoub, E. (2012). The story of the initial dip in fMRI. *Neuroimage*, *62*(2), 1103-1108. https://doi.org/10.1016/j.neuroimage.2012.03.005
Hua, J., Liu, P., Kim, T., Donahue, M., Rane, S., Chen, J. J., Qin, Q., & Kim, S. G. (2019). MRI techniques to measure arterial and venous cerebral blood volume. *Neuroimage*, *187*, 17-31. https://doi.org/10.1016/j.neuroimage.2018.02.027
Huang, C. B., Zhou, J. W., Lu, Z. L., Feng, L. X., & Zhou, Y. F. (2009). Binocular combination in anisometropic amblyopia [Article]. *Journal of Vision*, *9*(3), 16, Article 17. https://doi.org/10.1167/9.3.17
Huang, P. C., & Chen, C. C. (2016). Contrast Gain Control in Plaid Pattern Detection. *Plos One*, *11*(10), Article e0164171. https://doi.org/10.1371/journal.pone.0164171
Huang, X. Y., Elyada, Y. M., Bosking, W. H., Walker, T., & Fitzpatrick, D. (2014). Optogenetic Assessment of Horizontal Interactions in Primary Visual Cortex. *Journal of Neuroscience*, *34*(14), 4976-4990. https://doi.org/10.1523/jneurosci.4116-13.2014
Huang, Y. Z., Chen, R. S., Rothwell, J. C., & Wen, H. Y. (2007). The after-effect of human theta burst stimulation is NMDA receptor dependent [Article]. *Clinical Neurophysiology*, *118*(5), 1028-1032. https://doi.org/10.1016/j.clinph.2007.01.021
Huang, Y. Z., Edwards, M. J., Rounis, E., Bhatia, K. P., & Rothwell, J. C. (2005). Theta burst stimulation of the human motor cortex. *Neuron*, *45*(2), 201-206. https://doi.org/10.1016/j.neuron.2004.12.033
Hubel, D. H., & Wiesel, T. N. (1962). RECEPTIVE FIELDS, BINOCULAR INTERACTION AND FUNCTIONAL ARCHITECTURE IN CATS VISUAL CORTEX. *Journal of Physiology-London*, *160*(1), 106-&. https://doi.org/10.1113/jphysiol.1962.sp006837
Hubel, D. H., & Wiesel, T. N. (1974). SEQUENCE REGULARITY AND GEOMETRY OF ORIENTATION COLUMNS IN MONKEY STRIATE CORTEX. *Journal of Comparative Neurology*, *158*(3), 267-294. https://doi.org/10.1002/cne.901580304
Huber, L., Goense, J., Kennerley, A. J., Ivanov, D., Krieger, S. N., Lepsien, J., Trampel, R., Turner, R., & Moller, H. E. (2014). Investigation of the neurovascular coupling in positive and negative BOLD responses in human brain at 7 T. *Neuroimage*, *97*, 349-362. https://doi.org/10.1016/j.neuroimage.2014.04.022
Huber, L., Uludag, K., & Moller, H. E. (2019). Non-BOLD contrast for laminar fMRI in humans: CBF, CBV, and CMRO2. *Neuroimage*, *197*, 742-760. https://doi.org/10.1016/j.neuroimage.2017.07.041
Hulme, S. R., Jones, O. D., & Abraham, W. C. (2013). Emerging roles of metaplasticity in behaviour and disease. *Trends in Neurosciences*, *36*(6), 353-362. https://doi.org/10.1016/j.tins.2013.03.007
Hupe, J. M., Signorelli, C. M., & Alais, D. (2019). Two paradigms of bistable plaid motion reveal independent mutual inhibition processes [Article]. *Journal of Vision*, *19*(4), 16, Article 5. https://doi.org/10.1167/19.4.5

Hyder, F., Patel, A. B., Gjedde, A., Rothman, D. L., Behar, K. L., & Shulman, R. G. (2006). Neuronal-glial glucose oxidation and glutamatergic-GABAergic function. *J Cereb Blood Flow Metab*, *26*(7), 865-877. https://doi.org/10.1038/sj.jcbfm.9600263

Hyder, F., Sanganahalli, B. G., Herman, P., Coman, D., Maandag, N. J., Behar, K. L., Blumenfeld, H., & Rothman, D. L. (2010). Neurovascular and Neurometabolic Couplings in Dynamic Calibrated fMRI: Transient Oxidative Neuroenergetics for Block-Design and Event-Related Paradigms. *Front Neuroenergetics*, *2*. https://doi.org/10.3389/fnene.2010.00018

Iacaruso, M. F., Gasler, I. T., & Hofer, S. B. (2017). Synaptic organization of visual space in primary visual cortex. *Nature*, *547*(7664), 449-+. https://doi.org/10.1038/nature23019

Iadecola, C. (2017). The Neurovascular Unit Coming of Age: A Journey through Neurovascular Coupling in Health and Disease. *Neuron*, *96*(1), 17-42. https://doi.org/10.1016/j.neuron.2017.07.030

Ido, Y., Chang, K., & Williamson, J. R. (2004). NADH augments blood flow in physiologically activated retina and visual cortex [Article]. *Proceedings of the National Academy of Sciences of the United States of America*, *101*(2), 653-658. https://doi.org/10.1073/pnas.0307458100

Ilic, T. V., Meintzschel, F., Cleff, U., Ruge, D., Kessler, K. R., & Ziemann, U. (2002). Short-interval paired-pulse inhibition and facilitation of human motor cortex: the dimension of stimulus intensity [Article]. *Journal of Physiology-London*, *545*(1), 153-167. https://doi.org/10.1113/jphysiol.2002.030122

Ip, I. B., Berrington, A., Hess, A. T., Parker, A. J., Emir, U. E., & Bridge, H. (2017). Combined fMRI-MRS acquires simultaneous glutamate and BOLD-fMRI signals in the human brain [Article]. *Neuroimage*, *155*, 113-119. https://doi.org/10.1016/j.neuroimage.2017.04.030

Ip, I. B., & Bridge, H. (2021). Investigating the neurochemistry of the human visual system using magnetic resonance spectroscopy [Review; Early Access]. *Brain Struct Funct*, 15. https://doi.org/10.1007/s00429-021-02273-0

Ip, I. B., Emir, U. E., Lunghi, C., Parker, A. J., & Bridge, H. (2021). GABAergic inhibition in the human visual cortex relates to eye dominance. *Scientific Reports*, *11*(1), Article 17022. https://doi.org/10.1038/s41598-021-95685-1

Isaacson, J. S., & Scanziani, M. (2011). How Inhibition Shapes Cortical Activity. *Neuron*, *72*(2), 231-243. https://doi.org/10.1016/j.neuron.2011.09.027

Jack, C. R., Thompson, R. M., Butts, R. K., Sharbrough, F. W., Kelly, P. J., Hanson, D. P., Riederer, S. J., Ehman, R. L., Hangiandreou, N. J., & Cascino, G. D. (1994). SENSORY-MOTOR CORTEX - CORRELATION OF PRESURGICAL MAPPING WITH FUNCTIONAL MR-IMAGING AND INVASIVE CORTICAL MAPPING [Article]. *Radiology*, *190*(1), 85-92. https://doi.org/10.1148/radiology.190.1.8259434

Jakobsson, P. (1985). BINOCULAR INTERACTION IN THE VEP TO GRATING STIMULATION .1. ORIENTATIONAL EFFECTS. *Acta Ophthalmologica*, *63*(2), 183-191. https://doi.org/10.1111/j.1755-3768.1985.tb01532.x

Jang, J., Song, M., & Paik, S. B. (2020). Retino-Cortical Mapping Ratio Predicts Columnar and Salt-and-Pepper Organization in Mammalian Visual Cortex [Article]. *Cell Reports*, *30*(10), 3270-+. https://doi.org/10.1016/j.celrep.2020.02.038

Jelen, L. A., King, S., Mullins, P. G., & Stone, J. M. (2018). Beyond static measures: A review of functional magnetic resonance spectroscopy and its potential to investigate dynamic glutamatergic abnormalities in schizophrenia [Review]. *Journal of Psychopharmacology*, *32*(5), 497-508. https://doi.org/10.1177/0269881117747579

Jia, F., Xie, X. Q., & Zhou, Y. F. (2004). Short-term depression of synaptic transmission from rat lateral geniculate nucleus to primary visual cortex in vivo. *Brain Research*, *1002*(1-2), 158-161. https://doi.org/10.1016/j.brainres.2004.01.001

Jobst, B. C., Bartolomei, F., Diehl, B., Frauscher, B., Kahane, P., Minotti, L., Sharan, A., Tardy, N., Worrell, G., & Gotman, J. (2020). Intracranial EEG in the 21st Century. *Epilepsy Currents*, *20*(4), 180-188, Article 1535759720934852. https://doi.org/10.1177/1535759720934852

Jonas, E., & Kording, K. P. (2017). Could a Neuroscientist Understand a Microprocessor? [Article]. *Plos Computational Biology*, *13*(1), 24, Article e1005268. https://doi.org/10.1371/journal.pcbi.1005268

Jones, O. P., Alfaro-Almagro, F., & Jbabdi, S. (2018). An empirical, 21st century evaluation of phrenology [Article]. *Cortex*, *106*, 26-35. https://doi.org/10.1016/j.cortex.2018.04.011

Kaczor, P. T., & Mozrzymas, J. W. (2017). Key Metabolic Enzymes Underlying Astrocytic Upregulation of GABAergic Plasticity. *Frontiers in Cellular Neuroscience*, *11*, Article 144. https://doi.org/10.3389/fncel.2017.00144

Kaderali, S., Kim, Y. J., Reynaud, A., & Mullen, K. T. (2015). The Role of Human Brain Area hMT plus in the Perception of Global Motion Investigated With Repetitive Transcranial Magnetic Stimulation (rTMS) [Article]. *Brain Stimulation*, *8*(2), 200-207. https://doi.org/10.1016/j.brs.2014.11.001

Kakei, S., Hoffman, D. S., & Strick, P. L. (1999). Muscle and movement representations in the primary motor cortex. *Science*, *285*(5436), 2136-2139. https://doi.org/10.1126/science.285.5436.2136

Kamitani, Y., & Tong, F. (2005). Decoding the visual and subjective contents of the human brain. *Nature Neuroscience*, *8*(5), 679-685. https://doi.org/10.1038/nn1444

Kammer, T. (1999). Phosphenes and transient scotomas induced by magnetic stimulation of the occipital lobe: their topographic relationship [Article]. *Neuropsychologia*, *37*(2), 191-198. https://doi.org/10.1016/S0028-3932(98)00093-1

Kammer, T., Puls, K., Erb, M., & Grodd, W. (2005). Transcranial magnetic stimulation in the visual system. II. Characterization of induced phosphenes and scotomas [Article]. *Experimental Brain Research*, *160*(1), 129-140. https://doi.org/10.1007/s00221-004-1992-0

Kammer, T., Puls, K., Strasburger, H., Hill, N. J., & Wichmann, F. A. (2005). Transcranial magnetic stimulation in the visual system. I. The psychophysics of visual suppression [Article]. *Experimental Brain Research*, *160*(1), 118-128. https://doi.org/10.1007/s00221-004-1991-1

Kang, M. S., Lee, S. H., Kim, J., Heeger, D., & Blake, R. (2010). Modulation of spatiotemporal dynamics of binocular rivalry by collinear facilitation and pattern-dependent adaptation. *Journal of Vision*, *10*(11), Article 3. https://doi.org/10.1167/10.11.3

Kastner, S., Demmer, I., & Ziemann, U. (1998). Transient visual field defects induced by transcranial magnetic stimulation over human occipital pole [Article]. *Experimental Brain Research*, *118*(1), 19-26. https://doi.org/10.1007/s002210050251

Kastrup, A., Baudewig, J., Schnaudigel, S., Huonker, R., Becker, L., Sohns, J. M., Dechent, P., Klingner, C., & Witte, O. W. (2008). Behavioral correlates of negative BOLD signal changes in the primary somatosensory cortex. *Neuroimage*, *41*(4), 1364-1371. https://doi.org/10.1016/j.neuroimage.2008.03.049

Kato, H. K., Gillet, S. N., & Isaacson, J. S. (2015). Flexible Sensory Representations in Auditory Cortex Driven by Behavioral Relevance. *Neuron*, *88*(5), 1027-1039. https://doi.org/10.1016/j.neuron.2015.10.024

Katyal, S., Engel, S. A., He, B., & He, S. (2016). Neurons that detect interocular conflict during binocular rivalry revealed with EEG. *Journal of Vision*, *16*(3), Article 18. https://doi.org/10.1167/16.3.18

Katz, L. C., Gilbert, C. D., & Wiesel, T. N. (1989). Local circuits and ocular dominance columns in monkey striate cortex [Article]. *J Neurosci*, *9*(4), 1389-1399. https://doi.org/10.1523/JNEUROSCI.09-04-01389.1989

Katzner, S., Born, G., & Busse, L. (2019). V1 microcircuits underlying mouse visual behavior. *Current Opinion in Neurobiology*, *58*, 191-198. https://doi.org/10.1016/j.conb.2019.09.006

Katzner, S., Busse, L., & Carandini, M. (2011). GABA(A) Inhibition Controls Response Gain in Visual Cortex [Article]. *Journal of Neuroscience*, *31*(16), 5931-5941. https://doi.org/10.1523/jneurosci.5753-10.2011

Kauppinen, R. A., & Williams, S. R. (1991). NONDESTRUCTIVE DETECTION OF GLUTAMATE BY H-1 NUCLEAR-MAGNETIC-RESONANCE SPECTROSCOPY IN CORTICAL BRAIN-SLICES FROM THE GUINEA-PIG - EVIDENCE FOR CHANGES IN DETECTABILITY DURING SEVERE ANOXIC INSULTS [Article]. *Journal of Neurochemistry*, *57*(4), 1136-1144. https://doi.org/10.1111/j.1471-4159.1991.tb08271.x

Kay, K., Jamison, K. W., Vizioli, L., Zhang, R. Y., Margalit, E., & Ugurbil, K. (2019). A critical assessment of data quality and venous effects in sub-millimeter fMRI [Article]. *Neuroimage*, *189*, 847-869. https://doi.org/10.1016/j.neuroimage.2019.02.006

Keller, A. J., Dipoppa, M., Roth, M. M., Caudill, M. S., Ingrosso, A., Miller, K. D., & Scanziani, M. (2020). A Disinhibitory Circuit for Contextual Modulation in Primary Visual Cortex. *Neuron*, *108*(6). https://doi.org/10.1016/j.neuron.2020.11.013

Keller, A. J., & Martin, K. A. C. (2015). Local Circuits for Contrast Normalization and Adaptation Investigated with Two-Photon Imaging in Cat Primary Visual Cortex [Article]. *Journal of Neuroscience*, *35*(27), 10078-10087. https://doi.org/10.1523/jneurosci.0906-15.2015

Khammash, D., Simmonite, M., Polk, T. A., Taylor, S. F., & Meehan, S. K. (2019a). Probing short-latency cortical inhibition in the visual cortex with transcranial magnetic stimulation: A reliability study [Article]. *Brain Stimulation*, *12*(3), 702-704. https://doi.org/10.1016/j.brs.2019.01.013

Khammash, D., Simmonite, M., Polk, T. A., Taylor, S. F., & Meehan, S. K. (2019b). Temporal Dynamics of Corticocortical Inhibition in Human Visual Cortex: A TMS Study [Article]. *Neuroscience*, *421*, 31-38. https://doi.org/10.1016/j.neuroscience.2019.10.003

Kiemes, A., Davies, C., Kempton, M. J., Lukow, P. B., Bennallick, C., Stone, J. M., & Modinos, G. (2021). GABA, Glutamate and Neural Activity: A Systematic Review With Meta-Analysis of Multimodal H-1-MRS-fMRI Studies. *Frontiers in Psychiatry*, *12*, Article 644315. https://doi.org/10.3389/fpsyt.2021.644315

Kim, H. W., Kim, C. Y., & Blake, R. (2017). Monocular Perceptual Deprivation from Interocular Suppression Temporarily Imbalances Ocular Dominance [Article]. *Current Biology*, *27*(6), 884-889. https://doi.org/10.1016/j.cub.2017.01.063

Kim, S. G. (2018). Biophysics of BOLD fMRI investigated with animal models. *Journal of Magnetic Resonance*, *292*, 82-89. https://doi.org/10.1016/j.jmr.2018.04.006

Kim, S. G., & Ogawa, S. (2012). Biophysical and physiological origins of blood oxygenation level-dependent fMRI signals. *Journal of Cerebral Blood Flow and Metabolism*, *32*(7), 1188-1206. https://doi.org/10.1038/jcbfm.2012.23

Kim, Y. J., Gheiratmand, M., & Mullen, K. T. (2013). Cross-orientation masking in human color vision: Application of a two-stage model to assess dichoptic and monocular sources of suppression. *Journal of Vision*, *13*(6), Article 15. https://doi.org/10.1167/13.6.15

Kim, Y. J., & Mullen, K. T. (2015). The dynamics of cross-orientation masking at monocular and interocular sites [Article]. *Vision Research*, *116*, 80-91. https://doi.org/10.1016/j.visres.2015.09.008

Kingdom, F. A. A., Jennings, B. J., & Georgeson, M. A. (2018). Adaptation to interocular difference [Article]. *Journal of Vision*, *18*(5), 11, Article 9. https://doi.org/10.1167/18.5.9

Kingsmith, P. E., Grigsby, S. S., Vingrys, A. J., Benes, S. C., & Supowit, A. (1994). EFFICIENT AND UNBIASED MODIFICATIONS OF THE QUEST THRESHOLD METHOD - THEORY, SIMULATIONS, EXPERIMENTAL EVALUATION AND PRACTICAL IMPLEMENTATION [Article]. *Vision Research*, *34*(7), 885-912. https://doi.org/10.1016/0042-6989(94)90039-6

Kirchberger, L., Mukherjee, S., Schnabel, U. H., Van Beest, E. H., Barsegyan, A., Levelt, C. N., Heimel, J. A., Lorteije, J. A. M., Van der Togt, C., Self, M. W., & Roelfsema, P. R. (2021). The essential role of recurrent processing for figure-ground perception in mice. *Science Advances*, *7*(27), Article eabe1833. https://doi.org/10.1126/sciadv.abe1833

Kisler, K., Nelson, A. R., Montagne, A., & Zlokovic, B. V. (2017). Cerebral blood flow regulation and neurovascular dysfunction in Alzheimer disease. *Nat Rev Neurosci*, *18*(7), 419-434. https://doi.org/10.1038/nrn.2017.48

Kleiner, M., Brainard, D., & Pelli, D. (2007). What's new in Psychtoolbox-3? [Meeting Abstract]. *Perception*, *36*, 14-14.

Klink, P. C., Brascamp, J. W., Blake, R., & van Wezel, R. J. A. (2010). Experience-Driven Plasticity in Binocular Vision. *Current Biology*, *20*(16), 1464-1469. https://doi.org/10.1016/j.cub.2010.06.057

Kohn, A. (2007). Visual adaptation: Physiology, mechanisms, and functional benefits [Review]. *Journal of Neurophysiology*, *97*(5), 3155-3164. https://doi.org/10.1152/jn.00086.2007

Kolasinski, J., Hinson, E. L., Divanbeighi Zand, A. P., Rizov, A., Emir, U. E., & Stagg, C. J. (2019). The dynamics of cortical GABA in human motor learning. *J Physiol*, *597*(1), 271-282. https://doi.org/10.1113/JP276626

Koo, B., Choi, B., Park, H., & Yoon, K. J. (2019). Past, Present, and Future of Brain Organoid Technology. *Molecules and Cells*, *42*(9), 617-627. https://doi.org/10.14348/molcells.2019.0162

Koolschijn, R. S., Shpektor, A., Clarke, W. T., Ip, I. B., Dupret, D., Emir, U. E., & Barron, H. C. (2021). Memory recall involves a transient break in excitatory-inhibitory balance [Article]. *Elife*, *10*, 29, Article e70071. https://doi.org/10.7554/eLife.70071; 10.7554/eLife.70071.sa1; 10.7554/eLife.70071.sa2

Kosslyn, S. M., Pascual-Leone, A., Felician, O., Camposano, S., Keenan, J. P., Thompson, W. L., Ganis, G., Sukel, K. E., & Alpert, N. M. (1999). The role of Area 17 in visual imagery: Convergent evidence from PET and rTMS. *Science*, *284*(5411), 167-170. https://doi.org/10.1126/science.284.5411.167

Kovacs, I., Papathomas, T. V., Yang, M., & Feher, A. (1996). When the brain changes its mind: Interocular grouping during binocular rivalry. *Proceedings of the National Academy of Sciences of the United States of America*, *93*(26), 15508-15511. https://doi.org/10.1073/pnas.93.26.15508

Kozyrev, V., Eysel, U. T., & Jancke, D. (2014). Voltage-sensitive dye imaging of transcranial magnetic stimulation-induced intracortical dynamics. *Proceedings of the National Academy of Sciences of the United States of America*, *111*(37), 13553-13558. https://doi.org/10.1073/pnas.1405508111

Kozyrev, V., Staadt, R., Eysel, U. T., & Jancke, D. (2018). TMS-induced neuronal plasticity enables targeted remodeling of visual cortical maps [Article]. *Proceedings of the National Academy of Sciences of the United States of America*, *115*(25), 6476-6481. https://doi.org/10.1073/pnas.1802798115

Krauss, J. K., Lipsman, N., Aziz, T., Boutet, A., Brown, P., Chang, J. W., Davidson, B., Grill, W. M., Hariz, M. I., Horn, A., Schulder, M., Mammis, A., Tass, P. A., Volkmann, J., & Lozano, A. M. (2021). Technology of deep brain stimulation: current status and future directions. *Nature Reviews Neurology*, *17*(2), 75-87. https://doi.org/10.1038/s41582-020-00426-z

Krawchuk, M. B., Ruff, C. F., Yang, X. L., Ross, S. E., & Vazquez, A. L. (2020). Optogenetic assessment of VIP, PV, SOM and NOS inhibitory neuron activity and cerebral blood flow regulation in mouse somato-sensory cortex. *Journal of Cerebral Blood Flow and Metabolism*, *40*(7), 1427-1440, Article 0271678x19870105. https://doi.org/10.1177/0271678x19870105

Krieger, S. N., Streicher, M. N., Trampel, R., & Turner, R. (2012). Cerebral blood volume changes during brain activation. *Journal of Cerebral Blood Flow and Metabolism*, *32*(8), 1618-1631. https://doi.org/10.1038/jcbfm.2012.63

Kriegeskorte, N., Cusack, R., & Bandettini, P. (2010). How does an fMRI voxel sample the neuronal activity pattern: Compact-kernel or complex spatiotemporal filter? *Neuroimage*, *49*(3), 1965-1976. https://doi.org/10.1016/j.neuroimage.2009.09.059

Kriegeskorte, N., & Diedrichsen, J. (2016). Inferring brain-computational mechanisms with models of activity measurements. *Philosophical Transactions of the Royal Society B-Biological Sciences*, *371*(1705). https://doi.org/10.1098/rstb.2016.0278

Kriegeskorte, N., Simmons, W. K., Bellgowan, P. S. F., & Baker, C. I. (2009). Circular analysis in systems neuroscience: the dangers of double dipping. *Nature Neuroscience*, *12*(5), 535-540. https://doi.org/10.1038/nn.2303

Kujirai, T., Caramia, M. D., Rothwell, J. C., Day, B. L., Thompson, P. D., Ferbert, A., Wroe, S., Asselman, P., & Marsden, C. D. (1993). CORTICOCORTICAL INHIBITION IN HUMAN MOTOR CORTEX [Article]. *Journal of Physiology-London*, *471*, 501-519. https://doi.org/10.1113/jphysiol.1993.sp019912

Kullander, K., & Topolnik, L. (2021). Cortical disinhibitory circuits: cell types, connectivity and function. *Trends in Neurosciences*, *44*(8), 643-657. https://doi.org/10.1016/j.tins.2021.04.009

Kuravi, P., & Vogels, R. (2018). GABAergic and cholinergic modulation of repetition suppression in inferior temporal cortex. *Scientific Reports*, *8*, Article 13160. https://doi.org/10.1038/s41598-018-31515-1

Kwon, M. Y., Legge, G. E., Fang, F., Cheong, A. M. Y., & He, S. (2009). Adaptive changes in visual cortex following prolonged contrast reduction [Article]. *Journal of Vision*, *9*(2), 16, Article 20. https://doi.org/10.1167/9.2.20

Laing, C. R., & Chow, C. C. (2002). A spiking neuron model for binocular rivalry. *Journal of Computational Neuroscience*, *12*(1), 39-53. https://doi.org/10.1023/a:1014942129705

Lea-Carnall, C. A., El-Deredy, W., Williams, S. R., Stagg, C. J., & Trujillo-Barreto, N. J. (2021). From synaptic activity to human in vivo quantification of neurotransmitter dynamics: a neural modelling approach [Preprint posted online March 12, 2021]. *bioRxiv*. https://doi.org/10.1101/2021.03.11.434540

Lee, J. H., Durand, R., Gradinaru, V., Zhang, F., Goshen, I., Kim, D. S., Fenno, L. E., Ramakrishnan, C., & Deisseroth, K. (2010). Global and local fMRI signals driven by neurons defined optogenetically by type and wiring. *Nature*, *465*(7299), 788-792. https://doi.org/10.1038/nature09108

Lee, J. H., Koch, C., & Mihalas, S. (2017). A Computational Analysis of the Function of Three Inhibitory Cell Types in Contextual Visual Processing. *Frontiers in Computational Neuroscience*, *11*, Article 28. https://doi.org/10.3389/fncom.2017.00028

Lee, J. H., Stile, C. L., Bice, A. R., Rosenthal, Z. P., Yan, P., Snyder, A. Z., Lee, J. M., & Bauer, A. Q. (2021). Opposed hemodynamic responses following increased excitation and parvalbumin-based inhibition. *Journal of Cerebral Blood Flow and Metabolism*, *41*(4), 841-856, Article 0271678x20930831. https://doi.org/10.1177/0271678x20930831

Lee, L., Boorman, L., Glendenning, E., Christmas, C., Sharp, P., Redgrave, P., Shabir, O., Bracci, E., Berwick, J., & Howarth, C. (2020). Key Aspects of Neurovascular Control Mediated by Specific Populations of Inhibitory Cortical Interneurons. *Cerebral Cortex*, *30*(4), 2452-2464. https://doi.org/10.1093/cercor/bhz251

Lee, S. H., Kwan, A. C., Zhang, S. Y., Phoumthipphavong, V., Flannery, J. G., Masmanidis, S. C., Taniguchi, H., Huang, Z. J., Zhang, F., Boyden, E. S., Deisseroth, K., & Dan, Y. (2012). Activation of specific interneurons improves

V1 feature selectivity and visual perception. *Nature*, *488*(7411), 379-+. https://doi.org/10.1038/nature11312
Lefaucheur, J. P., Aleman, A., Baeken, C., Benninger, D. H., Brunelin, J., Di Lazzaro, V., Filipovic, S. R., Grefkes, C., Hasan, A., Hummel, F. C., Jaaskelainen, S. K., Langguth, B., Leocani, L., Londero, A., Nardone, R., Nguyen, J. P., Nyffeler, T., Oliveira-Maia, A. J., Oliviero, A., . . . Ziemann, U. (2020). Evidence-based guidelines on the therapeutic use of repetitive transcranial magnetic stimulation (rTMS): An update (2014-2018) [Review]. *Clinical Neurophysiology*, *131*(2), 474-528. https://doi.org/10.1016/j.clinph.2019.11.002
Lehky, S. R. (1988). AN ASTABLE-MULTIVIBRATOR MODEL OF BINOCULAR-RIVALRY. *Perception*, *17*(2), 215-228. https://doi.org/10.1068/p170215
Lesmes, L. A., Jeon, S. T., Lu, Z. L., & Dosher, B. A. (2006). Bayesian adaptive estimation of threshold versus contrast external noise functions: The quick TvC method. *Vision Research*, *46*(19), 3160-3176. https://doi.org/10.1016/j.visres.2006.04.022
Levelt, W. J. M. (1966). ALTERNATION PROCESS IN BINOCULAR RIVALRY. *British Journal of Psychology*, *57*, 225-&. https://doi.org/10.1111/j.2044-8295.1966.tb01023.x
Levelt, W. J. M. (1968). *On binocular rivalry*. Mouton.
Levy, L. M., Ziemann, U., Chen, R., & Cohen, L. G. (2002). Rapid modulation of GABA in sensorimotor cortex induced by acute deafferentation [Article]. *Annals of Neurology*, *52*(6), 755-761. https://doi.org/10.1002/ana.10372
Lewis, L. D., Setsompop, K., Rosen, B. R., & Polimeni, J. R. (2016). Fast fMRI can detect oscillatory neural activity in humans. *Proceedings of the National Academy of Sciences of the United States of America*, *113*(43), E6679-E6685. https://doi.org/10.1073/pnas.1608117113
Li, B. S., Virtanen, J. P., Oeltermann, A., Schwarz, C., Giese, M. A., Ziemann, U., & Benali, A. (2017). Lifting the veil on the dynamics of neuronal activities evoked by transcranial magnetic stimulation. *Elife*, *6*, Article e30552. https://doi.org/10.7554/eLife.30552
Li, B. W., & Freeman, R. D. (2011). Neurometabolic coupling differs for suppression within and beyond the classical receptive field in visual cortex. *Journal of Physiology-London*, *589*(13), 3175-3190. https://doi.org/10.1113/jphysiol.2011.205039
Li, B. W., Peterson, M. R., Thompson, J. K., Duong, T., & Freeman, R. D. (2005). Cross-orientation suppression: Monoptic and dichoptic mechanisms are different. *Journal of Neurophysiology*, *94*(2), 1645-1650. https://doi.org/10.1152/jn.00203.2005
Li, H., Heise, K. F., Chalavi, S., Puts, N. A. J., Edden, R. A. E., & Swinnen, S. P. (2022). The role of MRS-assessed GABA in human behavioral performance. *Prog Neurobiol*, 102247. https://doi.org/10.1016/j.pneurobio.2022.102247
Liang, C. L., Ances, B. M., Perthen, J. E., Moradi, F., Liau, J., Buracas, G. T., Hopkins, S. R., & Buxton, R. B. (2013). Luminance contrast of a visual stimulus modulates the BOLD response more than the cerebral blood flow response in the human brain. *Neuroimage*, *64*, 104-111. https://doi.org/10.1016/j.neuroimage.2012.08.077
Lien, A. D., & Scanziani, M. (2013). Tuned thalamic excitation is amplified by visual cortical circuits. *Nature Neuroscience*, *16*(9), 1315-U1207. https://doi.org/10.1038/nn.3488
Lin, A. L., Fox, P. T., Hardies, J., Duong, T. Q., & Gao, J. H. (2010). Nonlinear coupling between cerebral blood flow, oxygen consumption, and ATP production in human visual cortex. *Proc Natl Acad Sci U S A*, *107*(18), 8446-8451. https://doi.org/10.1073/pnas.0909711107
Lin, A. L., Fox, P. T., Yang, Y. H., Lu, H. Z., Tan, L. H., & Gao, J. H. (2008). Evaluation of MRI models in the measurement of CMRO2 and its relationship with CBF. *Magnetic Resonance in Medicine*, *60*(2), 380-389. https://doi.org/10.1002/mrm.21655
Lin, A. L., Fox, P. T., Yang, Y. H., Lu, H. Z., Tan, L. H., & Gao, J. H. (2009). Time-dependent correlation of cerebral blood flow with oxygen metabolism in activated human visual cortex as measured by fMRI. *Neuroimage*, *44*(1), 16-22. https://doi.org/10.1016/j.neuroimage.2008.08.029
Lin, Y., Stephenson, M. C., Xin, L. J., Napolitano, A., & Morris, P. G. (2012). Investigating the metabolic changes due to visual stimulation using functional proton magnetic resonance spectroscopy at 7 T [Article]. *Journal of Cerebral Blood Flow and Metabolism*, *32*(8), 1484-1495. https://doi.org/10.1038/jcbfm.2012.33
Lin, Y. J., Shukla, L., Dugue, L., Valero-Cabre, A., & Carrasco, M. (2021). Transcranial magnetic stimulation entrains alpha oscillatory activity in occipital cortex. *Scientific Reports*, *11*(1), Article 18562. https://doi.org/10.1038/s41598-021-96849-9

Ling, S., Pearson, J., & Blake, R. (2009). Dissociation of Neural Mechanisms Underlying Orientation Processing in Humans. *Current Biology*, *19*(17), 1458-1462. https://doi.org/10.1016/j.cub.2009.06.069
Litwin-Kumar, A., Rosenbaum, R., & Doiron, B. (2016). Inhibitory stabilization and visual coding in cortical circuits with multiple interneuron subtypes. *Journal of Neurophysiology*, *115*(3), 1399-1409. https://doi.org/10.1152/jn.00732.2015
Liu, B. H., Li, P. Y., Sun, Y. J. J., Li, Y. T., Zhang, L. I., & Tao, H. W. (2010). Intervening inhibition underlies simple-cell receptive field structure in visual cortex. *Nature Neuroscience*, *13*(1), 89-U256. https://doi.org/10.1038/nn.2443
Liu, B. H., Li, Y. T., Ma, W. P., Pan, C. J., Zhang, L. I., & Tao, H. W. (2011). Broad Inhibition Sharpens Orientation Selectivity by Expanding Input Dynamic Range in Mouse Simple Cells. *Neuron*, *71*(3), 542-554. https://doi.org/10.1016/j.neuron.2011.06.017
Liu, T. T. (2020). MRI in systems medicine. *Wiley Interdiscip Rev Syst Biol Med*, *12*(1), e1463. https://doi.org/10.1002/wsbm.1463
Logothetis, N. K. (2002). The neural basis of the blood-oxygen-level-dependent functional magnetic resonance imaging signal. *Philosophical Transactions of the Royal Society of London Series B-Biological Sciences*, *357*(1424), 1003-1037. https://doi.org/10.1098/rstb.2002.1114
Logothetis, N. K., Leopold, D. A., & Sheinberg, D. L. (1996). What is rivalling during binocular rivalry? *Nature*, *380*(6575), 621-624. https://doi.org/10.1038/380621a0
Lomber, S. G. (2017). What is the function of auditory cortex when it develops in the absence of acoustic input? [Article]. *Cognitive Development*, *42*, 49-61. https://doi.org/10.1016/j.cogdev.2017.02.007
Lopez-Munoz, F., Boya, J., & Alamo, C. (2006). Neuron theory, the cornerstone of neuroscience, on the centenary of the Nobel Prize award to Santiago Ramon y Cajal [Article]. *Brain Research Bulletin*, *70*(4-6), 391-405. https://doi.org/10.1016/j.brainresbull.2006.07.010
Lourenco, C. F., & Laranjinha, J. (2021). Nitric Oxide Pathways in Neurovascular Coupling Under Normal and Stress Conditions in the Brain: Strategies to Rescue Aberrant Coupling and Improve Cerebral Blood Flow. *Frontiers in Physiology*, *12*, Article 729201. https://doi.org/10.3389/fphys.2021.729201
Lourenco, J., Koukouli, F., & Bacci, A. (2020). Synaptic inhibition in the neocortex: Orchestration and computation through canonical circuits and variations on the theme. *Cortex*, *132*, 258-280. https://doi.org/10.1016/j.cortex.2020.08.015
Lu, H., Golay, X., Pekar, J. J., & Van Zijl, P. C. (2003). Functional magnetic resonance imaging based on changes in vascular space occupancy. *Magn Reson Med*, *50*(2), 263-274. https://doi.org/10.1002/mrm.10519
Luber, B., & Lisanby, S. H. (2014). Enhancement of human cognitive performance using transcranial magnetic stimulation (TMS) [Review]. *Neuroimage*, *85*, 961-970. https://doi.org/10.1016/j.neuroimage.2013.06.007
Lunghi, C., Burr, D. C., & Morrone, C. (2011). Brief periods of monocular deprivation disrupt ocular balance in human adult visual cortex. *Current Biology*, *21*(14), R538-R539. https://doi.org/10.1016/j.cub.2011.06.004
Lunghi, C., Burr, D. C., & Morrone, M. C. (2013). Long-term effects of monocular deprivation revealed with binocular rivalry gratings modulated in luminance and in color. *Journal of Vision*, *13*(6), Article 1. https://doi.org/10.1167/13.6.1
Lunghi, C., Emir, U., Morrone, M. C., Burr, D. C., & Bridge, H. (2014). Transient monocular deprivation affects binocular rivalry and GABA concentrations in adult human visual cortex. *Journal of Vision*, *14*(10), 378-378. https://doi.org/10.1167/14.10.378
Lunghi, C., Emir, U. E., Morrone, M. C., & Bridge, H. (2015). Short-Term Monocular Deprivation Alters GABA in the Adult Human Visual Cortex [Article]. *Current Biology*, *25*(11), 1496-1501. https://doi.org/10.1016/j.cub.2015.04.021
Maffei, A., Nataraj, K., Nelson, S. B., & Turrigiano, G. G. (2006). Potentiation of cortical inhibition by visual deprivation [Article]. *Nature*, *443*(7107), 81-84. https://doi.org/10.1038/nature05079
Maffei, A., & Turrigiano, G. G. (2008). Multiple modes of network homeostasis in visual cortical layer 2/3 [Article]. *Journal of Neuroscience*, *28*(17), 4377-4384. https://doi.org/10.1523/jneurosci.5298-07.2008
Mahmoud, S., Gharagozloo, M., Simard, C., & Gris, D. (2019). Astrocytes Maintain Glutamate Homeostasis in the CNS by Controlling the Balance between Glutamate Uptake and Release [Review]. *Cells*, *8*(2), 27, Article 184. https://doi.org/10.3390/cells8020184

Mangia, S., Giove, F., & DiNuzzo, M. (2012). Metabolic Pathways and Activity-Dependent Modulation of Glutamate Concentration in the Human Brain [Article]. *Neurochemical Research*, *37*(11), 2554-2561. https://doi.org/10.1007/s11064-012-0848-4

Mangia, S., Tkac, I., Gruetter, R., Van de Moortele, P. F., Maraviglia, B., & Ugurbil, K. (2007). Sustained neuronal activation raises oxidative metabolism to a new steady-state level: evidence from H-1 NMR spectroscopy in the human visual cortex [Article]. *Journal of Cerebral Blood Flow and Metabolism*, *27*(5), 1055-1063. https://doi.org/10.1038/sj.jcbfm.9600401

Maniglia, M., Trotter, Y., & Aedo-Jury, F. (2019). TMS reveals inhibitory extrastriate cortico-cortical feedback modulation of V1 activity in humans [Article; Early Access]. *Brain Struct Funct*, *224*(9), 3399-3408. https://doi.org/10.1007/s00429-019-01964-z

Mantini, D., Corbetta, M., Romani, G. L., Orban, G. A., & Vanduffel, W. (2013). Evolutionarily Novel Functional Networks in the Human Brain? [Article]. *Journal of Neuroscience*, *33*(8), 3259-3275. https://doi.org/10.1523/jneurosci.4392-12.2013

Marg, E., & Rudiak, D. (1994). PHOSPHENES INDUCED BY MAGNETIC STIMULATION OVER THE OCCIPITAL BRAIN - DESCRIPTION AND PROBABLE SITE OF STIMULATION [Article]. *Optometry and Vision Science*, *71*(5), 301-311. https://doi.org/10.1097/00006324-199405000-00001

Marr, D., & Hildreth, E. (1980). THEORY OF EDGE-DETECTION. *Proceedings of the Royal Society Series B-Biological Sciences*, *207*(1167), 187-217. https://doi.org/10.1098/rspb.1980.0020

Martin, D. L., & Rimvall, K. (1993). REGULATION OF GAMMA-AMINOBUTYRIC-ACID SYNTHESIS IN THE BRAIN [Review]. *Journal of Neurochemistry*, *60*(2), 395-407. https://doi.org/10.1111/j.1471-4159.1993.tb03165.x

Martin, K. A. C., Roth, S., & Rusch, E. S. (2014). Superficial layer pyramidal cells communicate heterogeneously between multiple functional domains of cat primary visual cortex. *Nature Communications*, *5*, Article 5252. https://doi.org/10.1038/ncomms6252

Martinez-Maestro, M., Labadie, C., & Moeller, H. E. (2019). Dynamic metabolic changes in human visual cortex in regions with positive and negative blood oxygenation level-dependent response [Article]. *Journal of Cerebral Blood Flow and Metabolism*, *39*(11), 2295-2307. https://doi.org/10.1177/0271678x18795426

Masainoto, K., Vazquez, A., Wang, P., & Kim, S. G. (2008). Trial-by-trial relationship between neural activity, oxygen consumption, and blood flow responses. *Neuroimage*, *40*(2), 442-450. https://doi.org/10.1016/j.neuroimage.2007.12.011

McGovern, D. P., Roach, N. W., & Webb, B. S. (2012). Perceptual Learning Reconfigures the Effects of Visual Adaptation. *Journal of Neuroscience*, *32*(39), 13621-13629. https://doi.org/10.1523/jneurosci.1363-12.2012

McKeefry, D. J., Gouws, A., Burton, M. P., & Morland, A. B. (2009). The Noninvasive Dissection of the Human Visual Cortex: Using fMRI and TMS to Study the Organization of the Visual Brain. *Neuroscientist*, *15*(5), 489-506. https://doi.org/10.1177/1073858409334424

McLean, J., & Palmer, L. A. (1996). Contrast adaptation and excitatory amino acid receptors in cat striate cortex. *Visual Neuroscience*, *13*(6), 1069-1087. https://doi.org/10.1017/s0952523800007720

Meese, T. S., & Baker, D. H. (2009). Cross-orientation masking is speed invariant between ocular pathways but speed dependent within them. *Journal of Vision*, *9*(5). https://doi.org/10.1167/9.5.2

Meese, T. S., & Baker, D. H. (2013). A common rule for integration and suppression of luminance contrast across eyes, space, time, and pattern. *I-Perception*, *4*(1), 1-16. https://doi.org/10.1068/i0556

Meese, T. S., & Holmes, D. J. (2007). Spatial and temporal dependencies of cross-orientation suppression in human vision. *Proceedings of the Royal Society B-Biological Sciences*, *274*(1606), 127-136. https://doi.org/10.1098/rspb.2006.3697

Meese, T. S., Summers, R. J., Holmes, D. J., & Wallis, S. A. (2007). Contextual modulation involves suppression and facilitation from the center and the surround [Review]. *Journal of Vision*, *7*(4), 21, Article 7. https://doi.org/10.1167/7.4.7

Mekle, R., Kuhn, S., Pfeiffer, H., Aydin, S., Schubert, F., & Ittermann, B. (2017). Detection of metabolite changes in response to a varying visual stimulation paradigm using short-TE H-1 MRS at 7 T [Article]. *Nmr in Biomedicine*, *30*(2), 9, Article e3672. https://doi.org/10.1002/nbm.3672

Mentch, J., Spiegel, A., Ricciardi, C., & Robertson, C. E. (2019). GABAergic Inhibition Gates Perceptual Awareness During Binocular Rivalry [Article]. *Journal of Neuroscience*, *39*(42), 8398-8407. https://doi.org/10.1523/jneurosci.0836-19.2019

Mescher, M., Merkle, H., Kirsch, J., Garwood, M., & Gruetter, R. (1998). Simultaneous in vivo spectral editing and water suppression. *Nmr in Biomedicine*, *11*(6), 266-272. https://doi.org/10.1002/(sici)1099-1492(199810)11:6<266::aid-nbm530>3.0.co;2-j

Mikellidou, K., Gouws, A. D., Clawson, H., Thompson, P., Morland, A. B., & Keefe, B. D. (2016). An Orientation Dependent Size Illusion Is Underpinned by Processing in the Extrastriate Visual Area, LO1 [Article]. *I-Perception*, *7*(5), 21, Article 2041669516667628. https://doi.org/10.1177/2041669516667628

Miles, W. (1929). Ocular dominance demonstrated by unconscious sighting [Article]. *Journal of Experimental Psychology*, *12*, 113-126. https://doi.org/10.1037/h0075694

Millman, D. J., Ocker, G. K., Caldejon, S., Kato, I., Larkin, J. D., Lee, E. K., Luviano, J., Nayan, C., Nguyen, T. V., North, K., Seid, S., White, C., Lecoq, J., Reid, C., Buice, M. A., & de Vries, S. E. J. (2020). VIP interneurons in mouse primary visual cortex selectively enhance responses to weak but specific stimuli. *Elife*, *9*, Article e55130. https://doi.org/10.7554/eLife.55130

Moliadze, V., Zhao, Y. Q., Eysel, U., & Funke, K. (2003). Effect of transcranial magnetic stimulation on single-unit activity in the cat primary visual cortex [Article]. *Journal of Physiology-London*, *553*(2), 665-679. https://doi.org/10.1113/jphysiol.2003.050153

Molnar, Z., & Pollen, A. (2014). How unique is the human neocortex? [Editorial Material]. *Development*, *141*(1), 11-16. https://doi.org/10.1242/dev.101279

Monier, C., Chavane, F., Baudot, P., Graham, L. J., & Fregnac, Y. (2003). Orientation and direction selectivity of synaptic inputs in visual cortical neurons: A diversity of combinations produces spike tuning [Article]. *Neuron*, *37*(4), 663-680. https://doi.org/10.1016/s0896-6273(03)00064-3

Monteggia, L. M., Heimer, H., & Nestler, E. J. (2018). Meeting Report: Can We Make Animal Models of Human Mental Illness? *Biological Psychiatry*, *84*(7), 542-545. https://doi.org/10.1016/j.biopsych.2018.02.010

Moon, H. S., Jiang, H. Y., Vo, T. T., Jung, W. B., Vazquez, A. L., & Kim, S. G. (2021). Contribution of Excitatory and Inhibitory Neuronal Activity to BOLD fMRI. *Cerebral Cortex*, *31*(9), 4053-4067. https://doi.org/10.1093/cercor/bhab068

Moradi, F., Buracas, G. T., & Buxton, R. B. (2012). Attention strongly increases oxygen metabolic response to stimulus in primary visual cortex. *Neuroimage*, *59*(1), 601-607. https://doi.org/10.1016/j.neuroimage.2011.07.078

Moradi, F., & Buxton, R. B. (2013). Adaptation of cerebral oxygen metabolism and blood flow and modulation of neurovascular coupling with prolonged stimulation in human visual cortex. *Neuroimage*, *82*, 182-189. https://doi.org/10.1016/j.neuroimage.2013.05.110

Moradi, F., & Heeger, D. J. (2009). Inter-ocular contrast normalization in human visual cortex. *Journal of Vision*, *9*(3), Article 13. https://doi.org/10.1167/9.3.13

Moreno-Bote, R., Rinzel, J., & Rubin, N. (2007). Noise-induced alternations in an attractor network model of perceptual bistability. *Journal of Neurophysiology*, *98*(3), 1125-1139. https://doi.org/10.1152/jn.00116.2007

Moroz, L. L., Romanova, D. Y., & Kohn, A. B. (2021). Neural versus alternative integrative systems: molecular insights into origins of neurotransmitters. *Philosophical Transactions of the Royal Society B-Biological Sciences*, *376*(1821), Article 20190762. https://doi.org/10.1098/rstb.2019.0762

Morrone, M. C., Burr, D. C., & Maffei, L. (1982). FUNCTIONAL IMPLICATIONS OF CROSS-ORIENTATION INHIBITION OF CORTICAL VISUAL CELLS .1. NEUROPHYSIOLOGICAL EVIDENCE. *Proceedings of the Royal Society Series B-Biological Sciences*, *216*(1204), 335-354. https://doi.org/10.1098/rspb.1982.0078

Morrone, M. C., Burr, D. C., & Speed, H. D. (1987). CROSS-ORIENTATION INHIBITION IN CAT IS GABA MEDIATED. *Experimental Brain Research*, *67*(3), 635-644. https://doi.org/10.1007/BF00247294

Mountcastle, V. B. (1957). MODALITY AND TOPOGRAPHIC PROPERTIES OF SINGLE NEURONS OF CATS SOMATIC SENSORY CORTEX. *Journal of Neurophysiology*, *20*(4), 408-434. https://doi.org/10.1152/jn.1957.20.4.408

Mrsic-Flogel, T. D., Hofer, S. B., Ohki, K., Reid, R. C., Bonhoeffer, T., & Hubener, M. (2007). Homeostatic regulation of eye-specific responses in visual cortex during ocular dominance plasticity. *Neuron*, *54*(6), 961-972. https://doi.org/10.1016/j.neuron.2007.05.028

Mueller, J. K., Grigsby, E. M., Prevosto, V., Petraglia, F. W., Rao, H., Deng, Z. D., Peterchev, A. V., Sommer, M. A., Egner, T., Platt, M. L., & Grill, W. M. (2014). Simultaneous transcranial magnetic stimulation and single-neuron recording in alert non-human primates [Article]. *Nature Neuroscience*, *17*(8), 1130-1136. https://doi.org/10.1038/nn.3751

Mullinger, K. J., Cherukara, M. T., Buxton, R. B., Francis, S. T., & Mayhew, S. D. (2017). Post-stimulus fMRI and EEG responses: Evidence for a neuronal origin hypothesised to be inhibitory. *Neuroimage*, *157*, 388-399. https://doi.org/10.1016/j.neuroimage.2017.06.020

Mullins, P. G. (2018). Towards a theory of functional magnetic resonance spectroscopy (fMRS): A meta-analysis and discussion of using MRS to measure changes in neurotransmitters in real time [Article]. *Scandinavian Journal of Psychology*, *59*(1), 91-103. https://doi.org/10.1111/sjop.12411

Murphy, S. C., Palmer, L. M., Nyffeler, T., Muri, R. M., & Larkum, M. E. (2016). Transcranial magnetic stimulation (TMS) inhibits cortical dendrites [Article]. *Elife*, *5*, 12, Article e13598. https://doi.org/10.7554/eLife.13598

Muthukumaraswamy, S. D., Edden, R. A. E., Jones, D. K., Swettenham, J. B., & Singh, K. D. (2009). Resting GABA concentration predicts peak gamma frequency and fMRI amplitude in response to visual stimulation in humans. *Proceedings of the National Academy of Sciences of the United States of America*, *106*(20), 8356-8361. https://doi.org/10.1073/pnas.0900728106

Muthukumaraswamy, S. D., Evans, C. J., Edden, R. A. E., Wise, R. G., & Singh, K. D. (2012). Individual variability in the shape and amplitude of the BOLD-HRF correlates with endogenous GABAergic inhibition. *Human Brain Mapping*, *33*(2), 455-465. https://doi.org/10.1002/hbm.21223

Myers, J. F. M., Nutt, D. J., & Lingford-Hughes, A. R. (2016). gamma-aminobutyric acid as a metabolite: Interpreting magnetic resonance spectroscopy experiments [Article]. *Journal of Psychopharmacology*, *30*(5), 422-427. https://doi.org/10.1177/0269881116639298

Nagai, J., Yu, X. Z., Papouin, T., Cheong, E. J., Freeman, M. R., Monk, K. R., Hastings, M. H., Haydon, P. G., Rowitch, D., Shaham, S., & Khakh, B. S. (2021). Behaviorally consequential astrocytic regulation of neural circuits. *Neuron*, *109*(4), 576-596. https://doi.org/10.1016/j.neuron.2020.12.008

Nagaoka, T., Zhao, F. Q., Wang, P., Harel, N., Kennan, R. P., Ogawa, S., & Kim, S. G. (2006). Increases in oxygen consumption without cerebral blood volume change during visual stimulation under hypotension condition. *Journal of Cerebral Blood Flow and Metabolism*, *26*(8), 1043-1051. https://doi.org/10.1038/sj.jcbfm.9600251

Nassi, J. J., Lomber, S. G., & Born, R. T. (2013). Corticocortical Feedback Contributes to Surround Suppression in V1 of the Alert Primate. *Journal of Neuroscience*, *33*(19), 8504-U8440. https://doi.org/10.1523/jneurosci.5124-12.2013

Natan, R. G., Briguglio, J. J., Mwilambwe-Tshilobo, L., Jones, S. I., Aizenberg, M., Goldberg, E. M., & Geffen, M. N. (2015). Complementary control of sensory adaptation by two types of cortical interneurons. *Elife*, *4*, Article e09868. https://doi.org/10.7554/eLife.09868.001

Natan, R. G., Rao, W., & Geffen, M. N. (2017). Cortical Interneurons Differentially Shape Frequency Tuning following Adaptation. *Cell Reports*, *21*(4), 878-890. https://doi.org/10.1016/j.celrep.2017.10.012

Nguyen, V. A., Freeman, A. W., & Alais, D. (2003). Increasing depth of binocular rivalry suppression along two visual pathways. *Vision Research*, *43*(19), 2003-2008. https://doi.org/10.1016/s0042-6989(03)00314-6

Niell, C. M., & Scanziani, M. (2021). How Cortical Circuits Implement Cortical Computations: Mouse Visual Cortex as a Model. *Annual Review of Neuroscience*, *44*, 517-546. https://doi.org/10.1146/annurev-neuro-102320-085825

Nippert, A. R., Biesecker, K. R., & Newman, E. A. (2018). Mechanisms Mediating Functional Hyperemia in the Brain [Review]. *Neuroscientist*, *24*(1), 73-83. https://doi.org/10.1177/1073858417703033

Noest, A. J., van Ee, R., Nijs, M. M., & van Wezel, R. J. A. (2007). Percept-choice sequences driven by interrupted ambiguous stimuli: A low-level neural model. *Journal of Vision*, *7*(8), Article 10. https://doi.org/10.1167/7.8.10

Norcia, A. M., Appelbaum, L. G., Ales, J. M., Cottereau, B. R., & Rossion, B. (2015). The steady-state visual evoked potential in vision research: A review [Article]. *Journal of Vision*, *15*(6), 46, Article 4. https://doi.org/10.1167/15.6.4

Northoff, G., Walter, M., Schulte, R. F., Beck, J., Dydak, U., Henning, A., Boeker, H., Grimm, S., & Boesiger, P. (2007). GABA concentrations in the human anterior cingulate cortex predict negative BOLD responses in fMRI. *Nature Neuroscience*, *10*(12), 1515-1517. https://doi.org/10.1038/nn2001

Nurminen, L., Peromaa, T., & Laurinen, P. (2010). Surround suppression and facilitation in the fovea: Very long-range spatial interactions in contrast perception. *Journal of Vision*, *10*(13), Article 9. https://doi.org/10.1167/10.13.9

Nys, J., Scheyltjens, I., & Arckens, L. (2015). Visual system plasticity in mammals: the story of monocular enucleation-induced vision loss. *Front Syst Neurosci*, *9*, 60. https://doi.org/10.3389/fnsys.2015.00060

O'Herron, P., Chhatbar, P. Y., Levy, M., Shen, Z. M., Schramm, A. E., Lu, Z. Y., & Kara, P. (2016). Neural correlates of single-vessel haemodynamic responses in vivo. *Nature*, *534*(7607), 378-+. https://doi.org/10.1038/nature17965

Ogawa, S., Lee, T. M., Kay, A. R., & Tank, D. W. (1990). Brain magnetic resonance imaging with contrast dependent on blood oxygenation. *Proc Natl Acad Sci U S A*, *87*(24), 9868-9872. https://doi.org/10.1073/pnas.87.24.9868

Olah, S., Komlosi, G., Szabadics, J., Varga, C., Toth, E., Barzo, P., & Tamas, G. (2007). Output of neurogliaform cells to various neuron types in the human and rat cerebral cortex. *Front Neural Circuits*, *1*, 4. https://doi.org/10.3389/neuro.04.004.2007

Olah, S., Miklos, F., Gergely, K., Csaba, V., Rita, B., Pal, B., & Gabor, T. (2009). Regulation of cortical microcircuits by unitary GABA-mediated volume transmission. *Nature*, *461*(7268), 1278-U1113. https://doi.org/10.1038/nature08503

Oliet, S. H. R., Piet, R., & Poulain, D. A. (2001). Control of glutamate clearance and synaptic efficacy by glial coverage of neurons. *Science*, *292*(5518), 923-926. https://doi.org/10.1126/science.1059162

Olman, C. A., Inati, S., & Heeger, D. J. (2007). The effect of large veins on spatial localization with GE BOLD at 3 T: Displacement, not blurring [Article]. *Neuroimage*, *34*(3), 1126-1135. https://doi.org/10.1016/j.neuroimage.2006.08.045

Ortuno, T., Grieve, K. L., Cao, R., Cudeiro, J., & Rivadulla, C. (2014). Bursting thalamic responses in awake monkey contribute to visual detection and are modulated by corticofugal feedback. *Frontiers in Behavioral Neuroscience*, *8*, 198, Article 198. https://doi.org/10.3389/fnbeh.2014.00198

Oshea, R. P., Sims, A. J. H., & Govan, D. G. (1997). The effect of spatial frequency and field size on the spread of exclusive visibility in binocular rivalry. *Vision Research*, *37*(2), 175-183. https://doi.org/10.1016/s0042-6989(96)00113-7

Overstreet-Wadiche, L., & McBain, C. J. (2015). Neurogliaform cells in cortical circuits. *Nature Reviews Neuroscience*, *16*(8), 458-468. https://doi.org/10.1038/nrn3969

Ozeki, H., Finn, I. M., Schaffer, E. S., Miller, K. D., & Ferster, D. (2009). Inhibitory stabilization of the cortical network underlies visual surround suppression. *Neuron*, *62*(4), 578-592. https://doi.org/10.1016/j.neuron.2009.03.028

Ozeki, H., Sadakane, O., Akasaki, T., Naito, T., Shimegi, S., & Sato, H. (2004). Relationship between excitation and inhibition underlying size tuning and contextual response modulation in the cat primary visual cortex. *Journal of Neuroscience*, *24*(6), 1428-1438. https://doi.org/10.1523/jneurosci.3852-03.2004

Park, T. I. H., Smyth, L. C. D., Aalderink, M., Woolf, Z. R., Rustenhoven, J., Lee, K., Jansson, D., Smith, A., Feng, S., Correia, J., Heppner, P., Schweder, P., Mee, E., & Dragunow, M. (2022). Routine culture and study of adult human brain cells from neurosurgical specimens. *Nature Protocols*, *17*(2), 190-221. https://doi.org/10.1038/s41596-021-00637-8

Parker, D. B., & Razlighi, Q. R. (2019). The Benefit of Slice Timing Correction in Common fMRI Preprocessing Pipelines. *Frontiers in Neuroscience*, *13*, Article 821. https://doi.org/10.3389/fnins.2019.00821

Parkin, B. L., Ekhtiari, H., & Walsh, V. F. (2015). Non-invasive Human Brain Stimulation in Cognitive Neuroscience: A Primer [Review]. *Neuron*, *87*(5), 932-945. https://doi.org/10.1016/j.neuron.2015.07.032

Pascual-Leone, A., Bartres-Faz, D., & Keenan, J. P. (1999). Transcranial magnetic stimulation: studying the brain-behaviour relationship by induction of 'virtual lesions'. *Philosophical Transactions of the Royal Society B-Biological Sciences*, *354*(1387), 1229-1238. https://doi.org/10.1098/rstb.1999.0476

Pascual-Leone, A., Walsh, V., & Rothwell, J. (2000). Transcranial magnetic stimulation in cognitive neuroscience - virtual lesion, chronometry, and functional connectivity [Review]. *Current Opinion in Neurobiology*, *10*(2), 232-237. https://doi.org/10.1016/s0959-4388(00)00081-7

Pascualleone, A., Vallssole, J., Wassermann, E. M., & Hallett, M. (1994). RESPONSES TO RAPID-RATE TRANSCRANIAL MAGNETIC STIMULATION OF THE HUMAN MOTOR CORTEX [Article]. *Brain*, *117*, 847-858. https://doi.org/10.1093/brain/117.4.847

Pashut, T., Magidov, D., Ben-Porat, H., Wolfus, S., Friedman, A., Perel, E., Lavidor, M., Bar-Gad, I., Yeshurun, Y., & Korngreen, A. (2014). Patch-clamp recordings of rat neurons from acute brain slices of the somatosensory

cortex during magnetic stimulation. *Frontiers in Cellular Neuroscience*, *8*, Article 145. https://doi.org/10.3389/fncel.2014.00145
Pasley, B. N., Allen, E. A., & Freeman, R. D. (2009). State-Dependent Variability of Neuronal Responses to Transcranial Magnetic Stimulation of the Visual Cortex [Article]. *Neuron*, *62*(2), 291-303. https://doi.org/10.1016/j.neuron.2009.03.012
Pastukhov, A., Garcia-Rodriguez, P. E., Haenicke, J., Guillamon, A., Deco, G., & Braun, J. (2013). Multi-stable perception balances stability and sensitivity. *Frontiers in Computational Neuroscience*, *7*, Article 17. https://doi.org/10.3389/fncom.2013.00017
Payne, S. (2016). Physiological Basis. In *Cerebral Autoregulation* (pp. 1-18). https://doi.org/10.1007/978-3-319-31784-7_1
Pearson, J., Naselaris, T., Holmes, E. A., & Kosslyn, S. M. (2015). Mental Imagery: Functional Mechanisms and Clinical Applications. *Trends in Cognitive Sciences*, *19*(10), 590-602. https://doi.org/10.1016/j.tics.2015.08.003
Peck, K. K., Sunderland, A., Peters, A. M., Butterworth, S., Clark, P., & Gowland, P. A. (2001). Cerebral activation during a simple force production task: changes in the time course of the haemodynamic response. *Neuroreport*, *12*(13), 2813-2816. https://doi.org/10.1097/00001756-200109170-00012
Pell, G. S., Roth, Y., & Zangen, A. (2011). Modulation of cortical excitability induced by repetitive transcranial magnetic stimulation: Influence of timing and geometrical parameters and underlying mechanisms [Review]. *Progress in Neurobiology*, *93*(1), 59-98. https://doi.org/10.1016/j.pneurobio.2010.10.003
Pelli, D. G. (1997). The VideoToolbox software for visual psychophysics: Transforming numbers into movies [Article]. *Spatial Vision*, *10*(4), 437-442. https://doi.org/10.1163/156856897x00366
Perea, G., Yang, A., Boyden, E. S., & Sur, M. (2014). Optogenetic astrocyte activation modulates response selectivity of visual cortex neurons in vivo. *Nature Communications*, *5*, Article 3262. https://doi.org/10.1038/ncomms4262
Perez-Garci, E., Larkum, M. E., & Nevian, T. (2013). Inhibition of dendritic Ca2+ spikes by GABA(B) receptors in cortical pyramidal neurons is mediated by a direct G(i/o)-beta gamma-subunit interaction with Ca(v)1 channels. *Journal of Physiology-London*, *591*(7), 1599-1612. https://doi.org/10.1113/jphysiol.2012.245464
Petrov, Y., Carandini, M., & McKee, S. (2005). Two distinct mechanisms of suppression in human vision. *Journal of Neuroscience*, *25*(38), 8704-8707. https://doi.org/10.1523/Jneurosci.2871-05.2005
Petrov, Y., & Mckee, S. P. (2009). The time course of contrast masking reveals two distinct mechanisms of human surround suppression. *Journal of Vision*, *9*(1), 21 21-11. https://doi.org/10.1167/9.1.21
Peyrache, A., & Destexhe, A. (2019). Electrophysiological monitoring of inhibition in mammalian species, from rodents to humans. *Neurobiology of Disease*, *130*, Article 104500. https://doi.org/10.1016/j.nbd.2019.104500
Pirttila, T. R. M., Hakumaki, J. M., & Kauppinen, R. A. (1993). H-1 NUCLEAR-MAGNETIC-RESONANCE SPECTROSCOPY STUDY OF CEREBRAL GLUTAMATE IN AN EXVIVO BRAIN PREPARATION OF GUINEA-PIG [Article]. *Journal of Neurochemistry*, *60*(4), 1274-1282. https://doi.org/10.1111/j.1471-4159.1993.tb03287.x
Polania, R., Nitsche, M. A., & Ruff, C. C. (2018). Studying and modifying brain function with non-invasive brain stimulation. *Nature Neuroscience*, *21*(2), 174-187. https://doi.org/10.1038/s41593-017-0054-4
Polimeni, J. R., & Lewis, L. D. (2021). Imaging faster neural dynamics with fast fMRI: A need for updated models of the hemodynamic response. *Prog Neurobiol*, 102174. https://doi.org/10.1016/j.pneurobio.2021.102174
Poplawsky, A. J., Iordanova, B., Vazquez, A. L., Kim, S. G., & Fukuda, M. (2021). Postsynaptic activity of inhibitory neurons evokes hemodynamic fMRI responses. *Neuroimage*, *225*, Article 117457. https://doi.org/10.1016/j.neuroimage.2020.117457
Pouille, F., Marin-Burgin, A., Adesnik, H., Atallah, B. V., & Scanziani, M. (2009). Input normalization by global feedforward inhibition expands cortical dynamic range. *Nature Neuroscience*, *12*(12), 1577-U1131. https://doi.org/10.1038/nn.2441
Priebe, N. J. (2016). Mechanisms of Orientation Selectivity in the Primary Visual Cortex. *Annual Review of Vision Science, Vol 2*, *2*, 85-107. https://doi.org/10.1146/annurev-vision-111815-114456
Priebe, N. J., & Ferster, D. (2006). Mechanisms underlying cross-orientation suppression in cat visual cortex. *Nature Neuroscience*, *9*(4), 552-561. https://doi.org/10.1038/nn1660
Priebe, N. J., & Ferster, D. (2008). Inhibition, spike threshold, and stimulus selectivity in primary visual cortex. *Neuron*, *57*(4), 482-497. https://doi.org/10.1016/j.neuron.2008.02.005

Proulx, S. (2022). *Model Simulation of Binocular Rivalry for the Study of Monocular Deprivation*. In (Version v0.1.0) Zenodo. https://doi.org/10.5281/zenodo.6257173
Proulx, S., McLellan, A., Yu, H., & Farivar, F. (2020). *Inhibitory rTMS Modulation of the Occipital Pole Decreases Cortical Suppression of Liminal Contrast Perception* Version 1). https://doi.org/10.5281/zenodo.4101627
Proulx, S., Safi-Harb, M., LeVan, P., An, D., Watanabe, S., & Gotman, J. (2014). Increased sensitivity of fast BOLD fMRI with a subject-specific hemodynamic response function and application to epilepsy [Article]. *Neuroimage*, *93*, 59-73. https://doi.org/10.1016/j.neuroimage.2014.02.018
Proulx, S., Sheynin, Y., Hess, R., Farivar, R. (2020, June 23 to July 3). What Can MR Spectroscopy Measures of Occipital GABA tell about Visual Plasticity in Human Adult? 26th Annual Meeting of the Organization for Human Brain Mapping, Canada. https://doi.org/10.5281/zenodo.4034898
Provencher, S. W. (1993). ESTIMATION OF METABOLITE CONCENTRATIONS FROM LOCALIZED IN-VIVO PROTON NMR-SPECTRA. *Magnetic Resonance in Medicine*, *30*(6), 672-679. https://doi.org/10.1002/mrm.1910300604
Provencher, S. W. (2001). Automatic quantitation of localized in vivo H-1 spectra with LCModel. *Nmr in Biomedicine*, *14*(4), 260-264. https://doi.org/10.1002/nbm.698
Rae, C. D. (2014). A Guide to the Metabolic Pathways and Function of Metabolites Observed in Human Brain H-1 Magnetic Resonance Spectra [Article]. *Neurochemical Research*, *39*(1), 1-36. https://doi.org/10.1007/s11064-013-1199-5
Raichle, M. E., & Mintun, M. A. (2006). Brain work and brain imaging. *Annual Review of Neuroscience*, *29*, 449-476. https://doi.org/10.1146/annurev.neuro.29.051605.112819
Rangelov, D., Muller, H. J., & Taylor, P. C. J. (2015). Occipital TMS at phosphene detection threshold captures attention automatically. *Neuroimage*, *109*, 199-205. https://doi.org/10.1016/j.neuroimage.2015.01.035
Reid, R. C., & Alonso, J. M. (1995). Specificity of monosynaptic connections from thalamus to visual cortex. *Nature*, *378*(6554), 281-284. https://doi.org/10.1038/378281a0
Rideaux, R., & Welchman, A. E. (2018). Proscription supports robust perceptual integration by suppression in human visual cortex [Article]. *Nature Communications*, *9*, 14, Article 1502. https://doi.org/10.1038/s41467-018-03400-y
Riesen, G., Norcia, A. M., & Gardner, J. L. (2019). Humans Perceive Binocular Rivalry and Fusion in a Tristable Dynamic State [Article]. *Journal of Neuroscience*, *39*(43), 8527-8537. https://doi.org/10.1523/jneurosci.0713-19.2019
Robertson, C. E., Ratai, E. M., & Kanwisher, N. (2016). Reduced GABAergic Action in the Autistic Brain [Article]. *Current Biology*, *26*(1), 80-85. https://doi.org/10.1016/j.cub.2015.11.019
Roerig, B., & Chen, B. (2002). Relationships of Local Inhibitory and Excitatory Circuits to Orientation Preference Maps in Ferret Visual Cortex. *Cerebral Cortex*, *12*(2), 187-198. https://doi.org/10.1093/cercor/12.2.187
Romero, M. C., Davare, M., Armendariz, M., & Janssen, P. (2019). Neural effects of transcranial magnetic stimulation at the single-cell level [Article]. *Nature Communications*, *10*, 11, Article 2642. https://doi.org/10.1038/s41467-019-10638-7
Rosburg, T., Marinou, V., Haueisen, J., Smesny, S., & Sauer, H. (2004). Effects of lorazepam on the neuromagnetic mismatch negativity (MMNm) and auditory evoked field component N100m. *Neuropsychopharmacology*, *29*(9), 1723-1733. https://doi.org/10.1038/sj.npp.1300477
Ross, J., & Speed, H. D. (1991). CONTRAST ADAPTATION AND CONTRAST MASKING IN HUMAN VISION. *Proceedings of the Royal Society B-Biological Sciences*, *246*(1315), 61-69. https://doi.org/10.1098/rspb.1991.0125
Ross, J. M., & Hamm, J. P. (2020). Cortical Microcircuit Mechanisms of Mismatch Negativity and Its Underlying Subcomponents. *Frontiers in Neural Circuits*, *14*, Article 13. https://doi.org/10.3389/fncir.2020.00013
Rothman, D. L., Behar, K. L., Hyder, F., & Shulman, R. G. (2003). In vivo NMR studies of the glutamate neurotransmitter flux and neuroenergetics: Implications for brain function [Review]. *Annual Review of Physiology*, *65*, 401-427. https://doi.org/10.1146/annurev.physiol.65.092101.142131
Rouder, J. N., Morey, R. D., Speckman, P. L., & Province, J. M. (2012). Default Bayes factors for ANOVA designs [Article]. *Journal of Mathematical Psychology*, *56*(5), 356-374. https://doi.org/10.1016/j.jmp.2012.08.001
Roumani, D., & Moutoussis, K. (2012). Binocular rivalry alternations and their relation to visual adaptation. *Frontiers in Human Neuroscience*, *6*, Article 35. https://doi.org/10.3389/fnhum.2012.00035
Roy, C. S., & Sherrington, C. S. (1890). On the Regulation of the Blood-supply of the Brain. *The Journal of physiology*, *11*(1-2), 85-158.117. https://doi.org/10.1113/jphysiol.1890.sp000321

Rusakov, D. A., & Stewart, M. G. (2021). Synaptic environment and extrasynaptic glutamate signals: The quest continues. *Neuropharmacology*, *195*, Article 108688. https://doi.org/10.1016/j.neuropharm.2021.108688
Rusu, C. V., Murakami, M., Ziemann, U., & Triesch, J. (2014). A Model of TMS-induced I-waves in Motor Cortex [Article]. *Brain Stimulation*, *7*(3), 401-414. https://doi.org/10.1016/j.brs.2014.02.009
Sadaghiani, S., Ugurbil, K., & Uludag, K. (2009). Neural activity-induced modulation of BOLD poststimulus undershoot independent of the positive signal. *Magn Reson Imaging*, *27*(8), 1030-1038. https://doi.org/10.1016/j.mri.2009.04.003
Sadeh, S., & Clopath, C. (2021). Inhibitory stabilization and cortical computation. *Nature Reviews Neuroscience*, *22*(1), 21-37. https://doi.org/10.1038/s41583-020-00390-z
Saha, R., Wu, K., Bloom, R. P., Liang, S., Tonini, D., & Wang, J. P. (2022). A review on magnetic and spintronic neurostimulation: challenges and prospects. *Nanotechnology*, *33*(18), Article 182004. https://doi.org/10.1088/1361-6528/ac49be
Said, C. P., & Heeger, D. J. (2013). A Model of Binocular Rivalry and Cross-orientation Suppression. *Plos Computational Biology*, *9*(3), Article e1002991. https://doi.org/10.1371/journal.pcbi.1002991
Salminen-Vaparanta, N., Noreika, V., Revonsuo, A., Koivisto, M., & Vanni, S. (2012). Is selective primary visual cortex stimulation achievable with TMS? *Human Brain Mapping*, *33*(3), 652-665. https://doi.org/10.1002/hbm.21237
Salminen-Vaparanta, N., Vanni, S., Noreika, V., Valiulis, V., Moro, L., & Revonsuo, A. (2014). Subjective Characteristics of TMS-Induced Phosphenes Originating in Human V1 and V2. *Cerebral Cortex*, *24*(10), 2751-2760. https://doi.org/10.1093/cercor/bht131
Salvador, R., Wenger, C., & Miranda, P. C. (2015). Investigating the cortical regions involved in MEP modulation in tDCS [Article]. *Frontiers in Cellular Neuroscience*, *9*, 11, Article 405. https://doi.org/10.3389/fncel.2015.00405
Samaha, J., Gosseries, O., & Postle, B. R. (2017). Distinct Oscillatory Frequencies Underlie Excitability of Human Occipital and Parietal Cortex. *Journal of Neuroscience*, *37*(11), 2824-2833. https://doi.org/10.1523/jneurosci.3413-16.2017
Sandberg, K., Blicher, J. U., Del Pin, S. H., Andersen, L. M., Rees, G., & Kanai, R. (2016). Improved estimates for the role of grey matter volume and GABA in bistable perception [Article]. *Cortex*, *83*, 292-305. https://doi.org/10.1016/j.cortex.2016.08.006
Sanganahalli, B. G., Herman, P., Rothman, D. L., Blumenfeld, H., & Hyder, F. (2016). Metabolic demands of neural-hemodynamic associated and disassociated areas in brain. *J Cereb Blood Flow Metab*, *36*(10), 1695-1707. https://doi.org/10.1177/0271678X16664531
Sasaki, T., Kodama, S., Togashi, N., Shirota, Y., Sugiyama, Y., Tokushige, S., Inomata-Terada, S., Terao, Y., Ugawa, Y., & Hamada, M. (2018). The intensity of continuous theta burst stimulation, but not the waveform used to elicit motor evoked potentials, influences its outcome in the human motor cortex. *Brain Stimulation*, *11*(2), 400-410. https://doi.org/10.1016/j.brs.2017.12.003
Scanziani, M. (2000). GABA spillover activates postsynaptic GABA(B) receptors to control rhythmic hippocampal activity. *Neuron*, *25*(3), 673-681. https://doi.org/10.1016/s0896-6273(00)81069-7
Schaeffer, S., & Iadecola, C. (2021). Revisiting the neurovascular unit. *Nature Neuroscience*, *24*(9), 1198-1209. https://doi.org/10.1038/s41593-021-00904-7
Schaeffner, L. F., & Welchman, A. E. (2017). Mapping the visual brain areas susceptible to phosphene induction through brain stimulation. *Experimental Brain Research*, *235*(1), 205-217. https://doi.org/10.1007/s00221-016-4784-4
Schousboe, A., Bak, L. K., & Waagepetersen, H. S. (2013). Astrocytic Control of Biosynthesis and Turnover of the Neurotransmitters Glutamate and GABA. *Frontiers in endocrinology*, *4*, 102. https://doi.org/10.3389/fendo.2013.00102
Schousboe, A., & Waagepetersen, H. S. (2007). GABA: Homeostatic and pharmacological aspects. In J. M. Tepper, E. D. Abercrombie, & J. P. Bolam (Eds.), *Gaba and the Basal Ganglia: From Molecules to Systems* (Vol. 160, pp. 9-19). Elsevier Science Bv. https://doi.org/10.1016/s0079-6123(06)60002-2
Schulz, A., Miehl, C., Berry, M. J., & Gjorgjieva, J. (2021). The generation of cortical novelty responses through inhibitory plasticity. *Elife*, *10*, Article e65309. https://doi.org/10.7554/eLife.65309

Scocchia, L., Valsecchi, M., & Triesch, J. (2014). Top-down influences on ambiguous perception: the role of stable and transient states of the observer [Review]. *Frontiers in Human Neuroscience*, *8*, 18, Article 979. https://doi.org/10.3389/fnhum.2014.00979

Sears, S. M. S., & Hewett, S. J. (2021). Influence of glutamate and GABA transport on brain excitatory/inhibitory balance. *Experimental Biology and Medicine*, *246*(9), 1069-1083. https://doi.org/10.1177/1535370221989263

Seay, M. J., Natan, R. G., Geffen, M. N., & Buonomano, D. V. (2020). Differential Short-Term Plasticity of PV and SST Neurons Accounts for Adaptation and Facilitation of Cortical Neurons to Auditory Tones. *Journal of Neuroscience*, *40*(48), 9224-9235. https://doi.org/10.1523/jneurosci.0686-20.2020

Sedigh-Sarvestani, M., Vigeland, L., Fernandez-Lamo, I., Taylor, M. M., Palmer, L. A., & Contreras, D. (2017). Intracellular, In Vivo, Dynamics of Thalamocortical Synapses in Visual Cortex. *Journal of Neuroscience*, *37*(21), 5250-5262. https://doi.org/10.1523/jneurosci.3370-16.2017

Seeman, S. C., Campagnola, L., Davoudian, P. A., Hoggarth, A., Hage, T. A., Bosma-Moody, A., Baker, C. A., Lee, J. H., Mihalas, S., Teeter, C., Ko, A. L., Ojemann, J. G., Gwinn, R. P., Silbergeld, D. L., Cobbs, C., Phillips, J., Lein, E., Murphy, G., Koch, C., . . . Jarsky, T. (2018). Sparse recurrent excitatory connectivity in the microcircuit of the adult mouse and human cortex. *Elife*, *7*, Article e37349. https://doi.org/10.7554/eLife.37349

Semyanov, A., Walker, M. C., Kullmann, D. M., & Silver, R. A. (2004). Tonically active GABA(A) receptors: modulating gain and maintaining the tone. *Trends in Neurosciences*, *27*(5), 262-269. https://doi.org/10.1016/j.tins.2004.03.005

Sengpiel, F., Baddeley, R. J., Freeman, T. C. B., Harrad, R., & Blakemore, C. (1998). Different mechanisms underlie three inhibitory phenomena in cat area 17. *Vision Research*, *38*(14), 2067-2080. https://doi.org/10.1016/S0042-6989(97)00413-6

Sengpiel, F., Jirmann, K.-U., Vorobyov, V., & Eysel, U. T. (2005). Strabismic Suppression Is Mediated by Inhibitory Interactions in the Primary Visual Cortex. *Cerebral Cortex*, *16*(12), 1750-1758. https://doi.org/10.1093/cercor/bhj110

Sengpiel, F., & Vorobyov, V. (2005). Intracortical origins of interocular suppression in the visual cortex. *Journal of Neuroscience*, *25*(27), 6394-6400. https://doi.org/10.1523/jneurosci.0862-05.2005

Shenoy, K. V., Sahani, M., & Churchland, M. M. (2013). Cortical Control of Arm Movements: A Dynamical Systems Perspective. In S. E. Hyman (Ed.), *Annual Review of Neuroscience, Vol 36* (Vol. 36, pp. 337-359). https://doi.org/10.1146/annurev-neuro-062111-150509

Sheth, S. A., Nemoto, M., Guiou, M., Walker, M., Pouratian, N., & Toga, A. W. (2004). Linear and nonlinear relationships between neuronal activity, oxygen metabolism, and hemodynamic responses. *Neuron*, *42*(2), 347-355. https://doi.org/10.1016/s0896-6273(04)00221-1

Sheynin, Y., Proulx, S., & Hess, R. F. (2019). Temporary monocular occlusion facilitates binocular fusion during rivalry [Article]. *Journal of Vision*, *19*(5), 17, Article 23. https://doi.org/10.1167/19.5.23

Shibata, K., Sasaki, Y., Bang, J. W., Walsh, E. G., Machizawa, M. G., Tamaki, M., Chang, L. H., & Watanabe, T. (2017). Overlearning hyperstabilizes a skill by rapidly making neurochemical processing inhibitory-dominant [Article]. *Nature Neuroscience*, *20*(3), 470-475. https://doi.org/10.1038/nn.4490

Shirinpour, S., Hananeia, N., Rosado, J., Tran, H., Galanis, C., Vlachos, A., Jedlicka, P., Queisser, G., & Opitz, A. (2021). Multi-scale modeling toolbox for single neuron and subcellular activity under Transcranial Magnetic Stimulation [Article]. *Brain Stimulation*, *14*(6), 1470-1482. https://doi.org/10.1016/j.brs.2021.09.004

Shmuel, A., Augath, M., Oeltermann, A., & Logothetis, N. K. (2006). Negative functional MRI response correlates with decreases in neuronal activity in monkey visual area V1. *Nature Neuroscience*, *9*(4), 569-577. https://doi.org/10.1038/nn1675

Shmuel, A., Yacoub, E., Pfeuffer, J., Van de Moortele, P. F., Adriany, G., Hu, X. P., & Ugurbil, K. (2002). Sustained negative BOLD, blood flow and oxygen consumption response and its coupling to the positive response in the human brain. *Neuron*, *36*(6), 1195-1210. https://doi.org/10.1016/s0896-6273(02)01061-9

Shpiro, A., Moreno-Bote, R., Rubin, N., & Rinzel, J. (2009). Balance between noise and adaptation in competition models of perceptual bistability. *Journal of Computational Neuroscience*, *27*(1), 37-54. https://doi.org/10.1007/s10827-008-0125-3

Sibson, N. R., Dhankhar, A., Mason, G. F., Rothman, D. L., Behar, K. L., & Shulman, R. G. (1998). Stoichiometric coupling of brain glucose metabolism and glutamatergic neuronal activity [Article]. *Proceedings of the*

National Academy of Sciences of the United States of America, *95*(1), 316-321. https://doi.org/10.1073/pnas.95.1.316

Simon, A. B., Griffeth, V. E., Wong, E. C., & Buxton, R. B. (2013). A novel method of combining blood oxygenation and blood flow sensitive magnetic resonance imaging techniques to measure the cerebral blood flow and oxygen metabolism responses to an unknown neural stimulus. *Plos One*, *8*(1), e54816. https://doi.org/10.1371/journal.pone.0054816

Singh, M. F., Braver, T. S., Cole, M. W., & Ching, S. N. (2020). Estimation and validation of individualized dynamic brain models with resting state fMRI. *Neuroimage*, *221*, Article 117046. https://doi.org/10.1016/j.neuroimage.2020.117046

Sipe, G. O., Petravicz, J., Rikhye, R. V., Garcia, R., Mellios, N., & Sur, M. (2021). Astrocyte glutamate uptake coordinates experience-dependent, eye-specific refinement in developing visual cortex. *Glia*, *69*(7), 1723-1735. https://doi.org/10.1002/glia.23987

Skerswetat, J., Formankiewicz, M. A., & Waugh, S. J. (2016). Very few exclusive percepts for contrast-modulated stimuli during binocular rivalry. *Vision Research*, *121*, 10-22. https://doi.org/10.1016/j.visres.2016.01.002

Skerswetat, J., Formankiewicz, M. A., & Waugh, S. J. (2018). More superimposition for contrast-modulated than luminance-modulated stimuli during binocular rivalry [Article]. *Vision Research*, *142*, 40-51. https://doi.org/10.1016/j.visres.2017.10.002

Smith, A. T., Singh, K. D., Williams, A. L., & Greenlee, M. W. (2001). Estimating receptive field size from fMRI data in human striate and extrastriate visual cortex. *Cerebral Cortex*, *11*(12), 1182-1190. https://doi.org/10.1093/cercor/11.12.1182

Smith, A. T., Williams, A. L., & Singh, K. D. (2004). Negative BOLD in the visual cortex: evidence against blood stealing. *Human Brain Mapping*, *21*(4), 213-220. https://doi.org/10.1002/hbm.20017

Solomon, S. G., & Kohn, A. (2014). Moving Sensory Adaptation beyond Suppressive Effects in Single Neurons [Review]. *Current Biology*, *24*(20), R1012-R1022. https://doi.org/10.1016/j.cub.2014.09.001

Song, X. M., Hu, X.-W., Li, Z., Gao, Y., Ju, X., Liu, D.-Y., Wang, Q.-N., Xue, C., Cai, Y.-C., Bai, R., Tan, Z.-L., & Northoff, G. (2021). Reduction of higher-order occipital GABA and impaired visual perception in acute major depressive disorder. *Molecular Psychiatry*. https://doi.org/10.1038/s41380-021-01090-5

Sousa, A. M. M., Meyer, K. A., Santpere, G., Gulden, F. O., & Sestan, N. (2017). Evolution of the Human Nervous System Function, Structure, and Development [Review]. *Cell*, *170*(2), 226-247. https://doi.org/10.1016/j.cell.2017.06.036

Sparing, R., Dambeck, N., Stock, K., Meister, I. G., Huetter, D., & Boroojerdi, B. (2005). Investigation of the primary visual cortex using short-interval paired-pulse transcranial magnetic stimulation (TMS) [Article]. *Neuroscience Letters*, *382*(3), 312-316. https://doi.org/10.1016/j.neulet.2005.03.036

Spiegel, D. P., Hansen, B. C., Byblow, W. D., & Thompson, B. (2012). Anodal Transcranial Direct Current Stimulation Reduces Psychophysically Measured Surround Suppression in the Human Visual Cortex [Article]. *Plos One*, *7*(5), 9, Article e36220. https://doi.org/10.1371/journal.pone.0036220

Stagg, C. J. (2014). Magnetic Resonance Spectroscopy as a tool to study the role of GABA in motor-cortical plasticity [Review]. *Neuroimage*, *86*, 19-27. https://doi.org/10.1016/j.neuroimage.2013.01.009

Stagg, C. J., Bachtiar, V., & Johansen-Berg, H. (2011a). The Role of GABA in Human Motor Learning [Article]. *Current Biology*, *21*(6), 480-484. https://doi.org/10.1016/j.cub.2011.01.069

Stagg, C. J., Bachtiar, V., & Johansen-Berg, H. (2011b). What are we measuring with GABA magnetic resonance spectroscopy? *Commun Integr Biol*, *4*(5), 573-575. https://doi.org/10.4161/cib.4.5.16213

Stagg, C. J., & Nitsche, M. A. (2011). Physiological Basis of Transcranial Direct Current Stimulation. *Neuroscientist*, *17*(1), 37-53. https://doi.org/10.1177/1073858410386614

Stagg, C. J., O'Shea, J., & Johansen-Berg, H. (2010). Imaging the effects of rTMS-induced cortical plasticity. *Restor Neurol Neurosci*, *28*(4), 425-436. https://doi.org/10.3233/RNN-2010-0553

Stagg, C. J., Wylezinska, M., Matthews, P. M., Johansen-Berg, H., Jezzard, P., Rothwell, J. C., & Bestmann, S. (2009). Neurochemical Effects of Theta Burst Stimulation as Assessed by Magnetic Resonance Spectroscopy. *Journal of Neurophysiology*, *101*(6), 2872-2877. https://doi.org/10.1152/jn.91060.2008

Stange, A., Myoga, M. H., Lingner, A., Ford, M. C., Alexandrova, O., Felmy, F., Pecka, M., Siveke, I., & Grothe, B. (2013). Adaptation in sound localization: from GABA(B) receptor-mediated synaptic modulation to perception. *Nature Neuroscience*, *16*(12), 1840-1847. https://doi.org/10.1038/nn.3548

Stefanovic, B., Warnking, J. M., & Pike, G. B. (2004). Hemodynamic and metabolic responses to neuronal inhibition. *Neuroimage*, *22*(2), 771-778. https://doi.org/10.1016/j.neuroimage.2004.01.036

Stepanyants, A., Martinez, L. M., Ferecsko, A. S., & Kisvarday, Z. F. (2009). The fractions of short- and long-range connections in the visual cortex. *Proceedings of the National Academy of Sciences of the United States of America*, *106*(9), 3555-3560. https://doi.org/10.1073/pnas.0810390106

Stettler, D. D., Das, A., Bennett, J., & Gilbert, C. D. (2002). Lateral connectivity and contextual interactions in macaque primary visual cortex. *Neuron*, *36*(4), 739-750. https://doi.org/10.1016/s0896-6273(02)01029-2

Stokes, M. G., Barker, A. T., Dervinis, M., Verbruggen, F., Maizey, L., Adams, R. C., & Chambers, C. D. (2013). Biophysical determinants of transcranial magnetic stimulation: effects of excitability and depth of targeted area [Article]. *Journal of Neurophysiology*, *109*(2), 437-444. https://doi.org/10.1152/jn.00510.2012

Suarez, H., Koch, C., & Douglas, R. (1995). MODELING DIRECTION SELECTIVITY OF SIMPLE CELLS IN STRIATE VISUAL-CORTEX WITHIN THE FRAMEWORK OF THE CANONICAL MICROCIRCUIT. *Journal of Neuroscience*, *15*(10), 6700-6719. https://doi.org/10.1523/JNEUROSCI.15-10-06700.1995

Sugie, N. (1982). NEURAL MODELS OF BRIGHTNESS PERCEPTION AND RETINAL RIVALRY IN BINOCULAR VISION. *Biological Cybernetics*, *43*(1), 13-21. https://doi.org/10.1007/bf00337283

Sui, J., Adali, T., Yu, Q. B., Chen, J. Y., & Calhoun, V. D. (2012). A review of multivariate methods for multimodal fusion of brain imaging data. *Journal of Neuroscience Methods*, *204*(1), 68-81. https://doi.org/10.1016/j.jneumeth.2011.10.031

Suppa, A., Huang, Y. Z., Funke, K., Ridding, M. C., Cheeran, B., Di Lazzaro, V., Ziemann, U., & Rothwell, J. C. (2016). Ten Years of Theta Burst Stimulation in Humans: Established Knowledge, Unknowns and Prospects [Article]. *Brain Stimulation*, *9*(3), 323-335. https://doi.org/10.1016/j.brs.2016.01.006

Tajima, S., Watanabe, M., Imai, C., Ueno, K., Asamizuya, T., Sun, P., Tanaka, K., & Cheng, K. (2010). Opposing Effects of Contextual Surround in Human Early Visual Cortex Revealed by Functional Magnetic Resonance Imaging with Continuously Modulated Visual Stimuli. *Journal of Neuroscience*, *30*(9), 3264-3270. https://doi.org/10.1523/jneurosci.4473-09.2010

Takado, Y., Takuwa, H., Sampei, K., Urushihata, T., Takahashi, M., Shimojo, M., Uchida, S., Nitta, N., Shibata, S., Nagashima, K., Ochi, Y., Ono, M., Maeda, J., Tomita, Y., Sahara, N., Near, J., Aoki, I., Shibata, K., & Higuchi, M. (2022). MRS-measured glutamate versus GABA reflects excitatory versus inhibitory neural activities in awake mice. *Journal of Cerebral Blood Flow and Metabolism*, *42*(1), 197-212, Article 0271678x211045449. https://doi.org/10.1177/0271678x211045449

Tang, A. D., Bennett, W., Bindoff, A. D., Bolland, S., Collins, J., Langley, R. C., Garry, M. I., Summers, J. J., Hinder, M. R., Rodger, J., & Canty, A. J. (2021). Subthreshold repetitive transcranial magnetic stimulation drives structural synaptic plasticity in the young and aged motor cortex [Article]. *Brain Stimulation*, *14*(6), 1498-1507. https://doi.org/10.1016/j.brs.2021.10.001

Thompson, B., Mansouri, B., Koski, L., & Hess, R. F. (2008). Brain plasticity in the adult: Modulation of function in amblyopia with rTMS. *Current Biology*, *18*(14), 1067-1071. https://doi.org/10.1016/j.cub.2008.06.052

Thompson, S. K., Engel, S. A., & Olman, C. A. (2014). Larger neural responses produce BOLD signals that begin earlier in time. *Frontiers in Neuroscience*, *8*, 159. https://doi.org/10.3389/fnins.2014.00159

Thut, G., Veniero, D., Romei, V., Miniussi, C., Schyns, P., & Gross, J. (2011). Rhythmic TMS Causes Local Entrainment of Natural Oscillatory Signatures. *Current Biology*, *21*(14), 1176-1185. https://doi.org/10.1016/j.cub.2011.05.049

Tkac, I., Starcuk, Z., Choi, I. Y., & Gruetter, R. (1999). In vivo H-1 NMR spectroscopy of rat brain at 1 ms echo time. *Magnetic Resonance in Medicine*, *41*(4), 649-656. https://doi.org/10.1002/(sici)1522-2594(199904)41:4<649::aid-mrm2>3.0.co;2-g

Tolhurst, D. J., & Thompson, P. G. (1975). Orientation illusions and after-effects: inhibition between channels. *Vision Res*, *15*, 967-972. https://doi.org/10.1016/0042-6989(75)90238-2

Tong, F., Meng, M., & Blake, R. (2006). Neural bases of binocular rivalry. *Trends in Cognitive Sciences*, *10*(11), 502-511. https://doi.org/10.1016/j.tics.2006.09.003

Tremblay, R., Lee, S., & Rudy, B. (2016). GABAergic Interneurons in the Neocortex: From Cellular Properties to Circuits. *Neuron*, *91*(2), 260-292. https://doi.org/10.1016/j.neuron.2016.06.033

Tremblay, S., Beaule, V., Proulx, S., de Beaumont, L., Marjanska, M., Doyon, J., Pascual-Leone, A., Lassonde, M., & Theoret, H. (2013). Relationship between transcranial magnetic stimulation measures of intracortical

inhibition and spectroscopy measures of GABA and glutamate plus glutamine [Article]. *Journal of Neurophysiology*, *109*(5), 1343-1349. https://doi.org/10.1152/jn.00704.2012
Tricoire, L., & Vitalis, T. (2012). Neuronal nitric oxide synthase expressing neurons: a journey from birth to neuronal circuits. *Frontiers in Neural Circuits*, *6*, Article 82. https://doi.org/10.3389/fncir.2012.00082
Uhlirova, H., Kılıç, K., Tian, P., Sakadžić, S., Gagnon, L., Thunemann, M., Desjardins, M., Saisan, P. A., Nizar, K., Yaseen, M. A., Hagler, D. J., Vandenberghe, M., Djurovic, S., Andreassen, O. A., Silva, G. A., Masliah, E., Kleinfeld, D., Vinogradov, S., Buxton, R. B., . . . Devor, A. (2016). The roadmap for estimation of cell-type-specific neuronal activity from non-invasive measurements. *Philosophical Transactions of the Royal Society B: Biological Sciences*, *371*(1705), 20150356. https://doi.org/10.1098/rstb.2015.0356
Uhlirova, H., Kılıç, K., Tian, P. F., Thunemann, M., Desjardins, M., Saisan, P. A., Sakadzic, S., Nese, T. V., Mateo, C., Cheng, Q., Weldy, K. L., Razoux, F., Vandenberghe, M., Cremonesi, J. A., Ferri, C. G. L., Nizar, K., Sridhar, V. B., Steed, T. C., Abashin, M., . . . Devor, A. (2016). Cell type specificity of neurovascular coupling in cerebral cortex. *Elife*, *5*. https://doi.org/10.7554/elife.14315
Uludag, K., Dubowitz, D. J., Yoder, E. J., Restom, K., Liu, T. T., & Buxton, R. B. (2004). Coupling of cerebral blood flow and oxygen consumption during physiological activation and deactivation measured with fMRI. *Neuroimage*, *23*(1), 148-155. https://doi.org/10.1016/j.neuroimage.2004.05.013
Urban, A., Rancillac, A., Martinez, L., & Rossier, J. (2012). Deciphering the neuronal circuitry controlling local blood flow in the cerebral cortex with optogenetics in PV::Cre transgenic mice. *Frontiers in Pharmacology*, *3*, Article 105. https://doi.org/10.3389/fphar.2012.00105
Uusitalo, M. A., & Ilmoniemi, R. J. (1997). Signal-space projection method for separating MEG or EEG into components [Article]. *Medical & Biological Engineering & Computing*, *35*(2), 135-140. https://doi.org/10.1007/bf02534144
Vafaee, M. S., & Gjedde, A. (2000). Model of blood-brain transfer of oxygen explains nonlinear flow-metabolism coupling during stimulation of visual cortex. *Journal of Cerebral Blood Flow and Metabolism*, *20*(4), 747-754. https://doi.org/10.1097/00004647-200004000-00012
Valero-Cabre, A., Amengual, J. L., Stengel, C., Pascual-Leone, A., & Coubard, O. A. (2017). Transcranial magnetic stimulation in basic and clinical neuroscience: A comprehensive review of fundamental principles and novel insights. *Neuroscience and Biobehavioral Reviews*, *83*, 381-404. https://doi.org/10.1016/j.neubiorev.2017.10.006
Valle-Inclan, F., Blanco, M. J., Soto, D., & Leiros, L. (2008). A new method to assess eye dominance [Article]. *Psicologica*, *29*(1), 55-64.
van Ee, R. (2009). Stochastic variations in sensory awareness are driven by noisy neuronal adaptation: evidence from serial correlations in perceptual bistability. *Journal of the Optical Society of America a-Optics Image Science and Vision*, *26*(12), 2612-2622. https://doi.org/10.1364/josaa.26.002612
Van Horn, J. D. (2006, Jun). Cognitive Neuroimaging: History, Developments, and Directions. [Cognitive neurosciences iii, third edition]. Conference of the Summer-Institute-in-Cognitive-Neuroscience, Lake Tahoe, CA.
van Loon, A. M., Knapen, T., Scholte, H. S., St John-Saaltink, E., Donner, T. H., & Lamme, V. A. F. (2013). GABA Shapes the Dynamics of Bistable Perception [Article]. *Current Biology*, *23*(9), 823-827. https://doi.org/10.1016/j.cub.2013.03.067
van Versendaal, D., Rajendran, R., Saiepour, M. H., Klooster, J., Smit-Rigter, L., Sommeijer, J. P., De Zeeuw, C. I., Hofer, S. B., Heimel, J. A., & Levelt, C. N. (2012). Elimination of Inhibitory Synapses Is a Major Component of Adult Ocular Dominance Plasticity [Article]. *Neuron*, *74*(2), 374-383. https://doi.org/10.1016/j.neuron.2012.03.015
Vazquez, A. L., Fukuda, M., & Kim, S. G. (2012). Evolution of the dynamic changes in functional cerebral oxidative metabolism from tissue mitochondria to blood oxygen. *J Cereb Blood Flow Metab*, *32*(4), 745-758. https://doi.org/10.1038/jcbfm.2011.198
Vazquez, A. L., Fukuda, M., & Kim, S. G. (2018). Inhibitory Neuron Activity Contributions to Hemodynamic Responses and Metabolic Load Examined Using an Inhibitory Optogenetic Mouse Model. *Cerebral Cortex*, *28*(11), 4105-4119. https://doi.org/10.1093/cercor/bhy225
Verhagen, J., & Wagenmakers, E. J. (2014). Bayesian Tests to Quantify the Result of a Replication Attempt. *Journal of Experimental Psychology-General*, *143*(4), 1457-1475. https://doi.org/10.1037/a0036731

Vernet, M., Brem, A. K., Farzan, F., & Pascual-Leone, A. (2015). Synchronous and opposite roles of the parietal and prefrontal cortices in bistable perception: A double-coil TMS-EEG study [Article]. *Cortex*, *64*, 78-88. https://doi.org/10.1016/j.cortex.2014.09.021

Vidyasagar, T. R. (1990). PATTERN ADAPTATION IN CAT VISUAL-CORTEX IS A COOPERATIVE PHENOMENON. *Neuroscience*, *36*(1), 175-179. https://doi.org/10.1016/0306-4522(90)90360-g

Vizi, E. S., Fekete, A., Karoly, R., & Mike, A. (2010). Non-synaptic receptors and transporters involved in brain functions and targets of drug treatment. *British Journal of Pharmacology*, *160*(4), 785-809. https://doi.org/10.1111/j.1476-5381.2009.00624.x

Waagepetersen, H. S., Sonnewald, U., & Schousboe, A. (1999). The GABA paradox: Multiple roles as metabolite, neurotransmitter, and neurodifferentiative agent. *Journal of Neurochemistry*, *73*(4), 1335-1342. https://doi.org/10.1046/j.1471-4159.1999.0731335.x

Wade, A. R., & Rowland, J. (2010). Early Suppressive Mechanisms and the Negative Blood Oxygenation Level-Dependent Response in Human Visual Cortex. *Journal of Neuroscience*, *30*(14), 5008-5019. https://doi.org/10.1523/Jneurosci.6260-09.2010

Wagenmakers, E. J., Love, J., Marsman, M., Jamil, T., Ly, A., Verhagen, J., Selker, R., Gronau, Q. F., Dropmann, D., Boutin, B., Meerhoff, F., Knight, P., Raj, A., van Kesteren, E. J., van Doorn, J., Smira, M., Epskamp, S., Etz, A., Matzke, D., . . . Morey, R. D. (2018). Bayesian inference for psychology. Part II: Example applications with JASP [Article]. *Psychonomic Bulletin & Review*, *25*(1), 58-76. https://doi.org/10.3758/s13423-017-1323-7

Wagenmakers, E. J., Marsman, M., Jamil, T., Ly, A., Verhagen, J., Love, J., Selker, R., Gronau, Q. F., Smira, M., Epskamp, S., Matzke, D., Rouder, J. N., & Morey, R. D. (2018). Bayesian inference for psychology. Part I: Theoretical advantages and practical ramifications [Article]. *Psychonomic Bulletin & Review*, *25*(1), 35-57. https://doi.org/10.3758/s13423-017-1343-3

Wagenmakers, E. J., Verhagen, J., & Ly, A. (2016). How to quantify the evidence for the absence of a correlation [Article]. *Behavior Research Methods*, *48*(2), 413-426. https://doi.org/10.3758/s13428-015-0593-0

Wald, L. L., & Polimeni, J. R. (2017). Impacting the effect of fMRI noise through hardware and acquisition choices - Implications for controlling false positive rates. *Neuroimage*, *154*, 15-22. https://doi.org/10.1016/j.neuroimage.2016.12.057

Walker, G. A., Ohzawa, I., & Freeman, R. D. (1998). Binocular cross-orientation suppression in the cat's striate cortex. *Journal of Neurophysiology*, *79*(1), 227-239. https://doi.org/10.1152/jn.1998.79.1.227

Wang, L., Kloc, M., Maher, E., Erisir, A., & Maffei, A. (2019). Presynaptic GABA(A) Receptors Modulate Thalamocortical Inputs in Layer 4 of Rat V1. *Cerebral Cortex*, *29*(3), 921-936. https://doi.org/10.1093/cercor/bhx364

Wang, L., & Maffei, A. (2014). Inhibitory Plasticity Dictates the Sign of Plasticity at Excitatory Synapses. *Journal of Neuroscience*, *34*(4), 1083-1093. https://doi.org/10.1523/jneurosci.4711-13.2014

Wang, M. X., McGraw, P., & Ledgeway, T. (2020). Short-term monocular deprivation reduces inter-ocular suppression of the deprived eye [Article]. *Vision Research*, *173*, 29-40. https://doi.org/10.1016/j.visres.2020.05.001

Waterston, M. L., & Pack, C. C. (2010). Improved Discrimination of Visual Stimuli Following Repetitive Transcranial Magnetic Stimulation. *Plos One*, *5*(4). https://doi.org/10.1371/journal.pone.0010354

Watson, A. B. (2017). QUEST plus : A general multidimensional Bayesian adaptive psychometric method. *Journal of Vision*, *17*(3), Article 10. https://doi.org/10.1167/17.3.10

Watson, A. B., & Pelli, D. G. (1983). QUEST - A BAYESIAN ADAPTIVE PSYCHOMETRIC METHOD [Article]. *Perception & Psychophysics*, *33*(2), 113-120. https://doi.org/10.3758/bf03202828

Webb, B. S., Dhruv, N. T., Solomon, S. G., Tailby, C., & Lennie, P. (2005). Early and late mechanisms of surround suppression in striate cortex of macaque. *Journal of Neuroscience*, *25*(50), 11666-11675. https://doi.org/10.1523/Jneurosci.3414-05.2005

Weber, A. I., Krishnamurthy, K., & Fairhall, A. L. (2019). Coding Principles in Adaptation. In J. A. Movshon & B. A. Wandell (Eds.), *Annual Review of Vision Science, Vol 5* (Vol. 5, pp. 427-449). https://doi.org/10.1146/annurev-vision-091718-014818

Weise, K., Numssen, O., Thielscher, A., Hartwigsen, G., & Knosche, T. R. (2020). A novel approach to localize cortical TMS effects. *Neuroimage*, *209*, Article 116486. https://doi.org/10.1016/j.neuroimage.2019.116486

Werner, J. S., & Chalupa, L. M. (2004). *The visual neurosciences*. MIT Press.

Wernicke, C. (1874). *Der aphasische symptomencomplex: Eine psychologische studie auf anatomischer basis.* Breslau, Cohn & Weigert.
Whitmire, C. J., & Stanley, G. B. (2016). Rapid Sensory Adaptation Redux: A Circuit Perspective. *Neuron*, *92*(2), 298-315. https://doi.org/10.1016/j.neuron.2016.09.046
Wikipedia, c. (29 September 2021 01:06 UTC). *Canny edge detector*. Wikipedia, The Free Encyclopedia. Retrieved 24 October 2021 16:55 UTC from https://en.wikipedia.org/w/index.php?title=Canny_edge_detector&oldid=1047102602
Wikipedia: the free encyclopedia. (2018). *Balloonist theory*. Retrieved April 1 from https://en.wikipedia.org/wiki/Balloonist_theory
Wilson, H. R. (2003). Computational evidence for a rivalry hierarchy in vision. *Proceedings of the National Academy of Sciences of the United States of America*, *100*(24), 14499-14503. https://doi.org/10.1073/pnas.2333622100
Wilson, H. R., Blake, R., & Lee, S. H. (2001). Dynamics of travelling waves in visual perception. *Nature*, *412*(6850), 907-910. https://doi.org/10.1038/35091066
Wilson, M., Andronesi, O., Barker, P. B., Bartha, R., Bizzi, A., Bolan, P. J., Brindle, K. M., Choi, I. Y., Cudalbu, C., Dydak, U., Emir, U. E., Gonzalez, R. G., Gruber, S., Gruetter, R., Gupta, R. K., Heerschap, A., Henning, A., Hetherington, H. P., Huppi, P. S., . . . Howe, F. A. (2019). Methodological consensus on clinical proton MRS of the brain: Review and recommendations [Review]. *Magnetic Resonance in Medicine*, *82*(2), 527-550. https://doi.org/10.1002/mrm.27742
Wilson, M. T., Fulcher, B. D., Fung, P. K., Robinson, P. A., Fornito, A., & Rogasch, N. C. (2018). Biophysical modeling of neural plasticity induced by transcranial magnetic stimulation [Review]. *Clinical Neurophysiology*, *129*(6), 1230-1241. https://doi.org/10.1016/j.clinph.2018.03.018
Wilson, N. R., Runyan, C. A., Wang, F. L., & Sur, M. (2012). Division and subtraction by distinct cortical inhibitory networks in vivo. *Nature*, *488*(7411), 343-348. https://doi.org/10.1038/nature11347
Wischnewski, M., & Schutter, D. (2015). Efficacy and Time Course of Theta Burst Stimulation in Healthy Humans [Review]. *Brain Stimulation*, *8*(4), 685-692. https://doi.org/10.1016/j.brs.2015.03.004
Wolters, A., Sandbrink, F., Schlottmann, A., Kunesch, E., Stefan, K., Cohen, L. G., Benecke, R., & Classen, J. (2003). A temporally asymmetric Hebbian rule governing plasticity in the human motor cortex [Article]. *Journal of Neurophysiology*, *89*(5), 2339-2345. https://doi.org/10.1152/jn.00900.2002
Wu, Y., Wang, W., Diez-Sampedro, A., & Richerson, G. B. (2007). Nonvesicular inhibitory neurotransmission via reversal of the GABA transporter GAT-1. *Neuron*, *56*(5), 851-865. https://doi.org/10.1016/j.neuron.2007.10.021
Wunderlich, K., Schneider, K. A., & Kastner, S. (2005). Neural correlates of binocular rivalry in the human lateral geniculate nucleus. *Nature Neuroscience*, *8*(11), 1595-1602. https://doi.org/10.1038/nn1554
Xing, J., & Heeger, D. J. (2001). Measurement and modeling of center-surround suppression and enhancement. *Vision Research*, *41*(5), 571-583. https://doi.org/10.1016/s0042-6989(00)00270-4
Yacoub, E., Harel, N., & Ugurbil, K. (2008). High-field fMRI unveils orientation columns in humans. *Proceedings of the National Academy of Sciences of the United States of America*, *105*(30), 10607-10612. https://doi.org/10.1073/pnas.0804110105
Yang, Y. P., Jin, J. Z., Zhou, Y. F., & Zhou, T. D. (2003). GABA(A) and GABA(B) receptors mediated inhibition affect the pattern adaptation of relay cells in the dorsal lateral geniculate nucleus (LGNd) of cats. *Brain Research*, *959*(2), 295-303, Article Pii s0006-8993(02)03765-4. https://doi.org/10.1016/s0006-8993(02)03765-4
Yang, Z. Y., Heeger, D. J., Blake, R., & Seidemann, E. (2015). Long-range traveling waves of activity triggered by local dichoptic stimulation in V1 of behaving monkeys. *Journal of Neurophysiology*, *113*(1), 277-294. https://doi.org/10.1152/jn.00610.2013
Yoon, J. H., Maddock, R. J., Rokem, A., Silver, M. A., Minzenberg, M. J., Ragland, J. D., & Carter, C. S. (2010). GABA Concentration Is Reduced in Visual Cortex in Schizophrenia and Correlates with Orientation-Specific Surround Suppression. *Journal of Neuroscience*, *30*(10), 3777-3781. https://doi.org/10.1523/Jneurosci.6158-09.2010
Yousry, T. A., Schmid, U. D., Alkadhi, H., Schmidt, D., Peraud, A., Buettner, A., & Winkler, P. (1997). Localization of the motor hand area to a knob on the precentral gyrus - A new landmark. *Brain*, *120*, 141-157. https://doi.org/10.1093/brain/120.1.141

Yu, X., Qian, C. Q., Chen, D. Y., Dodd, S. J., & Koretsky, A. P. (2014). Deciphering laminar-specific neural inputs with line-scanning fMRI [Article]. *Nature Methods*, *11*(1), 55-+. https://doi.org/10.1038/nmeth.2730

Zappe, A. C., Uludag, K., & Logothetis, N. K. (2008). Direct measurement of oxygen extraction with fMRI using 6% CO2 inhalation. *Magn Reson Imaging*, *26*(7), 961-967. https://doi.org/10.1016/j.mri.2008.02.005

Zenger-Landolt, B., & Heeger, D. J. (2003). Response suppression in V1 agrees with psychophysics of surround masking. *Journal of Neuroscience*, *23*(17), 6884-6893. https://doi.org/10.1523/JNEUROSCI.23-17-06884.2003

Zewdie, E., & Kirton, A. (2016). Chapter 1 - TMS Basics: Single and Paired Pulse Neurophysiology. In A. Kirton & D. L. Gilbert (Eds.), *Pediatric Brain Stimulation* (pp. 3-22). Academic Press. https://doi.org/https://doi.org/10.1016/B978-0-12-802001-2.00001-1

Zhang, H., & Sulzer, D. (2003). Glutamate spillover in the striatum depresses dopaminergic transmission by activating group I metabotropic glutamate receptors. *Journal of Neuroscience*, *23*(33), 10585-10592. https://doi.org/10.1523/JNEUROSCI.23-33-10585.2003

Zhang, P., Bao, M., Kwon, M., He, S., & Engel, S. A. (2009). Effects of Orientation-Specific Visual Deprivation Induced with Altered Reality. *Current Biology*, *19*(22), 1956-1960. https://doi.org/10.1016/j.cub.2009.10.018

Zhou, J. W., Clavagnier, S., & Hess, R. F. (2013). Short-term monocular deprivation strengthens the patched eye's contribution to binocular combination. *Journal of Vision*, *13*(5), 1-10. https://doi.org/10.1167/13.5.12

Zhou, Y. M., Lai, C. S. W., Bai, Y., Li, W., Zhao, R. H., Yang, G., Frank, M. G., & Gan, W. B. (2020). REM sleep promotes experience-dependent dendritic spine elimination in the mouse cortex. *Nature Communications*, *11*(1), Article 4819. https://doi.org/10.1038/s41467-020-18592-5

Ziemann, U. (2020). I-waves in motor cortex revisited. *Experimental Brain Research*, *238*(7-8), 1601-1610. https://doi.org/10.1007/s00221-020-05764-4

Ziemann, U., Lonnecker, S., Steinhoff, B. J., & Paulus, W. (1996). The effect of lorazepam on the motor cortical excitability in man [Article]. *Exp Brain Res*, *109*(1), 127-135. https://doi.org/10.1007/BF00228633

Annex A: WHAT SHOULD WE BE LOOKING FOR IN THE BRAIN? COMPUTATIONS.

A.1 The importance of relevant observations The human mind attempts to understand nature by creating abstract explanatory theories or models from existing observations. The empirical approach dominating modern science is to challenge these models by testing predictions derived from them. Performing these tests on new observations, made in different contexts, allows to select the explanatory models that are also predictive and generalizable – empirically tested models are more likely true or useful. Prediction testing also produces new observations often better targeting the relevant aspects of the object of a given scientific field. Importantly, theory defines the observations that are relevant to be made and relevant observations, even made for exploration, feedback on the theory, helping to refine and formalize it. This makes the field progress until it reaches corners where theory fails and observations consequently no longer relevant. In this opinion paper, I will illustrate the importance of making relevant observations through examples from the history of neuroscience, and argue that the most important question in system's neuroscience should ask what is the most relevant observation to make. I will propose *computation* as the answer and illustrate an experimental strategy for producing such relevant observations.

A.2 Observations in neuroscience Irrelevant observations can obviously lead to wrong theories. In ancient Greece and during the Renaissance, the observation of vast networks of cavities throughout the body during anatomical dissections led to the now obviously wrong Balloonist theory, where liquids or air flowing through these networks allow for functions of the "soul" (Wikipedia: the free encyclopedia, 2018). Even good theory can lead to dead ends when based on irrelevant observations. Early 19th century phrenologists had it right about modular brain functions that map on the gyrification pattern of the brain. Their error was to also postulate that the gyrification pattern impacted the outer shape of the skull, implying that someone's mental abilities can be predicted from the shape of that person's head, and leading them to collect actually unpredictive head shape observations (Jones et al., 2018). The idea of a modular brain organization however also predicted that sufficiently localized lesions should produce specific clinical symptoms. It is the more relevant observation of *lesion-symptom*

relations, pioneered by anatomists like Paul Broca (1861) and Carl Wernicke (1874) and still used today in clinical neurology, that established and refined the modular brain model. Note that an observation here is more than the objectivization of a lesion or the report of a symptom. It is rather the cooccurrence or the relation between the two. As used in this paper, an observation is the operationalization of some elements of a theory – if a brain module exists, damaging it will produce related symptoms. An observation should therefore be seen as a practical conceptual tool carved out of theory. If any relevant to the nature of the brain, probing it with such conceptual observations will have knowledge progress – looking for lesion-symptom relations contributed to the mapping of brain functions, looking for skull shape-mental ability relations did not.

New theories contributed new observations, each deepening our understanding of the brain. Giving up on a transcendent nature of the mind, behavioral psychology viewed the brain as a black-box programable machine to be understood through stimuli generating responses or inputs being transformed into outputs – we understood that the brain can link a ringing bell with food from the bell (input), reliably predicting salivation (output) in Pavlov's conditioned dogs. Here it is the *input-output relation* that became the relevant conceptual observation. Behavioral psychology greatly contributed to understanding the brain through the categorization of these relations and the description of their formation and extinction. However, observations of complex, weakly predictable input-output relations eventually cumulated – now try to predict what (input) will trigger your dog to chew on the couch (output). An input-output relation can change in an instant, e.g. the intensity needed to detect a stimulus increases as soon as you divert attention away from it. The black box must entail some flexibility, which was accommodated by cognitive theories of the brain that built on the earlier described modular model of the brain. As these modules flexibly interact, they could define different internal brain states that modulate the input-output relation. Here, the relevant observation is the *brain state*. Attention, emotion and working memory might now seem obvious "things", but they could not be scientifically circumscribed before cognitive psychology observed them as brain states.

Finally, behavioralist and cognitivist views both imply that the brain processes information. Information enters the brain as inputs, operations are performed, transforming the information, likely multiple times before the results are relayed as outputs – the brain computes. As early as in the late 19th century, Ramón y Cajal proposed a type of cell later called neuron as the material substrate for computations, integrating inputs at its dendrites and generating outputs through its axon (Lopez-Munoz et al., 2006). These now well understood integrate-and-fire properties and the advancement of recording technics propelled the observation of *neuronal firing* to the level of a gold-standard for understanding the brain – if neurons fire, the brain is computing, and vice versa.

A.3 System's neuroscience System's neuroscience tends to integrate all the above-mentioned observations in experiments carefully controlling/monitoring the inputs and outputs of the brain, manipulating brain states and assessing the effect of brain lesions. Not to mentioning other important observations, it is heavily based on neuronal firing, the central observation to which, for the good reason described above, the others are referred to. Another important aspect of the field is the strive for fully circumscribing and describing a given system, ideally in a formal mathematical way – descriptions of the oculomotor system do not consider the effects of attention until they are involved, and efforts are made to thigh the different modules involved into a comprehensive computational model.

These efforts are however constantly faced with the mind-boggling complexity of brain functions. Whether we could ever achieve a true understanding of the brain, in the sense that one could "fix" a broken implementation, is a warranted question. Jonas and Kording (2017) addressed that very question by applying current state-of-the-art neuroscience tools (or observations) to study a fully-known man-made surrogate brain: a micro-processor. They provocatively concluded that the detailed descriptions they obtained of the micro-processor could not possibly yield the understanding one would hope from this relatively simple system that a group of engineers designed within few months.

A.4 Computations What are we, neuroscientists, doing wrong? Probably nothing. But I would like to propose that all we need is to conceptualize the observation most relevant to the

computing function of brain – and that observation would be a *computation*. A firing neurons computes, but what *is* the computation? Certainly more than the fired output. A computation would be fully described from some information taken as inputs by a computing unit, transformed and relayed as outputs. Its observation would require reading information both from the input and output of the unit, allowing to describing how they relate, or alternatively rewiring the input and/or output of the unit and assess the effects. Obvious technical challenges apart, an interesting example of how to observe a computation comes from the rerouting of visual information to the auditory cortex of deaf cats, which supports boosted visual performance (Lomber, 2017). Cooling inactivation revealed a specific auditory area specifically supported the same kind of computation irrespective of its visual (in deaf cats) or auditory (in hearing cats) inputs: localizing stimulus in space. Directly manipulating inputs to the computing unit allowed to observe the computation, to disambiguate the functional role of the area. I think that observations of this kind, and others to be discussed, focused on computations, will fuel further progress by allowing targeted probing of the very nature of the computing brain.

A.5 Bibliography

Broca, P. (1861). Remarques sur le siege de la faculté du langage articulé; suivies d'une observation d'aphemie (perte de la parole). *Bulletins de La Société Anatomique (Paris)*, *6*, 330-357; 398-407.

Jonas, E., & Kording, K. P. (2017). Could a Neuroscientist Understand a Microprocessor? [Article]. *Plos Computational Biology*, *13*(1), 24, Article e1005268. https://doi.org/10.1371/journal.pcbi.1005268

Jones, O. P., Alfaro-Almagro, F., & Jbabdi, S. (2018). An empirical, 21st century evaluation of phrenology [Article]. *Cortex*, *106*, 26-35. https://doi.org/10.1016/j.cortex.2018.04.011

Lomber, S. G. (2017). What is the function of auditory cortex when it develops in the absence of acoustic input? [Article]. *Cognitive Development*, *42*, 49-61. https://doi.org/10.1016/j.cogdev.2017.02.007

Lopez-Munoz, F., Boya, J., & Alamo, C. (2006). Neuron theory, the cornerstone of neuroscience, on the centenary of the Nobel Prize award to Santiago Ramon y Cajal [Article]. *Brain Research Bulletin*, *70*(4-6), 391-405. https://doi.org/10.1016/j.brainresbull.2006.07.010

Wernicke, C. (1874). *Der aphasische symptomencomplex: Eine psychologische studie auf anatomischer basis.* Breslau, Cohn & Weigert.

Wikipedia: the free encyclopedia. (2018). *Balloonist theory*. Retrieved April 1 from https://en.wikipedia.org/wiki/Balloonist_theory

Annex B: MODELS OF BINOCULAR RIVALRY AND ALTERATION OF INTEROCULAR BALANCE

Bistable perception occurs whenever two qualitatively different images can be consciously perceived in alternation from stimulation with a single, physically stable image. Numerous examples of such ambiguous stimuli can produce bistable percepts across visual domains ranging from higher-level object recognition, as in the famous young lady versus old women illusion (Fig.1A), to depth (Fig.1B), motion perception (Fig.1C) and others. Binocular rivalry paradigms, where two physically dissimilar images are dichoptically presented, one to each eye (Fig.1D), are often used to study bistable perception. Just as a woman cannot be physically young and old at the same time, the world cannot *be* different whether it is seen from the left of the right eye. The brain therefore suppresses one, or multiple possible internal representations of this world such that only one reaches consciousness, and dominates perception at any given time. This selection and suppression process is intrinsically unstable, the dominant percept eventually vanishing and the suppressed one taking over, alternating

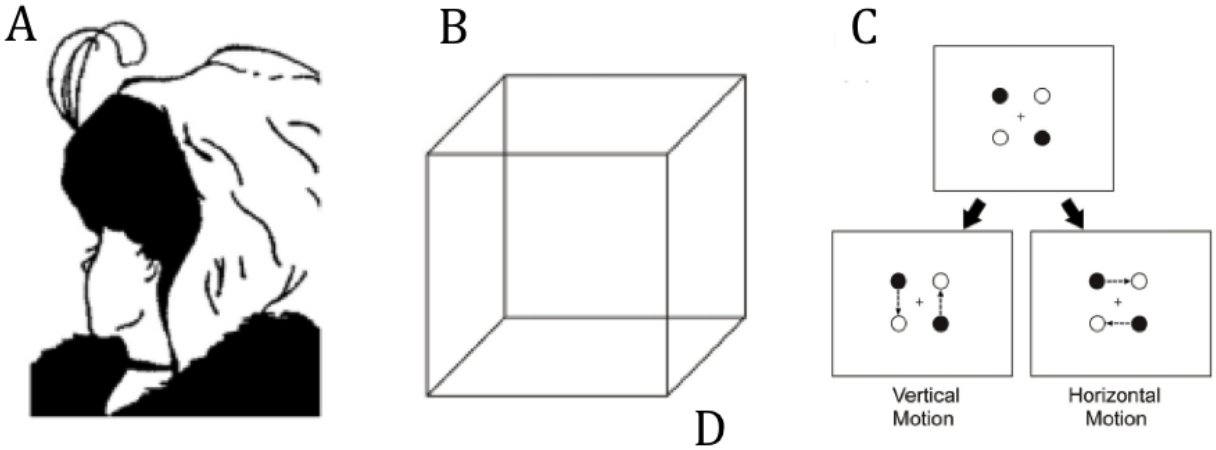

Figure 1. Examples of ambiguous stimuli in A. object recognition (either an old women or a young lady can be perceived), B. depth perception (the front face of the cube can either be the upper or the lower square) and C. motion perception (the circles simultaneously alternating between a white and a black fill can be perceived as apparent vertical of horizontal motion). Adapted from *Scocchia et al. Front Hum Neurosci. 2014*. In binocular rivalry in D., two orthogonal gratings are dichoptically presented, one to each eye. With relatively small stimulus size, perception is dominated by either one orientations, which alternate over time, rather than by a plaid overlay. Adapted from *Tong et al, Trends Cogn Sci. 2006*.

every few seconds, hence bistability. Although some stimulus characteristics or top-down cognitive processes like attention can modulate the stochastic statistics of duration of dominance periods, switches are inevitable (Blake & Logothetis, 2002).

The following essay will first describe the key computational features generating bistability in models of binocular rivalry and bistable perception in general. Although a review of the large body of literature on binocular rivalry and its ongoing debates would be of most interest for the current work, an adequate description covering all existing computational models addressing binocular rivalry can hardly be achieved in this manuscript with reasonable length. Instead, reference to other models and their key features will be made throughout the following sections whenever deemed appropriate. This will allow to further focus on the computational implications of a putative role for the inhibitory neurotransmitter GABA, and of the effect of unbalancing interocular interactions on the dynamics of rivalry. Finally, an implementation of one particular model will be challenged to account for some data from my lab where both neurotransmitter concentrations and rivalry dynamics were measured before and after altering the interocular balance with monocular deprivation.

B.1 THE GENERIC MODEL OF RIVALRY

B.1.1 Mutual inhibition

Early modeling work on binocular rivalry used competitive inhibition for the establishment of dominance of one percept over the other (Blake, 1989; Lehky, 1988; Sugie, 1982), a mechanism that still today is central to the vast majority of models (Blake & Wilson, 2011; Scocchia et al., 2014). In its minimalist form, a model would include two units, X1 and X2, respectively responding to excitatory inputs I_1 and I_2 with an activity level X_1 and X_2 as follow:

$$\tau \partial X_1 = I_1 - X_1$$
$$\tau \partial X_2 = I_2 - X_2 \qquad [1]$$

This could represent a red right-tilted grating in the right eye stimulating unit X1 and a green left-tilted grating in the left eye stimulating unit X2, such that the activity level in a given unit,

here solely dependent on the strength of the inputs, reflects the strength of the percept corresponding to the physical image it is driven by (Fig.1A). Mutual inhibition between the two units:

$$\tau\partial X_1 = I_1 - X_1 - \gamma S[X_2]$$
$$\tau\partial X_2 = I_2 - X_2 - \gamma S[X_1] \quad [2]$$

, where the level of activity of one suppresses activity of the other with gain *gamma* after non-linear transformation (S[*X*]=X^{18} for *X*>=0 and S[*X*]=0 for *X*<0), will introduce a winner-takes-all competition. An ever slight advantage in activity level of one unit, say X1, may it be by chance, will have it maximally suppress its opponent X2, while lifting inhibition on itself at the same time. Initiated at 0 and responding to the introduction of constant inputs I_1 slightly larger than I_2, X_1 and X_2 will rapidly converge respectively to their maximum and minimum, and dominance of perception of a red right-tilted grating will be established (Fig.2C).

B.1.2 Adaptation

Driving inputs and mutual inhibition alone are not sufficient for bistability, since the system becomes stable once dominance is established. Another element is needed to disrupt dominance and allow alternations. In our minimalist model, adaptation, depicted as recurrent self-inhibitory connections in Fig.1A and akin to neuronal fatigue, goes as follow:

$$\tau\partial X_1 = I_1 - (1+A_1)X_1 - \gamma S[X_2]$$
$$\tau\partial X_2 = I_2 - (1+A_2)X_2 - \gamma S[X_1] \quad [3]$$

$$\tau_A\partial A_1 = -A_1 + \alpha S[X_1]$$
$$\tau_A\partial A_2 = -A_2 + \alpha S[X_2] \quad [4]$$

, where A_1 and A_2 stand for the adaptation level of each unit and modulate the leak term. Adaptation levels are themselves controlled by the differential equations [4], which represents slow (tau_A >> *tau*) leaky integrators of the level of activity of the corresponding unit. Given this, adaptation will slowly accumulate for the highly active dominant X1 unit (Fig.1D, bottom panel), and as it does, it gradually reduces the activity level of the same unit (Fig.1D, top panel), *ergo* leading to dynamic interactions involving disinhibition of the suppressed X2 unit and inhibition of the dominant X1 unit by the increasingly active X2 unit. This culminates with rapid reversal of dominance once activity level of the (previously highly) suppressed X2 exceeds that of the (now

much less) dominant X1, and after the process can start over. Whether this fatigue, generally referred to as adaptation, is implemented similarly to physiological spike-rate adaptation by up-regulating the leak of the input integrator as above (Noest et al., 2007; van Loon et al., 2013) and/or as synaptic depression where the gain of the excitatory inputs to, or the inhibitory inputs from, the highly active unit is reduced (Laing & Chow, 2002), the behavior of the system will be the same: dominance and suppression wane over time and bistability emerges.

B.1.3 Noise

One must note that adaptation is not an absolute requirement for bistability (Brascamp et al., 2006; Moreno-Bote et al., 2007; Shpiro et al., 2009). If strong enough, and accompanied by mutual inhibition, Gaussian noise of mean 0 and standard deviation *sigma* added to the input signal as follow:

$$\tau\partial X_1 = I_1 - X_1 - \gamma S[X_2] + N(0, \sigma_{X1})$$
$$\tau\partial X_2 = I_2 - X_2 - \gamma S[X_1] + N(0, \sigma_{X2}) \qquad [5]$$

can momentarily overcome the mutual inhibition-induced dominance and trigger alternations (Fig.2E). Using such a mechanism to generate bistability takes us from the deterministic oscillator-based model described above to a stochastic attractor-based model, which although not explicit in the derivation in [5], represents the two perceptual alternatives as stable minima, the attractors, on an energy plane (Moreno-Bote et al., 2007). Whether triggering a perceptual switch is best explain by energizing an activity space with noise or by attenuating activity level associated with the dominant percept through adaptation processes is an ongoing debate, but an accurate match to experimental data likely requires a balance between both (Shpiro et al., 2009). Importantly, at least some level of noise, whether implemented in the inputs or as fluctuations in the gain of adaptation gain or synaptic depression, is most certainly required, as the deterministic nature of systems in which bistability relies solely on adaptation, as in [3] and [4], cannot produce the stochastic behavior, with gamma or log-normal distributed durations of dominance, that is a psychophysical hallmark of bistable perception (Levelt, 1968). Interestingly, the deterministic, yet chaotic behavior emerging from distributed neuronal network with Gaussian pattern of connectivity can mimic stochasticity and by producing

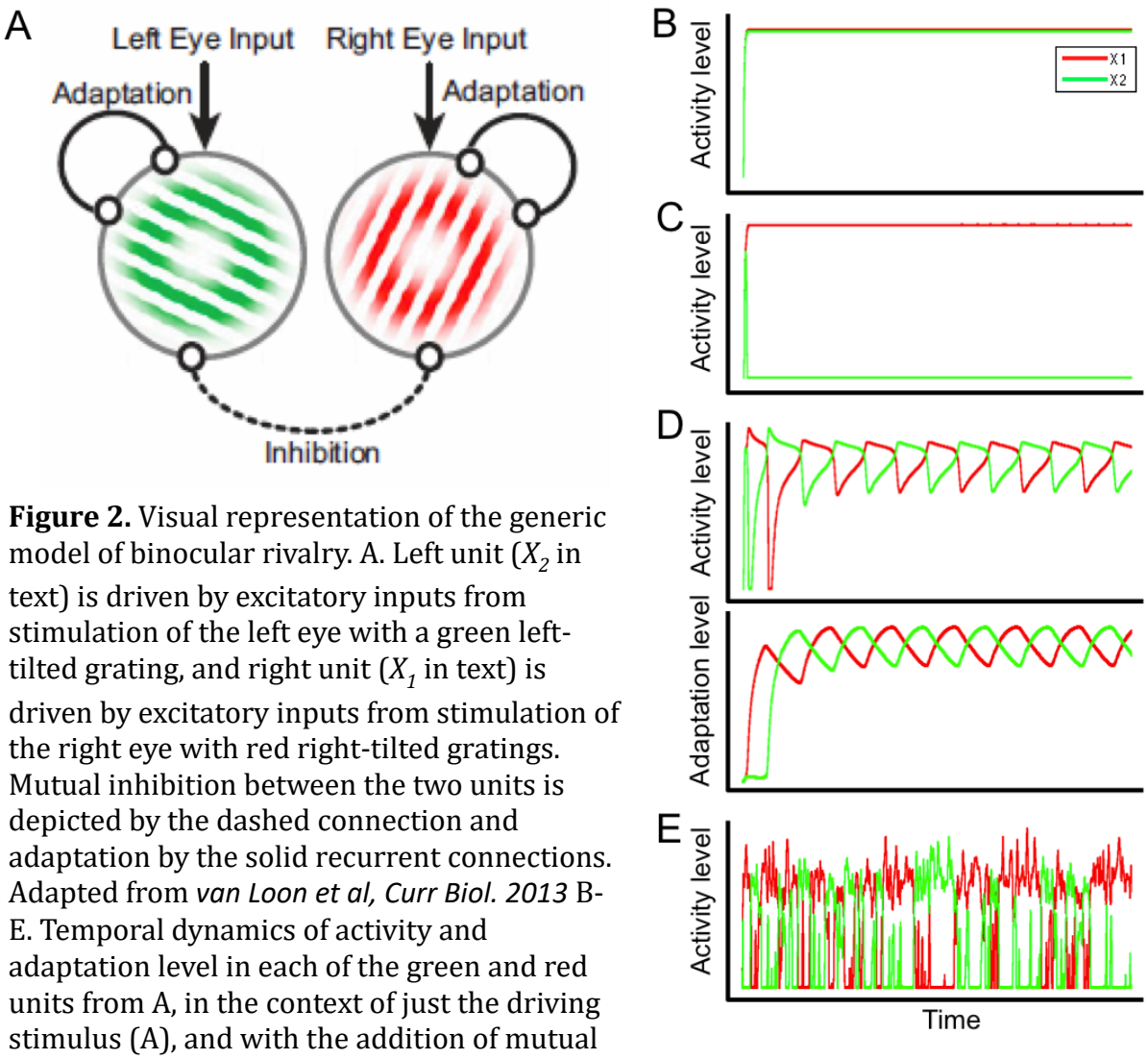

Figure 2. Visual representation of the generic model of binocular rivalry. A. Left unit (X_2 in text) is driven by excitatory inputs from stimulation of the left eye with a green left-tilted grating, and right unit (X_1 in text) is driven by excitatory inputs from stimulation of the right eye with red right-tilted gratings. Mutual inhibition between the two units is depicted by the dashed connection and adaptation by the solid recurrent connections. Adapted from *van Loon et al, Curr Biol. 2013* B-E. Temporal dynamics of activity and adaptation level in each of the green and red units from A, in the context of just the driving stimulus (A), and with the addition of mutual inhibition (B), mutual inhibition and slow adaptation (D) or mutual inhibition and input noise (E). See text for details.

gamma-distributed dominance durations (Laing & Chow, 2002), challenging this idea of an absolute requirement of noise to accurately account for empirical data.

B.2 The role GABAergic inhibition in the competition process

As described above, the role of competitive inhibition is central to the majority of models of binocular rivalry and bistable perception in general, but surprisingly enough, to the best of my knowledge, this assumption has been put to experimental challenge only very recently. (van

Loon et al., 2013) made use of a generic low-level model of bistable perception implementing both adaptation and input noise in a single stage (see later sections for a detailed description of the model) in order to predict the effect of changes in the level of (putatively GABAergic) mutual inhibition on the duration of dominance periods. Using both Magnetic Resonance Spectroscopy measures of GABA in the occipital cortex and pharmacological modulation of the $GABA_A$ receptor, they confirmed the predictions of the model in three types of bistable perception, including binocular rivalry. Subjects with higher GABA concentrations, and presumably higher levels of competitive inhibition, showed longer dominance durations as expected, and pharmacological inhibition of the receptor further suggested causality of the relation.

It is important to note at this point that the exact locus of the inhibition responsible for dominance is still a matter of debate (Blake & Wilson, 2011; Kovacs et al., 1996; Logothetis et al., 1996), just as is the relevance and nature of a hierarchical structure (Freeman, 2005; Wilson, 2003) and the importance of top-down interactions (Tong et al., 2006). Interestingly, (van Loon et al., 2013)'s relation between dominance durations and GABA concentrations was specific to the occipital cortex, as it was not found in the dorsolateral prefrontal cortex (DLPFC), a high-level region that may be implicated percept alternation (Vernet et al., 2015). This reinforces the idea that although competition can go on at higher levels, rivalry is likely initiated by competition at lower levels in the visual hierarchy (Blake & Wilson, 2011).

B.3 Monocular deprivation and unbalanced rivalry dynamics

The fully developed visual system is known to retain some potential for plastic changes, as revealed by various visual deprivation protocols in human adults (Boroojerdi et al., 2000; Kwon et al., 2009; Zhang et al., 2009). Plasticity induced by one such protocol involving a relatively short period (30 minutes to 3 hours) of monocular deprivation can bias vision towards a greater influence of the deprived eye during binocular combination (Zhou et al., 2013) and greater perceived contrast from the deprived relative to the non-deprived eye (Lunghi et al., 2011). Consistent with that is the fact that contrast sensitivity is increased in the deprived-eye and reciprocally decreased in the non-deprived one (Zhou et al., 2013). Not surprisingly, such

monocular deprivation treatment can also bias binocular rivalry dynamics toward longer dominance periods for the deprived-eye (Lunghi et al., 2011; 2013).

At first sight, these recent findings could point toward homeostatic modulation of contrast-gain mechanisms (Mrsic-Flogel et al., 2007). Given (van Loon et al., 2013)'s demonstration of the involvement of GABA in rivalry dynamics, couldn't monocular deprivation act through altering the balance of interocular mutual inhibitory connections? More importantly, the potency of monocular deprivation-induced plasticity offers an opportunity to challenge current computational models of binocular rivalry by offering a new way to alter processes underlying its dynamics.

B.4 Modeling the effect of unbalanced modulations on the rivalry dynamics

In this section, we will explore the dependence of dominance period durations on the different components of its underlying dynamics. In addition to balanced changes, i.e. identical changes to parameters related to the left and the right eye, I will attempt to offer a computational framework for the recent data on monocular deprivation reported above through the assessment of the effect of unbalanced, or unilateral parameter changes. Finally, the behavior of model will be compared to preliminary results from my lab where the dependence of binocular rivalry dynamics on the neurotransmitters GABA and glutamate was assessed using Magnetic Resonance Spectroscopy (MRS) (van Loon et al., 2013), both before and after ~3h of monocular deprivation (Lunghi et al., 2011; 2013).

Simulations will be limited to a single implementation of the generic computational model of binocular rivalry described above, the one from (van Loon et al., 2013), which incorporates all of mutual inhibition, adaptation and noise within a single stage. This decision is motivated by the ease of implementation of the model, which also has the advantage of already being shown by the investigators to reflect GABA-related effects on the rivalry dynamics, at least on the basis of inter-individual variations. It could have been of interest to explore more elaborate models implementing elements of hierarchical structure (Freeman, 2005; Wilson, 2003), top-down modulations (Tong et al., 2006) or distributed neuronal networks (Laing & Chow, 2002), but since our MRS-measures are limited to lower cortical visual areas and given the relatively high

explanatory power of generic single-stage models, it should suffice to capture most of the relevant processes.

B.3.1 Methods

B.3.1.1 Simulations

The levels of activity X_1 and X_2 of the model units X1 and X2 (Fig.2A) respectively responding to inputs I_1 and I_2 are governed by the following set of differential equations:

$$\begin{aligned}\tau\partial X_1 &= I_1 - (1+A_1)X_1 - \gamma_2 S[X_2] + N(0,\sigma_{X1}) \\ \tau\partial X_2 &= I_2 - (1+A_2)X_2 - \gamma_1 S[X_1] + N(0,\sigma_{X2})\end{aligned} \quad [6]$$

$$\begin{aligned}\tau_A\partial A_1 &= -A_1 + \alpha_1 S[X_1] \\ \tau_A\partial A_2 &= -A_2 + \alpha_2 S[X_2]\end{aligned} \quad [7]$$

It implements 1) mutual inhibition similar to [2], where X_1 suppresses X_2 with gain $gamma_1$ and X_2 suppresses X_1 with gain $gamma_2$ after non-linear transformation ($S[X]=X^{18}$ for $X>=0$ and $S[X]=0$ for $X<0$), 2) adaptation by modulation of the leak term with an adaptation levels A_1 and A_2 similar to [3] and 3) Gaussian noise of mean 0 and standard deviation $sigma_1$ and $sigma_2$ similar to [5]. Adaptation levels are governed by the slow (tau=1 whereas tau_A=125) leaky integrators of X_1 and X_2 with gain $alpha_1$ and $alpha_2$, similarly to [7]. Note that this exactly reproduces (van Loon et al., 2013)'s implementation, with the only difference that the *gamma* and *alpha* parameters can now be independently modulated for X1 and X2.

Using constant inputs I_1 and I_2, the dynamical system was solved for X_1, X_2, A_1 and A_2 by integrating the set of 4 differential equations from [5] and [6] in the Matlab computing environment from time 0 to 5000 (arbitrary units) using the Runge-Kutta method as implement in the ode45.m function. All variable solved were restricted to non-negative values and initiated at 0. Maximum time step allowed was 1 and relative tolerance 10^{-5}. An example of the time series obtained for X_1, X_2, A_1 and A_2 is shown in Fig3. From the reach of equilibrium (arbitrarily defined at 100 time units) to the end of the time series, periods of dominance were identified between to successive crossings of X_1 and X_2. Durations of X1 and X2 dominance periods were calculated and averaged.

When investigating the effect of balanced parameter changes, the two members of each parameter pair always shared the same value, and the value of only one parameter pair at a

time was modulated over its range across different simulations, while the other pairs were set to their reference value. Reference values and ranges are indicated in Table1. For example, when testing the effect of input strength I, $I_1 = I_2 = I$, where I varies within [0.95, 1.05] while $gamma_1 = gamma_2 = gamma = 3$, $sigma_1 = sigma_2 = sigma = 0.003$ and $alpha_1 = alpha_2 = alpha = 4$. This was iterated ten times for each of the parameter pairs explored.

For the investigation of unbalanced parameter changes, a similar scheme was used, with the only exception that the parameter corresponding to the first modeled unit X1 within a parameter pair was always set to its reference value, such that only parameters corresponding to X2 varied. For example, when testing the effect of input strength I, $I_1 = I$ but I_2 varies within [0.95, 1.05], while $gamma_1 = gamma_2 = gamma = 3$, $sigma_1 = sigma_2 = sigma = 0.003$ and $alpha_1 = alpha_2 = alpha = 4$. This was also iterated ten times for each of the parameter pairs to explore.

Table 1: Parameter space of simulations

Parameters	Reference Value	Range
I (I_1, I_2)	1	[0.95, 1.05]
$gamma$ ($gamma_1$, $gamma_2$)	3	[2.6, 3.4]
$sigma$ ($sigma_1$, $sigma_2$)	0.003	[0.001, 0.015]
$alpha$ ($apha_1$, $alpha_2$)	4	[3, 5]

B.3.1.2 Experimental acquisitions

Five subjects participated in this study so far, approved by the ethics committee of the Montreal Neurological Institute of Montréal. They all underwent a Magnetic Resonance Imaging (MRI) session, but one was not available for the follow-up behavioral session.

MRI acquisitions began with anatomical scans to allow the prescription of a 3x3x3cm^3 voxel for ^{1}H-MRS acquisition. These acquisitions used the MEGA-PRESS *J*-coupling editing sequence (Mescher et al., 1998) allowing measurement of GABA and glutamate neurotransmitters, the concentrations of which were normalized as ratios to the simultaneously acquired creatine signal. Two 8-minute measurements were acquired before and immediately after the start of monocular deprivation with an opaque black eye patch. Subjects then either monocularly read or watched television outside the scanner for the ~3 hours of the deprivation treatment before

coming back to the scanner for two other measurement immediately before and after removal of the patch.

In a follow-up behavioral session, the binocular rivalry dynamics was assessed similarly to (Lunghi et al., 2011). Using polarized filters, two orthogonal (-45° and +45° orientations) high-contrast gabor patches of 3cpd and size 1.5° were dichoptically and continuously presented within a squared frame to facilitate fusion. With fixation at the center of the gabor, subjects were instructed to press down a key assigned to one gabor whenever that gabor clearly dominated their visual field, and to release the key only when dominance was not clear anymore. A different key was assigned to the other gabor. The median durations of key presses during a 3-minute run were computed and averaged between two consecutive runs to yield one dominance duration measurement for each eye. Separated by about 15 minutes, two such measurements were obtained before and immediately after the same monocular deprivation treatment as administered during the MRI session.

B.3.2 Results

B.3.2.1 Simulations Results

A section of the time series of variables X_1, X_2, A_1 an A_2 obtained from one simulation using reference values for all parameters is shown in Fig.3A, along with the histogram of dominance period durations compiled across the ten iterations of the simulation (Fig3.B). The expected behavior is expressed, with high levels of activity alternating between X1 and X2. Adaptation levels vary more slowly and follow the activity level with some time lag, just as it would be expected from a slow leaky integrator. Note that the pattern closely resembles the one from Fig.2D, with the only exception of the addition of a little noise. This is not surprising since the

current simulation using [6] and [7] only differs from the simulation in Fig.2D, using [3] and [4], by the addition of the noise term. This noise did allow to break the determinism of the system, as can be seen from the distribution of dominance durations in Fig3.B. Although it does not fit well the expected gamma distribution, it is nevertheless *mostly* unimodal and skewed toward longer durations, as reported from human psychophysics. The few instances of very short duration are unexpected and will be discussed later.

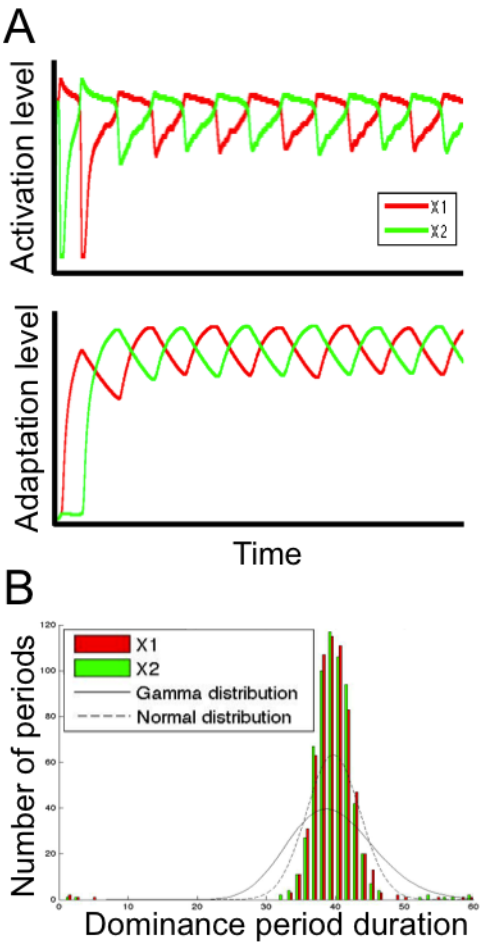

Figure 3. Simulation results when all parameters are set to their reference value. A. Time evolution of the activity and adaptation level of unit X1 and X2. B. Histogram of dominance period durations, collapsed across the ten iterations of the simulations. Gamma and normal distribution are fitted on the combination of X1 and X2 dominance periods.

The dependence of dominance period durations upon the different parameter tested is shown in Fig.4A-D. Open circles represent durations when both parameters of a pair were changed together according the value on the abscissa. Durations unexpectedly increased with input strength *I* (Fig.4A), but was directly related to mutual inhibition *gamma* (Fig.4B) as in (van Loon et al., 2013). Durations decreased with increases in both adaptation gain *alpha* (Fig.4C) and noise *sigma* (Fig.4D), but the later did so supra-linearly with larger changes in the upper noise range.

Filled circles in Fig.4 illustrate durations when only the parameter corresponding to unit X2 was changed according the value on the abscissa, the other parameter of the pair under examination being fixed to its reference value. The doted lines indicate durations when all parameters are set to their reference value. Increasing input strength I_2 increased X2 durations, almost linearly, and had the reciprocal effect on X1 durations (Fig.4A). Increasing inhibition from X2 to X1 while keeping fixed the inhibition from X1 to X2 allowed X2 to remain dominant

for longer periods of time, but that stronger inhibition on X1 left its dominance durations virtually unaffected (Fig.4B). The effect of unilateral changes in adaptation gain was similarly unilateral, with increases in $alpa_2$ decreasing durations of X2 only. Finally, the effect of noise is much richer. Making noisier only the inputs to X2 increased dominance duration of the later, and had roughly the mirror effect on X1 durations. Contrary to the effect of changing $sigma_1$

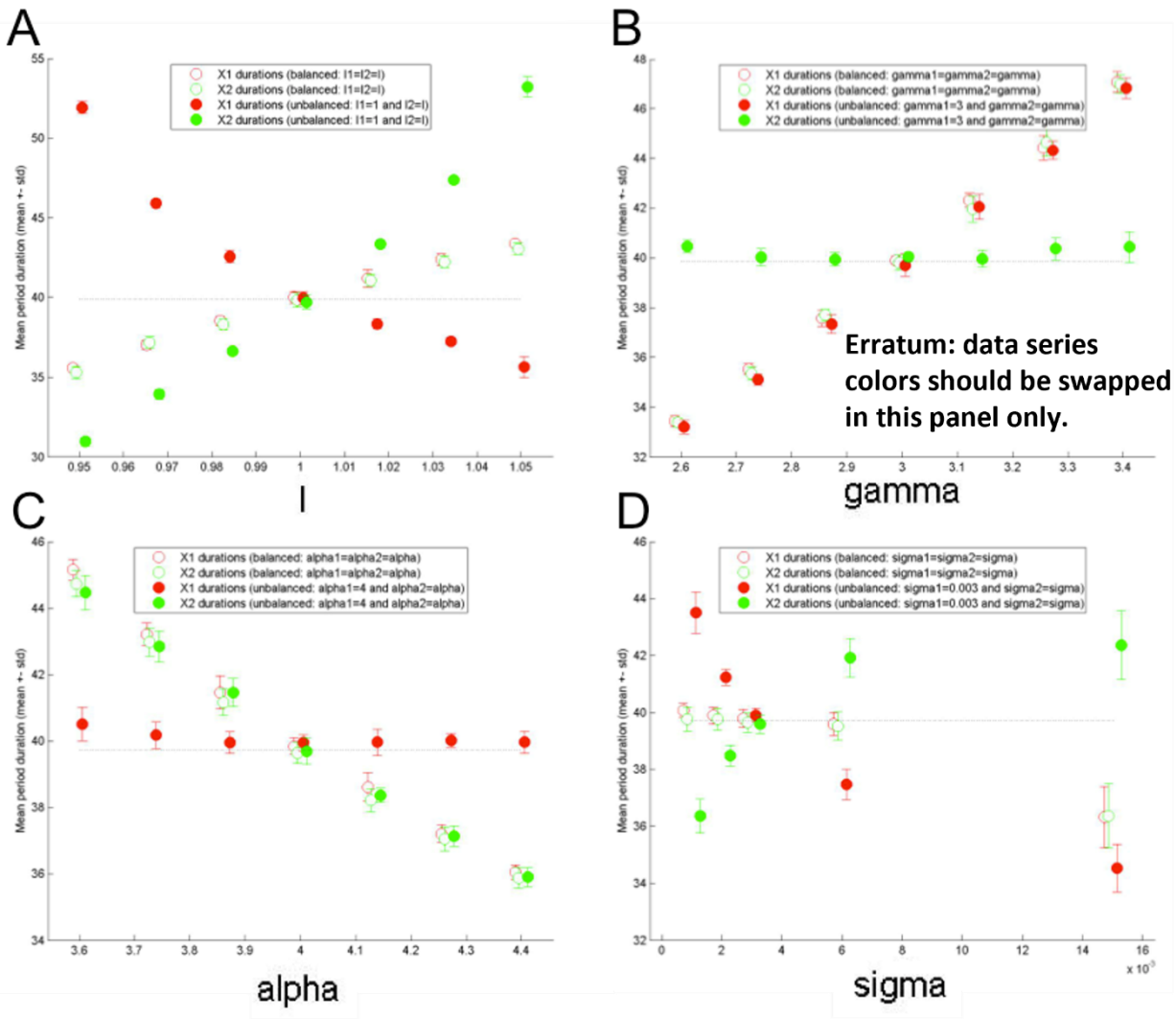

Figure 4. Dependence of dominance period durations on different parameter values. Durations of X1 and X2 dominance (mean and standard deviation across ten simulations) are respectively shown in red and green, and in the case of balanced (open circles) and unbalanced (filled circles) variations of the parameters. The dotted line indicate durations when all parameters are set to their reference value. A. Effect of variations of input *I*. B. Effect of variations of mutual inhibition gain *gamma*. C. Effect of variations of adaptation gain *alpha*. D. Effect of variations of noise gain *sigma*.

and *sigma*$_2$ together, which accelerated at higher noise level, the effects of unilateral changes of noise evolve rapidly in the lower and saturate in the higher noise range (Fig.4D).

B.3.2.2 Empirical Results

Results of the empirical experiment are summarized in Fig.5 and Fig.6. As expected from (Lunghi et al., 2011; 2013), monocular deprivation (MD) did bias the initially balanced interocular dynamics toward the deprived eye, with ratios of duration of percepts from the non-deprived over the deprived eye shifting from around one to lower values. MRS-measures of neurotransmitters did not show evidence of short-term effects of the transitions between binocular and monocular viewing at the onset and offset of the MD treatment. Viewing conditions will not be considered further and all four pre-MD measures (containing two measures during binocular and two during monocular viewing) will be taken as baseline, just as the four post-MD measures will be considered as reflecting time effects only, if any. Although MD did modulate neurotransmitter, it did so in an unsystematic manner, with both increases and decreases depending on the subject, for glutamate and especially GABA. No sham MD condition or control brain region was acquired, but the relevance of these changes to MD deprivation is supported by their correlation with the behavioral effects of the treatment reported below.

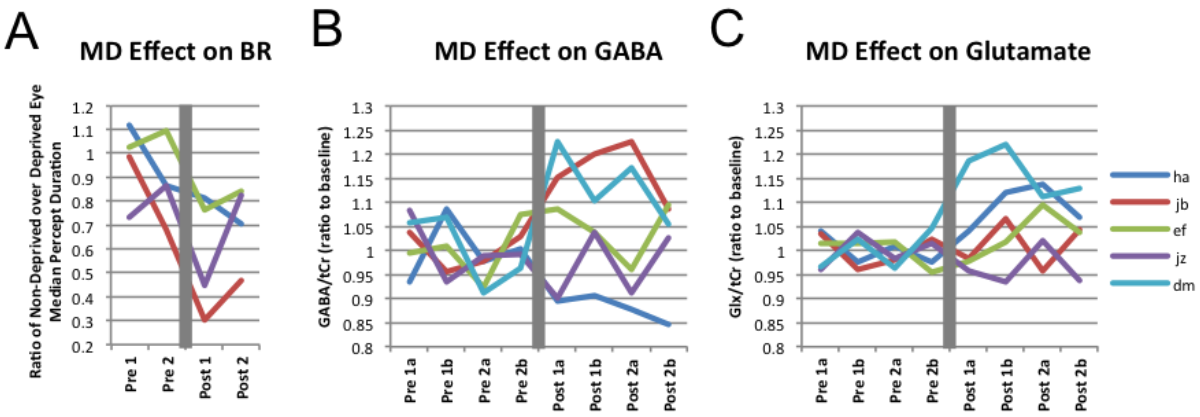

Figure 5. Empirical effect of monocular deprivation (MD) on binocular rivalry (BR) (A) and GABA (B) and glutamate (C) neurotransmitter concentrations. Thick vertical vertical lines mark the location of the 3-hour MD treatment. A. Ordinate axis reflect interocular balance expressed as a ratio of dominance period duration in the non-deprived eye over duration in the deprived eye. B-C. GABA and glutamate concentrations expressed as ratio to total creatine (tCr) normalized as ratio to baseline, calculated as the average of pre-MD measures.

A finer picture of the dynamics of BR is shown in Fig.6, left column, where median dominance durations before (left of the thick gray line) and after (right of the thick gray line) MD are resolved for percept coming from the deprived (middle row) and the non-deprived eye (bottom row). It can be observer that the shift in interocular balance shown in Fig.5A can arise from increased durations in the deprived eye and/or decreased durations in the non-deprived eye, and the proportions varies between the four subjects tested. Suggesting that the overall effect on the interocular balance might arise from different mechanisms depending on the subject, potentially explaining the highly variable MRS results. When expressed as percent change from baseline and compared to percent neurotransmitter changes in the middle and right columns, an inverse relation between GABA changes and dominance durations stands-out only for the non-deprived eye, such that an increase in GABA predicts a MD-related decrease of the non-

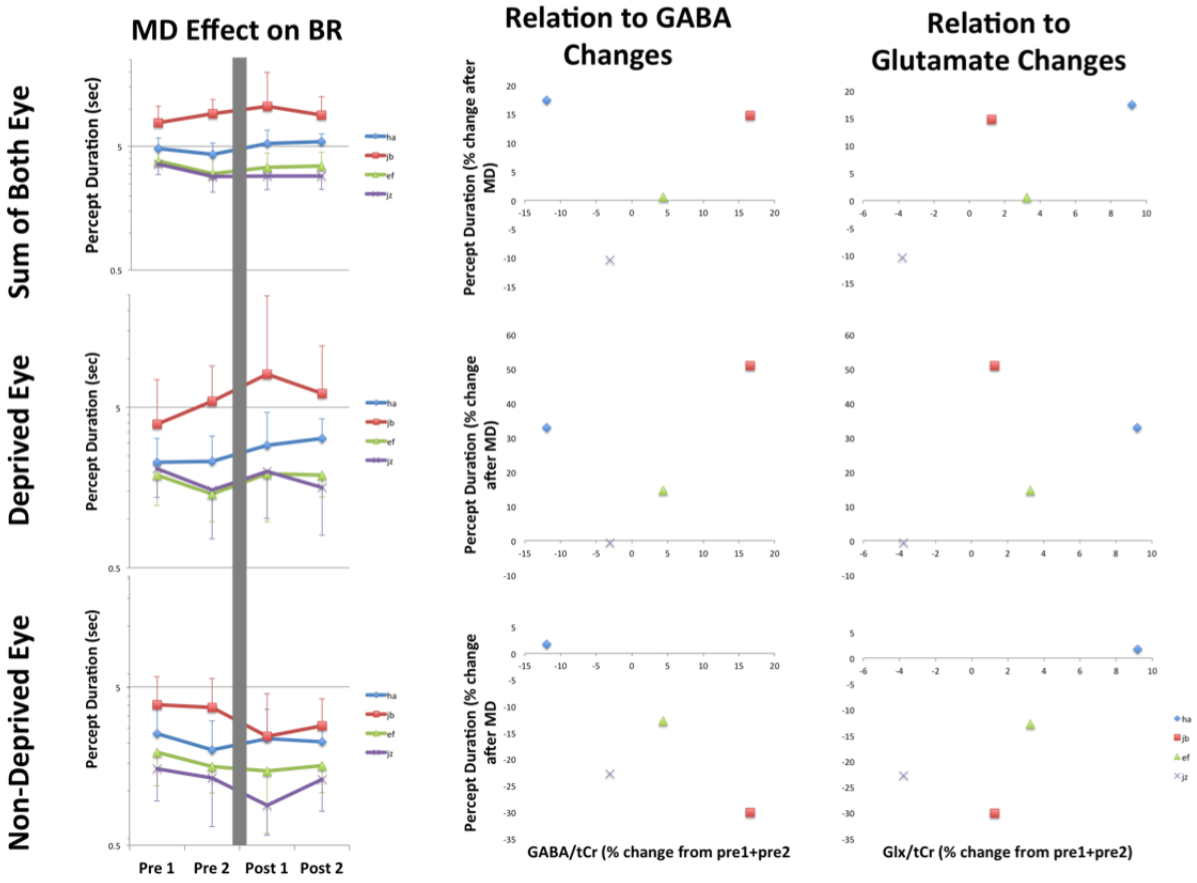

Figure 6. Detailed representation of the effect of monocular deprivation (MD) on binocular rivalry dynamics (left column), along with its relation with MD-induced neurotransmitter changes (middle and right column). Middle and bottom row uses median durations of dominance of percepts corresponding respectively to the deprived and non-deprived eye. The top row represents MD effects on BR that are unspecific to the eye by using the sum of durations from the two eyes. The thick gray line indicates the period of MD. In middle and right columns, both percept durations and neurotransmitter concentrations are expressed as percent change from baseline.

deprived-eye percept duration, and vice-versa. Increases in glutamate, on the other hand, seems to predict increased percept duration from both eye after MD, which is more evident in the first row where durations are summed across the eyes in order to better illustrate potential eye-*un*specific changes.

A pattern is emerging from these preliminary empirical data, whereby GABA modulations specifically predict non-deprived eye changes, and glutamate changes relate to dominance durations irrespective of the eye of origin (Fig.6). How does that compare to our simulation results? The patterns of dependence of dominance durations on *gamma* (Fig.4B) and *alpha* (Fig.4C) are candidate for the eye-specific GABA relation to durations, as unilateral modulations of the parameters for one unit (filled circles in Fig.4) also exhibit unit- (or eye-) specificity. Input strength *I* (Fig.4A) and *sigma* (Fig.4D) can be excluded, as unilateral modulations produced reciprocal changes in the two units, a pattern we don't observe between the deprived and non-deprived eye relation to GABA. All parameter modulations produced non-specific duration changes when the change in one member of a parameter pair equated the change in the other (Fig.4, open circles), and no specific candidate can be identified on the basis of this pattern of change alone.

B.3.3 Discussion

In the present work, we implemented a model of binocular rivalry in an attempt to account for the pattern of results we obtained from the empirical study of the effect of monocular deprivation on both MRS-measured concentrations of occipital GABA and glutamate and the psychophysically assessed dynamics of binocular rivalry. Before trying to relate simulation to empirical results, we must first assess the validity of the chosen model by comparing it against existing data on binocular rivalry.

B.3.3.1 Validity of the model

We observed earlier that durations produced by our model did not fit well the expected gamma distribution (Blake & Logothetis, 2002; Lunghi et al., 2011; Lunghi et al., 2013). More over, a few dominance periods of very short durations, completely outside of the main

distribution peak, were produced (Fig.3B). Closer inspection of time series simulated under the highest level of noise revealed that the only noise-driven dominance reversal present were actually incomplete, and were responsible for the observed very short dominance durations (Fig.7). More specifically, when noisy events brought activity of the suppressed unit at a higher level than the dominant one, but at a time when adaptation levels of the suppressed unit was still high, the switch of dominance could not be fully established and the two units returned into their respective dominant and suppressed states. A simple fixe for this misbehavior would be to remove the noise term from the fast dynamics of activity levels in [6] and rather introduce it into the slow dynamics of adaptation levels in [7]. This would not only make the distribution gamma-like as (van Ee, 2009) showed, but would likely prevent the observed incomplete noise-induced dominance reversals, as activity levels will only be influenced by noise through the adaptation process, which will then be the only driver of reversals, insuring their completeness. Such a reanalysis is however not needed as despite our distribution being non-gamma, it nevertheless shows the expected skewness and long tail of longer durations. The few very short durations certainly biased our dependent variable, the mean dominance duration, toward lower values, but it is unlikely to have affected most of our analysis, with the exception of simulations with varying noise levels, since the number of short off-distribution durations scaled-up with noise level (data not shown). This analysis of the effect of noise will therefore not be discussed further in the present work.

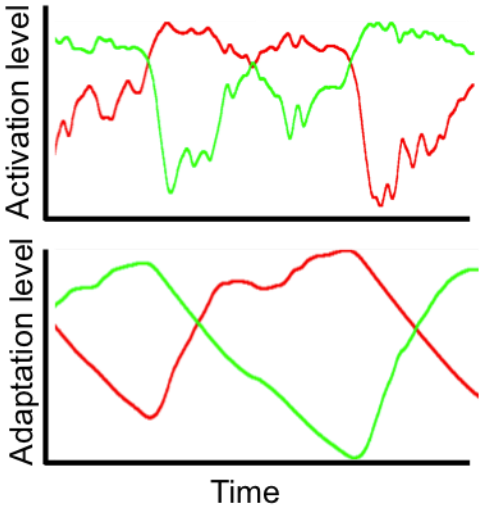

Figure 7. Example of noise-induced failed or incomplete dominance reversal. See text for details.

The effect of simulating variations in input strength *I* to one or the two eyes has a direct psychophysical equivalent that as been extensively studied, the contrast of the rivaling stimuli. Physically increasing the contrast of both left-eye and right-eye stimuli decreases dominance durations according to Levelt's fourth proposition (Levelt, 1968) and more recent experimental

data (Brascamp et al., 2006), but our model exhibited the inverse behavior (Fig.4A). Exploration of the full parameter space of a very similar model implementing all of mutual inhibition, adaptation and noise within a single stage (Shpiro et al., 2009) revealed an inverted U shape for the dependence of durations on input strength. The range of input strength we used might therefore be too high to reproduce experimental data.

Modulating contrast to only one eye while keeping fixed in the other was long thought to primarily affect dominance duration of the other eye, according to Levelt's second proposition (Levelt, 1968). Our model did comply with the expectation that inputs to X2 directly relate to dominance durations of the same unit, and inversely related to dominance duration of the other fixed-input X1 unit. The slopes of these relations are however of roughly the same magnitude, in violation of Levelt's second proposition. Recent psychophysical data suggests that the relative magnitude of these slopes depends on the level of the fixed contrast: a high fixed contrast comply with Levelt's and a low one produce the reverse (greater changes in the eye with variable inputs), while the middle range yield a pattern very similar to the behavior of our system (Shpiro et al., 2009).

Fitting the model on supplementary binocular rivalry data acquired at baseline while modulating contrast of the stimuli in one eye and in both eye would allow finding an appropriate input strength regime. Such an informed model should allow for more valid predictions of the effect of monocular patching, but interpretation should proceed with care until then.

For balanced modulation of the mutual inhibition gain parameters, our model not surprisingly matched the only relevant experimental data from (van Loon et al., 2013), with increased inhibition producing longer durations just as less measured GABA, or pharmacological down-regulation of $GABA_A$ receptor, yielded longer durations in humans. To the best of my knowledge, no data exist on unilateral changes in interocular inhibition and binocular rivalry.

Interestingly, although adaptation processes have received a lot of attention from various experimenters (Roumani & Moutoussis, 2012), to the best of my knowledge, none tried to assess the role of its gain on binocular rivalry. For example, although drifting stimuli ongoing

rivalry across a pre-adapted zone of the visual field is a clever way to demonstrate a causal role for adaptation (Blake et al., 2003), it does not inform on the gain of adaptation, which is the element of interest for the validation of our model. Experimentally modulating this gain might be challenging. We could however estimate it in each eye from the slope of the adaptation effect expressed as a function of contrast of the adaptor. In an approach similar to (van Loon et al., 2013), correlating inter-individual variations of these adaptation gain measures with binocular rivalry measures could help validating our model. Until then, validation of the dependence of dominance durations on adaptation gains expressed by our model will rely on the assumptions, entailed in the model's formalism, regarding the mechanisms through which adaptation affects binocular rivalry. These assumptions seem reasonable regarding the body of experimental data on the subject (Alais et al., 2010; Roumani & Moutoussis, 2012).

B.3.3.2 Mapping the effects of monocular deprivation on the model's simulation

As briefly mentioned in the results section, from the patterns of the simulation results, mutual inhibition and adaptation gain (Fig.4B-C) could both be considered as candidate to explain the relation between GABA and dominance durations specifically in non-deprived eye (Fig.6 middle column). We know from physiology that GABA neurotransmitter mediates interocular inhibition (Blake & Wilson, 2011), such that more of it should mean more mutual inhibition, hence higher *gamma*. Concordant with that, a direct relation between MRS-measured GABA and dominance duration as previously been shown (van Loon et al., 2013). Unless we are willing to consider a convoluted explanation involving sensitivity of MRS *baseline* GABA measures to mutual inhibition (direct relation in (van Loon et al., 2013)) and sensitivity of MRS measures of GABA *changes* to inhibition of mutual inhibition (our inverse relation), we should discard changes in mutual inhibition as the factor driving monocular deprivation-induced alterations of binocular rivalry.

The pattern of adaptation gain (Fig.4C) is interesting. For it to explain our GABA results, we could imagine a pool of GABA ready to be released on an adapting neuron that would consequently show reduced response. Importantly, the MRS-measured GABA would have to reflect the whole pool of GABA in order to be sensitive to the gain of adaptation, rather then adaptation itself, which would rather depend on the amount of released, or active GABA. This

may be far fetched, but it is not so far from common conceptualization of adaptation as recurrent self-inhibition or feedback inhibition, and the concept of adaptation is no stranger to GABAergic inhibition from some empirical studies (Heistek et al., 2010). Importantly, attributing our empirical results to a specific change in adaptation gain allows the testable prediction that monocular deprivation increases adaptation gain specifically in the non-deprived, and that contrary to common sense mutual inhibition is unchanged. Acquisition of the adaptation function in each eye as described earlier, as well as performance of simple dichoptic masking tasks should be sufficient to test those predictions.

The patterns of dependence of dominance durations on the model parameters (Fig.4) could not narrow down the number of candidate mechanisms explaining our empirical preliminarily evidence for an eye-*un*specific direct relation between glutamate and dominance durations (Fig.6 right column). It could be tempting to equate glutamate increase with increase in input strength for both eyes given the direction of the relation in the simulation of balanced changes in input strength (Fig.4A). One must however remember this direction of the relation, although consistent across our simulation and empirical results, is the inverse that observed empirically by physically modulating input strength through changing the contrast of the stimuli (Brascamp et al., 2006; Levelt, 1968). I am forced to conclude our simulations have very limited power helping to understand the mechanisms of the glutamatergic effect on dominance durations, and to appeal to metaplasticity phenomena (Hulme et al., 2013), where upregulating glutamate could favor other plastic changes, not captured by our model, affecting dominance duration similarly in both eyes.

B.4 Conclusion

Binocular rivalry and bistable perception in general is a broad and dynamic field where a variety of computational models are flourishing, and one must arm itself with patience to try to cover them all. It however fells gratifying that one of the simplest models available has such explanatory power. More importantly, the specific testable predictions its exploration allowed will be extremely useful to guide further empirical investigations.

B.5 BIBLIOGRAPHY

Alais, D., Cass, J., O'Shea, R. P., & Blake, R. (2010). Visual Sensitivity Underlying Changes in Visual Consciousness. *Current Biology*, *20*(15), 1362-1367. https://doi.org/10.1016/j.cub.2010.06.015

Blake, R. (1989). A NEURAL THEORY OF BINOCULAR-RIVALRY. *Psychological Review*, *96*(1), 145-167. https://doi.org/10.1037//0033-295x.96.1.145

Blake, R., & Logothetis, N. K. (2002). Visual competition. *Nature Reviews Neuroscience*, *3*(1), 13-23. https://doi.org/10.1038/nrn701

Blake, R., Sobel, K. V., & Gilroy, L. A. (2003). Visual motion retards alternations between conflicting perceptual interpretations. *Neuron*, *39*(5), 869-878. https://doi.org/10.1016/s0896-6273(03)00495-1

Blake, R., & Wilson, H. (2011). Binocular vision. *Vision Research*, *51*(7), 754-770. https://doi.org/10.1016/j.visres.2010.10.009

Boroojerdi, B., Prager, A., Muellbacher, W., & Cohen, L. G. (2000). Reduction of human visual cortex excitability using 1-Hz transcranial magnetic stimulation. *Neurology*, *54*(7), 1529-1531. https://doi.org/10.1212/wnl.54.7.1529

Brascamp, J. W., Van Ee, R., Noest, A. J., Jacobs, R., & van den Berg, A. V. (2006). The time course of binocular rivalry reveals a fundamental role of noise. *Journal of Vision*, *6*(11), 1244-1256. https://doi.org/10.1167/6.11.8

Freeman, A. W. (2005). Multistage model for binocular rivalry. *Journal of Neurophysiology*, *94*(6), 4412-4420. https://doi.org/10.1152/jn.00557.2005

Heistek, T. S., Lodder, J. C., Brussaard, A. B., Bosman, L. W. J., & Mansvelder, H. D. (2010). GABAergic inhibition shapes frequency adaptation of cortical activity in a frequency-dependent manner. *Brain Research*, *1321*, 31-39. https://doi.org/10.1016/j.brainres.2010.01.047

Hulme, S. R., Jones, O. D., & Abraham, W. C. (2013). Emerging roles of metaplasticity in behaviour and disease. *Trends in Neurosciences*, *36*(6), 353-362. https://doi.org/10.1016/j.tins.2013.03.007

Kovacs, I., Papathomas, T. V., Yang, M., & Feher, A. (1996). When the brain changes its mind: Interocular grouping during binocular rivalry. *Proceedings of the National Academy of Sciences of the United States of America*, *93*(26), 15508-15511. https://doi.org/10.1073/pnas.93.26.15508

Kwon, M. Y., Legge, G. E., Fang, F., Cheong, A. M. Y., & He, S. (2009). Adaptive changes in visual cortex following prolonged contrast reduction [Article]. *Journal of Vision*, *9*(2), 16, Article 20. https://doi.org/10.1167/9.2.20

Laing, C. R., & Chow, C. C. (2002). A spiking neuron model for binocular rivalry. *Journal of Computational Neuroscience*, *12*(1), 39-53. https://doi.org/10.1023/a:1014942129705

Lehky, S. R. (1988). AN ASTABLE-MULTIVIBRATOR MODEL OF BINOCULAR-RIVALRY. *Perception*, *17*(2), 215-228. https://doi.org/10.1068/p170215

Levelt, W. J. M. (1968). *On binocular rivalry*. Mouton.

Logothetis, N. K., Leopold, D. A., & Sheinberg, D. L. (1996). What is rivalling during binocular rivalry? *Nature*, *380*(6575), 621-624. https://doi.org/10.1038/380621a0

Lunghi, C., Burr, D. C., & Morrone, C. (2011). Brief periods of monocular deprivation disrupt ocular balance in human adult visual cortex. *Current Biology*, *21*(14), R538-R539. https://doi.org/10.1016/j.cub.2011.06.004

Lunghi, C., Burr, D. C., & Morrone, M. C. (2013). Long-term effects of monocular deprivation revealed with binocular rivalry gratings modulated in luminance and in color. *Journal of Vision*, *13*(6), Article 1. https://doi.org/10.1167/13.6.1

Mescher, M., Merkle, H., Kirsch, J., Garwood, M., & Gruetter, R. (1998). Simultaneous in vivo spectral editing and water suppression. *Nmr in Biomedicine*, *11*(6), 266-272. https://doi.org/10.1002/(sici)1099-1492(199810)11:6<266::aid-nbm530>3.0.co;2-j

Moreno-Bote, R., Rinzel, J., & Rubin, N. (2007). Noise-induced alternations in an attractor network model of perceptual bistability. *Journal of Neurophysiology*, *98*(3), 1125-1139. https://doi.org/10.1152/jn.00116.2007

Mrsic-Flogel, T. D., Hofer, S. B., Ohki, K., Reid, R. C., Bonhoeffer, T., & Hubener, M. (2007). Homeostatic regulation of eye-specific responses in visual cortex during ocular dominance plasticity. *Neuron*, *54*(6), 961-972. https://doi.org/10.1016/j.neuron.2007.05.028

Noest, A. J., van Ee, R., Nijs, M. M., & van Wezel, R. J. A. (2007). Percept-choice sequences driven by interrupted ambiguous stimuli: A low-level neural model. *Journal of Vision*, *7*(8), Article 10. https://doi.org/10.1167/7.8.10

Roumani, D., & Moutoussis, K. (2012). Binocular rivalry alternations and their relation to visual adaptation. *Frontiers in Human Neuroscience*, *6*, Article 35. https://doi.org/10.3389/fnhum.2012.00035

Scocchia, L., Valsecchi, M., & Triesch, J. (2014). Top-down influences on ambiguous perception: the role of stable and transient states of the observer [Review]. *Frontiers in Human Neuroscience*, *8*, 18, Article 979. https://doi.org/10.3389/fnhum.2014.00979

Shpiro, A., Moreno-Bote, R., Rubin, N., & Rinzel, J. (2009). Balance between noise and adaptation in competition models of perceptual bistability. *Journal of Computational Neuroscience*, *27*(1), 37-54. https://doi.org/10.1007/s10827-008-0125-3

Sugie, N. (1982). NEURAL MODELS OF BRIGHTNESS PERCEPTION AND RETINAL RIVALRY IN BINOCULAR VISION. *Biological Cybernetics*, *43*(1), 13-21. https://doi.org/10.1007/bf00337283

Tong, F., Meng, M., & Blake, R. (2006). Neural bases of binocular rivalry. *Trends in Cognitive Sciences*, *10*(11), 502-511. https://doi.org/10.1016/j.tics.2006.09.003

van Ee, R. (2009). Stochastic variations in sensory awareness are driven by noisy neuronal adaptation: evidence from serial correlations in perceptual bistability. *Journal of the Optical Society of America a-Optics Image Science and Vision*, *26*(12), 2612-2622. https://doi.org/10.1364/josaa.26.002612

van Loon, A. M., Knapen, T., Scholte, H. S., St John-Saaltink, E., Donner, T. H., & Lamme, V. A. F. (2013). GABA Shapes the Dynamics of Bistable Perception [Article]. *Current Biology*, *23*(9), 823-827. https://doi.org/10.1016/j.cub.2013.03.067

Vernet, M., Brem, A. K., Farzan, F., & Pascual-Leone, A. (2015). Synchronous and opposite roles of the parietal and prefrontal cortices in bistable perception: A double-coil TMS-EEG study [Article]. *Cortex*, *64*, 78-88. https://doi.org/10.1016/j.cortex.2014.09.021

Wilson, H. R. (2003). Computational evidence for a rivalry hierarchy in vision. *Proceedings of the National Academy of Sciences of the United States of America*, *100*(24), 14499-14503. https://doi.org/10.1073/pnas.2333622100

Zhang, P., Bao, M., Kwon, M., He, S., & Engel, S. A. (2009). Effects of Orientation-Specific Visual Deprivation Induced with Altered Reality. *Current Biology*, *19*(22), 1956-1960. https://doi.org/10.1016/j.cub.2009.10.018

Zhou, J. W., Clavagnier, S., & Hess, R. F. (2013). Short-term monocular deprivation strengthens the patched eye's contribution to binocular combination. *Journal of Vision*, *13*(5), 1-10. https://doi.org/10.1167/13.5.12

Annex C: Illustration of Signal Detection Theory to Model Within- and Between-Channel Processes

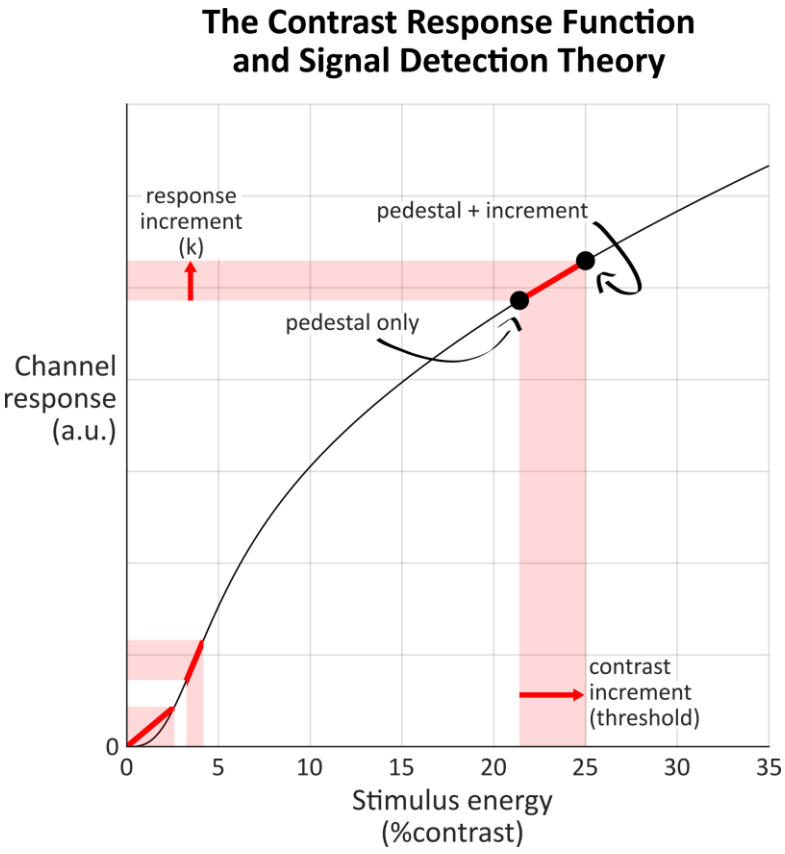

Figure C.1 Illustration of signal detection theory's account of psychophysical contrast thresholds. A hypothetical contrast response function (black trace) describes the response of a visual channel to the contrast energy of its preferred stimulus (a grating of given retinal position, spatial frequency, orientation, etc.). In a contrast discrimination task, a pedestal stimulus drives the channel to a baseline response level (red graphics elements; pedestal only). A small contrast increment to the pedestal produces a small response increment (red graphics elements; pedestal + increment). In a 2-interval-forced-choice task, the interval producing the largest response in the channel is picked, whether this was due to internal noise or true signal. Above-chance accuracy is therefore only achieved when response increments exceed a fixed value *k*. At high pedestal contrast, the system operates at low gain—shallow slope of the contrast response function (3rd set of red graphics from bottom left)—and a response increment *k* requires a large contrast increment, resulting in poor discrimination thresholds. With higher gains at lower pedestal contrast (2nd set of red graphics from bottom left), *k* is reached with smaller contrast increments, improving discrimination thresholds. A simple contrast detection task is a special case where pedestal contrast is zero, placing the system at the bottom of its dynamic range where the gain is again low and thresholds poor (1st set of red graphics from bottom left). Solving the contrast response function for the contrast increments producing a fixed response increment *k* allows to predict contrast increment thresholds across a range of the pedestal contrasts. *a.u.: arbitrary units; Code available at https://github.com/farivarlab/psychoCRFdemo.*

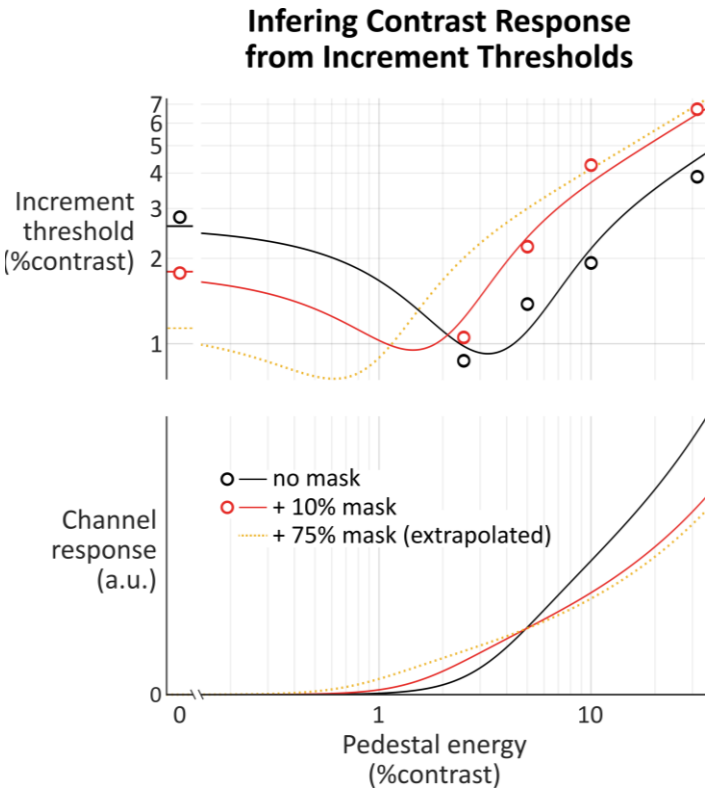

Figure C.2 Illustration of modeling within- and between-channel interactions. Top panel shows contrast discrimination thresholds (black and red circles) acquired across a range of pedestal contrasts. Bottom panel shows the corresponding contrast response functions (black and red traces; Equation [5.1]) fitted to top panel's thresholds. Relative to 0% contrast, increasing pedestal contrast successively facilitates (lowers thresholds) then suppresses (elevates thresholds) detection of contrast increments. Compared to the no mask condition (black circles and traces), adding a constant 10% cross-oriented mask (red circles and traces) facilitates the perception of low contrasts (lowers the threshold at 0% pedestal contrast) but suppresses the perception of high contrasts (elevates thresholds at >0% pedestal contrasts). The no-mask and 10%-mask data were modeled together in a single fit, and the effect of a 75% mask was extrapolated from that fit (yellow dotted trace). *Data and fits replotted and extrapolated from Meese et al. (2007) (observer RJS). Code available at https://github.com/farivarlab/psychoCRFdemo.*

C.1 Bibliography

Meese, T. S., Summers, R. J., Holmes, D. J., & Wallis, S. A. (2007). Contextual modulation involves suppression and facilitation from the center and the surround [Review]. *Journal of Vision*, *7*(4), 21, Article 7. https://doi.org/10.1167/7.4.7